

FACULTAD DE CIENCIAS
UNIVERSIDAD DE GRANADA
Departamento de Química Inorgánica



PROGRAMA DE DOCTORADO EN QUÍMICA

TESIS DOCTORAL

**NANOQUÍMICA CON BACTERIAS, BIOPOLÍMEROS
Y BIOFIBRAS. UNA NUEVA VÍA PARA EL
TRATAMIENTO DE INFECCIONES**

Laura Sabio Rodríguez

Granada. Abril de 2022

Directores de la Tesis Doctoral:
Prof. José Manuel Domínguez Vera
Dr. José Manuel Delgado López

Editor: Universidad de Granada. Tesis Doctorales
Autor: Laura Sabio Rodríguez
ISBN: 978-84-1117-757-3
URI: <https://hdl.handle.net/10481/80739>

NANOQUÍMICA CON BACTERIAS, BIOPOLÍMEROS Y BIOFIBRAS. UNA NUEVA VÍA PARA EL TRATAMIENTO DE INFECCIONES

Memoria de Tesis Doctoral presentada por
Laura Sabio Rodríguez
para aspirar al título de Doctor por la Universidad de Granada

Fdo.: Laura Sabio Rodríguez

DIRECTORES DE LA TESIS DOCTORAL:

Prof. José Manuel Domínguez Vera

Catedrático del Departamento de Química Inorgánica.
Universidad de Granada e Instituto de Biotecnología

Dr. José Manuel Delgado López

Investigador Ramón y Cajal del Departamento de Química Inorgánica.
Universidad de Granada

Los resultados del trabajo de investigación realizado durante el desarrollo de esta Tesis Doctoral han dado lugar a la publicación de artículos cuyos indicios de calidad son:

- Laura Sabio, Ana González, Gloria B. Ramírez-Rodríguez, José Gutiérrez-Fernández, Oscar Bañuelo, Mónica Olivares, Natividad Gálvez, José M. Delgado-López, and Jose M. Dominguez-Vera. Probiotic cellulose: Antibiotic-free Biomaterials with Enhanced Antibacterial Activity. *Acta Biomaterialia* (2021), 124, 244-253. ISSN 1742-7061
<https://doi.org/10.1016/j.actbio.2021.01.039>

Indicios de calidad:

Datos del Journal Citation Reports

- Impact Factor (2020): 8.947
 - Categorías (posición/número de revistas):
ENGINEERING, BIOMEDICAL (10/89)
MATERIALS SCIENCE, BIOMATERIALS (5/41)
 - Cuartil: Q1
- Laura Sabio, Andrea Sosa, José M. Delgado-López, and Jose M. Dominguez-Vera. Two-Sided Antibacterial Cellulose Combining Probiotics and Silver Nanoparticles. *Molecules* (2021), 26(10), 2848. eISSN 1420-3049
<https://doi.org/10.3390/molecules26102848>

Indicios de calidad:

Datos del Journal Citation Reports

- Impact Factor (2020): 4.412
- Categorías (posición/número de revistas):
BIOCHEMISTRY & MOLECULAR BIOLOGY - SCIE (115/295)
CHEMISTRY, MULTIDISCIPLINARY - SCIE (63/178)
- Cuartil: Q2

- Ana González, Laura Sabio, Carmen Hurtado, Gloria B. Ramírez-Rodríguez, Vipul Vansal, José M. Delgado-López, and Jose M. Dominguez-Vera. Entrapping Living Probiotics into Collagen Scaffold: A New Class of Biomaterials for Antibiotic-Free Therapy of Bacterial Vaginosis. *Advanced Materials Technologies* (2020), 2000137, 1-8. ISSN 2365-709X
<https://doi.org/10.1002/admt.202000137>

Indicios de calidad:

Datos del Journal Citation Reports

- Impact Factor (2020): 7.848
- Categorías (posición/número de revistas):
MATERIALS SCIENCE, MULTIDISCIPLINARY (60/334)
Cuartil: Q1

- Laura Sabio, Juan de Vicente Álvarez-Manzaneda, Jose M. Dominguez-Vera, and José M. Delgado-López. Hybrid Living Material with tunable viscoelasticity through bacterial proliferation. *Submitted* (2022),

Dichos resultados también han dado lugar a la publicación de dos patentes:

- Mónica Olivares Martín, Oscar Bañuelo Hortigüela, Ana Isabel González Garnica, Laura Sabio Rodríguez, Gloria Belén Ramírez Rodríguez, José Manuel Delgado López, and José Manuel Domínguez Vera. **BIOCOMPOSITES COMPRISING PROBIOTICS, COLLAGEN AND BACTERIAL EXTRACELLULAR POLYSACCHARIDES AND USES THEREOF**. PCT, P18057EP00, 2020. Transferida a BIOSEARCH S.A.
- José Manuel Delgado López, José Manuel Domínguez Vera, Natividad Gálvez Rodríguez, Ana Isabel González Garnica, Laura Sabio Rodríguez, y Gloria Belén Ramírez Rodríguez. **BIOMATERIAL COMPUESTO POR CELULOSA BACTERIANA Y PROBIÓTICOS Y USOS DEL MISMO**. PCT/EP2021 068166.

*A mis padres, Merche y Paco,
y a todos los que me habéis acompañado.*

"Happiness is only real when shared"
Christopher McCandless (Into the Wild, Jon Krakauer)

Esta Tesis Doctoral se ha llevado a cabo en el Departamento de Química Inorgánica de la Facultad de Ciencias (Universidad de Granada), en el grupo BIONANOMET (FQM-368). Gracias al Ministerio de Universidades por la concesión de mi beca de Formación de Profesorado Universitario (FPU16/01360) y a la financiación de los proyectos CTQ2015-64538-R, RTI2018-095794-A-C22 y PID2019-111461GB-I00. Gracias al Programa P10 del Plan Propio del Vicerrectorado de Investigación y Transferencia (UGR) por la beca de movilidad que se me concedió para realizar mi estancia breve.

En primer lugar, quiero agradecer a mi director de tesis, Josema, por ofrecerme la oportunidad de formar parte de este laboratorio, que ha pasado a ser mi segunda familia. Gracias por la confianza y por todo el esfuerzo que has invertido en mí en estos 6 años (que se dice pronto), por ayudarme a formarme como investigadora y como persona. Han sido años intensos, muy enriquecedores y, por supuesto, imposibles de olvidar. José, gracias por ser mi director, por las largas conversaciones, dentro y fuera del laboratorio. Qué gran suerte que aparecieras en nuestro grupo, para mí y para todos. Os agradezco especialmente vuestra implicación en estos últimos años, que han sido tan difíciles para mí tanto a nivel personal como profesional. También por vuestra paciencia y persistencia con la estancia predoctoral, a pesar de todos los inconvenientes que han surgido. Para mí, esta estancia ha sido un antes y un después en mi vida, y eso os lo agradeceré siempre. Quiero dar las gracias a todas las personas que han hecho que estos tres meses en Grenoble hayan sido tan fantásticos, empezando por Alexander. Gracias por tu implicación y por tu preocupación, por la experiencia en el ESRF y por haberme dado la oportunidad de analizar mis muestras allí. Agradezco el tiempo que me has brindado, Alicia, porque ha sido totalmente altruista por tu parte. Gracias por hacer que mi llegada a Grenoble fuese como estar en casa, por ofrecerme siempre tu ayuda. *Thank you, Andrew, for all the conversations and for all the days of climbing. I will always remember this past Christmas! Come whenever you want, here is your home. I would also like to*

thank all the people I met in ISTerre for their kindness, especially Alejandro, Luca, Benjamin, and Annette. También doy las gracias a todos los amigos que he dejado allí: Ana Torrubia, Ana, Clara, Claudia, Carmen, Alex, Víctor, Hamza, Lucie, Fernando y Samuel. Gracias por los días de esquí, por las cervezas y los paseos. Por todo el apoyo.

Gracias a Nati por sus abrazos y su amabilidad. Siempre respondiendo con una sonrisa, contagiando el buen ambiente. Gracias a Juan de Vicente Álvarez Manzaneda del Departamento de Física Aplicada de la UGR, por su tiempo y paciencia invertidos en enseñarme reología, un campo con un potencial que para mí era desconocido. Gracias a Manuel Martínez Bueno del Departamento de Microbiología de la UGR, por su ayuda y aportaciones experimentales.

Gracias al Centro de Investigación Científica de la UGR, y en especial a su personal por su profesionalidad. En particular quiero agradecer a Ana Santos el tiempo que hemos pasado juntas, que tan enriquecedor ha sido para mí, y las imágenes tan fantásticas de CLSM que han sido incluidas en nuestros artículos. También agradezco su esfuerzo a Conchi, Dani e Isabel Guerra por el maravilloso trabajo que llevan a cabo para la preparación y análisis de muestras en SEM, que tanta calidad les aporta a nuestras publicaciones.

Muchas gracias a Antonio de la Torre y a M^a Carmen, por su amabilidad y por estar ahí siempre que se les necesita. ¡Sin vosotros el departamento dejaría de funcionar!

Gracias a mi familia del laboratorio. ¿Qué puedo decir que no sepáis? Os estaré eternamente agradecida por vuestra maravillosa acogida, por los congresos, por las cervezas y los desayunos. Siempre agradeceré el tiempo que me habéis dedicado, en los buenos y en los malos momentos. Gracias Rocío, por ser tú. No existen palabras suficientes para describir todo lo que hemos vivido y todo lo que he aprendido de ti. Eres una persona maravillosa, y el Mola y tú os merecéis lo mejor. Os admiro muchísimo. Gracias Víctor por tu increíble optimismo tan contagioso. Aunque la situación sea complicada, siempre eres

capaz de sacarme una sonrisa. Siempre ofreces tu ayuda, no hay persona más transparente en este mundo. Gracias Migue por las conversaciones, por ofrecerme siempre tu punto de vista y tu apoyo. Deseo que todo te vaya genial. Gracias Ana por ser la madre del laboratorio, tu organización nos ha salvado de muchas desgracias y malos ratos. Gracias Marta, Jorge y Pedrito, por traernos un soplo de aire fresco desde Soria. Sois unas personas maravillosas y me siento muy afortunada de haberos conocido. Dispuestos a ayudar y a ofrecer siempre su hombro para mi desahogo. Sabéis que podéis contar conmigo para lo que sea. Gracias Belén por aparecer en el laboratorio y traernos aire de levante de 5 barras 😊. Al poco de llegar te convertiste en una pieza clave del laboratorio y de mi vida. Has pasado momentos muy duros, y yo doy las gracias por haber podido estar cerca de ti. Las palabras sobran si hay un abrazo a tiempo (o un sticker...). Cuando se juntan las ganas de comer con el hambre, ya sabemos lo que puede pasar. Que se prepare el mundo que allá vamos. Gracias Gloria por decidir quedarte con nosotros. Eres un ejemplo a seguir, un ejemplo de lucha y constancia, nunca te falta una sonrisa y palabras amables. Siempre disponible para tomar un cubata, digo, un bocata... También quiero dar las gracias a las nuevas incorporaciones y os mando mucha fuerza, Pablo, Gloria P. y Rafa.

Gracias Félix. Cuando te fuiste, una parte del laboratorio se fue contigo. Gracias por tu ayuda durante el tiempo que estuviste con nosotros, por las excursiones y las charlas sobre fotografía y pájaros. Eres una gran persona y te considero un gran amigo.

Gracias a todos los que forman y formaron parte del Departamento. Podría escribir una hoja de cada uno de vosotros, porque todos sois especiales para mí. Gracias Antonio. Te parecerá una tontería, pero me diste un golpe de realidad antes de irme de estancia, cosa que no olvidaré y que me hizo plantearme las cosas con otra perspectiva. Gracias por quitarle hierro a esos granos de arena que a veces se convierten en montañas. Gracias a los

radioquímicos, Abel, Pablo, Pili y Víctor (cuidado con él, gran personaje); a los MOFers, Rodri, Kiko, Rebeca, Lydia, Javi, Cristina, y Pedro; y a los magnéticos, Ismael, M^a del Mar, Aritz, y Juanra. Gracias a Chiqui, por darme esperanzas con el trabajo y la estancia. Gracias a Virginia y a Carmen, que fueron el nexo de unión de todos los “jóvenes”. Gracias Víctor Karim por la mano de Fátima; llámalo suerte, llámalo karma o llámalo energía, pero desde entonces las cosas me han ido mejor jeje. Gracias a todo el profesorado del Departamento, que tanto me han enseñado en todos los años que he sido parte de la Universidad, en especial a Antonillo, Sara, Puri, Enrique y José María.

Gracias también a mis compañeros de Bioquímica. A Laura Hidalgo, por nuestras terapias infinitas. Ánimo, te mereces lo mejor y vales muchísimo. A Nacho, Alex, Caro, Jesús, Álvaro y Germán. Gracias por todo el apoyo durante y después de la carrera.

Gracias a toda mi familia: a todos mis titos, mis primos y mi hermano, Gonzalo. A mis padres, Merche y Paco, por darme la vida que he tenido, por luchar siempre para ofrecernos lo mejor y por apoyarme en mis decisiones. Esto ha podido ser una realidad gracias a vosotros, a vuestro tiempo y esfuerzo incansable. Gracias a mi abuela Charo y a mi abuela Encarna, que, aunque ya no esté, sigue conmigo, motivándome todos los días para seguir luchando. No ha habido persona más admirable que ella.

GRACIAS Manu. Por enseñarme a trabajar en el laboratorio, por ofrecerte siempre a ayudar. Te sacrificas siempre por el bienestar de todos, sin importarte quién. Tienes un corazón enorme. Gracias por los viajes, las sorpresas que no te puedes aguantar, los abrazos, las ganas que le pones a todo, las excursiones, las escapadas, los picos conquistados... Me encantan tus locuras y tus caminos inventados. Gracias por todo el apoyo que me has brindado durante estos años. Tengo mucha ilusión en coleccionar más momentos maravillosos contigo, porque tú me has enseñado que la felicidad sólo es real cuando se comparte.



**RESUMEN Y ESTRUCTURA
DE LA TESIS DOCTORAL**

Esta Tesis Doctoral está dedicada al desarrollo de nuevas metodologías para la obtención de biomateriales mediante la integración de bacterias probióticas en matrices poliméricas (colágeno o celulosa bacteriana). La caracterización exhaustiva a nivel estructural del material híbrido resultante, sus propiedades mecánicas y sus prestaciones biológicas, han puesto de manifiesto su versatilidad para su uso en aplicaciones médicas reales, especialmente para el tratamiento de infecciones bacterianas evitando el uso de antibióticos.

Los resultados experimentales y su discusión se desarrollan en esta memoria divididos en 6 capítulos.

El **primer capítulo**, la introducción, se centra en los conceptos básicos de las áreas de investigación en las que se enmarca la presente Tesis Doctoral. Se discute el concepto “Biomaterial”, enfocando la discusión en sus aplicaciones en medicina. A continuación, se describen específicamente los dos biopolímeros empleados en esta Tesis: el colágeno y la celulosa bacteriana, detallando sus estructuras, importancia biológica, propiedades y, de forma más general, algunas de sus aplicaciones. Estos polímeros se han empleado como soportes para el desarrollo de nuevos materiales vivos (LMs), un concepto relativamente novedoso que describe biomateriales compuestos por una matriz inerte que incorpora entidades vivas, generalmente células.

En esta Tesis, hemos empleado bacterias probióticas como entidad viva. Así pues, la introducción prosigue abordando los tipos de bacterias con más interés actualmente en la industria biomédica, diferenciando aquellas que son beneficiosas para la salud humana, conocidas como bacterias probióticas, de las bacterias patógenas, que pueden infectar o provocar una enfermedad. Con respecto a las bacterias patógenas, se aborda la problemática de la aparición y desarrollo exponencial de bacterias resistentes a antibióticos, una de las mayores amenazas de salud global hoy en día.

Finalmente, se exponen los **objetivos** principales que se establecieron para esta Tesis Doctoral.

En el **segundo capítulo** se describe la síntesis de un nuevo tipo de LM en el que el colágeno autoensamblado actúa como matriz para las bacterias probióticas y sus exopolisacáridos (EPS), con objeto de tratar la vaginosis bacteriana (BV). Esta infección es la más común en mujeres en edad fértil y se caracteriza por un desajuste en la microbiota vaginal. La BV puede considerarse un modelo de infección donde bacterias de la microbiota vaginal luchan contra bacterias patógenas por predominar y sobrevivir, resultando en un estado sano o infección según predominen unas u otras. En este capítulo se desarrolla una estrategia para encapsular (y proteger) en matrices de colágenos tridimensionales a probióticos como *Lactobacillus fermentum* o *Lactobacillus acidophilus*, muy utilizados en la industria alimentaria. Dicha estrategia consistió en el autoensamblaje del colágeno en presencia de los probióticos, consiguiéndose la completa integración de la bacteria, la cual emplea su EPS para interactuar de forma específica con las fibras de colágeno, dando lugar a la formación de un LM con prestaciones mejoradas.

Los probióticos incorporados a esta matriz aumentan su estabilidad y actividad metabólica, incluso en condiciones adversas, con respecto a los probióticos libres. Además, este LM presenta una gran adherencia a los tejidos gracias a la presencia del colágeno. Estas propiedades hacen de este biomaterial una alternativa prometedora a los tratamientos convencionales de BV, puesto que su mayor adherencia a la vagina y su actividad prolongada (por su mayor estabilidad) evitarían las recaídas de dicha infección, uno de los puntos críticos en los tratamientos convencionales. El protocolo de obtención de este biomaterial y sus usos han sido protegidos según el Tratado de Cooperación en materia de Patentes (PCT, P18057EP00, 2020) y transferido a la empresa BIOSEARCH S.A. Asimismo, los resultados de este capítulo han sido publicados (*Adv. Mater. Tech.* 2020, 2000137).

El **tercer capítulo** se centra en la celulosa, otro biopolímero de gran importancia utilizado ampliamente en medicina. En este capítulo se desarrolla un biomaterial con dos componentes antibacterianos encapsulados en la celulosa bacteriana: un probiótico (*Lactobacillus fermentum*) y nanopartículas de plata. Para ello, se preparó una celulosa bacteriana “de doble cara”, una de ellas se funcionalizó con nanopartículas de plata y la opuesta con probióticos. La actividad antibacteriana de este biomaterial frente a *Pseudomonas aeruginosa* fue mayor que la que presentaron los controles de celulosa, celulosa-plata y celulosa-probiótico, lo que indica que existe cierta sinergia entre los dos componentes antibacterianos. Los resultados de este capítulo se publicaron en la revista *Molecules* 2021, 26, 2848.

En el **cuarto capítulo** hemos desarrollado una estrategia para conseguir un LM formado por probióticos (*L. fermentum* o *L. gasseri*) integrados en la matriz de celulosa bacteriana. Este protocolo se basa en el co-cultivo del probiótico y de la bacteria productora de celulosa, *A. xylinum*, para obtener la matriz de celulosa, y posteriormente se cambian a las condiciones de cultivo óptimas para el crecimiento del probiótico. De esta forma se induce el crecimiento exponencial del probiótico, que termina invadiendo totalmente la membrana de celulosa, desplazando a la bacteria productora de celulosa. Además, este protocolo evita el costoso y largo tratamiento de purificación que se emplea comúnmente para eliminar la bacteria productora de celulosa. Este biomaterial mostró actividad antibacteriana frente a *Staphylococcus aureus* y *Pseudomonas aeruginosa* y, lo que es más importante, frente a *S. aureus* y *P. aeruginosa* multirresistentes a antibióticos aislados de muestras de orina de pacientes reales. Es importante señalar que en todos los ensayos antibacterianos se emplearon medios y condiciones de cultivo óptimos para las bacterias patógenas, lo que pone de manifiesto el potencial real de este nuevo tipo de biomaterial como antibacteriano. Este LM ha sido patentado (PCT/EP2021 068166) y publicado en *Acta Biomaterialia* 2021, 124, 244.

En el **quinto capítulo** se llevó a cabo el estudio dinámico de las propiedades mecánicas (reológicas) del biomaterial obtenido tras la integración de *L. fermentum* en la celulosa bacteriana. Hemos observado como la proliferación del probiótico en la red de celulosa induce cambios muy significativos en las propiedades mecánicas del biomaterial. En particular, hemos observado cómo la viscoelasticidad de este biomaterial puede controlarse con el crecimiento bacteriano. Así pues, a baja densidad de probiótico, el biomaterial es un gel más viscoelástico que la propia matriz de celulosa, mientras que la proliferación masiva del probiótico en la matriz hace que el biomaterial adquiera propiedades mecánicas típicas de un sólido. Esta transformación de gel a sólido con el 'simple' paso del tiempo de cultivo (ed., proliferación) no había sido observada en ningún otro material vivo y abre la posibilidad de que este tipo de biomateriales puedan ser usados para su impresión 3D *in vivo* en diferentes aplicaciones biomédicas.

El **sexto capítulo** comienza con la síntesis y la caracterización estructural de la celulosa bacteriana producida por *Acetobacter xylinum*, tanto con las bacterias integradas en la estructura de celulosa como una vez purificada (tras eliminar las bacterias). También hemos estudiado cómo afectan las condiciones de cultivo y los métodos de secado a la estructura final de la celulosa bacteriana. Este estudio nos sirvió de base para afrontar el reto del alineamiento de las fibras de celulosa, con el fin de desarrollar una celulosa bacteriana ordenada que tuviera propiedades mecánicas mejoradas con respecto a la forma nativa. En este sentido, hemos desarrollado un método novedoso para obtener *in situ* celulosa con un alto grado de alineamiento de las fibras usando *A. xylinum* "magnética". El cultivo de estas bacterias en presencia de campos magnéticos da lugar a la formación de una fina lámina de celulosa. Su caracterización preliminar mediante AFM, SAXS y WAXS sugiere la presencia de anisotropía y cierto grado de orientación preferencial de las fibras de celulosa.



SUMMARY

This PhD thesis is devoted to the development of new methodologies for producing biomaterials by way of the adequate integration of probiotic bacteria into polymeric matrices (collagen or bacterial cellulose). An in-depth characterization of the resulting hybrid materials in terms of their structure, mechanical properties and biological performance has demonstrated their versatility for use in real medical applications, specifically the antibiotic-free treatment of bacterial infections.

The experimental results and corresponding discussions are outlined in six chapters as follow:

Chapter 1 introduces some of the basic concepts of the research areas in which this thesis is framed. The concept “Biomaterial” is defined, focusing the discussion on their applicability in medicine. Subsequently, the two most important biopolymers used in this thesis, namely collagen and bacterial cellulose, are described in detail, discussing their structures, biological importance, properties and, more generally, some of their applications. These biopolymers have been used as scaffolds to develop innovative living materials (LMs), a relatively new concept of biomaterial comprising an inert matrix that incorporates living entities, usually cells.

In this thesis, we have used probiotic bacteria as living entities instead. Thus, the introduction continues with a discussion of the most interesting bacterial types in the biomedical industry, differentiating between those that are beneficial to human health, known as probiotic bacteria, and pathogenic bacteria, which are known for their ability to infect or cause disease. With respect to pathogenic bacteria, we decided to focus on one of the greatest current global health threats, namely the emergence and exponential development of antibiotic-resistant bacteria. Finally, the main objectives of this thesis are clearly described.

Chapter 2 describes the first example of an LM, in which self-assembled collagen fibres serve as scaffolds for probiotic bacteria and their

exopolysaccharides (EPS), for the treatment of bacterial vaginosis (BV). BV is the most common infection in women of childbearing age and is characterised by an imbalance in the vaginal microbiota. BV can be considered a model of infection, with vaginal microbiota and pathogenic bacteria struggling for predominance and survival, thereby resulting in either a healthy state or infection, depending on the predominance of the former or the latter. In this chapter, we have developed a strategy to encapsulate (and protect) *Lactobacillus fermentum* or *Lactobacillus acidophilus*, two probiotics widely used in the food industry, in 3D collagen matrices. Thus, self-assembly of collagen in the presence of the probiotics resulted in the complete integration of the bacteria, which use their EPS to interact specifically with the collagen fibrils, thus leading to the formation of a LM with a good level of performance.

Specifically, the probiotics incorporated into the matrix increase their viability and metabolic activity, even under adverse conditions, in comparison to free probiotics. A further important aspect is the good adherence of this biomaterial to tissues due to the presence of collagen. These aspects make this type of biomaterial a very promising alternative for treating BV with probiotics, since its greater adherence to the vagina and its prolonged activity, due to its greater stability, would prevent relapses of this infection, one of the main disadvantages of conventional BV treatments. The protocol for obtaining this biomaterial, and its uses, have been protected under the Patent Cooperation Treaty (PCT, (P18057EP00, 2020) and transferred to the company BIOSEARCH SA. The results of this chapter have also been published (Adv. Mater. Tech. 2020, 2000137).

Chapter 3 moves the focus to cellulose, the other important biopolymer widely used in medicine. This chapter concerns the development of a biomaterial with two potentially antibacterial components encapsulated in the bacterial cellulose, namely a probiotic (*Lactobacillus fermentum*) and silver nanoparticles. For this purpose, a “double-sided” bacterial cellulose was prepared in which one side was functionalised with silver nanoparticles

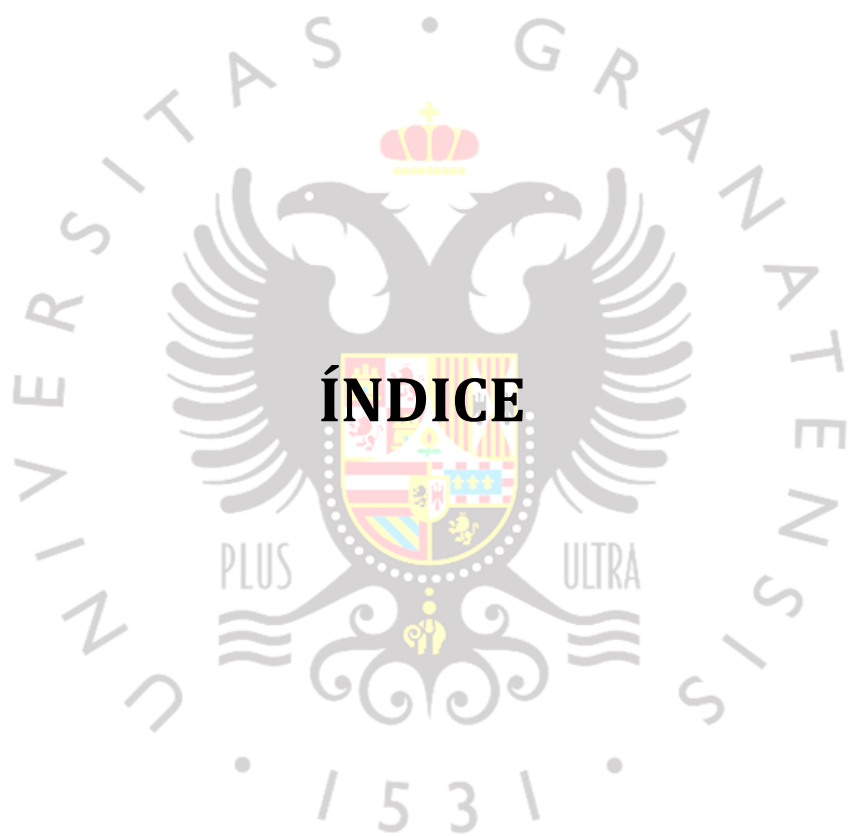
and the other with probiotics. The antibacterial activity of this biomaterial against *Pseudomonas aeruginosa* was higher than that of its cellulose, cellulose-silver and cellulose-probiotic counterparts, thus indicating a synergy between the two antibacterial components. The results of this chapter were published in the journal *Molecules* 2021, 26, 2848.

Chapter 4 presents other interesting example of LMs formed by integrating probiotics (*L. fermentum* or *L. gasseri*) into the bacterial cellulose matrix. This protocol is based on co-culture of the probiotic and the cellulose-producing bacterium *A. xylinum* under conditions initially favourable for *A. xylinum* to obtain the cellulose matrix, and subsequently switched to optimal culture conditions for growth of the probiotic. This induces exponential growth of the probiotic, which completely invades the cellulose membrane, displacing the cellulose-producing bacteria. Importantly, this protocol avoids the costly and time-consuming purification treatment commonly required to remove the cellulose-producing bacteria. This type of biomaterial showed antibacterial activity against *Staphylococcus aureus* and *Pseudomonas aeruginosa* and, more importantly, against multidrug resistant *S. aureus* and *P. aeruginosa* isolated from urine samples of real patients. Noticeably, all antibacterial assays were carried out in optimal media and culture conditions for the pathogenic bacteria, thus highlighting the great potential of this new type of biomaterial as an antibacterial agent. This biomaterial has been protected (PCT/EP2021 068166) and published in *Acta Biomaterialia* 2021, 124, 244.

The results described in **chapter 5** demonstrate the high level of performance that can be achieved upon the optimal integration of living entities into bacterial cellulose. We carried out a full dynamic study of the mechanical (rheological) properties of the biomaterial obtained after integrating the probiotic *L. fermentum* into bacterial cellulose and observed how proliferation of the probiotic in the cellulose network induces very significant changes in the mechanical properties of the biomaterial. In

particular, we observed how the viscoelasticity of this biomaterial can be tuned by bacterial proliferation. Thus, at low probiotic density, the biomaterial consists of a gel with a lower viscoelasticity than the matrix, while massive proliferation of the probiotic in the cellulose matrix causes the development of mechanical properties typical of a solid. This transformation from gel to solid with the “simple” passage of culture time (i.e., proliferation) has not been observed in any other living material and opens up the possibility that such biomaterials can be used for *in vivo* 3D printing in different biomedical applications.

The **chapter 6** starts with the synthesis and structural characterisation of the bacterial cellulose produced by *Acetobacter xylinum*, both with the bacteria incorporated into the cellulose structure and after purification, once bacteria were removed. We have also explored the impact of culture conditions and drying method on the bacterial cellulose structure. This study formed the cornerstone for tackling the challenge of aligning cellulose fibres with the aim of obtaining bacterial cellulose with improved mechanical properties compared to the native form. In this regard, we have developed a novel *in situ* method for obtaining cellulose with a high degree of fibre alignment using modified “magnetic” *A. xylinum*. Culture of these bacteria in the presence of magnetic fields results in the formation of a thin cellulose sheet. A preliminary structural characterization by AFM, SAXS and WAXS suggests the appearance of anisotropy and some degree of preferential orientation of the cellulose fibres.



ÍNDICE

ABBREVIATIONS AND DEFINITIONS	17
CHAPTER 1. INTRODUCTION	21
1. Biomaterials: materials for medicine	23
1.1. Collagen	26
1.2. Cellulose	30
2. Living Materials (LMs): at the frontier of synthetic biology and materials science	40
3. Bacteria: a micro-world of possibilities	48
3.1. Good (beneficial) versus bad (harmful) bacteria	50
3.2. Probiotics as cell factories and their applications	53
3.3. The antibiotic-resistance crisis. Probiotics, an alternative to antibiotics?	58
4. Objectives / Objetivos	66
5. References	68
CHAPTER 2. COLLAGEN-PROBIOTIC MATRIX. FOCUSING IN BACTERIAL VAGINOSIS (BV) TREATMENT	79
1. Introduction. Bacterial vaginosis	81
2. Results and discussion	85
3. Conclusions	102
4. Materials and methods	103
5. References	110
CHAPTER 3. TWO-SIDED ANTIBACTERIAL CELLULOSE COMBINING PROBIOTICS AND SILVER NANOPARTICLES	113
1. Introduction	115
2. Results and discussion	117
3. Conclusions	123
4. Materials and methods	124
5. References	128

CHAPTER 4. PROBIOTIC CELLULOSE: AN INNOVATIVE BIOMATERIAL FOR THE POST-ANTIBIOTIC ERA	131
1. Introduction. Skin infections	133
2. Results and discussion	136
3. Conclusions	150
4. Materials and methods	151
5. References	158
CHAPTER 5. HYBRID LIVING MATERIALS WITH TUNABLE VISCOELASTICITY THROUGH BACTERIAL PROLIFERATION	161
1. Introduction	163
2. Results and discussion	164
3. Conclusions	172
4. Materials and methods	177
5. References	181
CHAPTER 6. TOWARD ORDERED NANOCELLULOSE	183
1. Introduction	185
2. Results and discussion	188
3. Conclusions	201
4. Materials and methods	202
5. References	207
CONCLUSIONS/CONCLUSIONES	211

ABBREVIATIONS

2D	Two-dimensional
3D	Three-dimensional
AMR	Antimicrobial resistance
BC	Bacterial cellulose
BCS	Bacterial cellulose synthase
<i>bcs</i> ABCD	Bacterial cellulose synthesis ABCD operon
BSA	Bovine serum albumin
BV	Bacterial Vaginosis
CECT	<i>Colección Española de Cultivos Tipo</i>
CFU	Colony forming unit
CIC	<i>Centro de Investigación científica</i> (Centre for Scientific Instrumentation)
CNC	Cellulose nanocrystal
CNF	Cellulose nanofibers
CNM	Cellulose nanomaterial
col	Collagen
DNA	Desoxyribonucleic acid
ECDC	European Centre for Disease Prevention and Control
EFSA	European Food and Safety Authority
EIC	European Innovation Council
ELM	Engineered Living Material
EPS	Exopolysaccharide
ESKAPE	<i>Enterococcus faecium, Staphylococcus aureus, Klebsiella pneumoniae, Acinetobacter baumannii, Pseudomonas aeruginosa, and Enterobacteriaceae, which includes Escherichia coli</i>
ESRF	European Synchrotron Research Facility
FAO	Food and Agricultural Organizations of the United Nations
FD	Freeze-drying
FDA	Food and Drug Administration

GRAS	Generally Recognized As Safe
HIV	Human immunodeficiency virus
HLM	Hybrid Living Material
HS	Hestrin-Schramm (culture medium)
HSV	Herpes simplex virus
LAB	Lactic acid bacteria
LM	Living Material
LVR	Linear viscoelastic region
MDR	Multidrug resistant
MIC	Minimum Inhibitory Concentration
MRS	de Man, Rogosa and Sharpe (culture medium)
NLVR	Non-linear viscoelastic region
NP	Nanoparticle
OD	Optical density (A_{600nm})
PBS	Phosphate buffered saline solution
PC	Probiotic cellulose
PI	Propidium iodide
POM	Polyoxometalate
ROS	Reactive Oxygen Species
RT	Room temperature
rRNA	Ribosomal ribonucleic acid
scCO ₂	Supercritical CO ₂
SCFA	Short chain fatty acid
STI	Sexually transmitted infection
TNT	Trinitrotoluene
TSA	Trypticase Soy Agar (culture medium)
UD	Unidirectional
UDP-glucose	Uridine-5'-diphosphate- α -D-glucose
UGR	<i>Universidad de Granada</i> (University of Granada)
UTP	Uridine-triphosphate
WHO	World Health Organization

E	Compression modulus
ε	Strain
F_N	Normal Force
G'	Storage modulus
G''	Loss modulus
h	Gap separation
η	Viscosity
σ	Stress

TECHNIQUES

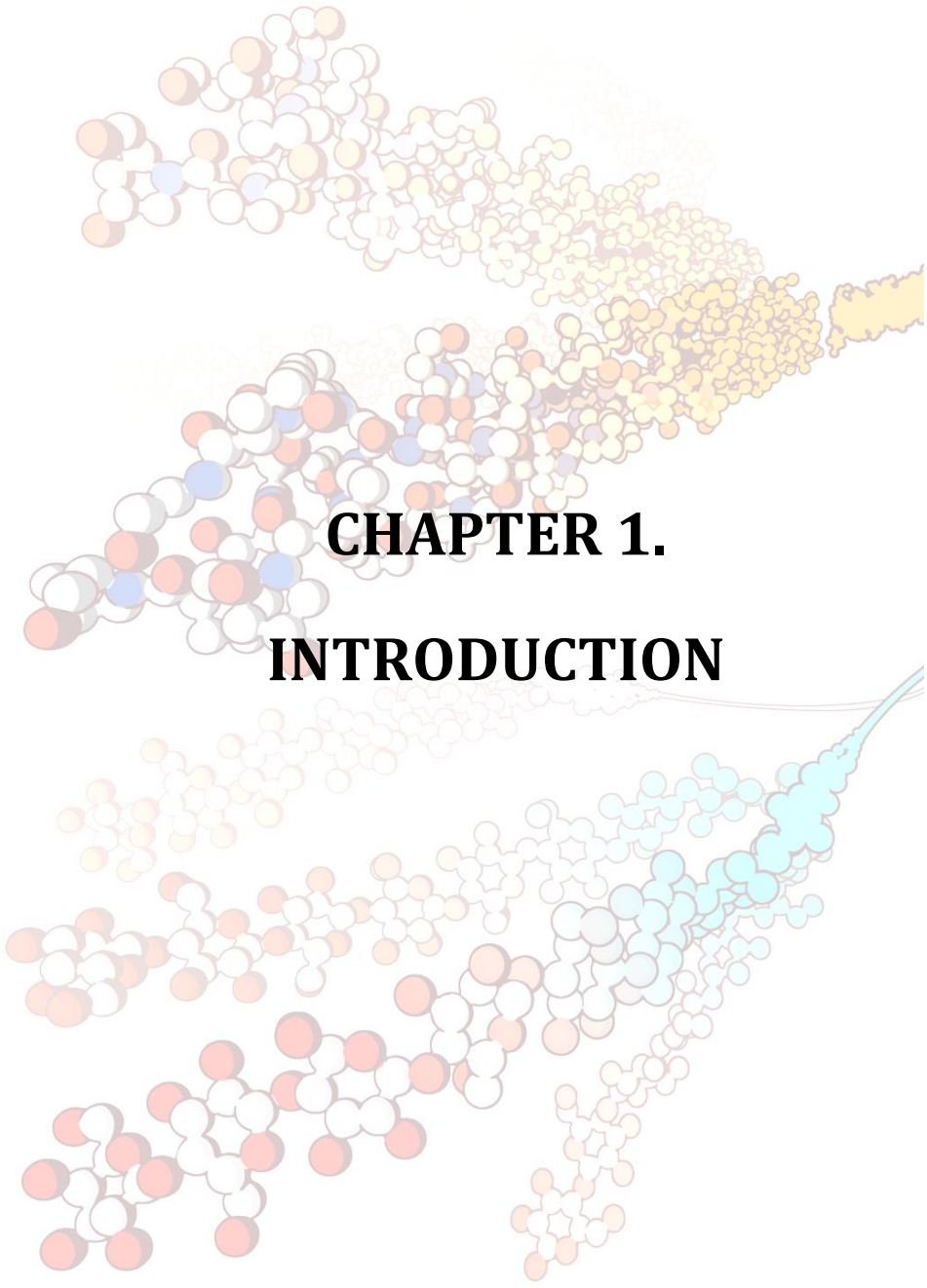
CLSM	Confocal laser scanning microscopy
FESEM	Field-emission scanning electron microscopy
FTIR	Fourier transform infrared spectroscopy
HAADF	High-angle annular dark-field
HR	High resolution
SAXS	Small-angle X-ray scattering
STEM	Scanning-transmission electron microscopy
TEM	Transmission electron microscopy
TGA	Thermogravimetric analysis
UV-vis	Ultraviolet-visible spectroscopy
WAXS	Wide-angle X-ray scattering
WAXTS	Wide-angle X-ray total scattering
XRD	X-ray diffraction

BACTERIA

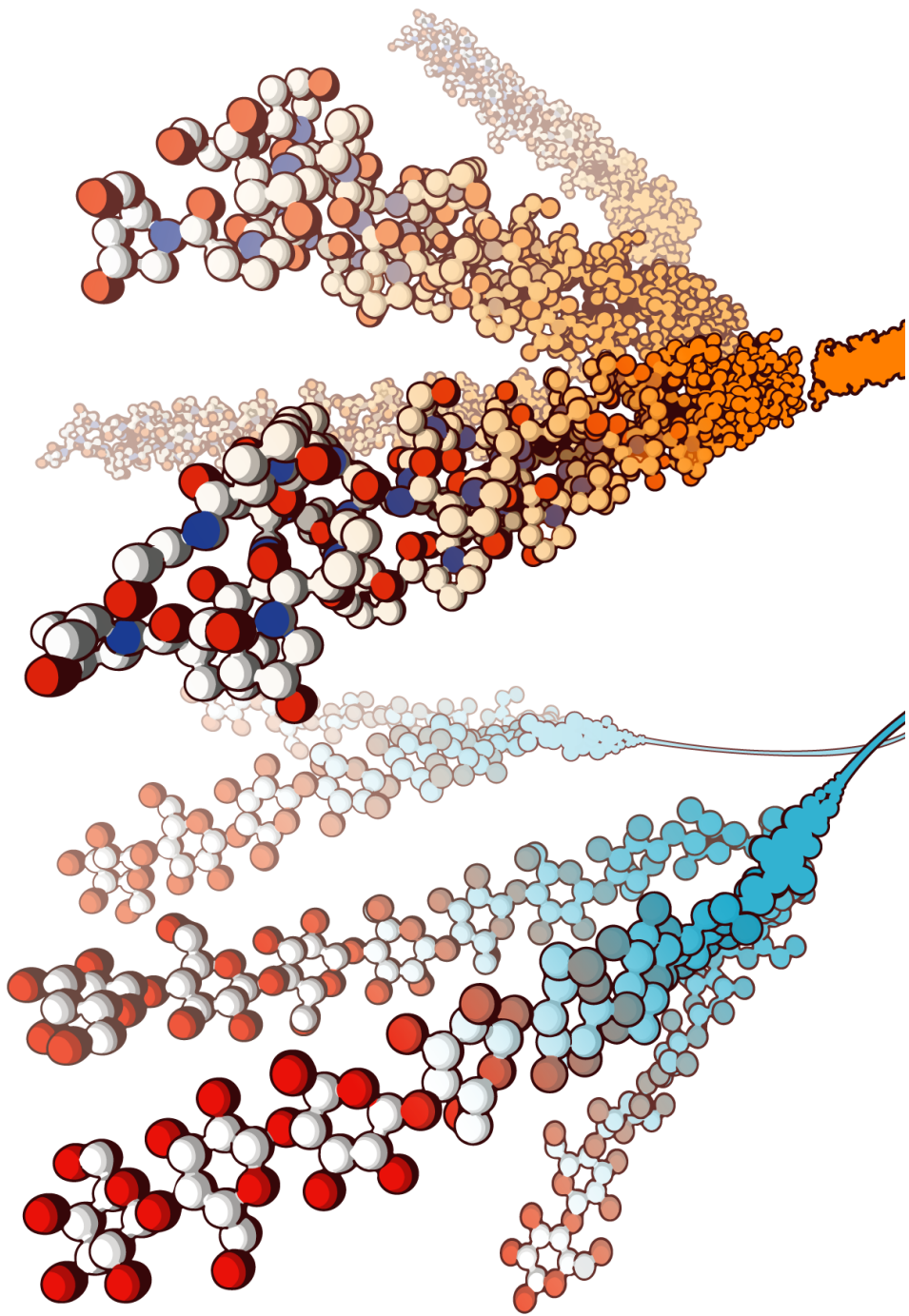
<i>Ax // Gx</i>	<i>Acetobacter xylinum // Gluconacetobacter xylinus</i>
<i>La</i>	<i>Lactobacillus acidophilus</i>
<i>Lf</i>	<i>Lactobacillus fermentum</i>
<i>Lg</i>	<i>Lactobacillus gasseri</i>
<i>MRSA</i>	Methicillin-resistant <i>Staphylococcus aureus</i>
<i>PA</i>	<i>Pseudomonas aeruginosa</i>
<i>SA</i>	<i>Staphylococcus aureus</i>

DEFINITIONS

Biomaterial	A material designed to take a form which can direct, through interaction with living systems, the course of any therapeutic or diagnostic procedure.
Microbiome	All the collective genome of our microbial inhabitants
Probiotic	Live microorganisms (bacteria or yeasts) which, when administrated in appropriate doses, confer health benefit to the host
Engineered Living material	Bioinspired materials composed, either entirely or partly, of living cells. They self-assemble via bottom-up process.
Hybrid Living Material	Bioinspired materials composed partly of living cells. They are built via top-down process.
Pathogen	Microorganisms that cause sickness.
Multidrug-resistant bacteria	Bacteria resistant to more than three antibiotic classes.



CHAPTER 1.
INTRODUCTION



1. Biomaterials: materials for medicine

The term “**biomaterial**” as we recognize it nowadays did not exist 70 years ago¹. Prior to that time, most implants rarely succeeded because of a deficient knowledge of sterilization and **biocompatibility** -defined as the ability of a material to carry out its required function without undesired effects-. In 1920s, metals were widely used (e.g., gold, silver, platinum, iron, steel, copper, nickel), being some of them well tolerated, but unsuitable mechanically. Afterwards, some types of alloys, ceramics and titanium were used with success in odontology and implants, and some years later the progress in synthetic polymers lead to the development of nylon (as suture), polyethylene and Teflon. Probably, the first study of biocompatibility in humans was done in case of cataracts, when natural lenses were replaced by intraocular ones. After World War II, in 1950, Sir Harold Ridley noted that poly(methyl methacrylate) had no undesirable immune responses². Henceforth, the development of materials designed for medical applications started, and it led to the manufacturing of functional materials such as silicones, hydrogels, hydroxyapatite, or bioglass. The contemporary era has adopted new materials in addition to metals, polymers, and ceramics, such as **hybrids** or **composites**³, but also some ideas are now strongly established in this field, such as phase separation, self-assembly or surface modification, and important progresses in protein adsorption, controlled release, tissue engineering, regenerative materials, and nanotechnology, are being fulfilled.

The biomaterial field can include virtually all the above materials. However, there is a controversy related to the meaning of “biomaterial”: the prefix “bio-” could refer to “something that comes from life” or “something employed to the benefit of life”³. Thus, a biomaterial was defined in 1999 as ‘*a material intended to interface with biological systems to evaluate, treat, augment or replace any tissue, organ or function of the body*’⁴, but others, as Larousse dictionary, took the opposite view and defines it as ‘*a solid material*

*which occurs in and is made by living organisms, such as chitin, fibrin or bone*⁵. The definition that managed a consensus in 2018, which entails their use only in healthcare (making it equivalent to 'biomedical material'), is as follows⁴:

"Biomaterial. *A material designed to take a form which can direct, through interaction with living systems, the course of any therapeutic or diagnostic procedure."*

In this sense, the potential biomedical applications of them include diagnosis, biosensing, antimicrobial efficacy, anticancer therapeutics, drug delivery, bioprinting, bioimaging, tissue engineering and regenerative medicine².

Instead of inorganic materials, there is an increasing trend to use bioinspired manufactured materials and molecules extracted from natural sources to improve the biocompatibility and biodegradability of them². At the same time, these biomaterials have remarkable mechanical properties and possess innate functions that increase their bioactivity and therapeutic potential⁶. Natural polymers include lipids, proteins, carbohydrates, proteoglycans, and nucleic acids (Table 1). They are used to fulfil a physical function, as a scaffold, carrier, or substrate for chemical modifications. Furthermore, these starting polymers possess intrinsic biological activity which provides bioactivity to the final material, and the combination of them or with synthetic materials also leads to the construction of advanced smart materials with improved chemical, mechanical, stimuli-responsiveness, immunogenicity and biocompatibility features².

Table 1. Natural polymers obtained from plants, animals and microorganisms used as biomaterials.

Lipids	Proteins	Carbohydrates	Proteoglycans	Nucleic acids
Fatty acids	Collagen	Monosaccharides	Aggrecan	DNA
Cholesterol	Gelatin	Oligosaccharides	Versican	RNA
Steroids	Silk	Cyclodextrin	Neurocan	Oligonucleotides
Liposomes	Elastin		Lumican	Nucleobases
Micelles	Keratin	Polysaccharides:		
	Titin	Glycosaminoglycan		
	Fibrin	Cellulose		
	Mucin	Methylcellulose		
	Amyloids	Amylose		
		Chitin		
		Starch		
		Dextran		
		Agarose		
		Alginate		

Living organisms synthesize high molecular weight biopolymers by enzymes that combine building blocks such as sugars, amino acids or hydroxy fatty acids. The following sections are focused in the most abundant mammalian polymer, the **collagen**, and the most abundant polymer in Earth, the **cellulose**. Natural abundances and unique properties make these polymers a widespread option for the development of composites and for application in almost every field. Indeed, the number of publications related with these polymers are in constant growth (Figure 1).

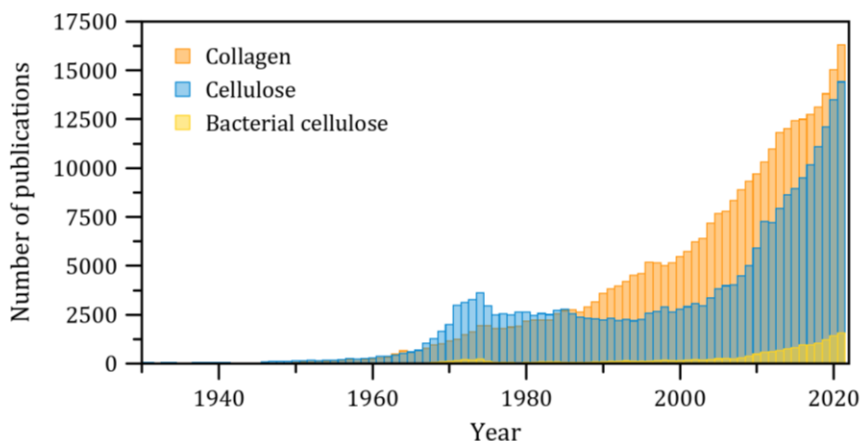


Figure 1. Number of total publications per year registered in the Web of Science using as topic “collagen”, “cellulose” and “bacterial cellulose”.

1.1. Collagen

Collagen is the most abundant protein in mammals, being the main structural protein in the extracellular matrix of connective tissues (e.g., cartilage, bone, tendons, skin...) ⁷. This protein is the responsible for the elastic and viscoelastic properties of the tissues, and their interactions with other molecules determines the mechanical properties and functionalities of tissues such as skin, tendon, cornea, blood vessel, cartilage and bone ⁷.

To date, 29 genetically different collagen types (fibrillars and non-fibrillars) have been identified, despite the localization and function of many of them are not known ⁸. Undoubtedly, collagen types I, II and III composed around 80-90% of the total collagen, being the **type I collagen** the most abundant. It consists of a triple-helix of two identical α_1 and one α_2 peptide chains, and each one is formed by the amino acid repeating sequence [Gly-X-Y]_n, where X and Y are proline and 4-hydroxyproline, respectively ⁹ (Figure 2).

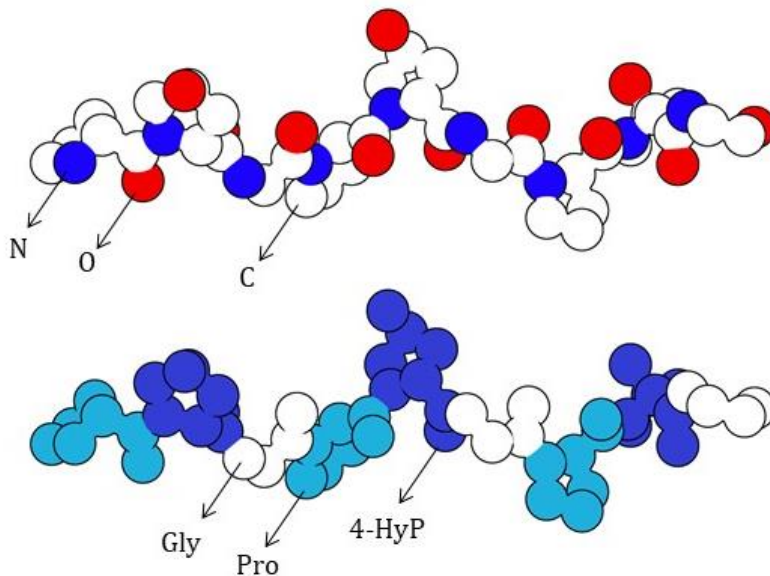


Figure 2. A small portion of a collagen type I molecule, coloured by atom (up) and by amino acid (down). N, nitrogen; O, Oxygen; C, Carbon; Gly, Glycine; Pro, Proline; 4-HyP, 4-Hydroxyproline. Image designed with “The Protein Imager”¹⁰ (<https://3dproteinimaging.com/protein-imager/>) using the Protein Data Bank (PDB) file *1cag*.

The three-peptide chains are synthesized inside the cell (mainly by fibroblasts) and assembled into a triple-helical structure containing large N- and C-terminal domains, the so-called pro-collagen. Pro-collagen is then secreted into the extracellular space, where the non-helical extensions are cleaved by specific proteinases, resulting in a collagen molecule that spontaneously self-assembles into microfibrils¹¹. These microfibrils self-assemble into fibrils which successively generate collagen fibers, showing a characteristic pattern of 67 nm where the overlapping regions alternates with gap regions (Figure 3). This high-density matrix of fibers has several microns in length, with diameters between 50 – 400 nm.

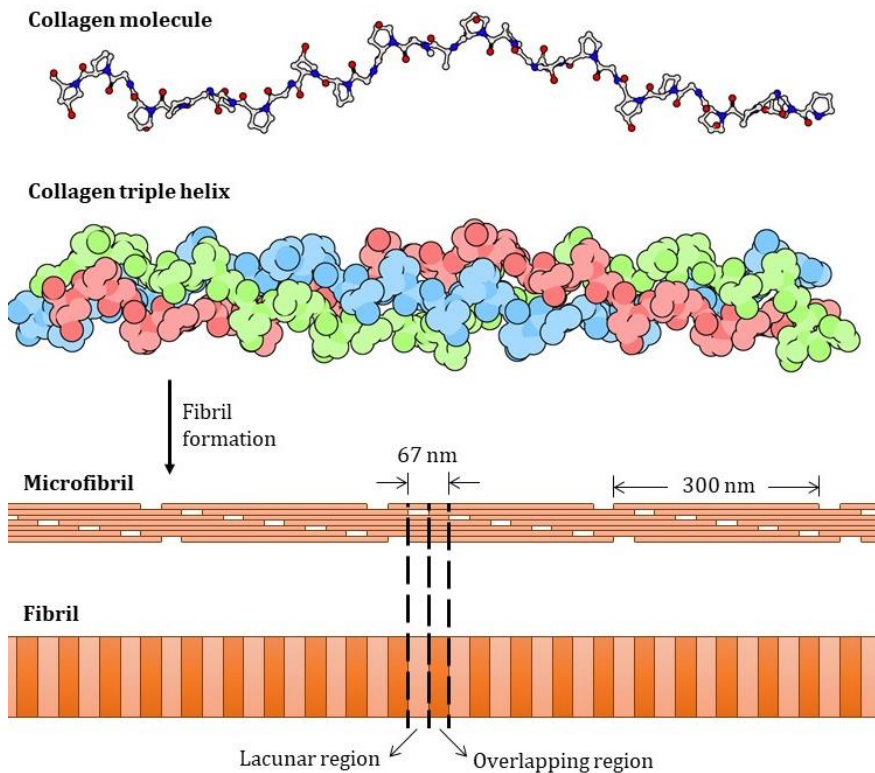


Figure 3. Illustration of an individual collagen type I molecule (coloured by atom), collagen triple helix (coloured by chain), collagen microfibril and collagen fibril. Images of collagen molecule and triple helix were designed with “The Protein Imager”¹⁰ (<https://3dproteinimaging.com/protein-imager/>) using the PDB file *1cag*.

Since this molecule has a particular structuration and is an endogenous constituent of the body, it entails inherent properties such as good biocompatibility and absorbability, hydrophilicity, an excellent cell-binding capacity, and it is involved in cell recognition pathways¹². Cells can attach to collagen by direct adhesion mechanisms, which consist in cell binding to specific protein domains through the expression of surface receptors, which can be also collagen-type specific¹³. In this regard, collagen entails a great potential as a tissue adhesive, either alone or in combination with other compounds^{14,15}.

For all the above reasons, collagen scaffolds are largely used in biomedicine. In addition to all the properties mentioned above, the length of the molecule, the type, the degree of crosslinking, and further processing result in the obtention of 3D scaffolds of various conformations. In this regard, tissue grafts, self-assembled hydrogels and fibers, freeze-dried sponges, collagen films and tubes, and template-produced materials are the most typical scaffolds used for optimal *ex vivo* cell growth, for drug or biological delivery, for cellular differentiation and encapsulation, and, specially, in **tissue engineering** and **tissue regeneration**^{7,16}. In these last fields, collagen plays a key role: the functionalization approaches allow the treatment of damaged tissues such as bone, cornea, cartilage, tendon, lung, intestine, kidney, muscle and even for neural repair or for wound healing^{12,17}. Collagen composites can be obtained when the protein is combined with other molecules such as antibiotics, vitamins, other biopolymers, and nanoparticles in order to enhance its desirable functions¹⁸⁻²⁰. The combination of collagen with nanoparticles and antibiotics is one of the employed strategies to address bacterial infections. Extensive research has evaluated the antimicrobial activity of collagen combined with antibiotics (such as gentamicin and rifampicin)²¹ or nanoparticles (e.g., silver nanoparticles)²² against pathogenic strains, as *Pseudomonas aeruginosa* and *Staphylococcus aureus*. These composites have antibacterial activity and *in vivo* experiments with rats demonstrated higher wound-healing rate over the application of only collagen. Other approach to enhance tissue regeneration speed and quality is the use of collagen as a cellular scaffold, for example osteoblasts in the case of bone regeneration¹⁸. In addition, the development of human models²³ and bioinks⁹ are nowadays relevant lines where collagen can play a key role.

Nevertheless, the use of collagen is not only limited to the biomedical field, but it is also exploited in other industrial fields as beverage and food supplementation, additives, packaging, cosmetics, and in leather and

pharmaceutical industries²³⁻²⁵. Collagen can be found in these fields in its natural state or as a derivative product, such as hydrolysate, gelatin, telocollagen, atelocollagen, gels, and powder¹¹.

For all the above purposes, collagen is mainly extracted from biological tissues. It can be obtained from tendon, skin, intestine, cornea, and blood vessels of ovine, porcine, equine and bovine sources¹². Despite being the main natural source of collagen, other sources, like marine species (such as sponges, jellyfishes and fish offal), are under investigation because they may avoid immune responses and cross-species disease transmission²⁶. Other approaches like cell-produced collagen (e.g., harvesting collagen type I from fibroblast culture), recombinant collagen (e.g., use of genetically engineered microorganisms to produce human collagen) and synthetic collagens, are also under investigation, but their low yields are the main drawback for its industrial application^{7,8,27}.

1.2. Cellulose

Cellulose is the most abundant macromolecule on Earth, and it is synthesized mainly by plants, but also by tunicates, algae, and several types of bacteria²⁸. This water-insoluble polymer consists of a polysaccharide chain with cellobiose (i.e., $\beta(1-4)$ linked D-glucopyranoses) as the building block (Figure 4A). Inter- and intramolecular hydrogen bonds stabilize the linear configuration of the polymer and promote parallel stacking of multiple cellulose chains forming elementary fibrils (2-4 nm in diameter, also called nanofibrils) that further aggregate into microfibrils (5-50 nm in diameter and several microns in length)^{29,30} (Figure 4B-E). Hydrogen bonds and the presence of many hydroxyl groups also allows the incorporation of water molecules within the structure, resulting in a such high water-holding capacity in the wet state (Figure 4D).

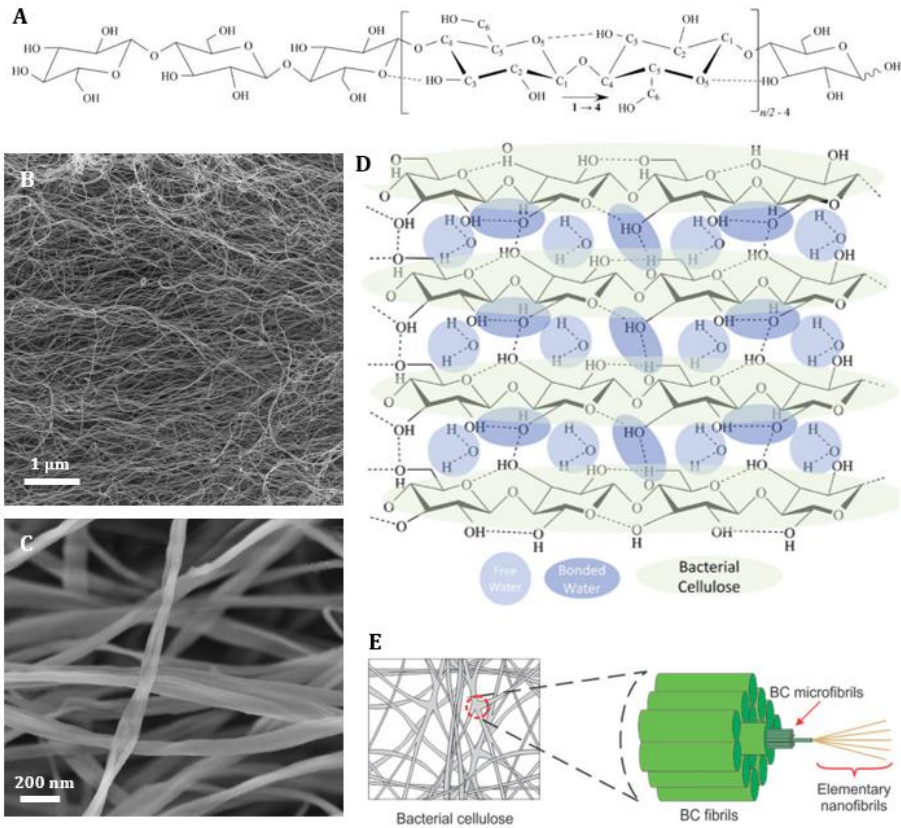


Figure 4. (A) Chemical composition of cellulose, where the cellobiose is the repeating unit. Image extracted from Zhong (2020)³¹. Scanning electron microscopy images showing the typical bacterial cellulose (BC) fiber arrangement (B) and the ribbon-like structure (C). (D) Molecular structure of hydrated BC. Image extracted from Portela *et al.* (2019)³⁷. (E) BC hierarchical structure. Image from Torres *et al.* (2019)³⁷.

These cellulose fibrils contain highly ordered (crystalline) regions alternating with disordered (amorphous) regions. Several polymorphs of crystalline cellulose (I, II, III, IV) can be found and have been extensively studied^{32,33}. Cellulose I (also referred to as ‘natural’ cellulose since it is naturally produced by many organisms) can be converted to the other polymorphs by chemical treatments (Figure 5A). The natural cellulose I also present two polymorphs, I α and I β , with triclinic and monoclinic crystalline

structure, respectively³⁴. Algae and bacteria synthesize cellulose I α , whereas plants mainly produce cellulose I β . As cellulose I α is metastable, an alkaline heat treatment can convert I α into I β . The conversion yield depends on the alkalinity and temperature but the complete conversion cannot be achieved.

Figure 5C-F shows the crystalline structure of I α and I β polymorphs. Although the crystalline structure and the unit cells (marked in dotted blue line for I α and solid red line for I β) are different, the variations in the cellulose chains are difficult to distinguish when the structure is viewed along the chain or fibril axis (c-axis). Three lattice planes with d-spacings of 0.39 nm, 0.53 nm, and 0.61 nm corresponds to planes (110)_{I α} , (010)_{I α} , and (100)_{I α} , or (200)_{I β} , (110)_{I β} , and (1-10)_{I β} , respectively. These planes produce three intense Bragg reflections when cellulose is studied by X-ray diffraction (Figure 5B). The only structural difference between I α and I β occur along the chain axis (or c-axis) direction (Figure 5C) Cellulose sheets are displaced (+c/4 in I α or alternating +c/4 and -c/4 in I β) along the (110)_{I α} or (200)_{I β} planes (also called “hydrogen-bonded” planes). This structural variation causes slight differences in peak positions (d-spacing) of the X-ray reflections (Figure 5B). Thus, identifying and distinguishing between the two polymorphs is not a simple task.

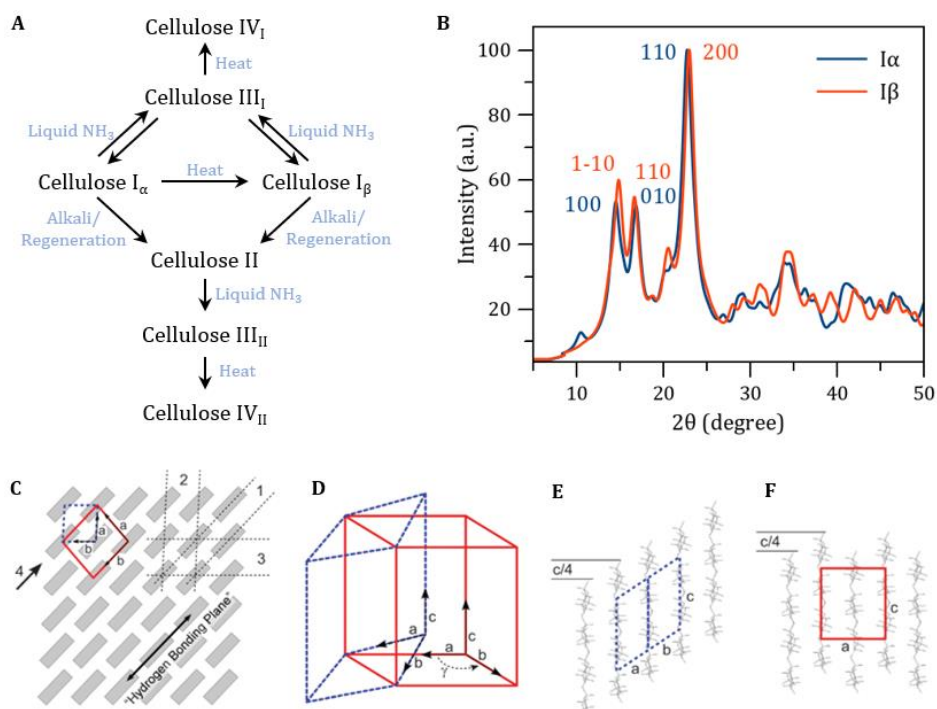


Figure 5. (A) Interconversions of cellulose polymorphs. (B) XRD patterns were calculated with Mercury software using the CIF files of I α (CCDC 1866391) and I β (CCDC 810597). (C-F) Representation of unit cells for cellulose I α (triclinic, dashed blue line) and I β (monoclinic, solid red line). (C) Projection along the chain direction with the I α (blue) and I β (red) unit cells superimposed on the cellulose I crystal lattice, showing the parallelogram shape of both unit cells when looking down the c-axis. In this orientation both unit cells have nearly identical molecular arrangements, sharing the three major lattice planes, labelled 1, 2, and 3, with the corresponding d-spacings of 0.39, 0.53, and 0.61. The corresponding lattice planes for 1, 2, and 3, are (110) $_t$, (010) $_t$, and (100) $_t$ for I α and (200) $_m$, (110) $_m$, and (1-10) $_m$ for I β . (D-F) View along the direction labelled 4 (i.e., [1-10] $_t$ for I α , and [010] $_m$ for I β), (D) relative configuration of I α with respect to I β unit cell, and the displacement of the hydrogen bonding sheets for (E) I α of +c/4, and for (F) I β alternating +c/4 and -c/4. Figure and caption extracted from Moon *et al.*³³

In particular, cellulose is produced by some bacteria (bacterial cellulose, BC, also called bacterial nanocellulose, BNC) as a fermentation product. Bacteria are prime cell factories that can effectively convert carbon and nitrogen sources into a large variety of intracellular and extracellular biopolymers. They can synthesize various classes of these biopolymers, such as polysaccharides (sugars or sugar acids connected by glycosidic linkages), polyamides (amino acids connected by peptide bonds), polyesters (hydroxy fatty acids linked by ester bonds) and polyphosphates (inorganic phosphates linked by anhydride bonds). Some strains of acetic acid bacteria synthesize a cellulose-based biofilm in the liquid-air interface with the aim of maintaining the cells oxygenated, supporting the diffusion of nutrients and by-products, avoiding drying and serving as a defensive barrier against damaging agents (such as other microorganisms or radiation)³⁴ (Figure 6). BC, as plant cellulose, is biodegradable, but the main advantage over vegetal cellulose is its high purity. BC is free of hemicellulose, pectin and lignin, and thus is a non-toxic and biocompatible material. Other properties derived from the thickness of the fibres, which are around 60 nm (one hundred times thinner than those of plants), are its higher surface area and water holding capacity. The mechanical properties of BC arise from the fiber arrangement in the three-dimensional network, which confers to the matrix a high elasticity, flexibility and mechanical strength. In addition, cellulose is transparent and chemically stable, even when immersed in extremely acidic or basic solutions at high temperatures. These unique properties led to the increase of its uses in biomedicine -specially in wound dressing and tissue regeneration applications^{29,34}- and other fields, such as electronics and sensors^{35,36}.

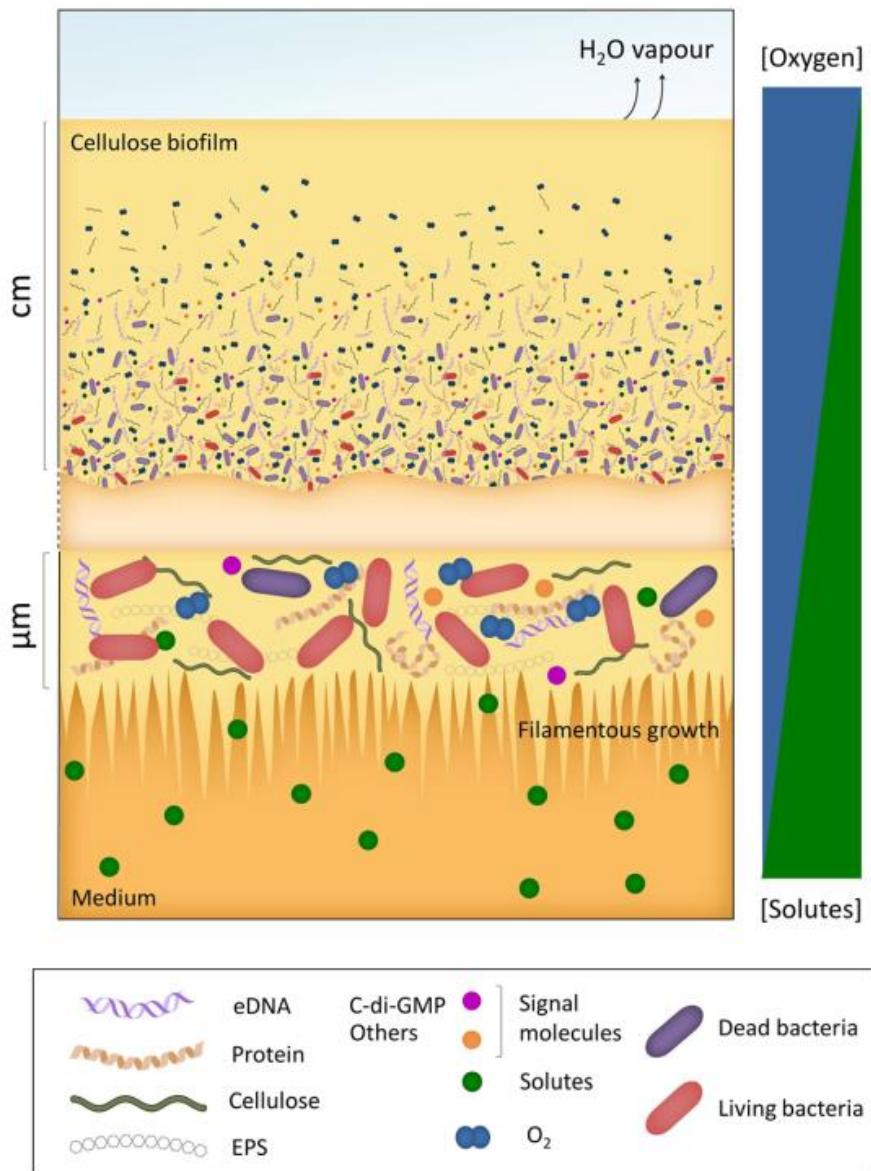


Figure 6. The structure of biofilm in acetic acid bacteria. Upper side centimetre (cm): BC biofilm formation occurs at the down surface due to solutes availability and oxygen diffusion across the matrix. In the upper surface, cell growth is limited due to evaporation and low solutes availability. Lower side micron (μm): BC biofilm formation in the early phase, with oxygen and solute availability. Image and caption extracted from Gullo *et al.* (2018)³⁷.

Many strains of bacteria are capable of produce cellulose, such as *Sarcina*, *Asaia*, *Agrobacterium*, *Rhizobium*, *Pseudomonas*, *Enterobacter*, *Salmonella*, *Alcaligenes* and *Acetobacter* genera³⁸⁻⁴⁰. *Acetobacter xylinum* (also known as *Komagataeibacter* or *Gluconacetobacter*) is a non-pathogenic, Gram negative, aerobic and rod-shaped acetic acid bacterium, and it was the first cellulose-producing bacteria discovered, identified by Brown in 1886⁴¹. Due to the high efficiency in producing cellulose (a single bacterium is able to polymerize 200000 glucoses in one second³¹), and the ability to produce cellulose from a wide range of carbon/nitrogen sources^{30,37}, *A. xylinum* has been established as a model bacterium for study the BC synthesis and as an useful tool in numerous industrial fields. The linear polymerization of BC is a process that involves several proteins and enzymes encoded by singular genes and the BC synthesis operon (*bcsABCD*), identified in this strain for the first time³⁴. These proteins guide the intracellular biosynthesis of nanocellulose, which starts with the conversion of glucose to glucose-6-phosphate; followed by the isomerization of glucose-6-phosphate to glucose-1-phosphate; then a uridine-triphosphate (UTP) is added to the molecule to produce uridine-5'-diphosphate- α -D-glucose (UDP-glucose); and finally, the cellulose synthase (BCS, EC 2.4.1.12) catalyse the transfer of UDP-glucose to the growing homopolymer (Figure 7). After, the single chains are secreted through the pores located in the bacterial cell wall.

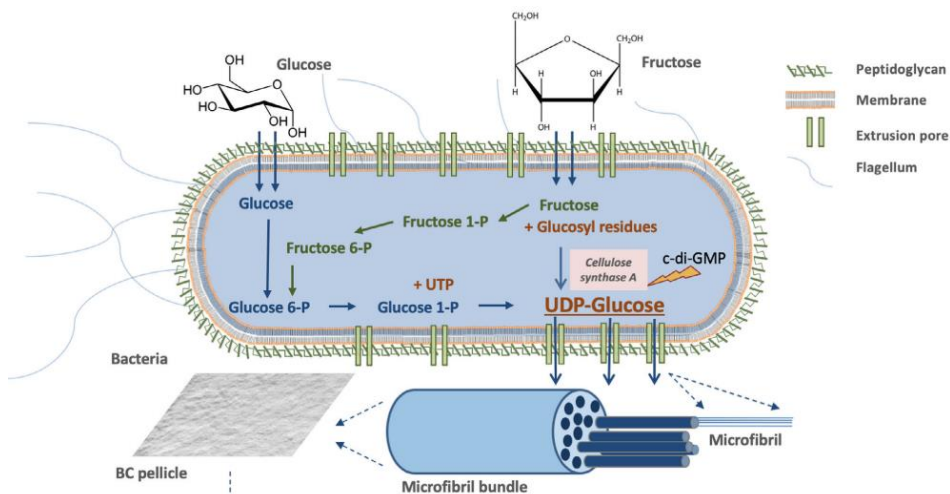


Figure 7. Scheme depicting the multistep process of BC synthesis. Image adapted from Portela *et al.* (2019)³⁴.

Microorganisms and culture conditions are the basis of BC production, and have a great influence on cellulose yield and properties. The network formation can be affected by the temperature, pH, dissolved oxygen, stirring speed, culture media, cultivation time, and additives. One of the most critical parameters is cultivation in static or dynamic (agitated conditions), which result in significantly different BC structures. Static condition yields denser networks of higher crystallinity⁴² whereas dynamic ones are faster, due to the better contact with the provided oxygen. Moreover, agitated cultures result in a lowering of $I\alpha$ percentage compared to static fermentations.

Thanks to all these properties, BC is in the market for different purposes and new applications are being discovered for the short-term future. Indeed, there are several trademarks based on BC, such as CELLULON™ Cellulose Liquid, Sun Artist®, Fibnano, AxCel®, Nanoderm™, Bionext®, Membracell®, Suprasorb® X, Biofill®, Gengiflex®, Xcell®, Nanollose®, etc. BC is widely applied in the following industries^{31,43}:

- Food industry. BC is considered as Generally Recognized As Safe (GRAS) food additives by the Food and Drug Administration (FDA).

The first industrial manufacturing of BC was first adopted in Philippines in 1970s, the so-called *nata de coco*. The static culture results in the obtention of a BC with a gelatin-like texture, high fiber content, and almost cholesterol-free. This pellicle is broadly used for desserts or food additives to change texture and flavours. On the other hand, the agitated fermentation has been used as a suspending agent in food, or even for the preparation of artificial meat. Moreover, dry films are exploited in food packaging, and dry powder is used with other materials as carrageenan, carboxymethylcellulose, xanthan gum, etc.

- Textile industry. Considering that BC is biodegradable and easily produced and purified, this material is a potential source to obtain plant-free rayon and fabric, avoiding petroleum-based fibers and the pollution generated by the processing of wood and cotton. Actually, Nanollose has developed a BC-based textile using coconut water, the Nullarbor™ fiber. This company defend the use of BC arguing that the yield of BC is higher than those of plants both in time and land; needs low energy and water; and they use industrial wastes to produce it.
- Personal care. Due to the high surface area of BC, it is possible to impregnate the pellicle with different nutrients or active molecules that can be released over the time. This permits its exploitation as a face mask, and not only for personal care, but also for treating skin diseases or burns.
- Biomedical applications. Within this field, BC is widely employed for wound dressing, artificial skin, drug delivery, scaffolds for tissue regeneration, biosensors, etc.

However, BC itself has no activity against bacterial infection, which is a frequent issue in some wounds, especially in chronic wounds. In order to overcome this limitation, BC composites have been developed. Thus, BC can be combined with organic (such as polymers, active agents and

nanomaterials) or inorganic materials (metals, metal oxides and solid particles) by different routes^{29,34,35,44–47}.

Several procedures have been explored in order to obtain new BC composites with novel advantages and properties while maintaining the original 3D network. According to the synthesis, the composites have an *in situ* or *ex situ* approach, i.e., modifications during the biosynthesis or modifications of BC hydrogel (Figure 8A)³⁵. On the one hand, an *in situ* modification could be the addition of metallic nanoparticles to the culture media⁴⁸ or the patterning by lithography⁴⁹, and on the other hand, an *ex situ* modification of BC can be achieved by a technique as simple as the impregnation with polymers or active compounds^{43,47}, or by microwave-assisted routes^{50,51}.

The alternative route to develop new BC-based materials is through the destruction of the natural network. This approach implies the matrix degradation, the use of crosslinkers, or the obtention of BC nanocrystals or whiskers (Figure 8B)⁵². In this sense, the use of cellulose nanocrystals suspensions is a widely used route to obtain, for example, novel composites that incorporate a Fe-Cu alloy to improve the antibacterial activity and Pb²⁺ elimination from water⁵³.

Chemical functionalization by conventional procedures becomes difficult in BC due to its poor solubility in water or organic solvents. However, some BC derivatives have been produced through the previous incorporation of reactive chemical groups, such as -N₃ for click chemistry or -NH₂ for condensation and esterification⁵⁴.

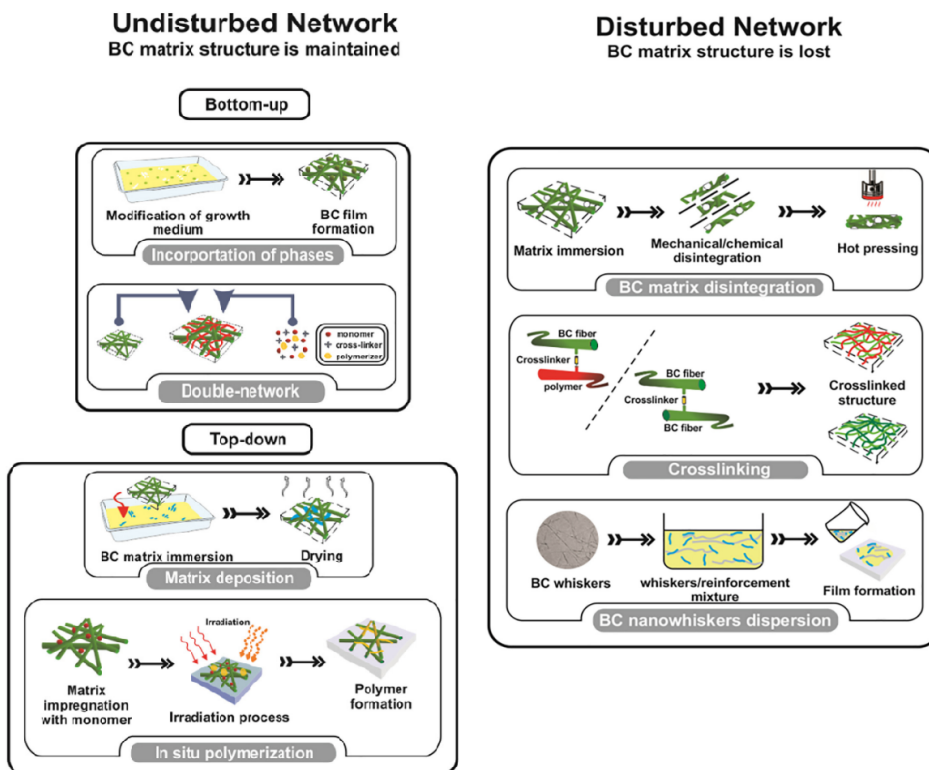


Figure 8. Approaches to modify the characteristics of BC by maintaining (A) or modifying (B) the natural three-dimensional network. Image adapted from Torres *et al.* (2019)⁵².

2. Living Materials (LMs). At the frontier of synthetic biology and materials science

Living organisms have the ability to build a multitude of complex, hierarchical, multifunctional ‘living’ materials, being bone, wood, and organs, among the most representative examples. Cells synthesize small molecules that act as building blocks of more complex macromolecules (e.g., proteins from aminoacids), that further self-assemble and grow to form such hierarchical materials with fascinating properties⁶³. When an external stimulus (or “input”) is applied, both cells and the materials can trigger a response in order to adapt to the new environment, resulting in a

modification of the material properties through changes in the composition or the arrangement. Such environmental stimuli arise from different origins: chemicals, pH, temperature, light irradiation, external forces, etc. Thus, living cells and materials can be viewed as natural sensors that can grow, self-regenerate and perform different responses depending on the environmental factors.

In the last years, synthetic replication of these natural living materials has been a matter of intense research to obtain engineered materials with higher level of performance. **Engineered Living Materials (ELMs)** are bioinspired materials composed, either entirely or partly, of living cells^{63,64}. Among them, biological ELMs are entirely composed of living cells and they self-assemble via a bottom-up process (e.g., cellulose produced by bacteria in culture)⁵⁵. ELMs partly composed of living cells are instead commonly referred to as hybrid living materials (HLMs) and are built with a top-down process resulting in the integration of the cells into polymers or scaffolds (e.g., 2D and 3D bioprinted hydrogels encapsulating bacteria). The European Union Commission has used these definitions in the recently launched EIC Pathfinder Challenge on “*Engineered Living Materials*”⁵⁶. The term ‘engineered’ is widely employed when the living entities are genetically modified cells⁵⁷. However, it is also used for other modifications directed to somehow modulate the functional performance of the material⁶⁶ (Figure 9). The combination of cells with nanoparticles to obtain novel properties is also an approach with great interest. For example, the surface functionalization of genetically engineered bacteria with magnetic nanoparticles allows the obtention of viable bioreporters that can be recovered with a magnet⁵⁸.

The living part, once included in the material, act as a responsive and multifunctional composite that modifies the material’s properties through environment-dependent mechanisms over its lifetime^{63,66}. Thus, when both components are present, cells and matrix, the viability and capabilities of the

living part and the scaffold properties must be addressed in order to establish the influence of the former on the latter, and vice versa. In general, living materials (ELM or HLM) are obtained when living cells are perfectly integrated in the matrix, generating new or enhanced features that cannot be obtained by the simple combination of the components. In this PhD thesis, we have prepared different class of living materials that according to the above definitions could be framed as biological ELMs or HLMs. However, we have used the general term Living Materials (LMs) to denote the materials here prepared to avoid any misleading.

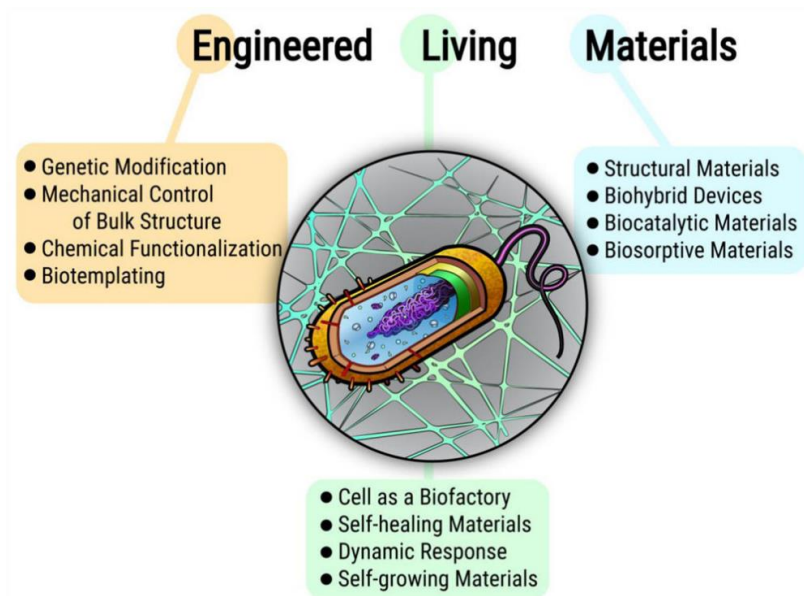


Figure 9. Properties of Engineered Living Materials. Figure extracted from Nguyen *et al.* (2019)⁵⁷.

As this is a fast-developing field, a taxonomy of ELMs and its emerging trends have recently begun to be established⁵⁹ (Figure 10). Thus, ELMs can be classified according to scale (from nano to macro); the approach (top-down or bottom-up); the type of living cells (wild-type or engineered bacteria, fungi, plant, unicellular algae...); the material properties; and the application field

(cell engineering, biosensors, construction, wound healing, controlled drug delivery, actuators, etc.⁶⁰⁻⁶²).

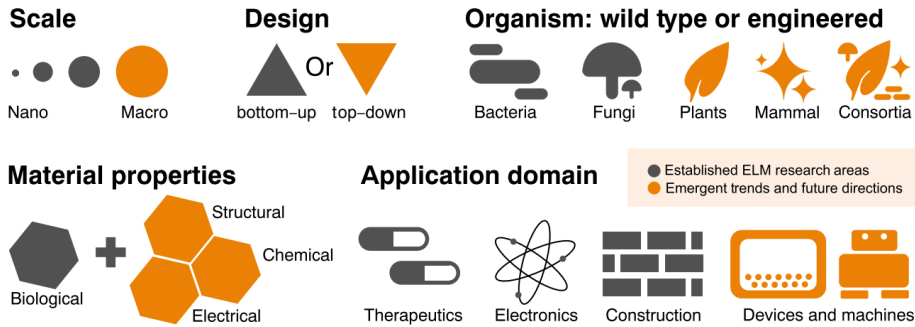


Figure 10. A taxonomy of ELMs research. The established ELMs research areas (in grey) include small-scale, control of bacteria and fungi, with applications in medicine, electronics and built field. New approaches (in orange), include macroscopic-scale with plants, mammalian cells, or consortia of cells. Some researchers are developing complex devices and machines. Image extracted and caption adapted from Srubar (2021)⁵⁹.

The most widely employed strategies to obtain novel or improved LMs are genetic engineering, cell coating, surface adhesion, microfluidics, electrospinning, and 3D bioprinting^{76,77}, and they can also be used in combination. Genetic engineering is usually applied to bacterial strains in order to modify extracellular matrix polymers or to produce a specific response to a specific stimulus; cell coating is a technology based on the application of a material on the cellular surface (as polymers or nanoparticles) to improve cell capabilities; the surface adhesion consist on the support of cells by natural or synthetic mechanisms to substrates; microfluidics comprise the control of fluid flow in the scale of microns in order to obtain nano- and microparticles, allowing the encapsulation of cells and organoids generation; the electrospinning permits the production of thin fibres to develop versatile and porous scaffolds; and finally, 3D bioprinting

enables the spatial arrangement of cells and matrix components for the development of complex structures, such as tissue models.

LMs are widely used for biomedical applications. In tissue regeneration, different cell types may constitute the living part while soft matrices compose the scaffolds. For instance, osteoblasts can be integrated in different scaffolds (such as a collagen/chitosan/hyaluronic acid hydrogels) combined with apatite to address bone tissue regeneration *in vivo*⁶³. The living cells control the synthesis of hydroxyapatite, thus producing the extracellular matrix main component for bone regeneration. Another case is the treatment of heart failure through the construction of a scaffold made of poly-3-amino-4-methoxybenzoic acid and grafted gel-foam, which supports cardiac fibroblasts⁶⁴. This polymer is a conductive matrix which enhances the propagation of the electrical impulse, and *in vivo* implantation resulted in an improved transmission of the impulse through the damaged tissue. On the other hand, in order to obtain actuators, certain cell types such as muscle cells (capable of make contractions) can be used to build soft-robots that can convert the contraction into an external output, such as light or colours⁶⁵.

Nowadays, bacteria are also widely used for bioremediation, and biomedical or biosensing applications, as long as some strains can be genetically engineered more easily. This is notably useful when the desirable response against a specific stimulus is the production of, for example, a metabolite of industrial interest, an enzyme or a chemically modified polymer, which may also affect a material property. Thus, the matrix can be combined with GRAS engineered bacteria such as probiotics (i.e., engineered *Lactococcus lactis* to induce human mesenchymal stem cells differentiation)⁶⁶, endospore-forming bacteria (i.e., *Bacillus subtilis*, to achieve longer lifetimes)⁶⁵, *Agrobacterium* and *Rhizobium*, or feasible model organisms, such as *Escherichia coli*. This latter bacterium has been broadly studied for several applications:

- To fight bacterial infections. *E. coli* has been engineered to improve the adhesion ability to dextran hydrogels and to produce a bacteriocin capable to kill multidrug resistant *S. aureus*⁶⁷.
- As biosensors. This model microorganism has been genetically modified to detect molecules like TNT, heavy metals or lactate⁶⁵.
- To secrete specific biofilm components. One of the main approaches to obtain the matrix components of HLMs is the use of bacteria as synthetic tools to obtain biofilms⁶². Bacteria secrete and assemble extracellular matrix components, in the form of polysaccharides, proteins, and DNA, during biofilm formation. *E. coli* can be engineered to synthesize curli nanofibers, which are amyloid proteins involved in cell adhesion, aggregation, and inflammatory responses⁶⁸. These fibers have been employed, for example, in mercury remediation and to build underwater adhesives^{62,69}. The main drawback of curli is its amyloid nature, which limits its application in biomedicine. To avoid this disadvantage, other authors engineered *E. coli* to produce Caf1, which is a non-amyloid protein naturally synthesized by *Yersinia pestis*⁶⁹. This protein is assembled by the bacterium through non-covalent interactions in highly thermal and chemical stable polymers, whose sequences can be modified to achieved new properties. This results in the obtention of heteropolymers with tunable properties, i.e., by incorporating osteopontin peptide domains to enhance bone formation by osteoblasts.
- For controlled drug release. Bacteria are microfabrics able to synthesize a wide range of products of industrial interest in large amounts. Although biofilm components are especially useful for material development, other synthetic pathways are investigated for the synthesis of nutritional compounds and antibiotics. For instance, an endotoxin-free *E. coli* has been opto-engineered and encapsulated in agarose hydrogels to produce deoxy-violacein (a drug with

antibacterial, antifungal and antitumoral properties) under blue light exposure⁶⁹.

Most of these living materials are based on strains of *E. coli* that can be genetically modified. However, the final approval of biomaterials to be used as medical devices in clinical applications requires the use of Generally Recognized as Safe (GRAS) species. In this sense, currently research is exploring the use of yeasts, specifically the model organism *Saccharomyces cerevisiae*, a GRAS eukaryotic microorganism genetically engineerable with a high ability to excrete recombinant proteins. Very recently, innovative ELM has been produced by co-culturing *Komagataeibacter rhaeticus* and *Saccharomyces cerevisiae*, taking inspiration from the symbiosis established in Kombucha tea⁷⁵. The former synthesizes BC naturally as a scaffold, and the second is genetically modified to produce recombinant proteins in response to external stimuli. Indeed, the symbiosis between them improved the synthesis of cellulose by the bacteria, allowing the formation of films with embedded yeasts. This approach can be applied to modify the BC physical properties (if the yeast is engineered to secrete cellulase) or to build biosensors (by inducing the synthesis of the green fluorescent protein in the presence of specific molecules).

As stated before, the viability and capabilities of the cells incorporated in HLMs are commonly assayed, but other characteristics of the hybrid, such as elasticity, viscosity, porosity, cytocompatibility, and lifetime, are also tested according to the applications. Among them, the **mechanical properties** are essential features that must be assayed for biomedical applications. Biomaterials in general, and living materials in particular, show different responses when a force is applied: elastic, plastic, and viscous deformations⁷⁰. Thus, this behaviour can be divided in elastic (e.g., typical of ceramics), elastoplastic (e.g., typical of metallic materials), or viscoelastic (e.g., typical of polymers). Moreover, the material can be classified in isotropic materials, such as glass, which exhibit uniform features in all directions; or in

anisotropic materials, such as wood, which display different responses according to the direction. The flow and deformation under diverse force systems is defined by the mechanical properties. In other words, they characterize the response of a material exposed to stresses and strains resulting from applied external forces. These mechanical properties also depend on the inherent structure and the environmental conditions (e.g., temperature). Thus, the importance of the mechanical properties lies in the fact that they define the biostability and the mechanical compatibility between the living materials and the target tissue, and the mechanical signals can even induce different physiological responses in cells⁷¹. Thus, biomaterials should have analogue mechanical properties with target tissues and support its mechanical stability during repair, in order to promote the healing. In this sense, there are important differences between tissues. For example, a scaffold designed for bone regeneration should have mechanical properties in close association with those of the surrounding bone⁷². Thus, the material used must be evaluated for its elastic modulus, tensile strength, compressive strength, flexural modulus, maximum strain, and fatigue. So, the materials used for scaffolds should match the range of cortical bone strengths (between 100 – 230 MPa); otherwise, it should be fixed with plates or wires to avoid failure of the material. On the contrary, for the development of wound dressing materials, the scaffolds employed are mostly hydrogels because of their controllable mechanical properties. Thus, mechanical properties of dermal scaffolds include stiffness, elastic modulus, tensile strength, viscoelasticity, stress stiffening effects, stress-relaxation rate, and more⁷³. Clinical practice in wound healing has proven that higher tension sutures increase scar tissue development, and that the stress and stiffness of wound fixation could also affect wound healing speed and quality. Thus, the mechanical properties of the biomaterial must be appropriate for the target tissue.

3. Bacteria: a micro-world of possibilities

Bacteria are microscopic single-celled organisms. They are found in every habitat on Earth –soil, rocks, oceans and even snow– either free or in organisms including plants, animals and humans⁷⁴. While some of them are harmful, the vast majority are not, and others are even beneficial to health. Bacteria, in addition to fungi, are vital to the planet’s ecosystems and in the cycling of nutrients.

The bacterial size usually ranges from 0.5 – 5 microns in length, and the cell structure is simple: they are prokaryotes, meaning they do not have organized nuclei or any other membrane-bound organelles, in contrast to eukaryotes. So, they have a unique internal space that contains the cytoplasm, where the DNA, ribosomes, and almost all the metabolic machinery are located (Figure 11). Bacteria cells are surrounded by an outer cell wall and an inner cell membrane. However, certain bacteria such as mycoplasma do not have an integral cell wall, and others may indeed have an external layer called the capsule. In addition, some types of bacteria have flagella or pili covering their cell wall, which allows the microbe move around and attach to a surface.

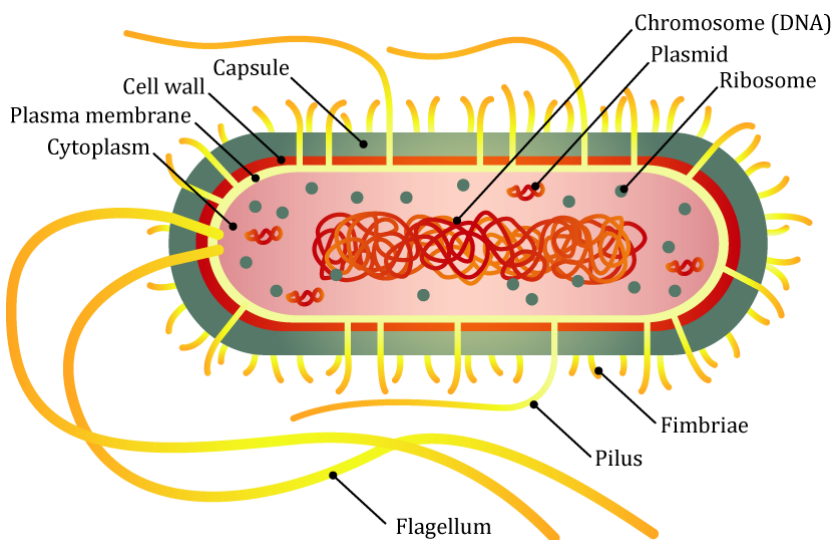


Figure 11. Bacterial cell structure.

There are several types of bacterial classifications. The most employed are those according to⁷⁵:

- Phenotypic analysis:
 - The basic shape. There are five groups: spherical (*cocci*), rod (*bacilli*), spiral (*spirilla*), comma-shaped (*vibrios*) or corkscrew (*spirochaetes*). They can exist as single cells, in pairs, chains (*strepto-*) or clusters (*staphylo-*).
 - Gram staining. Depending on the composition of the cell wall, can be classified as Gram-positives or Gram-negatives if they do not or do have an outer membrane, respectively (Figure 12A). This causes them to stain differently using the Gram staining technique (Figure 12B).
 - Oxygen toleration. While aerobic bacteria depend upon the presence of oxygen for proliferate, anaerobic bacteria cannot tolerate it. Facultative anaerobes can grow in both conditions.

- Taxonomy. It consists of a characterization, classification, and nomenclature of microorganisms, and it is based on analysis of the 16S ribosomal ribonucleic acid (rRNA) gene sequences to establish phylogenetic relationships.

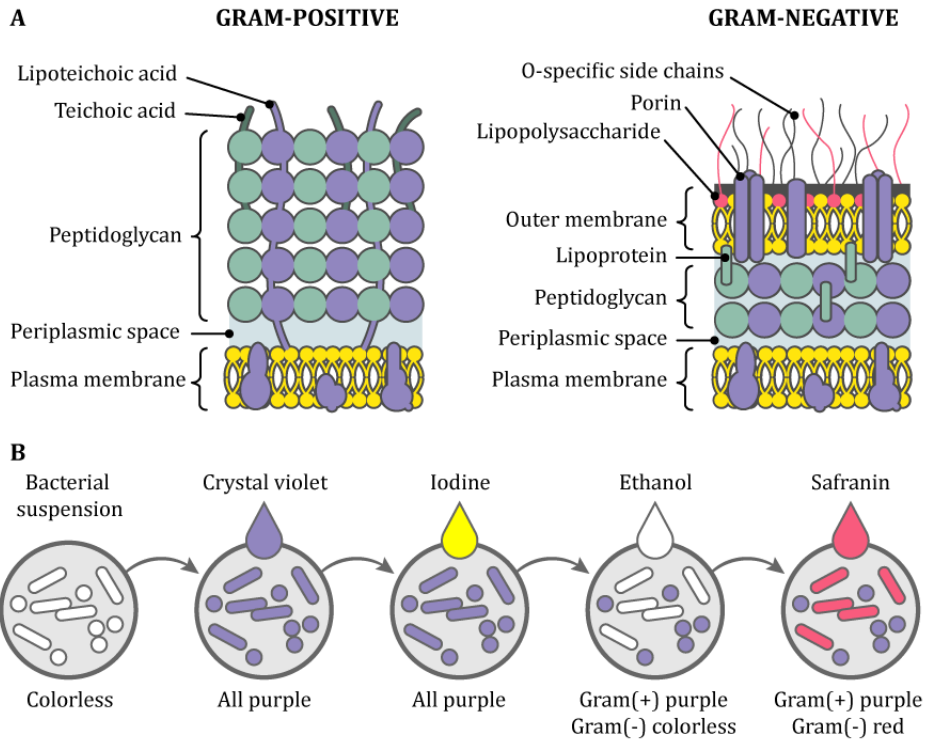


Figure 12. (A) Differences between Gram-positive and Gram-negative bacterial cell walls. **(B)** Gram staining procedure. The crystal violet stains all types of bacteria, but only Gram-positive ones retain the colour after the alcohol decolouration step, due to the dense peptidoglycan layer. The last step consists of staining of decolourised Gram-negative bacteria with safranin.

3.1. Good (beneficial) versus bad (harmful) bacteria

Microbes inhabit virtually every part of the human body, living on the skin, in the mouth, the throat, the gut, in the vagina⁷⁶, etc. All the collective genome of our microbial inhabitants are known as the **microbiome**⁷⁷. The human microbiome configuration includes trillions of microorganisms, outnumbering human cells by a ratio of 10:1. However, because of their small size, microorganisms constitute about 1 to 3 percent of the body's mass. Sometimes they cause sickness, but normally, microorganisms live in harmony with the host, providing vital functions in human health⁷⁸. For

example, the microbes in the gut (the gut microbiome) break down many of the proteins, lipids and carbohydrates in our diet into nutrients that we can then absorb. Moreover, they produce compounds like vitamins and anti-inflammatories that our genome is not able to produce. Nevertheless, in addition to our beneficial microbiome set, almost everyone hosts others microorganisms that can cause sickness, known as **pathogens**. However, pathogens cause no disease in healthy individuals; they coexist with their host and the microbiome. Nowadays, there is a great diversity of research on why and how some pathogens cause disease, or even the death, and under what circumstances.

The composition of the human microbiome patently varies over time. When a patient is ill or takes antibiotics, some bacterial types may be affected. Eventually, the microbiome becomes stable again, even if the preceding bacterial species does not⁷⁹. Other example in which microbiome experiences a dramatic variation is in the vagina of pregnant women. A newborn colonizes its own microbiome after leaving the sterile womb; passage through the birth canal provides the baby its first lot of microbes, so the vaginal microbiome matured to be healthy and safe for the neonate^{80,81}. In this context, the normal human microbiome has been deeply analyzed in order to correlate how its alteration can be associated with a disease or, even more, be its origin⁷⁶. Likewise, research is underway into which strains could be useful to improve health conditions.

Beneficial bacteria can be found in the body, but also in dairy products, among others. Actually, we have used microorganisms for centuries to obtain edible products from raw ones that we cannot digest properly or as a strategy to prolongate the life of them. For example, the fermentation of milk by bacteria of *Lactobacillus* genus can provide yoghurt and cheese. As a result of the fermentation process, *Lactobacillus* produces lactic acid, which lowers the milk pH to 4, leading the change in the organoleptic properties of milk and

avoiding the proliferation of non-desired microbes, such as foodborne pathogens⁸². These benign microbes are used in food and animal feeding as well⁸³, which improves the food quality and safety. These bacteria are known as **lactic acid bacteria** (LAB) and are classified as a type of **probiotic**. They also have the status of GRAS for use by the FDA⁸⁴. Probiotic concept was introduced in early 20th century by Russian scientist and Nobel Prize winner in Physiology or Medicine in 1908, Elie Metchnikoff⁷⁷. The actual definition of probiotics is that these “*are live microorganisms (bacteria or yeasts) which, when administrated in appropriate doses, confer health benefit to the host*” (FAO/WHO)^{85,86}. Their role in the well-being of humans includes (Figure 13):

- Metabolic activity of undigested carbohydrates, synthesis and bioavailability of bioactive compounds or secondary metabolites (such as antioxidants, bacteriocins, enzymes, vitamins, amino acids, oligosaccharides, short-chain fatty acids (SCFAs), exopolysaccharides, and immunomodulators)^{87,88}.
- Creating less desirables conditions for pathogens and viruses. The mechanisms by which LAB inhibit pathogenic bacteria remain unclear, but their ability to produce organic acids, hydrogen peroxide, and bacteriocins is believed to be responsible for the antimicrobial activity^{82,89}. Other mechanisms are the competition for nutrients and location, coaggregating with pathogens, and immune system stimulation⁹⁰.

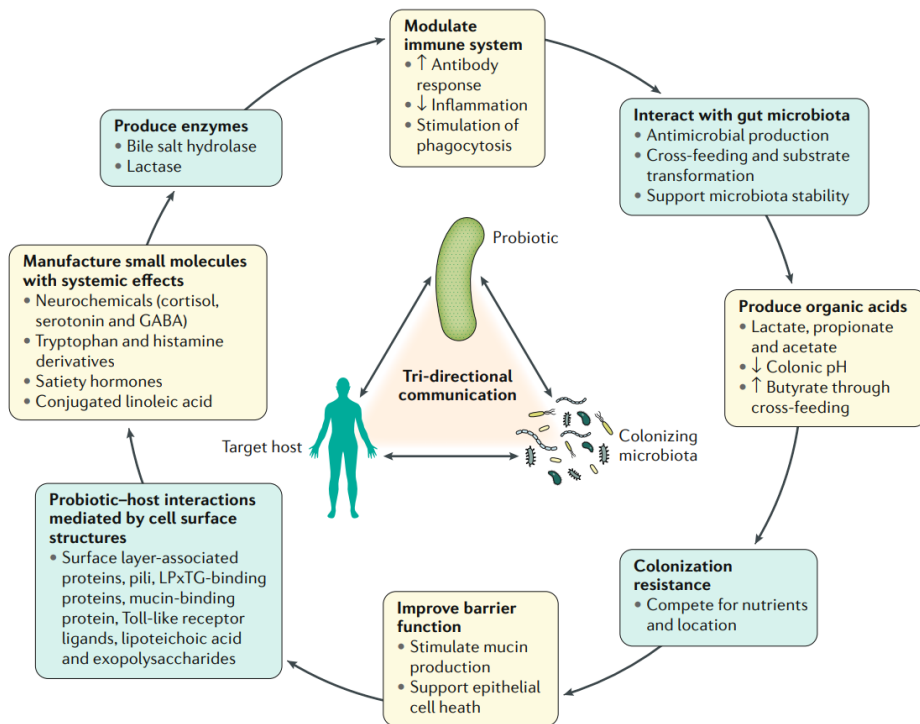


Figure 13. Probiotic mechanisms of action. GABA, gamma-aminobutyric acid. Image extracted from M. Sanders *et al.* (2019)⁹¹.

3.2. Probiotics as cell factories and their applications

Although diverse functional LAB have been applied in fermented foods worldwide, the market is constantly on the need to develop and diversify these products by, for example, using new species with different and specific functional properties. For this purpose, a growing number of scientific studies exploit new strains that are isolated from human sources in view of being considered safer for product development. However, novel isolation sources are currently being used, such as dairy products, fruits, grains, and waste⁹⁰. To be approved as a probiotic, the microbe must deal with the WHO and FAO specifications⁸⁶ (Figure 14).

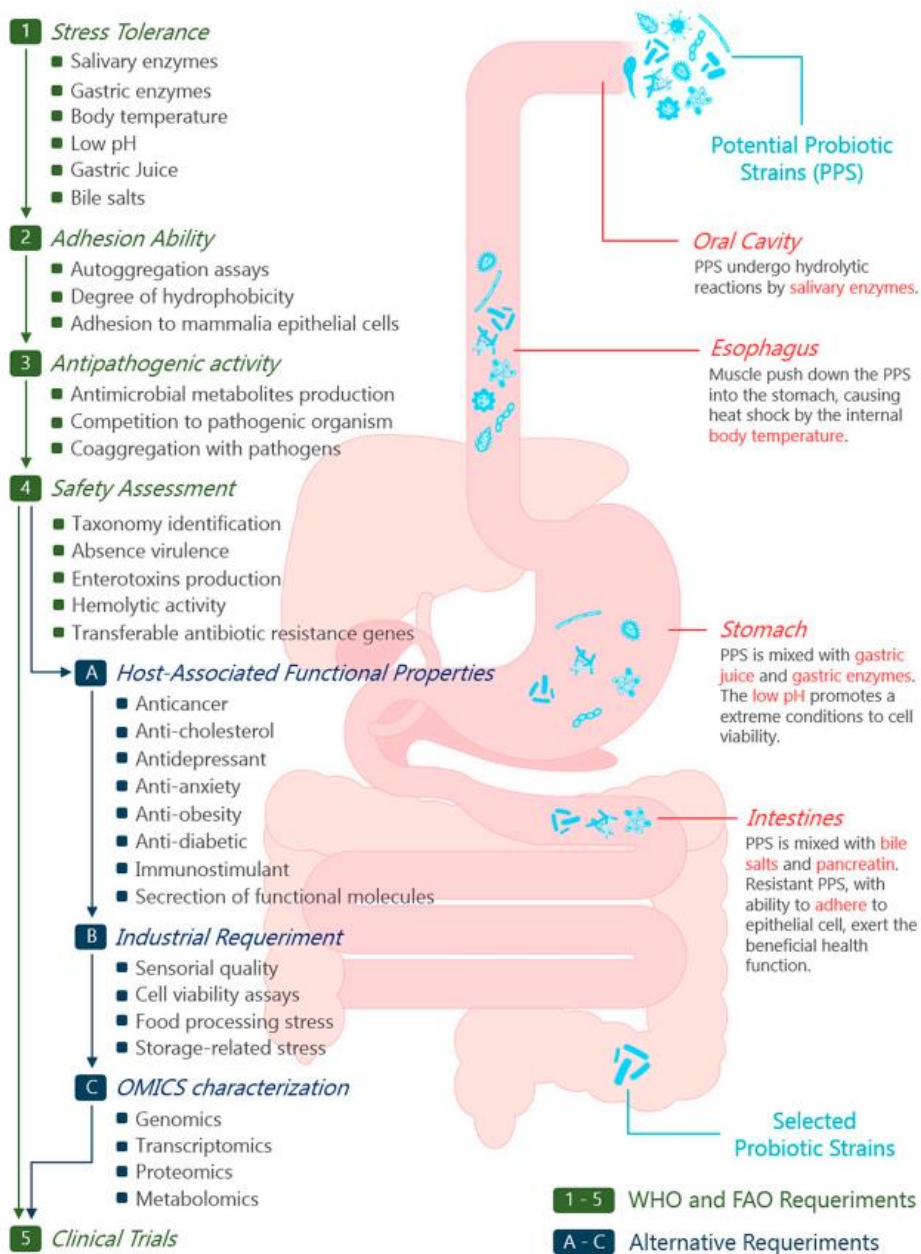


Figure 14. Screening approaches used for characterization of probiotics strains according to WHO/FAO and other studies. Image extracted from G. de Melo Pereira *et al.* (2018)⁹⁰.

The probiotic denomination includes LAB, *Bifidobacterium*, *Bacillus*, and yeasts. Among these, ***Lactobacillus*** is the predominant LAB group in animal and human digestive systems and comprise 183 recognized species, e.g., *L. acidophilus*, *L. fermentum*, *L. plantarum*, *L. casei*, *L. paracasei*, *L. reuteri*, *L. rhamnosus*, and *L. johnsonii*. The family of *Lactobacillaceae* is particularly extensive and varied, which makes taxonomy complicated, but also gives this LAB genus a high interest for several industrial applications. Regardless of the diversity, LAB have a positive impact in the wellbeing and health, and they also share some phenotypic features: they are low-GC, Gram-positive organisms, facultatively anaerobic or aerotolerant, non-sporulating and non-motile, and they ferment a wide range of carbon sources⁹². Metabolically, LAB can be classified as homofermentative (which produce exclusively lactic acid) or heterofermentative (if, in addition to lactic acid, produces several metabolites including ethanol, acetic acid, and carbon dioxide).

For all the above, LAB are used in fermented food and beverage, in edible films for food protection, as pre- and probiotic, in vaccines and drug delivery; the products of their carbon metabolism are used as food flavouring, acidulant, preservative and texturing, medical ingredients, in cosmetic manufacture, green chemicals and fuels; and the secondary metabolites are employed as antimicrobials and nutraceuticals⁹²⁻⁹⁴. Furthermore, interest in their use as cell factories is growing because of their valuable properties, such as high tolerance to ethanol, salts, low pH and wide temperature ranges⁹⁰. Probiotic preparations are to be considered medical or pharmaceutical products when aspects related to health, such as diagnosis of a disease, therapy prevention, or relief, are demanded. Thus far, the European Food Safety Authority (EFSA) has rejected all health requests made for probiotics, classifying them as food or dietary supplements⁹⁰. However, there are lots of successful examples in using microbes to manage microbial ecosystems⁹⁵:

- Wound healing. Recent evidence suggests that the application of wounds with commensal microorganisms can reduce infections after surgery and the use of antibiotics⁹⁶. Similar strategies are also being tested in treating atopic dermatitis and acute wounds⁹⁷.
- Probiotics in hospital cleaning. Antiseptic treatments are not completely effective, leaving dangerous pathogens that can live in surfaces for months and also give rise to increase antibiotic resistance. The use of cleaning agents with probiotics can be an efficient, alternative method to sanitize surfaces⁹⁸.
- Food safety. Probiotic use in chickens, dairy cows, and aquaculture has resulted in improved growth rates, decline in pathogen presence and antibiotic resistance genes, and improved product quality⁹⁹⁻¹⁰¹.
- Fighting infections in humans. Probiotics can diminish the duration and harshness of infectious diarrhoea by reaching the gut, although direct applications to oral cavity, vaginal tract and skin are being investigated^{91,102}.
- Stimulating an ecosystem to fight cancer. Antibiotics are commonly used in cancer treatment to reduce the risk of infection, but this affects the microbiota resulting in a lower therapy efficiency. Optimization of the microbiota to enhance immune situation will presumably improve the treatment of cancer^{103,104}.
- C-section delivery. A recent pilot study showed that infants delivered by C-section who received their mother's vaginal microorganisms developed a microbiota more similar to those of vaginally delivered infants¹⁰⁵. Future studies are required to determine whether vaginal seeding after C-section delivery provides any health benefit to the newborn.

There is growing evidence that the use of beneficial bacteria is a promising path forward for managing pathogenic microbes in humans^{95,102}. Although the LAB employed in industry are quite resistant to hard

environments, such as that of stomach (which is very oxidative and has low pH), the probiotics could experience an elevated damage before achieving their final location in the body. This is the main drawback in probiotic administration, and high effort for improving bacteria viability and functionality are being carried out. Therefore, one of the keys to the health applications associated with probiotics is the choice of an appropriate matrix to host and protect them, since dead or unprotected probiotics have reduced or no activity¹⁰⁶. To accomplish this aim, researchers have explored different approaches, being encapsulation the most studied¹⁰⁷. Thus, different encapsulation techniques and encapsulating food-grade materials are available in order to protect probiotics under unfavourable conditions, and improve their viability and capabilities (e.g., bacterial adhesion). Usually, the encapsulation process involves the embedding or coating of the microbe with biopolymers (alginate, pectin, carboxymethyl cellulose, chitosan), proteins (whey protein, human like collagen, gelatin) and lipids.

For example, one of the most investigated encapsulation structures are microgels¹⁰⁸. They are composed of a matrix of biopolymers with high porosity and large water content, such as calcium alginate. This polymer has been broadly employed for protect probiotics against gastrointestinal conditions, and the gelation is achieved just by adding a calcium chloride solution to the alginate. Thus, the procedure is fast and fully compatible with the bacterial viability: it does not involve high temperature, extreme pH or mechanical stresses. However, alginate gels are unstable under acidic environments or when chelating molecules are present. To avoid these drawbacks, the alginate can be combined with other polymers, such as starch, or built a cover around the alginate with another material, as chitosan. On the other hand, the encapsulation is also useful for protect LAB in fermented food through the industrial process, especially when they are used as starter cultures¹⁰⁹. These starter cultures are composed of one or more microorganisms that are added to the raw food in order to improve the

fermentation rate, increase the fermentation success and the uniformity of the final product between different batches. In conclusion, most studies into engineering protective matrices for probiotics were intended for food and nutraceuticals^{106,110-113}, yet little has been done regarding potentially fatal skin infections, including those occurring at hard-to-heal wounds such as following major surgery, war wounds, burns, and so on. In this sense, this Thesis focus in the obtention of living materials by the combination of LAB with their own or with other bacterial exopolysaccharides for self-encapsulation in order to enhance the compatibility between the encapsulating material and microorganisms, while improving other desired features such as the shelf-life, the adherence, the antimicrobial properties, etc.

3.3. The antibiotic-resistance crisis. Probiotics, an alternative to antibiotics?

Since the discovery of penicillin in 1928 by Alexander Fleming¹¹⁴, the development and use of antibiotics have accompanied humans throughout history. Although this discovery has saved millions of lives, antibiotics have become the prototypic factor associated with industrialization that negatively affects the gut microbiota and can have a long-term impact on it¹¹⁵. This is a reasonable result because most of these medicines were originally designed to have broad-spectrum effects¹¹⁶. Although antibiotics have a deep effect in the microbiota composition, the most alarming consequence of its use is the development of **antibiotic-resistant pathogens**. In fact, the emergence of **multidrug-resistant bacteria** (MDR, bacteria resistant to more than three antibiotic classes) is the result of overprescribed antibiotics, self-medication, and exposure to infections in hospitals¹¹⁷. In a few years, the isolation of MDR bacteria has been excessive (Figure 15).

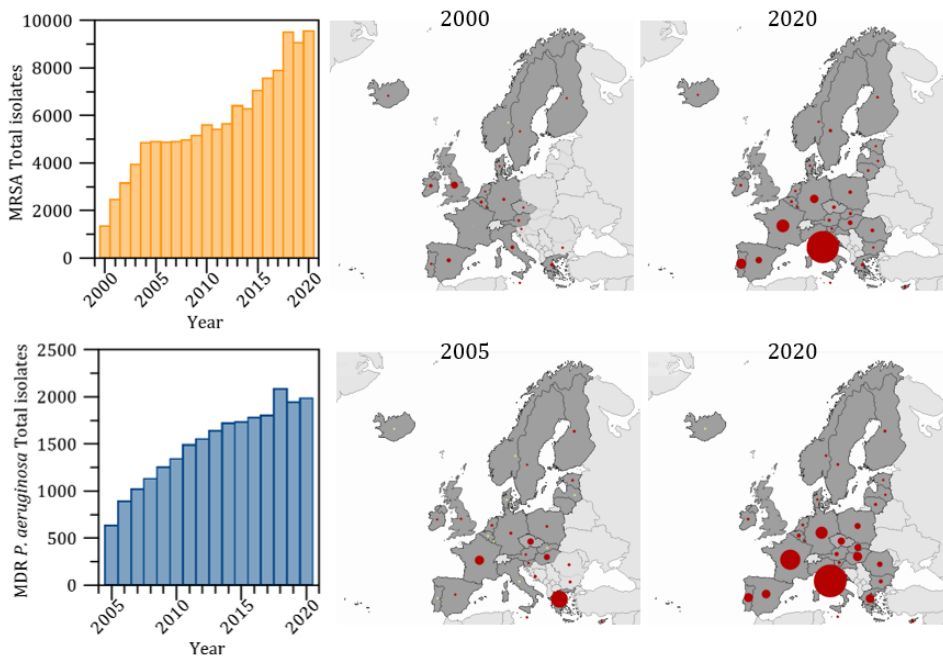


Figure 15. Surveillance Atlas of Infectious Diseases. Panels show the total number of resistant bacteria isolates. MRSA, Methicillin-Resistant *S. aureus*; MDR: Multidrug Resistant. Maps generated by the European Centre for Disease Prevention and Control (ECDC) (<https://atlas.ecdc.europa.eu/public/index.aspx>).

According to the World Health Organization (WHO), the increase of antibiotic-resistant bacteria is one of the biggest threats to global health¹¹⁸. In February 2017, the WHO published its list of pathogens for which new antimicrobial development is urgently needed. Within this large list, ESKAPE pathogens (*Enterococcus faecium*, *Staphylococcus aureus*, *Klebsiella pneumoniae*, *Acinetobacter baumannii*, *Pseudomonas aeruginosa*, and *Enterobacteriaceae*, which includes *Escherichia coli*) were designed “priority status”¹¹⁹. The ESKAPE pathogens exhibit virulence and multidrug resistance by the following mechanisms^{117,120}:

- Horizontal transfer of antibiotic resistance genes between bacteria.
- Antibiotic inactivation/alteration by the production of enzymes. Bacteria can destroy or modify antibiotics by the synthesis of enzymes

with hydrolytic activity or by the addition of chemical groups to key positions.

- Target site modifications. Mutations or bacterial modifications of the antibiotic target site can reduce or prevent the binding of the antibiotic molecule.
- Reducing antibiotic permeability and accumulation. Gram-negative bacteria are intrinsically less permeable to many drugs than Gram-positive due to their outer membrane (Figure 12A). In addition, mutations affecting the function or presence of outer membrane protein channels (i.e., porins) inhibit the penetration of antibiotics, but also the expression of bacterial efflux pumps can extrude drugs out of the cell.
- Other mechanisms and survival strategies. The growth within biofilms, the antibiotic tolerance and persistence, and the intracellular survival (some strains can be internalized within the host cells) can further impede antimicrobial activity.

Health and industry sectors deferred pre-pandemic antimicrobial resistance on an upstaging by COVID-19. This response was cautious but affected the process on battling resistances. In 2014, experts noted that drug-resistant infections could cause 10 million deaths per year by 2050 (Figure 16A)¹²¹. So, the war against antimicrobial resistance requires innovation, which is costly, and all countries around the world must have access to medication¹²² (Figure 16B). A recent study published in *The Lancet* journal conclude that in 2019, almost 5 million deaths were related to MDR bacteria¹²³ (Figure 17). It is important to keep in mind that the development of resistance to antibiotics is a natural ecological phenomenon and is the result of billions of years of evolution¹²⁰. On the one hand, studies of microorganisms of pristine sites (including permafrost¹²⁴), have shown that resistance occurs in the absence of human activity.

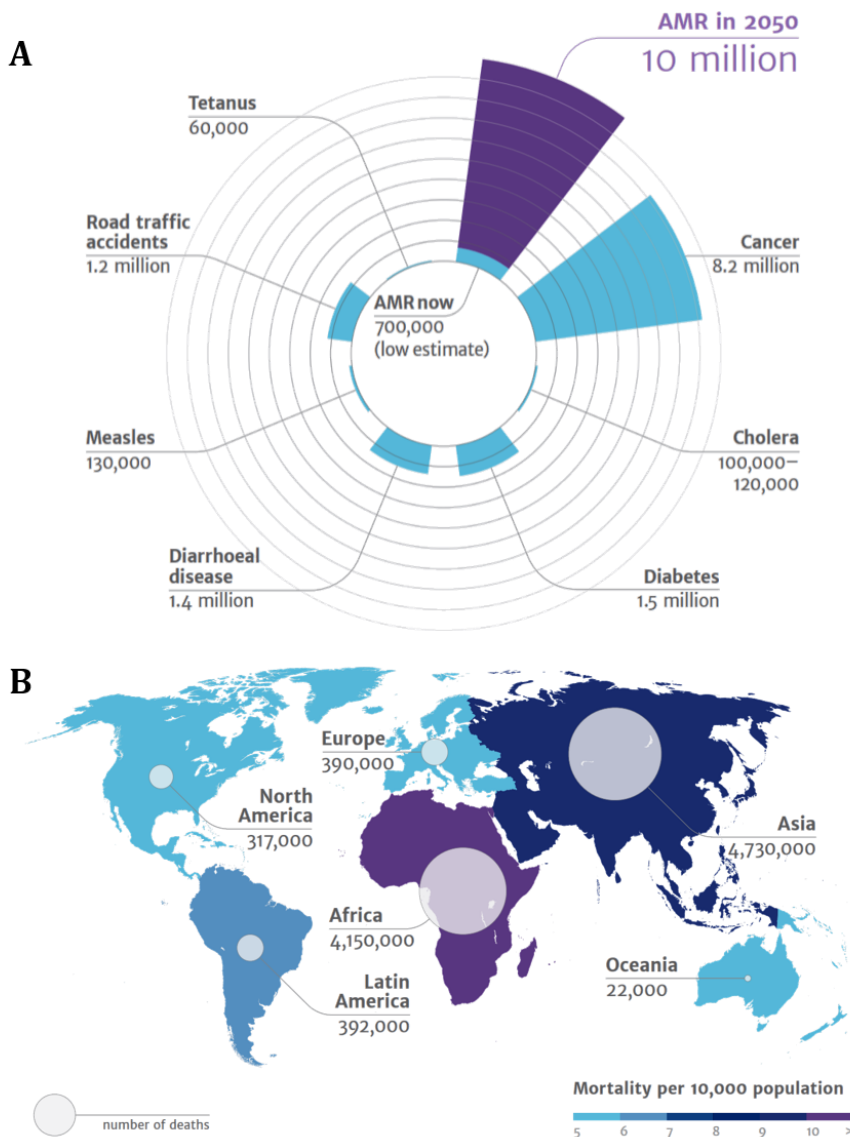


Figure 16. (A) Impact of antimicrobial resistance (AMR). Deaths attributable to AMR every year compared to other major causes of death. The estimated number of AMR will increase to 10 million by 2050, approaching the total number of deaths caused by all diseases today. **(B)** Deaths attributable to AMR in different parts of the world by 2050. The data was obtained after modelling the increase of AMR based on the information available in 2014. There is a tendency for reduced mortality continents with better economic conditions and more stringent antibiotic management. Figure extracted from O’Neil (2014)¹²⁵.

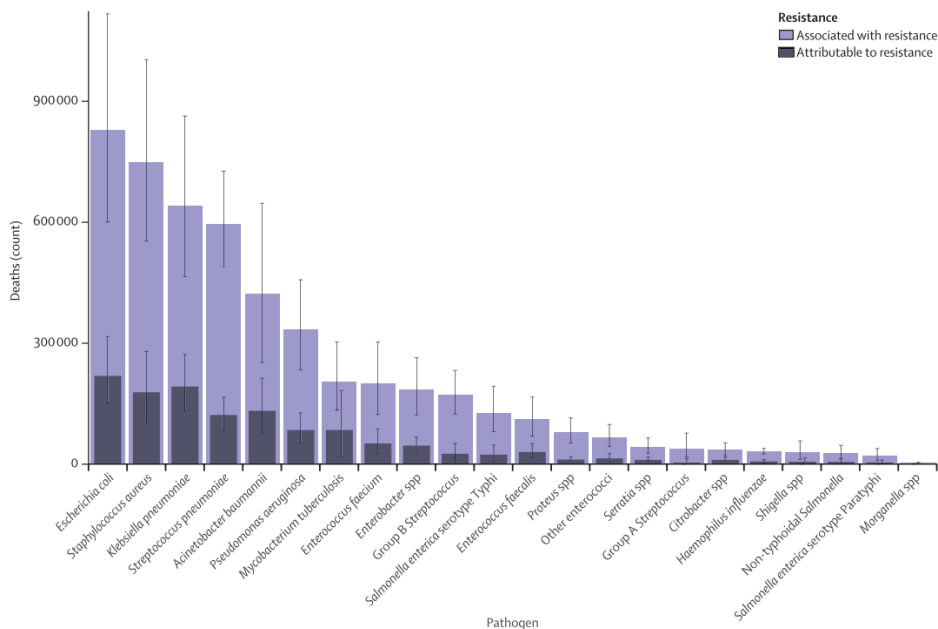


Figure 17. Global deaths (counts) attributable to and associated with antimicrobial resistance by pathogen, 2019. Error bars show 95% uncertainty intervals. Figure and caption extracted from Murray and collaborators (2022)¹²³.

On the other hand, most antibiotics that are used in human medicine are derived from antibiotic-producing microorganisms that expose other species in their local environment to antimicrobial molecules, favouring the selection of resistance^{126,127}. In addition, antibiotics has many intrinsic disadvantages, such as the innate toxicity of certain drugs. The rates of drug-induced nephrotoxicity range from 14% to 26% in adults, and it is the most common toxicity¹²⁸, but psychiatric and sensory disturbances, problems with muscles, tendons and nerves also have been reported¹²⁹. Antibiotics are often not fully metabolized by either humans or animals (in some cases, less than the 10%), and they are released to the aquatic environment where they may have negative effects on non-target species¹³⁰. These species include algae and cyanobacteria, which are the base of food chain in aquatic ecosystems, and any alteration may result in severe effects on other organisms at higher trophic levels.

In this sense, it is important to develop new strategies to fight resistance by investigating new pharmaceutical targets to combat microbial virulence, new methods to inhibit the genetic transfer of antibiotic resistance between bacteria, and new drugs that bolster host immunity against such pathogens. In addition, there are urgently needed new **antibiotic-free approaches** because of all the above mentioned, for prevention or therapy, such as the vaccine development, the immune stimulation, the use of antimicrobial enzymes or peptides, and nanoparticles (e.g., silver nanoparticles), and the phage, photodynamic light, monoclonal antibody and microbiota-based therapies^{117,131,132}. Nevertheless, there are still big challenges in the development of new strategies (Figure 18).

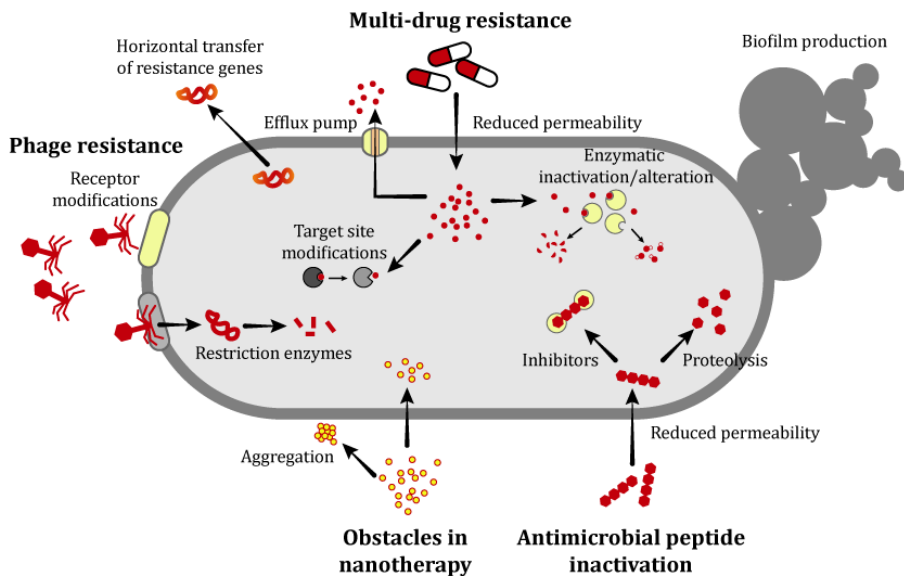


Figure 18. Pathways by which pathogens avoid the antimicrobial therapies.

Among these antibiotic-free approaches, probiotics can play an important role. Extensive research demonstrate that probiotic administration is a promising route to low the risk of acute respiratory and digestive tract

infections, which can be associated with a reduced antibiotic prescription¹⁰². In addition to being useful in prevention, they have been tested *in vitro* against pathogenic bacteria (e.g., *S. aureus* and *P. aeruginosa*), and *in vivo* in established infections. For example, some strains identified in human breast milk, such as *L. fermentum*, display antimicrobial activity *in vitro*¹³³, and certain probiotic strains and probiotic combinations like kefir can promote the wound healing by topical application¹³⁴. In both cases, the most employed bacteria are strains of *Lactobacillus*, *Bifidobacterium*, and *Bacillus subtilis* is also widely employed for antibacterial applications¹³⁵. Some mechanisms by which probiotics may fight pathogens have been established, but the vast majority are not well understood for the moment. Between them, the main mechanisms are the competition for the location and nutrients, the coaggregation with pathogens, the immune system stimulation, and the production of antimicrobial metabolites^{83,87,134} (Figure 19). These metabolites include organic acids such as acetic acid and lactic acid (inhibit the proliferation of pathogens), hydrogen peroxide (induces the formation of reactive oxygen species), bacteriocins (non-toxic antimicrobial peptides with the ability to kill other bacteria), and biofilm inhibitors (molecules that interfere with the pathogenic biofilm formation).

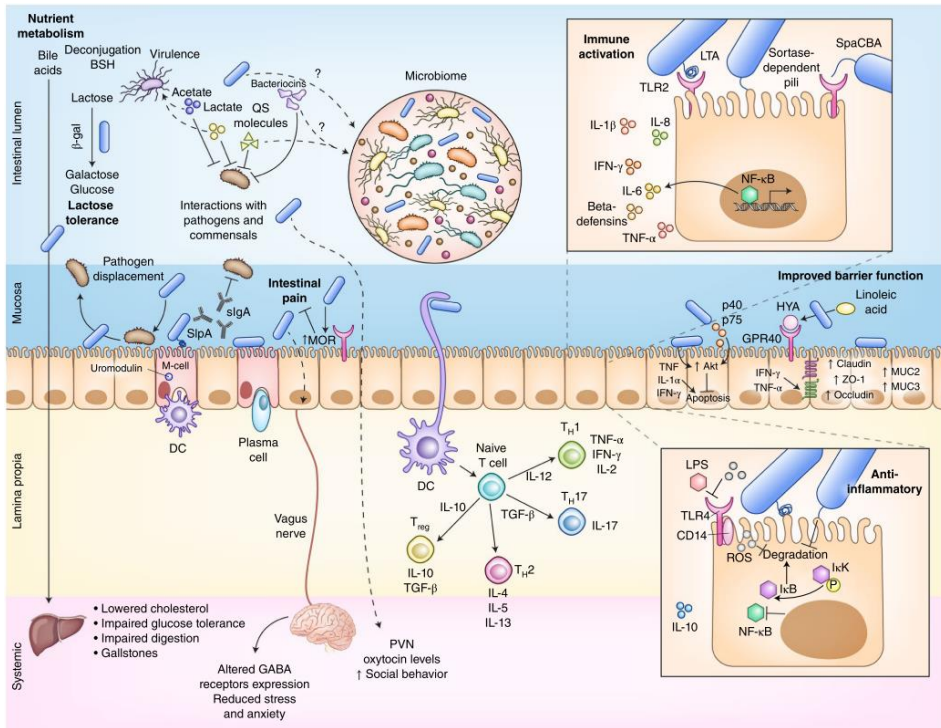


Figure 19. Mechanistic interactions between probiotics and the host and its microbiome. Probiotics may have several effects on the host, including metabolism of nutrients to improve digestion (e.g., lactose) or produce systemic effects (e.g., bile salts); direct and indirect pathogen antagonism (but potentially also promotion of virulence); improved barrier function, alteration of the microbiome; change of signaling to the nervous system; and immunomodulation. These may be contact-dependent and/or mediated by surface molecules (such as lipoteichoic acid (LTA), sEPS, SpaCBA and sortase-dependent pili), or by secreted molecules (such as short-chain fatty acids, bacteriocins, p40 and p75). Dashed lines represent putative mechanisms. BSH, bile salt hydrolase; β-gal, β-galactosidase; SlpA, S-layer protein A; sIgA, secreted immunoglobulin A; DC, dendritic cell; MOR, mu-opioid receptor; PVN, paraventricular nucleus of the hypothalamus; TGF-β, transforming growth factor beta; TLR, toll-like receptor; LPS, lipopolysaccharide; ROS, reactive oxygen species; T_H, T-helper cell; T_{reg}, regulatory T cell. Image and caption extracted from Suez *et al.* (2019)¹³⁶.

4. Objectives

The general objective of this Doctoral Thesis is the development of biomaterials based on the combination of probiotic bacteria with biocompatible polymers of biological importance, like collagen or bacterial cellulose, using mild conditions framed in the Green Chemistry. In fact, we will take special care to develop environmentally friendly and energy-efficient methods to produce the biomaterials, which is a very important aspect for potential industrial exploitation. In particular, the challenge of this work is the synthesis of new probiotic-based biomaterials for the therapy of bacterial infections as an alternative to antibiotics. According to the World Health Organization, the increase of antibiotic-resistant bacteria is one of the biggest threats to global health, and therefore, new antibacterial strategies are necessary. Probiotics could be an alternative to antibiotics but they are vulnerable in the hostile ambient of infected tissues. We will intend the integration of probiotics into the biocompatible matrix to render them stable and with enhanced activity. Likewise, we pretend the incorporation of other antibacterials, different to antibiotics, as silver nanoparticles, in these biomaterials. We will check the activity of all biomaterials against frequent pathogens as well as, against antibiotic-resistant strains.

Objetivos

El objetivo general de esta Tesis Doctoral es el desarrollo de biomateriales que combinen bacterias probióticas y polímeros biocompatibles con importancia biológica, como son el colágeno y la celulosa bacteriana. Para ello, se pretenden utilizar condiciones suaves, lo que permitiría enmarcar estos procedimientos dentro de lo que se conoce como Química Verde. En particular, este trabajo tiene como reto la síntesis de nuevos biomateriales basados en probióticos como alternativa a los antibióticos para el tratamiento de infecciones bacterianas. De acuerdo con la Organización Mundial de la Salud, el incremento del número de bacterias resistentes a antibióticos es una de las mayores amenazas para salud global y, por tanto, se requieren urgentemente nuevas estrategias antibacterianas. Los probióticos pueden ser una alternativa a los antibióticos, pero su mayor desventaja es que los tejidos con infecciones establecidas presentan un ambiente hostil, haciéndolos ser vulnerables. Nos proponemos la integración de los probióticos en una matriz biocompatible para proporcionarles estabilidad y mejorar su actividad. De la misma forma, también consideramos la incorporación de otros antibacterianos diferentes a los antibióticos, como son las nanopartículas de plata. Comprobaremos la actividad de todos estos biomateriales contra los patógenos más frecuentes, además de otras cepas que presentan resistencias a antibióticos.

5. References

1. Ratner, B. D. & Zhang, G. *A History of Biomaterials. Biomaterials Science* (Elsevier, 2020). doi:10.1016/b978-0-12-816137-1.00002-7
2. Datta, L. P., Manchineella, S. & Govindaraju, T. Biomolecules-derived biomaterials. *Biomaterials* **230**, 119633 (2020).
3. Moradali, M. F. & Rehm, B. H. A. Bacterial biopolymers: from pathogenesis to advanced materials. *Nat. Rev. Microbiol.* **18**, 195–210 (2020).
4. Williams, D. F. Biomaterials and biomedical materials. in *Definitions of Biomaterials for the Twenty-First Century* 15–23 (Elsevier, 2019). doi:10.1016/B978-0-12-818291-8.00002-X
5. Walker, P. M. B. *Larousse dictionary of science and technology*. (Larousse Press, 2006).
6. Joyce, K., Fabra, G. T., Bozkurt, Y. & Pandit, A. Bioactive potential of natural biomaterials: identification, retention and assessment of biological properties. *Signal Transduct. Target. Ther.* **6**, 1–28 (2021).
7. Sorushanova, A. *et al.* The Collagen Suprafamily: From Biosynthesis to Advanced Biomaterial Development. *Adv. Mater.* **31**, 1–39 (2019).
8. Rele, S. *et al.* D-Periodic Collagen-Mimetic Microfibers. *J. Am. Chem. Soc.* **129**, 14780–14787 (2007).
9. *Collagen. Structure and Mechanics*. (Springer US, 2008).
10. Tomasello, G., Armenia, I. & Molla, G. The Protein Imager: A full-featured online molecular viewer interface with server-side HQ-rendering capabilities. *Bioinformatics* **36**, 2909–2911 (2020).
11. Ramírez Rodríguez, G., Patrício, T. & Delgado López, J. *Natural polymers for bone repair. Bone Repair Biomaterials* (Elsevier Ltd, 2019). doi:10.1016/b978-0-08-102451-5.00008-1
12. Lin, K. *et al.* Advanced Collagen-Based Biomaterials for Regenerative Biomedicine. *Adv. Funct. Mater.* **29**, 1–16 (2019).
13. Heino, J. The collagen family members as cell adhesion proteins. *BioEssays* **29**, 1001–1010 (2007).
14. Yang, Q. *et al.* A bioinspired gallol-functionalized collagen as wet-tissue adhesive for biomedical applications. *Chem. Eng. J.* **417**, 127962 (2021).
15. Taguchi, T. *et al.* Bonding of soft tissues using a novel tissue adhesive consisting of a citric acid derivative and collagen. *Mater. Sci. Eng. C* **24**, 775–780 (2004).

16. Rubert Pérez, C. M., Panitch, A. & Chmielewski, J. A collagen peptide-based physical hydrogel for cell encapsulation. *Macromol. Biosci.* **11**, 1426–1431 (2011).
17. Chattopadhyay, S. & Raines, R. T. Review collagen-based biomaterials for wound healing. *Biopolymers* **101**, 821–833 (2014).
18. Zhang, D., Wu, X., Chen, J. & Lin, K. The development of collagen based composite scaffolds for bone regeneration. *Bioact. Mater.* **3**, 129–138 (2018).
19. Fu, J. H. *et al.* Degradable Chitosan-Collagen Composites Seeded with Cells as Tissue Engineered Heart Valves. *Hear. Lung Circ.* **26**, 94–100 (2017).
20. Zhou, H. *et al.* In-situ preparation of silver salts/collagen fiber hybrid composites and their photocatalytic and antibacterial activities. *J. Hazard. Mater.* **359**, 274–280 (2018).
21. Alvarez, G. S. *et al.* Antibiotic-loaded silica nanoparticle-collagen composite hydrogels with prolonged antimicrobial activity for wound infection prevention. *J. Mater. Chem. B* **2**, 4660–4670 (2014).
22. Rath, G., Hussain, T., Chauhan, G., Garg, T. & Goyal, A. K. Collagen nanofiber containing silver nanoparticles for improved wound-healing applications. *J. Drug Target.* **24**, 520–529 (2016).
23. Avila Rodríguez, M. I., Rodríguez Barroso, L. G. & Sánchez, M. L. Collagen: A review on its sources and potential cosmetic applications. *J. Cosmet. Dermatol.* **17**, 20–26 (2018).
24. Le, A., Morales-peñaloza, A. & Mart, M. Hydrolyzed Collagen—Sources and Applications. 1–16
25. Bhumbar, M. V., Bhagwat, P. K. & Dandge, P. B. Extraction and characterization of acid soluble collagen from fish waste: Development of collagen-chitosan blend as food packaging film. *J. Environ. Chem. Eng.* **7**, 102983 (2019).
26. Berillis, P. *Marine Collagen: Extraction and Applications. Research Trends in Biochemistry, Molecular Biology and Microbiology* (Academia, 2015).
27. Rutschmann, C., Baumann, S., Cabalzar, J., Luther, K. B. & Hennet, T. Recombinant expression of hydroxylated human collagen in *Escherichia coli*. *Appl. Microbiol. Biotechnol.* **98**, 4445–4455 (2014).
28. Moon, R. J., Martini, A., Nairn, J., Simonsen, J. & Youngblood, J. *Cellulose nanomaterials review: Structure, properties and nanocomposites. Chemical Society Reviews* **40**, (2011).
29. Sulaeva, I., Henniges, U., Rosenau, T. & Potthast, A. Bacterial cellulose

as a material for wound treatment: Properties and modifications. A review. *Biotechnol. Adv.* **33**, 1547–1571 (2015).

30. Lee, K. Y., Buldum, G., Mantalaris, A. & Bismarck, A. More than meets the eye in bacterial cellulose: Biosynthesis, bioprocessing, and applications in advanced fiber composites. *Macromol. Biosci.* **14**, 10–32 (2014).
31. Zhong, C. Industrial-Scale Production and Applications of Bacterial Cellulose. *Front. Bioeng. Biotechnol.* **8**, 1–19 (2020).
32. Lee, C. *et al.* Correlations of Apparent Cellulose Crystallinity Determined by XRD, NMR, IR, Raman, and SFG Methods. *Adv. Polym. Sci.* **271**, 115–132 (2015).
33. Moon, R. J., Martini, A., Nairn, J., Simonsen, J. & Youngblood, J. Cellulose nanomaterials review: Structure, properties and nanocomposites. *Chem. Soc. Rev.* **40**, 3941–3994 (2011).
34. Portela, R., Leal, C. R., Almeida, P. L. & Sobral, R. G. Minireview Bacterial cellulose: a versatile biopolymer for wound dressing applications. *Microb. Biotechnol.* **12**, 586–610 (2019).
35. Shah, N., Ul-Islam, M., Khattak, W. A. & Park, J. K. Overview of bacterial cellulose composites: A multipurpose advanced material. *Carbohydr. Polym.* **98**, 1585–1598 (2013).
36. Keshk, S. M. Bacterial Cellulose Production and its Industrial Applications. *J. Bioprocess. Biotech.* **04**, (2014).
37. Gullo, M., La China, S., Falcone, P. M. & Giudici, P. Biotechnological production of cellulose by acetic acid bacteria: current state and perspectives. *Appl. Microbiol. Biotechnol.* **102**, 6885–6898 (2018).
38. Karim, Z. & Afrin, S. Bacterial cellulose: Preparation and characterization. in *Cellulose-Reinforced Nanofibre Composites: Production, Properties and Applications* (eds. Jawaid, M., Boufi, S. & Khalil H.P.S., A.) 327–340 (Woodhead Publishing, Elsevier Ltd, 2017).
39. Kumagai, A. *et al.* Ultrafine Cellulose Fibers Produced by *Asaia bogorensis*, an Acetic Acid Bacterium. 2815–2821 (2011). doi:10.1021/bm2005615
40. Ma, T. *et al.* Bioresource Technology Cellulose synthesized by *Enterobacter* sp . FY-07 under aerobic and anaerobic conditions. *Bioresour. Technol.* **126**, 18–23 (2012).
41. Brown, A. J. XLIII.—On an acetic ferment which forms cellulose. *J. Chem. Soc. Trans.* **49**, 432–439 (1886).
42. Gao, H. *et al.* Comparison of bacterial nanocellulose produced by different strains under static and agitated culture conditions.

- Carbohydr. Polym.* **227**, 115323 (2020).
43. Azeredo, H. M. C., Barud, H., Farinas, C. S., Vasconcellos, V. M. & Claro, A. M. Bacterial Cellulose as a Raw Material for Food and Food Packaging Applications. *Front. Sustain. Food Syst.* **3**, (2019).
 44. Anton-Sales, I., Roig-Sanchez, S., Sánchez-Guisado, M. J., Laromaine, A. & Roig, A. Bacterial Nanocellulose and Titania Hybrids: Cytocompatible and Cryopreservable Cell Carriers. *ACS Biomater. Sci. Eng.* **6**, 4893–4902 (2020).
 45. Chang, S. T., Chen, L. C., Lin, S. Bin & Chen, H. H. Nano-biomaterials application: Morphology and physical properties of bacterial cellulose/gelatin composites via crosslinking. *Food Hydrocoll.* **27**, 137–144 (2012).
 46. Wahid, F. *et al.* Development of bacterial cellulose/chitosan based semi-interpenetrating hydrogels with improved mechanical and antibacterial properties. *Int. J. Biol. Macromol.* **122**, 380–387 (2019).
 47. Maneerung, T., Tokura, S. & Rujiravanit, R. Impregnation of silver nanoparticles into bacterial cellulose for antimicrobial wound dressing. *Carbohydr. Polym.* **72**, 43–51 (2008).
 48. Roig-Sanchez, S. *et al.* One-Step Biosynthesis of Soft Magnetic Bacterial Cellulose Spheres with Localized Nanoparticle Functionalization. *ACS Appl. Mater. Interfaces* **13**, 55569–55576 (2021).
 49. Roig-Sanchez, S., Fernández-Sánchez, C., Laromaine, A. & Roig, A. Bio and soft-imprinting lithography on bacterial cellulose films. *Mater. Today Chem.* **21**, (2021).
 50. Roig-Sanchez, S. *et al.* Nanocellulose films with multiple functional nanoparticles in confined spatial distribution. *Nanoscale Horizons* **4**, 634–641 (2019).
 51. Mira-Cuenca, C., Meslier, T., Roig-Sanchez, S., Laromaine, A. & Roig, A. Patterning Bacterial Cellulose Films with Iron Oxide Nanoparticles and Magnetic Resonance Imaging Monitoring. *ACS Appl. Polym. Mater.* **3**, 4959–4965 (2021).
 52. Torres, F. G., Arroyo, J. J. & Troncoso, O. P. Bacterial cellulose nanocomposites: An all-nano type of material. *Mater. Sci. Eng. C* **98**, 1277–1293 (2019).
 53. Greca, L. G., Lehtonen, J., Tardy, B. L., Guo, J. & Rojas, O. J. Biofabrication of multifunctional nanocellulosic 3D structures: A facile and customizable route. *Mater. Horizons* **5**, 408–415 (2018).
 54. Bethke, K. *et al.* Functionalized Cellulose for Water Purification, Antimicrobial Applications, and Sensors. *Adv. Funct. Mater.* **28**, 1–14

- (2018).
55. Lantada, A. D., Korvink, J. G. & Islam, M. Taxonomy for Engineered Living Materials. (2021).
 56. European Commission. EIC Pathfinder challenge: Engineered living materials. *European Innovation Council* (2021). Available at: https://eic.ec.europa.eu/eic-funding-opportunities/calls-proposals/eic-pathfinder-challenge-engineered-living-materials_en. (Accessed: 17th February 2022)
 57. Nguyen, P. Q., Courchesne, N.-M. D., Duraj-Thatte, A., Praveschotinunt, P. & Joshi, N. S. Engineered Living Materials: Prospects and Challenges for Using Biological Systems to Direct the Assembly of Smart Materials. *Adv. Mater.* **30**, 1704847 (2018).
 58. Zhang, D. *et al.* Functionalization of whole-cell bacterial reporters with magnetic nanoparticles. *Microb. Biotechnol.* **4**, 89–97 (2011).
 59. Srubar, W. V. Engineered Living Materials: Taxonomies and Emerging Trends. *Trends Biotechnol.* **39**, 574–583 (2021).
 60. Smith, R. S. H. *et al.* Hybrid Living Materials: Digital Design and Fabrication of 3D Multimaterial Structures with Programmable Biohybrid Surfaces. *Adv. Funct. Mater.* **30**, (2020).
 61. Hosseinidou, Z. *et al.* Bioengineered and biohybrid bacteria-based systems for drug delivery. *Adv. Drug Deliv. Rev.* **106**, 27–44 (2016).
 62. Rodrigo-Navarro, A., Sankaran, S., Dalby, M. J., del Campo, A. & Salmeron-Sanchez, M. Engineered living biomaterials. *Nat. Rev. Mater.* **6**, 1175–1190 (2021).
 63. Gilarska, A. *et al.* Addressing the Osteoporosis Problem-Multifunctional Injectable Hybrid Materials for Controlling Local Bone Tissue Remodeling. *ACS Appl. Mater. Interfaces* **13**, 49762–49779 (2021).
 64. Chen, S. *et al.* A conductive cell-delivery construct as a bioengineered patch that can improve electrical propagation and synchronize cardiomyocyte contraction for heart repair. *J. Control. Release* **320**, 73–82 (2020).
 65. Liu, S. & Xu, W. Engineered Living Materials-Based Sensing and Actuation. *Front. Sensors* **1**, 1–9 (2020).
 66. Qin, G., Panilaitis, B. J. & Kaplan, Z. S. D. L. A cellulosic responsive ‘living’ membrane. *Carbohydr. Polym.* **100**, 40–45 (2014).
 67. Guo, S. *et al.* Engineered Living Materials Based on Adhesin-Mediated Trapping of Programmable Cells. *ACS Synth. Biol.* **9**, 475–485 (2020).

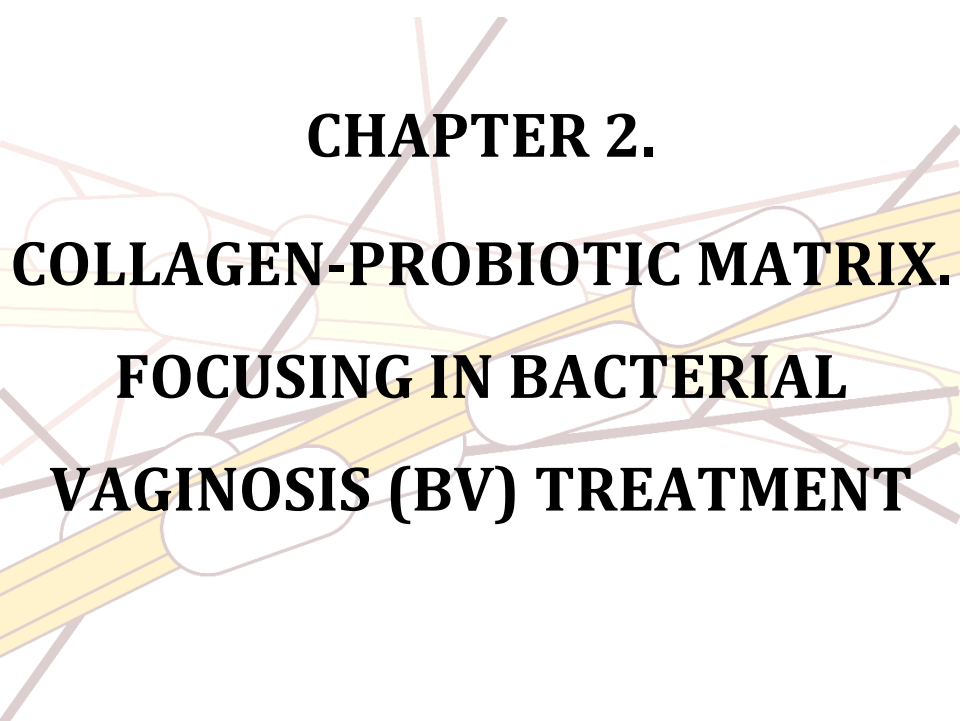
68. Barnhart, M. M. & Chapman, M. R. Curli biogenesis and function. *Annu. Rev. Microbiol.* **60**, 131–147 (2006).
69. Estrella, L. A. *et al.* Engineered Escherichia coli Biofilms Produce Adhesive Nanomaterials Shaped by a Patterned 43 kDa Barnacle Cement Protein. *Biomacromolecules* **22**, 365–373 (2021).
70. Wang, L., Wang, C., Wu, S., Fan, Y. & Li, X. Influence of the mechanical properties of biomaterials on degradability, cell behaviors and signaling pathways: Current progress and challenges. *Biomater. Sci.* **8**, 2714–2733 (2020).
71. Wang, Y. Biadaptability: An Innovative Concept for Biomaterials. *J. Mater. Sci. Technol.* **32**, 801–809 (2016).
72. Prasad, S. & Wong, R. C. W. Unraveling the mechanical strength of biomaterials used as a bone scaffold in oral and maxillofacial defects. *Oral Sci. Int.* **15**, 48–55 (2018).
73. Wang, Y., Armato, U. & Wu, J. Targeting Tunable Physical Properties of Materials for Chronic Wound Care. *Front. Bioeng. Biotechnol.* **8**, 1–14 (2020).
74. Graham, B. J. Bacteria. *National Human Genome Research Institute* Available at: <https://www.genome.gov/genetics-glossary/Bacteria>. (Accessed: 10th December 2021)
75. Morata de Ambrosini, V. I., Martín, M. C. & Merín, M. G. Classification of the Bacteria: Traditional. *Encycl. Food Microbiol. Second Ed.* **1**, 169–173 (2014).
76. Methé, B. A. *et al.* A framework for human microbiome research. *Nature* **486**, 214–2021 (2012).
77. Podolsky, S. H. Metchnikoff and the microbiome. *Lancet* **380**, 1810–1811 (2012).
78. MacDougall, R. NIH Human Microbiome Project defines normal bacterial makeup of the body. *National Institutes of Health* (2012). Available at: <https://www.nih.gov/news-events/news-releases/nih-human-microbiome-project-defines-normal-bacterial-makeup-body>. (Accessed: 5th December 2021)
79. Lloyd-Price, J. *et al.* Strains, functions and dynamics in the expanded Human Microbiome Project. *Nature* **550**, 61–66 (2017).
80. Walther-António, M. R. S. *et al.* Pregnancy's stronghold on the vaginal microbiome. *PLoS One* **9**, 1–10 (2014).
81. Freitas, A. C. *et al.* The vaginal microbiome of pregnant women is less rich and diverse, with lower prevalence of Mollicutes, compared to non-pregnant women. *Sci. Rep.* **7**, 1–16 (2017).

82. Gao, Z. *et al.* Inhibitory effect of lactic acid bacteria on foodborne pathogens: A review. *J. Food Prot.* **82**, 441–453 (2019).
83. Sadiq, F. A. *et al.* Lactic Acid Bacteria as Antifungal and Anti-Mycotoxigenic Agents: A Comprehensive Review. *Compr. Rev. Food Sci. Food Saf.* **18**, 1403–1436 (2019).
84. GRAS Notices. *U.S. Food & Drug Administration* (2021). Available at: <https://www.cfsanappsexternal.fda.gov/scripts/fdcc/index.cfm?set=GRASNotices>. (Accessed: 10th December 2021)
85. Bielecka, M. Probiotics in food. *Chem. Funct. Prop. Food Components, Third Ed.* 413–426 (2006). doi:10.1201/9781420009613.ch16
86. Araya, M. *et al.* *Guidelines for the Evaluation of Probiotics in Food.* (2002).
87. Indira, M., Venkateswarulu, T. C., Abraham Peele, K., Nazneen Bobby, M. & Krupanidhi, S. Bioactive molecules of probiotic bacteria and their mechanism of action: a review. *3 Biotech* **9**, 1–11 (2019).
88. Behnsen, J., Deriu, E., Sassone-Corsi, M. & Raffatellu, M. Probiotics: Properties, Examples, and Specific Applications. *Cold Spring Harb. Perspect. Med.* **3**, a010074–a010074 (2013).
89. Bäumlér, A. J. & Sperandio, V. Interactions between the microbiota and pathogenic bacteria in the gut. *Nature* **535**, 85–93 (2016).
90. de Melo Pereira, G. V., de Oliveira Coelho, B., Magalhães Júnior, A. I., Thomaz-Soccol, V. & Soccol, C. R. How to select a probiotic? A review and update of methods and criteria. *Biotechnol. Adv.* **36**, 2060–2076 (2018).
91. Sanders, M. E., Merenstein, D. J., Reid, G., Gibson, G. R. & Rastall, R. A. Probiotics and prebiotics in intestinal health and disease: from biology to the clinic. *Nat. Rev. Gastroenterol. Hepatol.* **16**, 605–616 (2019).
92. Bosma, E. F., Forster, J. & Nielsen, A. T. Lactobacilli and pediococci as versatile cell factories – Evaluation of strain properties and genetic tools. *Biotechnol. Adv.* **35**, 419–442 (2017).
93. Pop, O. L. *et al.* Edible films and coatings functionalization by probiotic incorporation: A review. *Polymers (Basel)*. **12**, 1–18 (2020).
94. Leroy, F. & De Vuyst, L. Lactic acid bacteria as functional starter cultures for the food fermentation industry. *Trends Food Sci. Technol.* **15**, 67–78 (2004).
95. Sonnenburg, J. L. & Sonnenburg, E. D. Vulnerability of the industrialized microbiota. *Science (80-.)*. **366**, (2019).
96. Kasatpibal, N. *et al.* Effectiveness of probiotic, prebiotic, and synbiotic

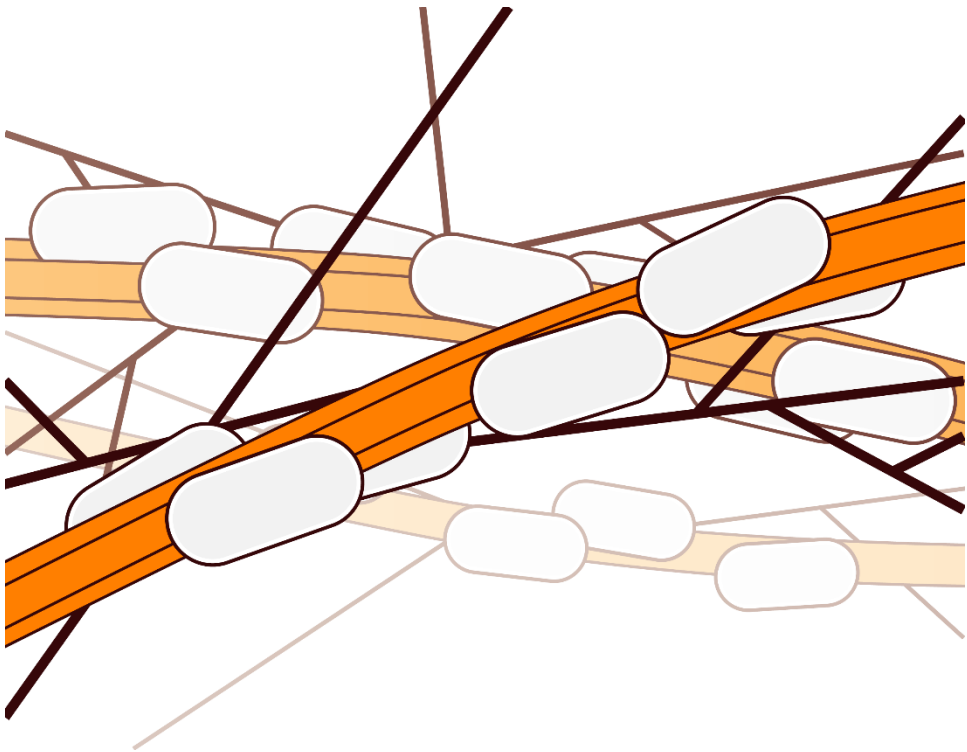
- therapies in reducing postoperative complications: A systematic review and network meta-analysis. *Clin. Infect. Dis.* **64**, S153–S160 (2017).
97. Valdéz, J. C., Peral, M. C., Rachid, M., Santana, M. & Perdigón, G. Interference of *Lactobacillus plantarum* with *Pseudomonas aeruginosa* in vitro and in infected burns: The potential use of probiotics in wound treatment. *Clin. Microbiol. Infect.* **11**, 472–479 (2005).
 98. Caselli, E. Hygiene: microbial strategies to reduce pathogens and drug resistance in clinical settings. *Microb. Biotechnol.* **10**, 1079–1083 (2017).
 99. Alagawany, M. *et al.* The use of probiotics as eco-friendly alternatives for antibiotics in poultry nutrition. *Environ. Sci. Pollut. Res.* **25**, 10611–10618 (2018).
 100. Uyeno, Y., Shigemori, S. & Shimosato, T. Effect of probiotics/prebiotics on cattle health and productivity. *Microbes Environ.* **30**, 126–132 (2015).
 101. Balcázar, J. L. *et al.* The role of probiotics in aquaculture. *Vet. Microbiol.* **114**, 173–186 (2006).
 102. King, S. *et al.* Does probiotic consumption reduce antibiotic utilization for common acute infections? A systematic review and meta-analysis. *Eur. J. Public Health* **29**, 494–499 (2019).
 103. Vétizou, M. *et al.* Anticancer immunotherapy by CTLA-4 blockade relies on the gut microbiota. *Science (80-.)*. **350**, 1079–1084 (2015).
 104. Sivan, A. *et al.* Commensal *Bifidobacterium* promotes antitumor immunity and facilitates anti-PD-L1 efficacy. *Science (80-.)*. **350**, 1084–1089 (2015).
 105. Dominguez-Bello, M. G. *et al.* Partial restoration of the microbiota of cesarean-born infants via vaginal microbial transfer. *Nat. Med.* **22**, 250–253 (2016).
 106. Burgain, J., Gaiani, C., Linder, M. & Scher, J. Encapsulation of probiotic living cells: From laboratory scale to industrial applications. *J. Food Eng.* **104**, 467–483 (2011).
 107. Yao, M. *et al.* Progress in microencapsulation of probiotics: A review. *Compr. Rev. Food Sci. Food Saf.* **19**, 857–874 (2020).
 108. Martín, M. J., Lara-Villoslada, F., Ruiz, M. A. & Morales, M. E. Microencapsulation of bacteria: A review of different technologies and their impact on the probiotic effects. *Innov. Food Sci. Emerg. Technol.* **27**, 15–25 (2015).

109. Kavitate, D., Kandasamy, S., Devi, P. B. & Shetty, P. H. Recent developments on encapsulation of lactic acid bacteria as potential starter culture in fermented foods – A review. *Food Biosci.* **21**, 34–44 (2018).
110. Vilela, C., Moreirinha, C., Almeida, A., Silvestre, A. J. D. & Freire, C. S. R. Zwitterionic Nanocellulose-Based Membranes for Organic Dye Removal. (2019).
111. Huq, T. *et al.* Alginate based nanocomposite for microencapsulation of probiotic: Effect of cellulose nanocrystal (CNC) and lecithin. *Carbohydr. Polym.* (2017). doi:10.1016/j.carbpol.2017.03.032
112. Singh, P. *et al.* Cellulose-based edible films for probiotic entrapment. *Food Hydrocoll.* (2019). doi:10.1016/j.foodhyd.2018.08.057
113. Singh, P. *et al.* On the viability, cytotoxicity and stability of probiotic bacteria entrapped in cellulose-based particles. *Food Hydrocoll.* (2018). doi:10.1016/j.foodhyd.2018.04.027
114. Fleming, A. On the antibacterial action of cultures of a penicillium, with special reference to their use in the isolation of B. influenzae. 1929. *Bulletin of the World Health Organization* **79**, 780–790 (2001).
115. Blaser, M. J. Antibiotic use and its consequences for the normal microbiome. *Science (80-.).* **352**, 544–545 (2016).
116. Schulfer, A. & Blaser, M. J. Risks of Antibiotic Exposures Early in Life on the Developing Microbiome. *PLoS Pathog.* **11**, 1–6 (2015).
117. Mulani, M. S., Kamble, E. E., Kumkar, S. N., Tawre, M. S. & Pardesi, K. R. Emerging Strategies to Combat ESKAPE Pathogens in the Era of Antimicrobial Resistance: A Review. *Front. Microbiol.* **10**, (2019).
118. Willyard, C. The drug-resistant bacteria that pose the greatest health threats. *Nature* **543**, 15 (2017).
119. Shrivastava, S. R., Shrivastava, P. S. & Ramasamy, J. World health organization releases global priority list of antibiotic-resistant bacteria to guide research, discovery, and development of new antibiotics. *JMS -J. Med. Soc.* **32**, 76–77 (2018).
120. Blair, J. M. A., Webber, M. A., Baylay, A. J., Ogbolu, D. O. & Piddock, L. J. V. Molecular mechanisms of antibiotic resistance. *Nat. Rev. Microbiol.* **13**, 42–51 (2015).
121. Willyard, C. Drug-resistant bacteria ranked. *Nature* **543**, 15 (2017).
122. Kwon, J. H. & Powderly, W. G. The post-antibiotic era is here. *Science (80-.).* **373**, 471 (2021).
123. Murray, C. J. *et al.* Global burden of bacterial antimicrobial resistance

- in 2019: a systematic analysis. *Lancet* **6736**, (2022).
124. Dcosta, V. M. *et al.* Antibiotic resistance is ancient. *Nature* **477**, 457–461 (2011).
 125. O’Neill, J. Antimicrobial Resistance: Tackling a crisis for the health and wealth of nations The Review on Antimicrobial Resistance Chaired. *Rev. Antimicrob. Resist.* (2014).
 126. Perry, J. A. & Wright, G. D. The antibiotic resistance ‘mobilome’: Searching for the link between environment and clinic. *Front. Microbiol.* **4**, 1–7 (2013).
 127. Forsberg, K. J. *et al.* The Shared Antibiotic Resistome of soil bacteria and human pathogens. *Science (80-.).* **337**, 1107–1111 (2012).
 128. Perazella, M. A. Pharmacology behind common drug nephrotoxicities. *Clin. J. Am. Soc. Nephrol.* **13**, 1897–1908 (2018).
 129. Marchant, J. When antibiotics turn toxic. *Nature* **555**, 431–433 (2018).
 130. Kovalakova, P. *et al.* Occurrence and toxicity of antibiotics in the aquatic environment: A review. *Chemosphere* **251**, 126351 (2020).
 131. De Oliveira, D. M. P. *et al.* Antimicrobial resistance in ESKAPE pathogens. *Clin. Microbiol. Rev.* **33**, (2020).
 132. O’Neill, J. *Tackling Drug-Resistant Infections Globally: Final Report and Recommendations. THE REVIEW ON ANTIMICROBIAL RESISTANCE* (2016).
 133. Marti, R. Antimicrobial potential of four *Lactobacillus* strains isolated from breast milk. **101**, 72–79 (2006).
 134. Tsiouris, C. G. & Tsiouri, M. G. Human microflora, probiotics and wound healing. *Wound Med.* **19**, 33–38 (2017).
 135. Su, Y., Liu, C., Fang, H. & Zhang, D. *Bacillus subtilis*: A universal cell factory for industry, agriculture, biomaterials and medicine. *Microb. Cell Fact.* **19**, 1–12 (2020).
 136. Suez, J., Zmora, N., Segal, E. & Elinav, E. The pros, cons, and many unknowns of probiotics. *Nat. Med.* **25**, 716–729 (2019).

The background features a stylized illustration of biological structures. It includes several yellow, cylindrical fibers representing collagen, some of which are bundled together. Interspersed among these fibers are various shapes representing cells or protein molecules, including some with circular heads and thin tails, and others that are more complex and interconnected. The overall style is clean and scientific, using a palette of yellow, brown, and white.

CHAPTER 2.
COLLAGEN-PROBIOTIC MATRIX.
FOCUSING IN BACTERIAL
VAGINOSIS (BV) TREATMENT



1. Introduction. Bacterial vaginosis

Bacterial vaginosis (BV), also known as vaginal bacteriosis, is the most frequent cause of vaginal disorders in women of reproductive age. The most common symptoms of BV are vaginal discharge, burning during urination, and itching¹. However, some women with BV have no symptoms. This disorder alone is not considered harmful, but complications can arise. BV condition increases the risk of developing a sexually transmitted infection (STI), such as human immunodeficiency virus (HIV) infection^{1,2}, gonorrhoea, chlamydia, trichomoniasis, herpes simplex virus (HSV) and human papilloma virus infections³. During pregnancy, BV can lead to early or preterm delivery, loss of pregnancy, or even infertility⁴ (Figure 1). Although BV can lead to serious complications, it is not considered an STI.

From a microbiology perspective, BV is characterized by a dysbiosis, the imbalance of normal vaginal microbiota. The health of the vaginal microbiota is believed to be maintained by lactic acid-producing organisms, such as lactobacilli¹. With a minute imbalance on the pH profile of the vaginal fluid (e.g., from pH 4 to 5 in a healthy vs unhealthy environment), these lactobacilli are suppressed by the overgrowth of pathogenic bacteria, such as *Gardnerella vaginalis*, *Mycoplasma* and *Mobiluncus* spp.^{3,5}, which are present in small populations when healthy, resulting in BV in reproductive-age women.

BACTERIAL VAGINOSIS (BV) FACTS

PREVALENCE^{1,2}

~1 IN 3 

women have BV, affecting more than 21 million in the U.S. each year

BV is the most common vaginal infection among women ages 14-49

Today, more than 4 million women are treated in the U.S. for BV annually

SIGNS AND SYMPTOMS OF BV^{1,3}

84% of women do not recognize the signs of BV

COMMON SYMPTOMS INCLUDE:

Unusual vaginal discharge

- White or gray
- Watery
- Strong fish-like odor

Vaginal irritation

- Itching around the outside of the vagina

WHAT CAUSES BV



BV is caused when the vagina has more harmful bacteria than good bacteria³

WHAT IF BV IS LEFT UNTREATED?

Women are more at risk for serious health concerns, including:³

- Increased risk of getting sexually transmitted diseases, including chlamydia, trichomoniasis, gonorrhea, herpes and HIV
- Pregnancy problems (e.g. pre-term birth, low birth weight)
- Pelvic inflammatory disease

WHAT BV TREATMENTS ARE CURRENTLY AVAILABLE?

The most commonly prescribed oral BV treatment regimen requires twice-a-day dosing for seven days. Adherence with the current leading therapies for the treatment of BV has been shown to be only approximately 50 percent.²

Figure 1. Bacterial Vaginosis facts: prevalence in the U.S., signs, causes, consequences and current treatments. Image extracted from Newark (2017)⁶.

From a chemical point of view, the vaginal environment of a healthy woman is dominated by the lactic acid, the main metabolite of the *Lactobacillus* family. Other short-chain fatty acids (SCFAs), such as acetic, propionic, and butyric acids associated with other typically harmful bacteria are present at almost 100-fold lower concentrations^{3,5}. The pH is therefore regulated by the lactic acid ($pK_a = 3.80$), which is found in healthy vaginal

fluid at concentrations of the order of 120 mM, leading pH values around 4. When BV develops, the decreasing population of *Lactobacilli* and the excessive growth of pathogenic bacteria modify the metabolite pattern: an increase of SCFAs and a dramatic decrease of lactic acid (Table 1). In particular, acetic acid, the main component of SCFAs, can reach concentrations about 120 mM from originally 2 mM, which leads to an increase of pH up to the value of 5, since the pK_a of acetic acid (4.86) is higher than that of lactic acid. Therefore, the pH of the vaginal fluid moves from 4 (healthy) to 5 (BV) and worsening the disease condition over time. The pH change is, in fact, a key parameter used in the diagnosis of BV. For instance, the Amsel method diagnoses BV when the vaginal fluid has a pH higher than 4.5⁷.

Table 1. Summary of the principal alterations when a BV has established.

Situation	Healthy (eubiosis)	Unhealthy (Bacterial vaginosis, dysbiosis)
Predominant bacteria	<i>Lactobacillus</i>	<i>Gardnerella vaginalis</i> <i>Mycoplasma</i> <i>Mobilincus</i> spp.
Chemical environment	Acidic: pH 4 [Lactic acid] = 120 mM [SCFAs (acetic acid)] = 1 mM	Lower acidity: pH 5 [Lactic acid] < 20 mM [SCFAs (acetic acid)] = 120 mM

BV has been traditionally treated with antibiotics, especially metronidazole and clindamycin, and more recently with new antibiotic-based therapies, as VivaGel®⁸. However, a number of drawbacks in existing treatment modalities necessitate the development of new routes of therapy⁹. First, treatments based on antibiotics do not avoid recurrences. Second, the development of antibiotic-resistant bacteria due to the excessive use of antibiotics remains the biggest challenge faced by modern medicine at

global level⁹⁻¹⁶. Therefore, antibiotic-free and more effective long-term therapies are critically needed. Recent approaches have considered creams or gels containing probiotics of the *Lactobacillus* family¹⁷. While promising, the efficiency of this approach will depend on the adhesion and proliferation levels of the probiotic within the BV-compromised micro-environment. In particular, the high pH of vaginal fluids during BV tends to hamper lactobacilli proliferation and subsequent therapy, leading to BV recurrences. The adhesion of lactobacilli can displace pathogens in epithelial cells, and their proliferation can restore the eubiotic chemical environment. Moreover, *Lactobacillus* spp. proved to be antagonistic against many viruses such as HIV and HSV¹⁸, which is an additional advantage in preventing STIs when BV is treated.

The phenomena related to the surface properties of beneficial lactobacilli such as adhesion and biofilm formation capabilities are involved in the permanence and colonization. Lactobacilli are Gram-positive organisms whose surface consists in a cell wall made of peptidoglycan grafted with proteins, teichoic acids, lipoteichoic acids and polysaccharides¹⁹. The adhesion mechanisms in lactobacilli involve non-specific factors, particularly hydrophobicity and surface charge, as well as specific components such as carbohydrates and proteins on the bacteria cell wall²⁰, that can anchor different cell surface components such as collagen and mucin. This recognition leads to an adhesive interaction and, finally, to the biofilm formation. The type and the strength of this association is strain-dependent, and the molecule recognized on the cell surface has a significant influence on the biofilm development. Nevertheless, the knowledge of the lactobacilli molecular mechanisms that mediate adhesion is still limited.

To overcome these challenges, we have developed a new strategy based on the use of a cytocompatible collagen-based matrix that protects probiotics and allows their effective localization and proliferation within the compromised vaginal fluids.

Collagen is the most abundant protein in mammals and the basic building block of extracellular matrices of different tissues. Collagen is considered an ideal natural polymer for tissue engineering due to its abundance and easy processing, flexibility, hydrophilicity, excellent biocompatibility and biodegradability and extremely low antigenicity²¹⁻²³. Collagen matrix provides innate biological informational guidance to cells that elicits cell attachment and promotes chemotactic response²⁴. Despite collagen scaffolds are being regularly designed and commercialized for tissue regeneration and drug delivery^{21,25}, the use of collagen scaffolds to incorporate living probiotics, that proliferate and form biofilms has not been explored so far. This work explores the ability of collagen scaffolds (col) to protect two biofilm-producing probiotics of the genus *Lactobacillus*, viz., *L. fermentum* (*Lf*) and *L. acidophilus* (*La*), resulting in hybrid materials, col-*Lf* and col-*La*, respectively, with enhanced healing properties against BV infections. Both materials correspond to biocomposites composed of collagen, probiotic, and the bacterial EPS (exopolysaccharides). col-*Lf* and col-*La* are able to restore the pH of a compromised simulated BV fluid to a healthy condition. Outstanding stability of these collagen entrapped probiotics, combined with high adhesion to the vaginal mucosa and the intrinsic cytocompatibility of the collagen matrix, make these materials very promising for nonantibiotic BV therapy.

2. Results and discussion

2.1. Collagen matrix as a scaffold for probiotics

Type I collagen is a predominant protein in the human body and the major organic component of the bone extracellular matrix. In bone tissues, collagen triple helices (monomers) are self-assembled at the molecular level in a periodic staggered array resulting in large fibrils with a characteristic banding pattern of 67 nm²⁶. This self-assembly is driven by an increase in

pH²⁷. Taking inspiration from this process, we mixed an acidic solution containing collagen monomers with a suspension of probiotics (*Lf* or *La*) in phosphate buffered saline solution (PBS, pH 7.4), as depicted in the scheme in Figure 2. The instantaneous pH increase induces the collagen self-assembly into a high-density matrix of fibers with several hundred microns in length, with diameters ranging between 50 – 400 nm (with an average diameter of 250 nm), and showing the characteristic D-banding pattern (67 nm). Optical images show how the collagen monomeric solution changes after the pH increase in absence (Figure 3A,B) and in presence of *Lf* and *La* (Figure 3C and E, respectively). As it is evident from the scanning electron microscopy (SEM) micrographs (Figure 4), using this simple one-pot procedure, *Lf* and *La* probiotics were successfully entrapped into the network of collagen fibers (Figure 4C,D and 4E,F, respectively). Further, the presence of probiotics did not alter the pH-induced structure and assembly of the collagen fibers, which were similar to those obtained in PBS without bacteria (Figure 4A,B). Likewise, bacteria enmesh neither affected the diameter of the fibers (Figure 4 G-I), but optical images show that collagen matrix acquired a white and more compact aspect (Figure 3C,E).

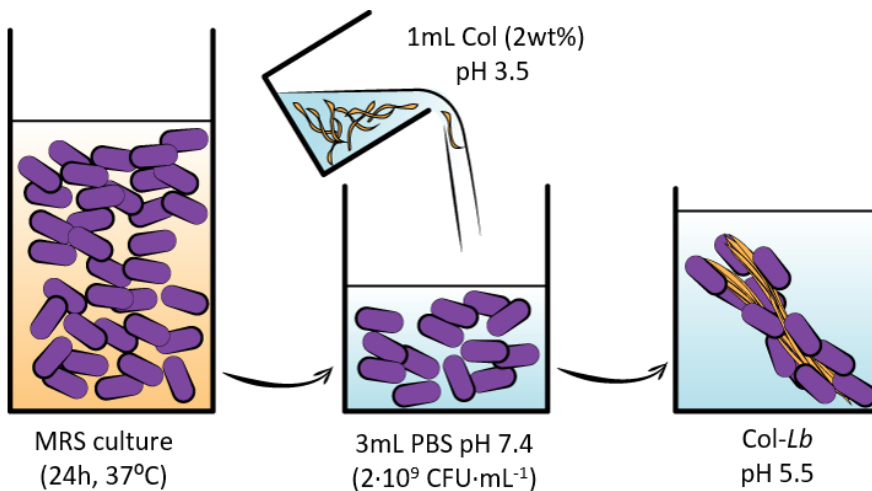


Figure 2. Schematic representation of lactobacilli's entrapment in the collagen matrix. *Lb* indicates both *Lf* or *La*.

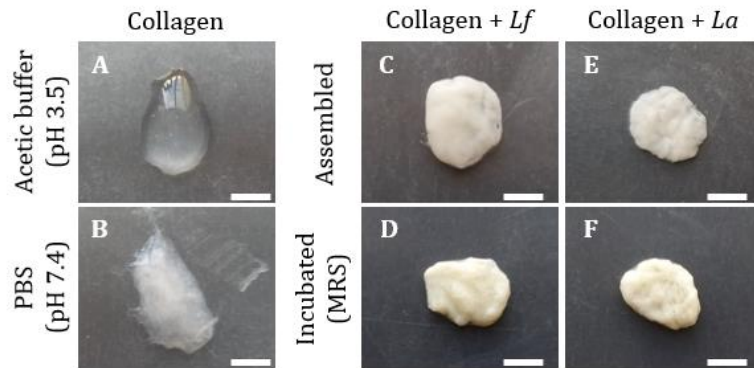


Figure 3. Photographs of the collagen solution (1% w/w) before **(A)** and after the pH-induced self-assembly **(B)**. The pictures of the biocomposites obtained when collagen assembles in presence of probiotics and after 24 h of incubation in MRS **(C,D for *Lf*, E,F for *La*)** show how bacteria affect the appearance of the matrix. Scale bar = 5 mm.

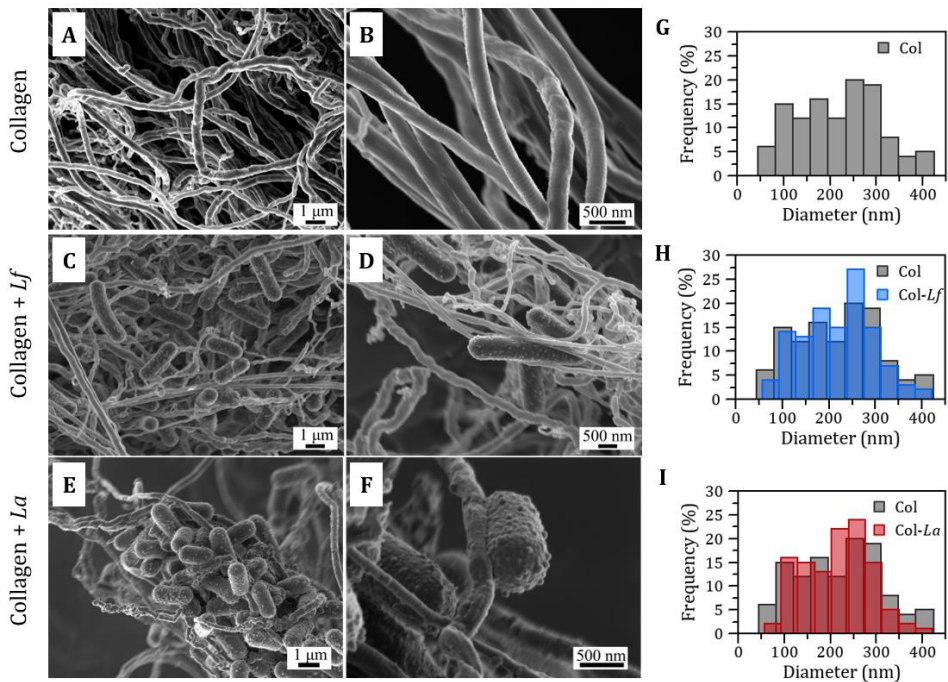


Figure 4. SEM micrographs of collagen fibers assembled in PBS in the absence **(A, B)** and in presence of the probiotic *Lf* **(C, D)** or *La* **(E, F)**. **(G-I)** Histograms represent the diameter distribution of collagen fibers in the absence (grey bars) and in the presence of *Lf* or *La* (blue and red bars, respectively). The diameters of 100 fibers from different SEM images were measured for each condition.

In order to assess the stability of the collagen scaffold after entrapping the probiotic, we carried out a study of the collagen degradation. The collagen release was monitored by the UV-vis absorption bands of tyrosine at 276 nm, phenyl-alanine at 258 nm, and peptide bonds at 205 nm. After 24h in PBS at 37 °C, the absorbance of the supernatant at 276 nm and 258 nm was negligible (Figure 5A). From the absorption band at 205 nm, and using an extinction coefficient of $5.91 \text{ g}^{-1}\text{cm}^{-1}$, we determined that 3% w/w of collagen was released from the scaffold after 24 h. Likewise, the level of released probiotics from the collagen scaffold was directly counted in a Neubauer chamber. A gradual release corresponding to the 15% of probiotics was observed during the first 6 h, and kept constant after 24 h (Figure 5B). Therefore, collagen degradation and probiotic release levels pointed out the stability of the material formed by entrapping probiotics into the collagen scaffold in PBS.

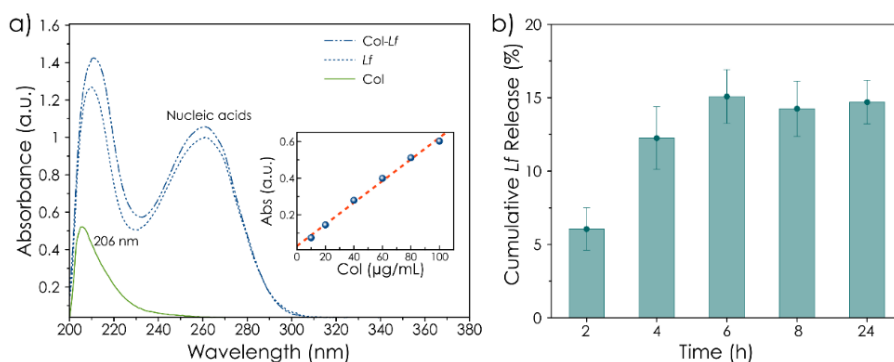


Figure 5. Stability of collagen matrix assembled in presence of *Lf* in simulated physiological conditions (PBS and 37 °C). **a)** UV-spectra of supernatant collected by centrifugation of collagen matrix (Col), *Lf* and Col with *Lf* after 24 hours in PBS. Inset displays the calibration plot for collagen quantification by UV-vis spectroscopy. After 24 hours, absorbance values at 206 nm of 0.52 for Col sample, corresponding with a collagen concentration in the supernatant of 83.22 $\mu\text{g}/\text{mL}$, indicates almost negligible scaffold degradation ($\sim 3 \text{ wt.}\%$). **b)** Cumulative *Lf* release from Col with *Lf* at 2, 4, 6, 8 and 24 hours. Results are expressed as percentage of released CFU with respect to the initial CFU with the standard deviations as error bars. Released *Lf* was measured by direct counting in a Neubauer chamber (BLAUBRAND®, Sigma).

Interestingly, when both probiotic-containing collagen materials were incubated in an optimal probiotic medium, such as de Man, Rogosa and Sharpe (MRS), the appearance of the material changed again, resulting in an even more compact material (Figure 3D,F). Figure 6A shows that the bacteria successfully proliferated and produced biofilms, which decorated the collagen fibers. These lactobacilli are high biofilm-producing probiotics, and EPS prevail as the major component of this polymeric matrix (Figure 6B,C). EPS play an important role in the formation of the biofilm, which is essential for bacteria to create a growth-conductive microenvironment in a substrate, in this case, the collagen fibers. The excellent integration of bacteria into the collagen matrix, witnessed by the formation of biofilms, is evident from Figure 7, showing how bacteria adhere to collagen fibers through their EPS. These materials, col-*Lf* and col-*La* hereafter, are in fact hybrid biocomposites formed by three constituents: the collagen matrix, the probiotic, and their bacterial EPS, being the latter the natural 'glue' of the other two components. This class of biocomposite has never been reported.

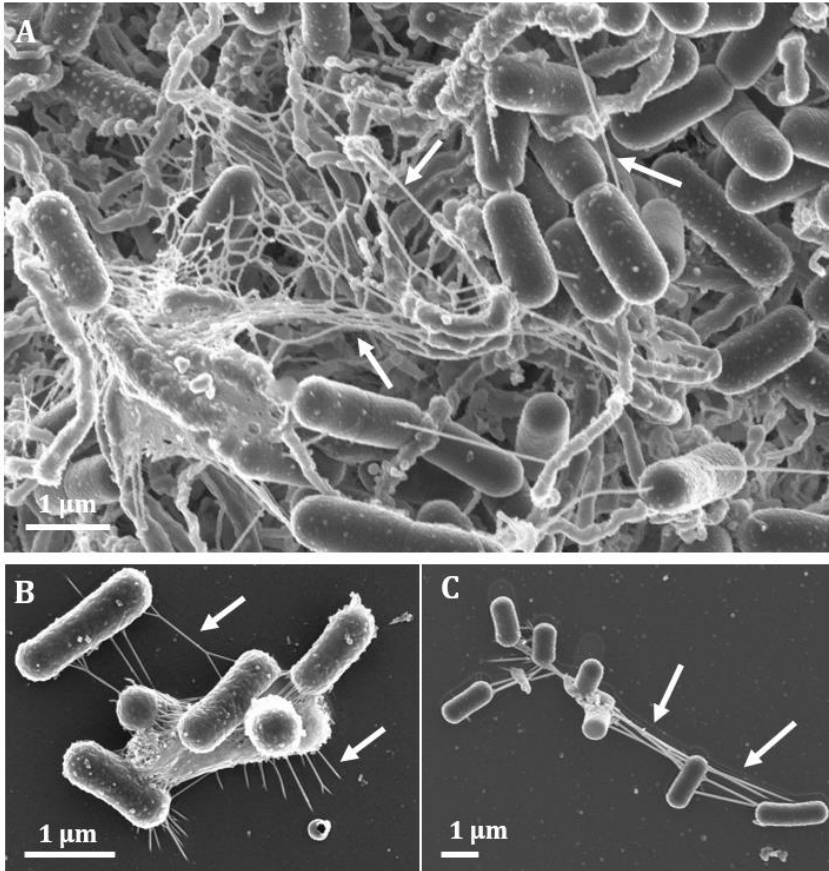


Figure 6. SEM micrographs of the biocomposite with *Lf* (A) and *Lf* pellet (B, C), both after incubation in MRS broth. The former is the so-called col-*Lf*. White arrows indicate the EPS.

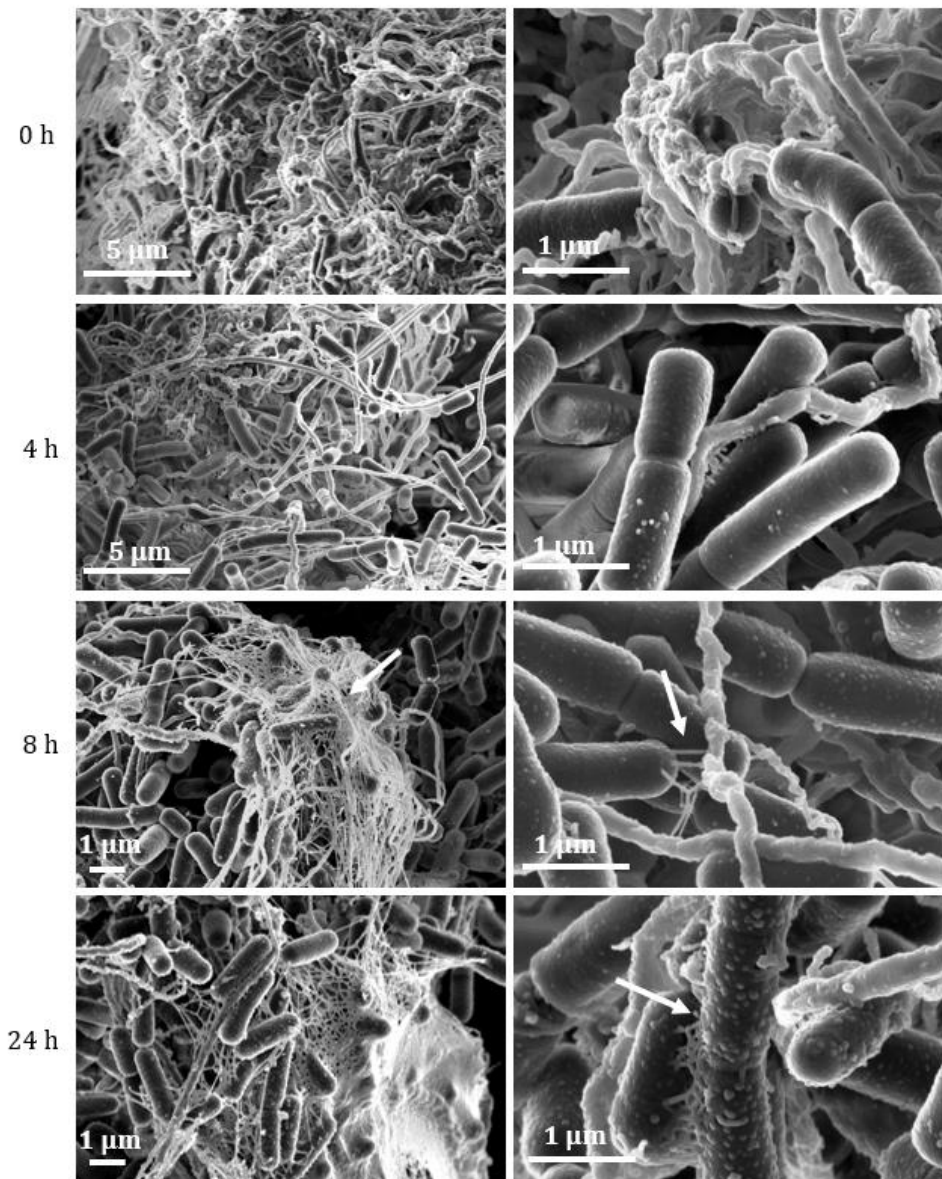


Figure 7. SEM micrographs confirming the proliferation of *Lf* in the presence of collagen and in optimal growing conditions, at different incubation times. The material obtained after incubation in MRS is the col-*Lf*. Arrows indicate the EPS.

The amount of EPS in the biocomposites were quantified by a standard sugar test. Values of 98 and 93.3 mg per gram of collagen were obtained for col-*Lf* and col-*La*, respectively. Interestingly, the initial materials obtained by incubating probiotics and collagen in PBS contained much lower sugar levels (10 and 18.6 mg g⁻¹, respectively). The drastic increase of sugar in the final biocomposites col-*Lf* and col-*La* is certainly due to the biofilm formation in the optimum MRS medium, in agreement with SEM images (Figure 8).

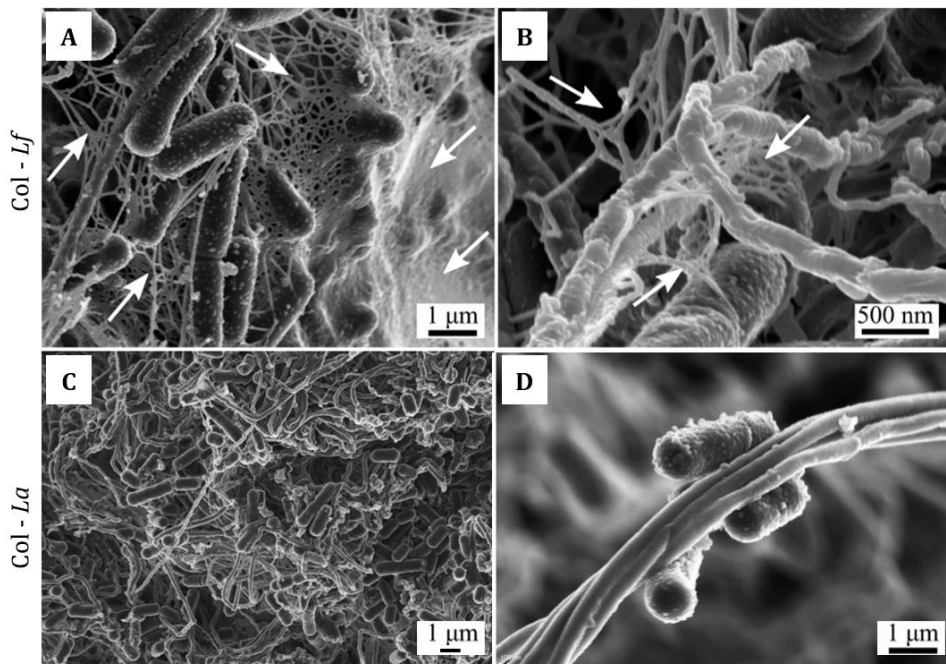


Figure 8. SEM micrographs of collagen assembled in the presence of *Lf* (A, B) or *La* (C, D) and incubated in MRS for 24 h (col-*Lf* and col-*La*). Arrows indicate the EPS.

The biocomposite col-*Lf* was further characterized at the macroscale by Fourier transform infrared spectroscopy (FTIR) and thermogravimetric analysis (TGA), and at the molecular scale by synchrotron X-ray wide-angle total scattering (WAXTS) (Figure 9). FTIR spectra and TGA of col-*Lf* show the main fingerprints of collagen fibers along with some signals assignable to the presence of bacteria (Figure 9a,b). WAXTS patterns of collagen and col-*Lf*

were similar (Figure 9c) with a broad peak centered at $ca. q = 13.25 \text{ nm}^{-1}$ due to the diffuse scattering of the collagen fibers. The Bragg peak at $q = 5.46 \text{ nm}^{-1}$ corresponds to the equatorial molecule-molecule averaged separation (i.e., the intermolecular lateral spacing) of the collagen triple-helix. This peak results in a d -spacing of 1.15 nm (inset, Figure 9c), which is in good agreement with the corresponding d -spacing of collagen in dry non-mineralized biological tissues^{28,29} and confirms that bacteria do not affect the macromolecular assembly of collagen fibers.

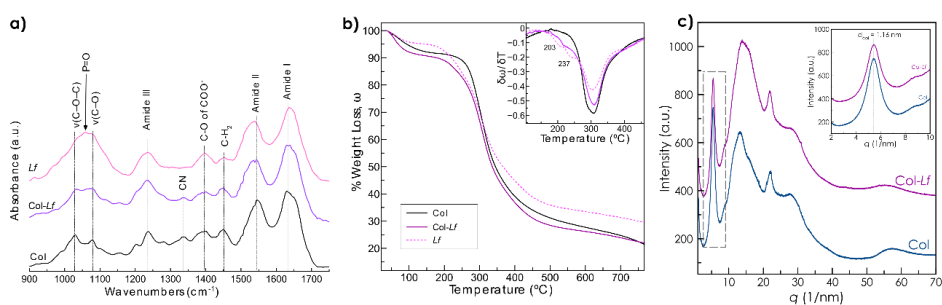


Figure 9. FTIR spectra **(a)** of collagen (Col), bacteria (*Lf*) and col-*Lf*. Collagen matrix shows peaks at 1030 and 1078 cm^{-1} corresponding to the C-O stretch of the carbohydrate's groups ($\nu(\text{C-O})$) and broad absorptions bands centered at 1650, 1550 and 1240 cm^{-1} which arise from amides I, II and III, respectively. Similar features were observed in the FTIR spectrum of col-*Lf* biocomposites. **(b)** TGA curves of collagen (Col), bacteria (*Lf*) and col-*Lf*. The curves show loss of water between room temperature and 150 °C and the decomposition of collagen between 230 and 600 °C. The inset in **b** shows the corresponding derivative TGA curves (DTG curves). TGA/DTG analysis of col-*Lf* biocomposites in addition shows a weight loss between 180 and 240 °C, which arise from the decomposition of *Lf*. Both characterizations confirm the effective incorporation of the bacteria into the collagen scaffolds. **(c)** WAXTS patterns of col and col-*Lf*, being q the scattering vector amplitude (i.e., $q = 4\pi\sin\theta/\lambda$). The inset shows the Bragg diffraction peak corresponding to the collagen-collagen lateral packing ($d = 2\pi/q = 1.15 \text{ nm}$).

2.2. Viability of probiotics in the collagen scaffold

Standard live/dead test based on the fluorophores SYTO 9 (green)/propidium iodide (PI, red) demonstrated that *Lf* and *La* bacteria were alive in the col-*Lf* and col-*La* materials (Figure 10A,B and C,D, respectively). As it is evident from Figure 10, the majority of *Lf* and *La* probiotics remained alive (green), with only a few dead bacteria found (red). Furthermore, side-view images (sum of successive *xy* sections, upper images in Figure 10A,C) show that lactobacilli penetrated and invaded the entire collagen matrix to form unique hybrid biomaterials. Interestingly, magnified top-view confocal images (Figure 10B,D) show the alignment of bacteria along the collagen scaffold, suggesting the existence of specific recognition of the collagen by both probiotics.

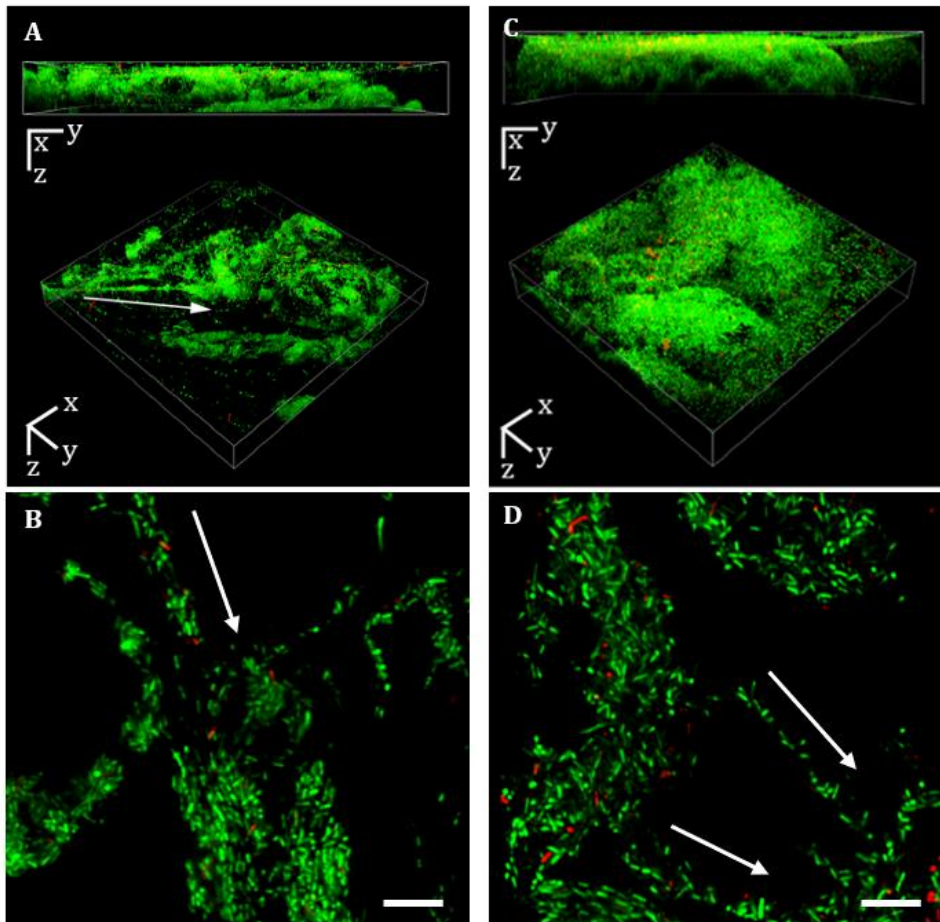


Figure 10. Confocal images of col-*Lf* (**A, B**) and col-*La* (**C, D**) stained with the SYTO9/PI (green/red) dyes. The 3D reconstructions dimensions are 318.20 μm x 318.20 μm x 38 μm for col-*Lf* (**A**), and 318.20 μm x 318.20 μm x 55 μm for col-*La* (**C**). They reveal that the bacteria penetrated and are fully integrated into the collagen matrix. The 2D images are composed by a z-section in each case, and show high viability and very few dead bacteria (red) in both biocomposites (**B** for *Lf*, and **D** for *La*). Scale bar = 10 μm . White arrows indicate how bacteria are specifically aligned along the collagen fibers. The images were obtained using the NIS Elements software.

2.3. Activity of probiotics in the collagen scaffold

The collagen matrix not merely acts as a hosting scaffold for probiotics, but also provides an additional protection during storage under harsh conditions (e.g., at 4 °C). Live bacteria excrete metabolites to the media and lactobacilli, in particular, excretes lactic acid, which regulates the pH at around 4 after incubation in optimal conditions. We measured the pH evolution to monitor the metabolic activity of the probiotics after storage under harsh conditions (4 °C). The pH evolution of fresh *Lf* and col-*Lf*, and *La* and col-*La* (without thermal treatment) and after storage at 4 °C during two, four, and eight weeks, as shown in Figure 11. Col-*Lf* induced a much higher drop of pH in MRS media in comparison to that of *Lf* (Figure 11A), supporting that probiotics embedded within the collagen matrix retain their metabolic activity and confirming that the collagen offers extra protection and enhances the shelf-life of probiotics. Similar behaviours were observed for the col-*La*/*La* pair after two and four weeks of storage at 4 °C. However, col-*La* stored for eight weeks showed much less activity (Figure 11B).

In addition, we assessed the metabolic activity of stored col-*Lf* and col-*La* at 4 °C using an assay developed by our team, that correlates the reductive capacity of bacteria to their metabolic activity, using an electrochromic polyoxometalate (POM)³⁰. Once reduced, POM exhibits an adsorption band in the UV-vis spectrum centered at 820 nm. The evolution of this absorption band after incubating aliquots from the supernatants of col-*Lf*/*Lf* and col-*La*/*La* cultures with an aqueous solution of POM was monitored (Figure 12A and B, respectively). The POM reduction activity in the MRS broth media is enhanced when the bacteria is embedded in the collagen matrix in comparison to those of free stored bacteria. Final values of col-*Lf* stored for two, four and eight weeks at 4 °C were similar to those for 'fresh' samples. Similar behaviour was observed for the col-*La*/*La* pair after two or eight weeks. Samples of col-*La* after eight weeks showed much

less capacity to reduce POM (Figure 12B), in agreement to their inferior ability to reduce pH noted above (Figure 11B).

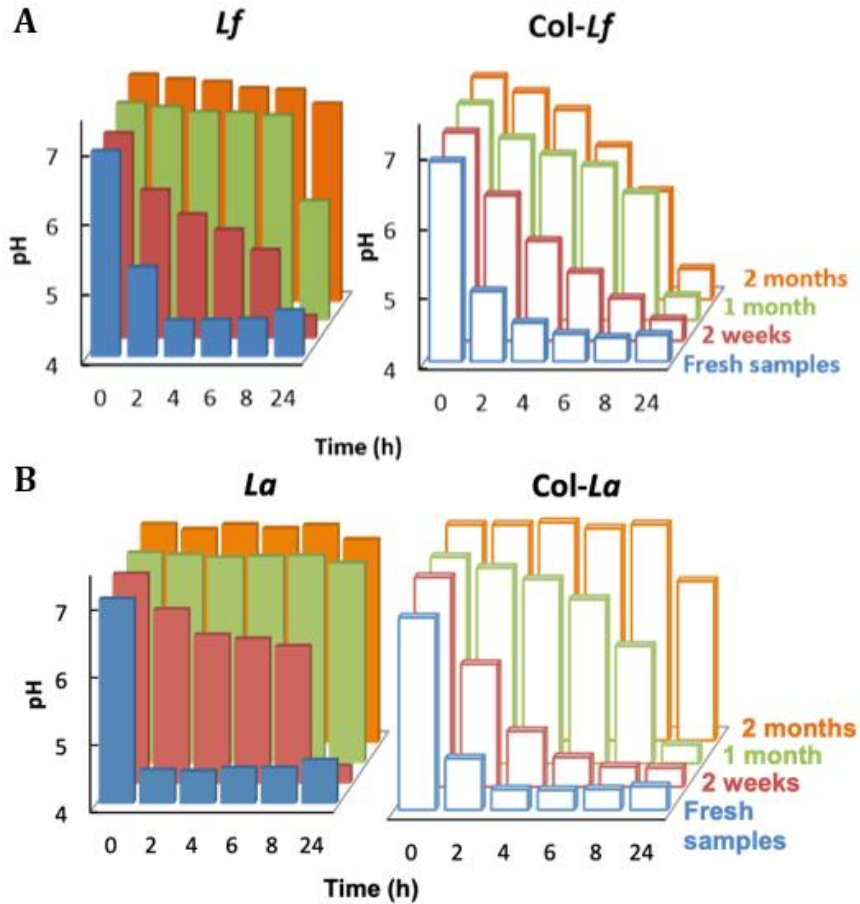


Figure 11. Bacterial activity after storage in harsh conditions (4 °C). **(A-B)** Time evolution of the pH in 1/10 diluted MRS media containing *Lf*, *La* (solid bars) or *col-Lf*, *col-La* (open bars) after storage for two (red), four (green) or eight weeks (orange) at 4 °C. The pH evolution of 'fresh' samples (blue) is also shown. Errors as standard deviations for these samples are all less than ± 0.2 . pH values for *col-Lf* vs. *Lf* and *col-La* vs. *La* were compared by Two-Way ANOVA followed by a Bonferroni's test resulting in p-values below 0.05 at each time point.

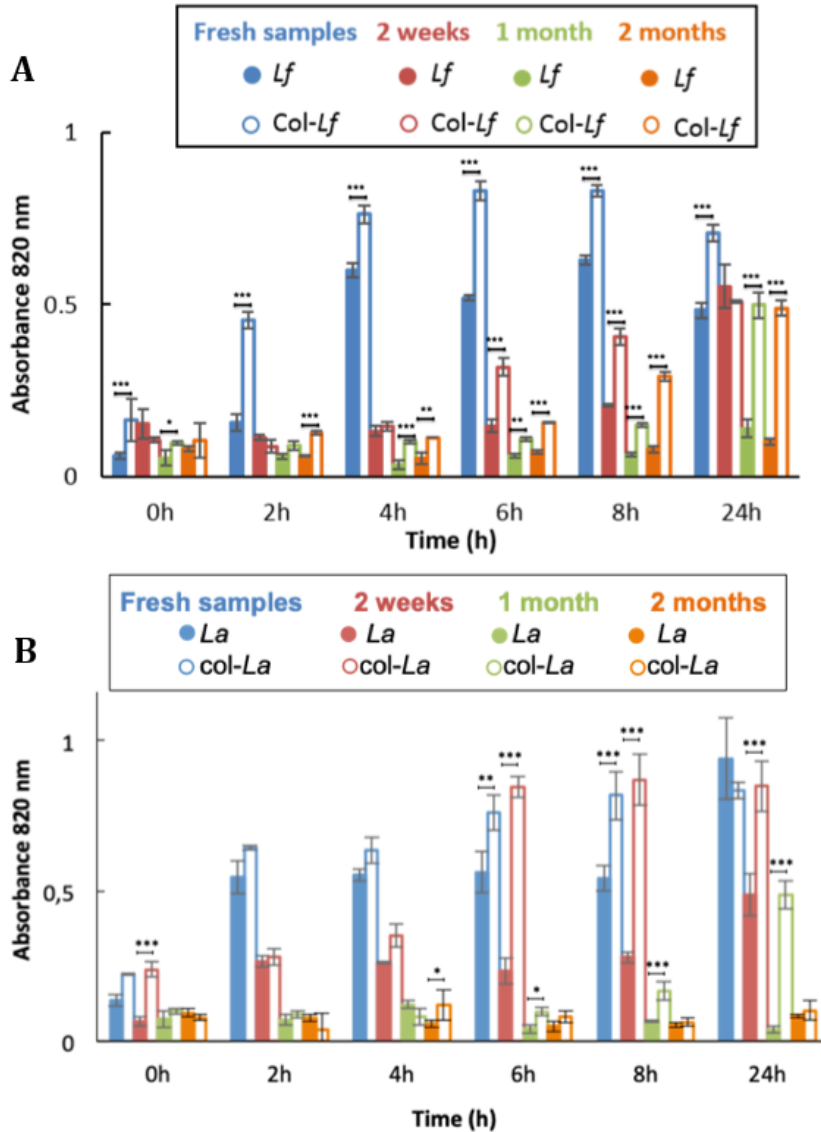


Figure 12. Time evolution of the POM reduction activity in 1/10 diluted MRS containing *Lf*, *La* (solid bars), or *col-Lf*, *col-La* (open bars) (**A** for *Lf* and **B** for *La*) after storage for two (red), four (green) or eight weeks (orange) at 4 °C. Evolution of the POM reduction activity of 'fresh' samples (blue) is also shown. The A^{820} drop observed for the fresh sample at 24h is due to the decrease of bacterial viability, and then its reducing capability, in the diluted MRS medium. Non-diluted MRS media cannot be used as it reduces POM. Statistical analysis was performed at each time point using Two-Way ANOVA followed by a Bonferroni's test (* $p < 0.05$; ** $p < 0.01$; *** $p < 0.001$).

These observations support that the collagen scaffold assists in maintaining the core cellular activity of probiotics, especially that of *Lf*, even after their exposure to extended harsh storage conditions. The retention of high metabolic and cellular activities is a critical parameter for the successful use of probiotics in antibiotic-free therapies.

2.4. The biocomposites col-*Lf* and col-*La* for BV therapy. Adhesion and activity

The adhesion of lactobacilli to the vaginal mucosa is of paramount relevance to efficiently treat BV with probiotics. Indeed, if a biomaterial containing highly proliferating probiotics does not adequately adhere to the vaginal mucosa, it would not offer much value for BV therapy. The adhesion capacity of col-*Lf*/*Lf* and col-*La*/*La* was evaluated with porcine mucin, which are heavily glycosylated proteins produced by epithelial tissues. This test is a well-established adhesion model^{31,32}. To assess the density of bacteria adhered to mucin in the wells, and after eliminate the unbounded bacteria, a fixing step at 60 °C was performed before the staining with crystal violet. This dye binds to the cell wall, and is used typically in the Gram's staining. After redissolution of the dye in citrate buffer, absorbance at 590 nm was measured. As shown in Figure 13A, the adhesion of col-*Lf* to mucin was sensibly higher than that of *Lf*, supporting the ability of collagen to enhance the adhesion of entrapped probiotics. The col-*La* formulation also exhibited a higher adhesion to mucin than the *La* probiotic alone (Figure 13B). On comparison of the adhesion of col-*Lf* and col-*La* to mucin, a higher signal corresponding to crystal violet was observed for col-*Lf*. This is likely due to the higher CFU value of col-*Lf* per mg of collagen in comparison to that of col-*La*, as discussed above.

The typical adhesion model also includes a treatment with bovine serum albumin (BSA) after the immobilization of mucin, in order to block

the remaining free sites of the protein-sensitive well plates after mucin immobilization. The experiments using BSA showed no significant difference to that of the corresponding experiments without BSA (Figure 13A and B for col-*Lf*/*Lf* and col-*La*/*La*, respectively). This confirms that the observed increase of absorbance is not due to the adsorption of collagen on the protein-binding plates, but to the adhesion of col-*Lf* and col-*La* on mucin.

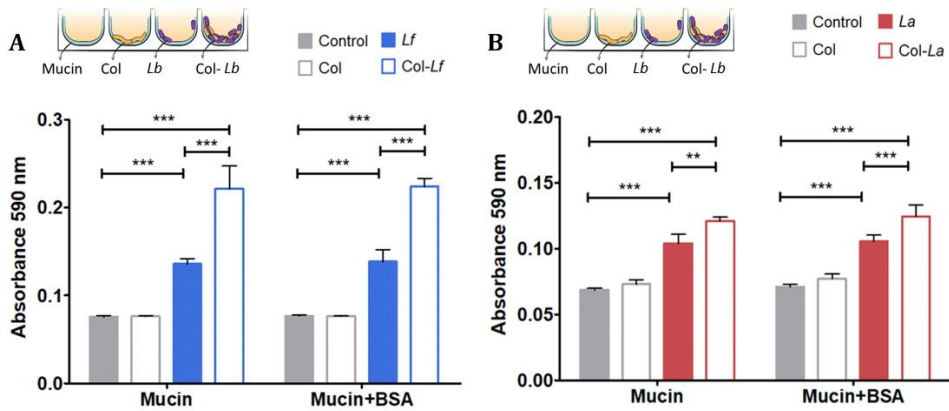


Figure 13. Schematic representations of the adhesion experiments are shown in upper panels. Evaluation of the adhesion of *Lf* (solid blue bar) and col-*Lf* (open blue bar) **(A)**, and *La* (solid red bar) and col-*La* (open red bar) **(B)** to immobilized porcine mucin. Absorbance at 590 nm correlates with the density of bacteria adhered to mucin. Absorbance values of controls (Mucin and Mucin + Col) are also included. Results while blocking with BSA (Mucin + BSA) or not (Mucin) are showed. Statistical analysis was performed using One-Way ANOVA followed by a Bonferroni's test (** $p < 0.01$; *** $p < 0.001$).

A decisive step to confirm the functionality of col-*Lf* and col-*La* for BV therapy is their capacity to restore the healthy conditions from a simulant BV fluid pH 5.0. As noted from Figure 14, both col-*Lf* and col-*La* were able to shift the pH of the BV medium to that of healthy conditions, pH 4. Metronidazole, the genuine antibiotic used in the treatment of BV, was unable to drop the pH of the simulated-BV medium, even at a high dose.

These results point out that, even if the simulated BV media (pH 5) diffuses and contacts with probiotics, these did not lose their activity and were capable to restore the pH to the physiological value (pH 4). This pH shift is certainly due to the excretion of lactic acid by the probiotics, confirming that bacteria remain alive and active once entrapped into the collagen matrix, as discussed above. Interestingly, the drop of pH with *Lf* and *La* without collagen was much slower and did not reach the healthy value of 4.0 (Figure 14).

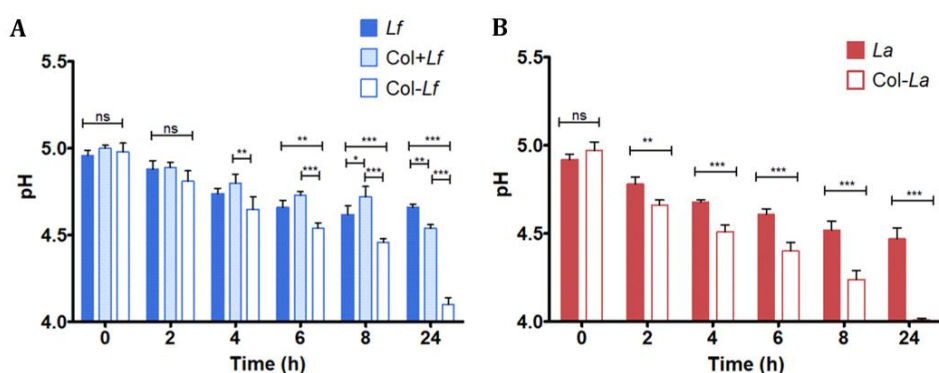


Figure 14. (A) pH evolution of simulated BV fluid (initial pH 5) in the presence of *Lf*, a mixture of collagen and *Lf* (col+*Lf*), and col-*Lf*. (B) pH evolution of simulated BV fluid in the presence of *La* and col-*La*. Statistical analysis was performed at each time point using Two-Way ANOVA followed by a Bonferroni's test (* p<0.05; ** p<0.01; *** p<0.001).

Two observations are worth highlighting from these results: *i*) the two materials, col-*Lf* and col-*La*, were capable of shifting the pH from the unhealthy BV medium (pH 5) to the healthy vaginal conditions (pH 4); and *ii*) the ability to reduce the pH of col-*Lf* and col-*La* is higher than those of *Lf* or *La*. Furthermore, we have shown that the capacity of probiotics to overcome the hostile BV medium and restore the physiological pH requires that the entrapment of probiotics within the collagen scaffold. In fact, when we tested a mixture of collagen and probiotics, instead of the biocomposites

col-*Lf*, the pH was not totally restored (Figure 14A). The mixture of the independent components failed to reach the physiological pH.

3. Conclusions

We have developed a new class of biomaterial-based formulation for BV therapy consisting of collagen as a cytocompatible matrix for effectively entrapping probiotic bacteria in a simple one-step synthesis. The high promise of this approach is shown through entrapping two BV-relevant probiotics, *Lactobacillus fermentum* and *Lactobacillus acidophilus*. Other probiotics may also be easily entrapped following the same procedure. Once *L. fermentum* and *L. acidophilus* are entrapped in the collagen fiber network, they remain alive, proliferate and show enhanced metabolic activity.

These entrapped probiotics (col-*Lf* and col-*La*) are capable of acclimatizing and proliferating in a hostile BV environment, whereas the respective non-entrapped bacteria, *Lf* and *La*, do not show credible performance. Through proliferation under BV conditions, these entrapped probiotics are able to restore the pH of the BV medium (pH 5) to a healthy pH of around 4. The restoration of healthy pH conditions should consequently promote further proliferation and activity of healthy vaginal microbiota via suppressing unhealthy bacteria.

In addition to the stability that the collagen matrix confers to the entrapped probiotics, col-*Lf* and col-*La* exhibit excellent adhesion to mucin, sensibly higher than those of *Lf* and *La*.

The combination of these properties makes these biomaterials ideal candidates for the treatment of BV, as they overcome the two critical limitations of the current probiotic-based therapies: high adhesion to the vaginal mucosa and protection of the probiotics in the hostile BV environment

4. Materials and methods

Reagents, bacteria sources and collagen

High purity reagents were purchased from Sigma-Aldrich. All solutions were prepared with ultrapure deionized water (18 M Ω ·cm). *Lactobacillus fermentum* (*Lf*, CECT5716) powder was obtained from Biosearch Life S.A. *Lactobacillus acidophilus* (*La*, CECT903, Moro 1900) was purchased from CECT (Colección Española de Cultivos Tipo, Spain). De Man, Rogosa and Sharpe medium (MRS) was purchased from Thermo Scientific. Type I collagen was extracted from equine tendon using the standardized manufacturing method of OPOCRIN S.p.A. (Corlo di Formigine, Modena, Italy)³³.

Entrapment of lactobacilli in the collagen matrix and preparation of the col-*Lf* and col-*La* biocomposites

La and *Lf* were separately inoculated in 100 mL of MRS broth and incubated for 24 h at 37 °C under continuous stirring (180 rpm). Subsequently, bacteria were collected by centrifugation (10000 g, 5 minutes), washed with saline solution (0.9% NaCl in water) and re-suspended in phosphate buffered saline (PBS, pH 7.4) to obtain a bacterial suspension with 2·10⁹ Colony Forming Unit (CFU) mL⁻¹. Then, 3 mL of bacteria suspension was mixed with 1 mL of collagen solution (1.5 mg mL⁻¹, pH 3.0) triggering to the formation of a 3D matrix of self-assembled collagen fibers in the presence of the probiotic. The collagen matrices with the entrapped bacteria were maintained for 30 minutes at 37 °C under continuous stirring (180 rpm) and then, washed with 10 mL of saline solution (0.9% NaCl in water) to remove the non-entrapped bacteria.

The collagen matrices with the entrapped bacteria were then incubated in 10 mL of MRS broth for 6 h at 37 °C in anaerobic conditions. The resulting

materials, referred to as col-*Lf* and col-*La*, were washed with saline solution and stored until further *ex-situ* characterizations.

Characterization of collagen-probiotic biocomposites

Field Emission Scanning Electron Microscopy (FESEM). Collagen matrices (with and without probiotics), col-*La* and col-*Lf* biocomposites were fixed in 1 mL of cacodylate buffer (0.1 M, pH 7.4) containing 2.5% of glutaraldehyde at 4 °C for 24 h. Subsequently, samples were washed with cacodylate buffer three times for 30 min at 4 °C. The samples were stained with osmium tetroxide (OsO₄) solution (1% v/v) for 2 hours in the dark, being then repeatedly rinsed with Milli-Q water to remove the excess of OsO₄ solution. Samples were then dehydrated at room temperature with ethanol/water mixtures of 50%, 70%, 90% and 100% (v/v) for 20 min each, being the last concentration repeated three times and dried at the CO₂ critical point. Finally, dehydrated samples were mounted on aluminum stubs using a carbon tape, sputtered with a thin carbon film, and analyzed using a FESEM (Zeiss SUPRA40V) of the Centre for Scientific Instrumentation (University of Granada, CIC-UGR).

The size (width) distribution of each condition was obtained by measuring 100 fibers of different SEM micrographs with ImageJ software (version 1.48v; NIH, Bethesda, MD).

Stability and degradability under physiological conditions (PBS and 37 °C)

Collagen release experiments. A collagen matrix (~3 mg) was introduced in 1mL of PBS (pH 7.4) solution and maintained 24 hours at 37 °C. At 24 hours, the sample was centrifuged (4500 g, 15 minutes) and PBS medium was collected. Same protocol was followed for col-*Lf* matrix and *Lf*. UV-vis spectrum of the collected PBS medium was recorded from 200 to 400 nm to quantify the amount of collagen release according to the calibration curve carried out by measuring the absorbance (at 206 nm) of different collagen solutions (10, 20, 40, 60, 80 and 100 µg/mL).

Bacterial release from col-Lf. The release of *L. fermentum* from the collagen-bacteria material was further assayed in PBS by direct counting in a Neubauer chamber (BLAUBRAND®, Sigma). The col-Lf was prepared as described, washed with saline solution, and incubated in 10 mL of PBS at 37 °C with stirring (180 rpm) for 24 h. After 2, 4, 6, 8 and 24 h of incubation, 1 mL was collected from the vial and an appropriate volume was used for direct counting. The Neubauer chamber was observed through an iScope (Euromex) microscope, under a 40x objective. The results are expressed as percentage of CFU released.

Quantification of exopolysaccharides (EPS). The standard phenol-sulfuric method was used for EPS quantification³⁴. Samples were immersed in 1 mL of saline solution containing with 500 µL of phenol (5% in water), and 2.5 mL of sulfuric acid and maintained in a water bath at 30 °C for 20 min. Absorbance of each sample was measured at 490 nm. EPS concentration was determined using the absorption coefficients obtained from a calibration curve and expressed in mg of sugar per g of collagen. Calibration curves were performed using a mixture of dextran and levan, the most characteristics components of the EPS excreted by lactobacilli. Each sample was tested in triplicate.

Fourier-Transform Infrared (FTIR) spectroscopy. FTIR spectra were collected on a Bruker Tensor 27 spectrometer under Attenuated total reflection configuration with a resolution of 3 cm⁻¹ by accumulation of 100 scans covering the 4000 - 400 cm⁻¹ spectral range.

Thermogravimetry analyses (TGA). TGA were performed using a Mettler-Toledo TGA/DSC1 thermal balance (Mettler-Toledo International Inc., Switzerland) with a heating rate of 5 °C/min up to 900 °C in nitrogen flow.

Wide-Angle Synchrotron X-Ray Total Scattering (WAXTS). WAXTS data were collected on a 1.0 mm diameter glass capillary filled with either dry collagen or collagen/bacteria matrices at the X04SA-MS Beamline of the Swiss Light

Source (SLS) of the Paul Scherrer Institut (Villigen, Switzerland). The beam energy was set at 16 keV (operational wavelength, $\lambda = 0.77627 \text{ \AA}$). Data were collected with the aid of the position sensitive single-photon counting MYTHEN II detector³⁵. The samples were freeze-dried at -40 °C (LyoQuest, Telstar) overnight prior FTIR, TGA and WAXTS characterizations. WAXTS patterns are represented as $I(q)$ as a function of the scattering vector amplitude, $q = 4\pi\sin\theta/\lambda$, being θ the scattering angle and λ the wavelength of the X-ray beam.

Viability and activity of entrapped probiotics

Live-dead viability assays by confocal laser scanning microscopy (CLSM). Bacterial viability in col-*Lf* and col-*La* were qualitatively evaluated with BacLight™ Bacterial Viability kit (Thermo-Fisher) following manufacturer's instructions. This assay consists in combining membrane impermeable DNA-binding stain, i.e., propidium iodide (PI), with membrane-permeable DNA-binding counterstain, SYTO 9, staining dead and live and dead bacteria, respectively. Confocal laser scanning microscopy (CSLM) images were collected with a Nikon Eclipse Ti-E A1 microscope equipped with 60x oil immersion objective. Images were analyzed with NIS Elements software. For acquiring SYTO 9 signals, 488 nm laser and 505–550 nm emission filter were used. For PI, 561 nm laser and 575 nm long-pass emission filter were used. The reconstruction of the three-dimensional image was obtained with 39 z-sections for col-*Lf* and 56 z-sections for col-*La*.

Bacteria activity of the biocomposites after storage at 4 °C. Collagen-probiotic biocomposite and the corresponding controls (naked probiotics) were stored at 4 °C for 2 weeks, 1 month and 2 months. After this time, samples and controls were separately added to 10 mL of MRS broth media and incubated at 37 °C and 180 rpm for 1 hour. Then, all samples were washed twice (3000 g, 5 min) with saline solution (0.9% NaCl in water). Subsequently, 10 mL of 1/10 diluted MRS broth media were added and

incubated at 37 °C and 180 rpm. 1/10 diluted MRS broth was used to avoid auto-reducing ability of non-diluted MRS broth. Aliquots of 1 mL were sequentially collected from each of the cultures' supernatants at scheduled times: 0, 2, 4, 6, 8 and 24 h. Aliquots were centrifuged (3000 g, 5 min) to remove any residual bacteria. The fermentation activity of the encapsulated living materials and the corresponding controls were monitored by pH measurements. To confirm the higher viability of collagen bacteria systems with respect to non-entrapped bacteria, we applied a procedure developed by us consisting on correlating the bacterial proliferation to its reductive capacity against the electrochromic polyoxometalate (POM), $[P_2MoV_{18}O_{62}]^{6-}$ ³⁶. 190 µL of each aliquot were added to a well containing 10 µL of a 10 mM solution of POM. Samples were left in dark at room temperature. Then, they were irradiated with UV light (365 nm) for 10 minutes and then the absorbance was measured in a Tecan's NanoQuant plate reader. Same experiments were performed on materials stored at room temperature (fresh samples). In addition, controls of free collagen were used to confirm that this material itself is not able to decrease pH or reduce POM. Each aliquot was tested in triplicate.

Bacterial adhesion and activity of col-Lf and col-La for BV treatment

In vitro assay of bacterial adhesion. The adhesion of col-probiotics and probiotics was assayed according to the method previously reported with slight modifications^{31,37}. In brief, the wells of Maxisorp plates (Nunc, Roskilde, Denmark) were incubated overnight at 4 °C with 100 µL of a 5 mg mL⁻¹ solution of porcine mucin (Sigma-Aldrich) in PBS pH 7.4. After immobilization, wells were washed three times with PBS and blocked with 2% BSA in PBS for 1 h. Bacterial pellets from 5 mL fractions of bacterial culture were collected by centrifugation (6000 g, 5 minutes), washed three times with PBS and resuspended in 5 mL of PBS. Upon removal of the BSA solution and washing three times the wells with PBS, the bacterial

suspension ($100\ \mu\text{L}$, $10^8\ \text{CFU mL}^{-1}$) was added. In the case of collagen-bacteria matrix samples, $25\ \mu\text{L}$ of collagen ($50\ \text{mg mL}^{-1}$ in $0.1\ \text{M}$ acetic acid) were added. The plate was incubated with *Lf* or *La* on an orbital shaker at $180\ \text{rpm}$ for $2\ \text{h}$ at $37\ ^\circ\text{C}$. Non-adhered bacteria were removed by washing the wells three times with $100\ \mu\text{L}$ of PBS, and the samples were fixed at $60\ ^\circ\text{C}$ for $20\ \text{min}$. Afterwards, the fixed cells were stained with crystal violet ($100\ \mu\text{L}$ per well, 0.1% solution) for $45\ \text{min}$ at room temperature. Finally, the wells were washed twice with $150\ \mu\text{L}$ of PBS and the stain bound to the bacteria was dissolved in $50\ \mu\text{L}$ of citrate buffer ($\text{pH}\ 4.3$) for $1\ \text{h}$. The absorbance was measured at $590\ \text{nm}$ using the microtiter plate reader (NanoQuant). Results were expressed as the mean of triplicates with a total volume of $200\ \mu\text{L}$, after collecting four replicates of $50\ \mu\text{L}$ in one well. Controls consisted of mucin and mucin-collagen, and samples were mucin-*Lf*, mucin-*La*, mucin-col-*La* and mucin-col-*Lf*, blocked or not with BSA.

Bacterial activity in a simulant BV fluid. The collagen-probiotic samples and controls were separately added to $10\ \text{mL}$ of simulant BV fluid and incubated at $37\ ^\circ\text{C}$ and $180\ \text{rpm}$. $1\ \text{L}$ of BV fluid, prepared according to the protocol previously reported³⁸ with slight modifications, contains NaCl , $3.51\ \text{g}$; KOH , $1.40\ \text{g}$; $\text{Ca}(\text{OH})_2$, $0.222\ \text{g}$; bovine serum albumin, $0.018\ \text{g}$; urea, $0.4\ \text{g}$; glycerol, $0.16\ \text{g}$; glucose, $10\ \text{g}$; lactic acid, $2\ \text{g}$; and acetic acid, $1\ \text{g}$. The pH was of 5.00 . Aliquots of $1\ \text{mL}$ were sequentially collected from each of the cultures' supernatants at scheduled times: 0 , 2 , 4 , 6 , 8 and $24\ \text{h}$. Aliquots were centrifuged ($3000\ \text{g}$, $5\ \text{min}$) to remove any residual bacteria. The pH of the entrapped living materials and the corresponding controls was measured to demonstrate the capacity of restoring the pH of the media. Two experiments controls were performed: first, a positive control, which consisted of a mixture of assembled collagen with the bacterial suspension (*Lf*) and second, a saturated solution of the antibiotic metronidazole. The procedure for the first control was the same that used for collagen-probiotic samples. For the second control, metronidazole powder ($100\ \text{mg}$) was

directly added to 10 mL of simulant BV fluid and incubated at 37 °C. The concentration of the antibiotic was close to saturation (11 mg mL⁻¹)³⁹. The pH of the mixture was 5.20 ± 0.10 and kept constant for 24 h. Each experiment was tested in triplicate.

Statistics. Results are expressed as average ± standard deviation as error bars (N=3). Statistical comparisons were performed using one-way or two-way ANOVA followed by Bonferroni's post hoc test using GraphPad Prism software (version 6.0). Differences between data sets were considered significant at p < 0.05.

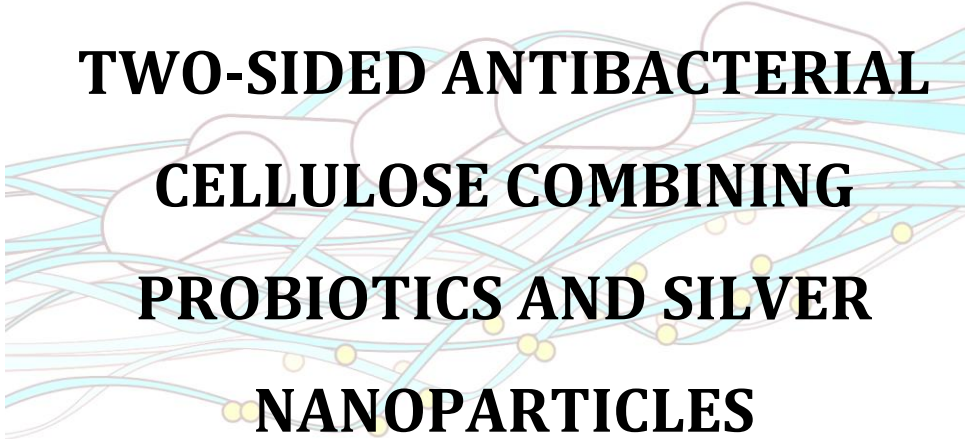
5. References

1. Onderdonk, A. B., Delaney, M. L. & Fichorova, R. N. The human microbiome during bacterial vaginosis. *Clin. Microbiol. Rev.* **29**, 223–238 (2016).
2. Alcaide, M. L. *et al.* Bacterial vaginosis is associated with loss of gamma delta T cells in the female reproductive tract in women in the Miami Women Interagency HIV Study (WIHS): A cross sectional study. *PLoS One* **11**, 1–14 (2016).
3. Aldunate, M. *et al.* Antimicrobial and immune modulatory effects of lactic acid and short chain fatty acids produced by vaginal microbiota associated with eubiosis and bacterial vaginosis. *Front. Physiol.* **6**, 1–23 (2015).
4. McGregor, James A. MD, CM Janice I. French, CNM, M. Bacterial Vaginosis in Pregnancy. *Obstet. Gynecol. Surv.* **55**, 1–19 (2000).
5. O'Hanlon, D. E., Moench, T. R. & Cone, R. A. Vaginal pH and microbicidal lactic acid when lactobacilli dominate the microbiota. *PLoS One* **8**, 1–8 (2013).
6. Newark, N. J. FDA Approves Symbiomix Therapeutics' Solosec™ (secnidazole) Oral Granules for the Treatment of Bacterial Vaginosis in Adult Women. *Symbiomix Therapeutics* (2017). Available at: <https://www.businesswire.com/news/home/20170918005768/en/>. (Accessed: 16th February 2022)
7. Amsel, R. *et al.* Nonspecific vaginitis. Diagnostic criteria and microbial and epidemiologic associations. *Am. J. Med.* **74**, 14–22 (1983).
8. Hegde, N., Velingkar, V. & Prabhakar, B. An Update on Design and Pharmacology of Dendritic Poly(l-lysine). *Int. J. Pept. Res. Ther.* **25**, 1539–1562 (2018).
9. Bradshaw, C. S. *et al.* High Recurrence Rates of Bacterial Vaginosis over the Course of 12 Months after Oral Metronidazole Therapy and Factors Associated with Recurrence. *J. Infect. Dis.* **193**, 1478–1486 (2006).
10. Bradshaw, C. S. & Sobel, J. D. Current Treatment of Bacterial Vaginosis-Limitations and Need for Innovation. *J. Infect. Dis.* **214**, S14–S20 (2016).
11. Richter, M. F. *et al.* Predictive compound accumulation rules yield a broad-spectrum antibiotic. *Nature* **545**, 299–304 (2017).
12. Seiple, I. B. *et al.* A platform for the discovery of new macrolide antibiotics. *Nature* **533**, 338–345 (2016).

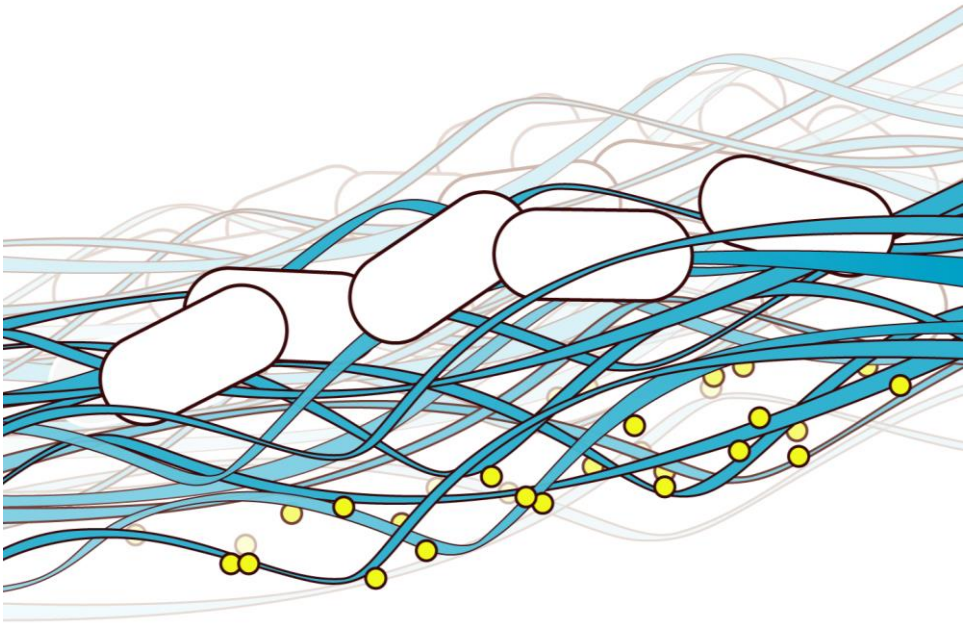
13. Li, Z. *et al.* Biofilm-Inspired Encapsulation of Probiotics for the Treatment of Complex Infections. *Adv. Mater.* **30**, 1803925 (2018).
14. Li, X. *et al.* Supramolecular Antibacterial Materials for Combatting Antibiotic Resistance. *Adv. Mater.* **31**, 1–28 (2019).
15. Vuotto, C., Longo, F. & Donelli, G. Probiotics to counteract biofilm-associated infections: promising and conflicting data. *Int. J. Oral Sci.* **6**, 189 (2014).
16. Schuyler, J. A. *et al.* Identification of intrinsically metronidazole-resistant clades of *Gardnerella vaginalis*. *Diagn. Microbiol. Infect. Dis.* **84**, 1–3 (2016).
17. Mogha, K. V. & Prajapati, J. B. Probiotics for treating bacterial vaginosis. *Rev. Med. Microbiol.* **27**, 87–94 (2016).
18. Abdelhamid, A. G., El-Masry, S. S. & El-Dougdoug, N. K. Probiotic *Lactobacillus* and *Bifidobacterium* strains possess safety characteristics, antiviral activities and host adherence factors revealed by genome mining. *EPMA J.* **10**, 337–350 (2019).
19. Elena, F. Phenotypic surface properties (aggregation , adhesion and biofilm formation) and presence of related genes in beneficial vaginal lactobacilli. 1761–1772 (2014). doi:10.1111/jam.12642
20. Lorca, G., Torino, M. I., Font De Valdez, G. & Ljungh, Å. Lactobacilli express cell surface proteins which mediate binding of immobilized collagen and fibronectin. *FEMS Microbiol. Lett.* **206**, 31–37 (2002).
21. Lin, K. *et al.* Advanced Collagen-Based Biomaterials for Regenerative Biomedicine. *Adv. Funct. Mater.* **29**, 1–16 (2019).
22. Lausch, A. J., Chong, L. C., Uludag, H. & Sone, E. D. Multiphasic Collagen Scaffolds for Engineered Tissue Interfaces. *Adv. Funct. Mater.* **28**, 1–9 (2018).
23. Ramírez Rodríguez, G., Patrício, T. & Delgado López, J. *Natural polymers for bone repair. Bone Repair Biomaterials* (Elsevier Ltd, 2019). doi:10.1016/b978-0-08-102451-5.00008-1
24. Stevens, M. M. Biomaterials for bone tissue engineering. *Mater. Today* **11**, 18–25 (2008).
25. Sorushanova, A. *et al.* The Collagen Suprafamily: From Biosynthesis to Advanced Biomaterial Development. *Adv. Mater.* **31**, 1–39 (2019).
26. Wang, Y. *et al.* The predominant role of collagen in the nucleation, growth, structure and orientation of bone apatite. *Nat. Mater.* **11**, 724–733 (2012).

27. Ramírez-Rodríguez, G. B., Iafisco, M., Tampieri, A., Gómez-Morales, J. & Delgado-López, J. M. pH-responsive collagen fibrillogenesis in confined droplets induced by vapour diffusion. *J. Mater. Sci. Mater. Med.* **25**, 2305–2312 (2014).
28. Fratzl, P., Fratzl-Zelman, N. & Klaushofer, K. Collagen packing and mineralization. An x-ray scattering investigation of turkey leg tendon. *Biophys. J.* **64**, 260–266 (1993).
29. Delgado-López, J. M. *et al.* The synergic role of collagen and citrate in stabilizing amorphous calcium phosphate precursors with platy morphology. *Acta Biomater.* **49**, 555–562 (2017).
30. González, A., Gálvez, N., Clemente-León, M. & Dominguez-Vera, J. M. Electrochromic polyoxometalate material as a sensor of bacterial activity. *Chem. Commun.* **51**, 10119–10122 (2015).
31. Miljkovic, M. *et al.* AggLb is the largest cell-aggregation factor from *Lactobacillus paracasei* subsp. *paracasei* bgnj1-64, functions in collagen adhesion, and pathogen exclusion in vitro. *PLoS One* **10**, 1–19 (2015).
32. Olivares, M., Díaz-Ropero, M. P., Martín, R., Rodríguez, J. M. & Xaus, J. Antimicrobial potential of four *Lactobacillus* strains isolated from breast milk. *J. Appl. Microbiol.* **101**, 72–79 (2006).
33. Tampieri, A. *et al.* Biologically inspired synthesis of bone-like composite: Self-assembled collagen fibers/hydroxyapatite nanocrystals. *J. Biomed. Mater. Res. - Part A* **67**, 618–625 (2003).
34. Dubois, M., Gilles, K. A., Hamilton, J. K., Rebers, P. A. & Smith, F. Colorimetric Method for Determination of Sugars and Related Substances. *Anal. Chem.* **28**, 350–356 (1956).
35. Bergamaschi, A. *et al.* The MYTHEN detector for X-ray powder diffraction experiments at the Swiss Light Source. *J. Synchrotron Radiat.* **17**, 653–668 (2010).
36. González, A., Gálvez, N., Clemente-León, M. & Dominguez-Vera, J. M. Electrochromic polyoxometalate material as a sensor of bacterial activity. *Chem. Commun.* **51**, 10119–10122 (2015).
37. Olivares, M., Díaz-Ropero, M. P., Martín, R., Rodríguez, J. M. & Xaus, J. Antimicrobial potential of four *Lactobacillus* strains isolated from breast milk. *J. Appl. Microbiol.* **101**, 72–79 (2006).
38. Owen, D. H. & Katz, D. F. A vaginal fluid simulant. *Contraception* **59**, 91–95 (1999).
39. Talkowsky, S. H. & He, Y. *Handbook of Aqueous Solubility Data*. (CRC Press, Boca Raton, FL 2003). p. 282

CHAPTER 3.



TWO-SIDED ANTIBACTERIAL CELLULOSE COMBINING PROBIOTICS AND SILVER NANOPARTICLES



1. Introduction

The dramatic increase of antibiotic-resistant bacteria is one of the biggest threats to global health¹. The development of innovative antibiotic-free antibacterials is, in fact, one of the most important challenges of material scientists^{2,3}. Two promising alternatives to antibiotics are the use of silver nanoparticles (AgNPs) and probiotics. AgNPs have received much attention as antibacterial agents⁴⁻⁸. Indeed, they are currently being used as antibacterials in medical devices, textiles, cosmetics, and food packaging⁹⁻¹². AgNPs present antimicrobial activity as a result of the slow oxidation of Ag⁰ to Ag⁺ by air oxygen. Ag⁺ interacts with Cys-rich proteins and perturbs their functionality, provokes RNA and DNA damages, and induces the production of highly toxic reactive oxygen species (ROS)^{8,13}. Nevertheless, it should be noted that some strains have developed resistance to AgNPs¹⁴.

Probiotics are live microorganisms known to provide health benefits to the host, either by restoring the natural balance of bacteria in the microbiota¹⁵, by excreting antipathogenic compounds¹⁶ or by restoring the pH of infected media to healthy values, as it occurs, for instance, in the therapy of bacterial vaginosis¹⁷.

Each antibacterial usually covers a specific group of microbes. Combining several antibacterial agents in a single biomaterial has, therefore, the advantage to broaden the activity spectrum, increase its efficiency and be effective against complex bacterial infections in which more than one pathogen is involved.

Taking all these aspects into account, we have explored the possibility of combining living probiotics and AgNPs in a matrix as bacterial cellulose (BC) to produce a new hybrid biomaterial with enhanced antibacterial properties. In principle, this approach has the drawback that probiotic bacteria, in particular *Lactobacilli*, are highly susceptible to AgNPs¹⁸. To overcome this issue, we have developed a two-sided material, in

which AgNPs and the probiotic *Lactobacillus fermentum* (*Lf*) are located on opposite BC faces, thus *Lf* being protected from the antibacterial AgNPs. In addition, the acidic environment caused by the excretion of lactic acid by *Lf* promotes Ag dissolution and ROS overproduction, thus increasing the bactericidal effect of AgNPs¹⁸.

BC is a polymer of glucose made by some aerobic bacteria that has been widely studied for biomedical applications and, in particular, as a wound-dressing material¹⁹⁻²¹. BC is chemically pure, biocompatible, and due to its higher surface area, it exhibits extraordinary efficacy to absorb wound exudates without adhering to the wound surface, thereby avoiding tissue damage upon removal.

However, BC itself has no activity against bacterial infection, which is a recurrent issue affecting chronic or acute wounds. Most of the strategies used to confer antibacterial properties to BC are based in the covalent or non-covalent incorporation of antibacterial polymers and peptides to the glucose fiber network^{22,23}. However, the chemical modification by covalent attachment of molecules to BC is difficult due to the poor solubility of BC, which makes necessary the employ of organic solvents, elevated temperatures, and long reaction times, limiting its large-scale production. The non-covalent incorporation of active biomolecules is chemically easier, but due to the weak interaction between BC and these biomolecules, the resulting biomaterial potentially suffers from shedding.

A strategy to produce antibacterial BC-derivatives that circumvents the chemical functionalization of BC and does not exhibit shedding has been the incorporation of Ag and TiO₂ nanoparticles into BC^{24,25}. Roig-Sanchez *et al.* have recently reported that, in fact, layers of BC can be decorated step-by-step with different nanoparticles (Ag and TiO₂, among others), thus creating a *mille-feuille* concept of multifunctional BC²⁴. On the other hand, we have

recently demonstrated that BC can incorporate a huge number of probiotics resulting in a living biomaterial with enhanced antibacterial activity²⁶.

2. Results and discussion

Taking advantages of these possibilities of BC, we have developed a BC derivative that combines two antibacterials with different mechanisms of action, AgNPs and living probiotics, *Lf*. We have used the step-by-step loading to host both antibacterials at opposite BC sides, thus obtaining a two-sided biomaterial (AgNP-BC-*Lf*) with a high density of alive and metabolically active probiotics on one surface and AgNPs on the opposite one, being probiotics preserved from the antibacterial AgNPs. No example of this type of antibacterial biomaterial has been reported so far.

Acetobacter xylinum (*Ax*) was used to obtain BC pellicles. Subsequently, probiotics and AgNPs were sequentially adsorbed on opposite faces of BC. First, one of the surfaces of BC was immersed in a probiotic culture (Step 1, Figure 1A). The adsorption of *Lf* on BC occurred very fast, and after a few hours, the number of loaded probiotics practically did not increase with incubation time. The resulting sample (BC-*Lf*) was repeatedly washed and then stained with the standard SYTO9/propidium iodide (PI) dyes to study the viability (live/dead) and allocation of probiotics within BC by confocal laser scanning microscopy (CLSM). As illustrated in Figure 2A and D, *Lf* only penetrated a few layers of BC. The dense fibril network does not allow the penetration of probiotics into the entire BC. The high density of live probiotics (green spots), points out that the transfer from the culture to the cellulose did not affect the probiotic viability.

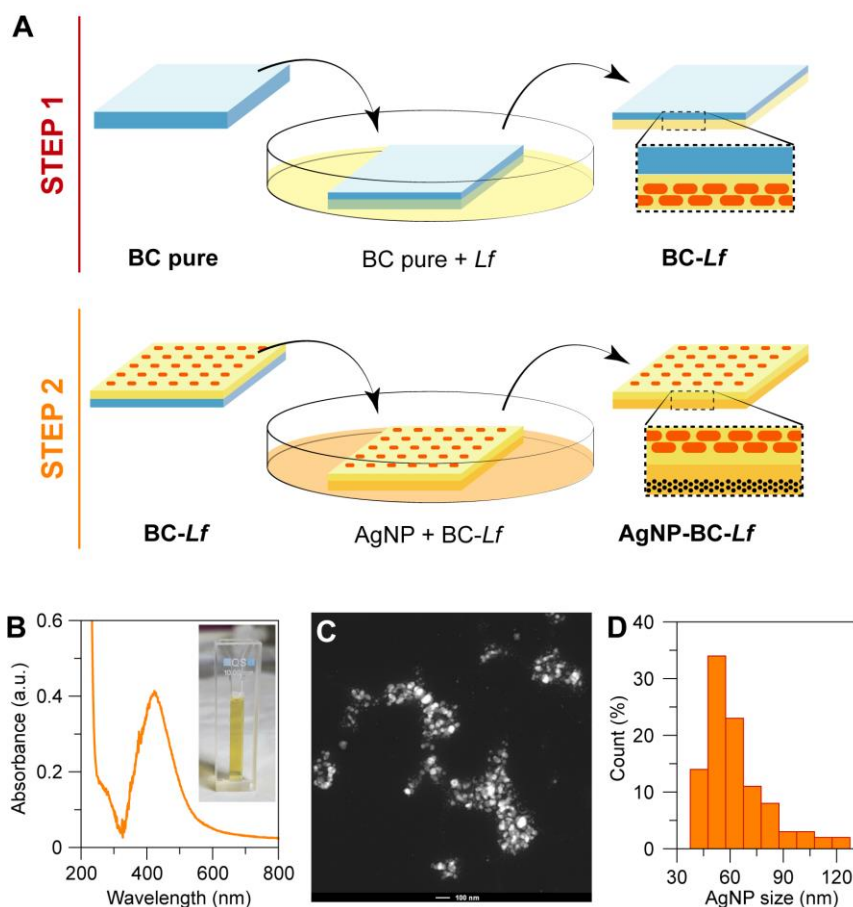


Figure 1. (A) Graphical representation of the experimental protocol used to obtain the two-sided BC. The first step involves the adsorption of probiotics followed by the impregnation of the opposite BC side with AgNPs. The resulting material is referred to as AgNPs-BC-Lf. **(B)** The UV-vis spectrum showed the expected absorbance band centered at 420 nm, in agreement with AgNPs with a mean diameter of 50 nm. The inset in B corresponds to a picture of an AgNPs solution. **(C)** HAADF-STEM micrograph of AgNPs (scale bar is 100 nm). **(D)** Diameter distribution of AgNPs (n = 100).

In a second step, the opposite surface, free of probiotics, was functionalized with AgNPs (Step 2, Figure 1A). AgNPs with average diameter of 50 nm (Figure 1B,C) were synthesized by the Turkevich method, using

citrate as a reducing and capping agent²⁷. A suite of materials with different contents of AgNPs was obtained by incubating BC-*Lf* in the AgNPs-containing solution at different times, ranging from 5 to 30 min. The resulting materials were stained with SYTO9/PI and visualized by CLSM (Figure 2). We found that the longer the incubation time, the higher the number of dead probiotics (red spots) in the opposite face to that in contact with AgNPs (Figure 2B, C). This result was expected since, while probiotics cannot diffuse through the BC network, AgNPs (and Ag⁺ ions) diffuse through the entire BC structure, contacting the probiotics and affecting their viability. In any case, the number of no viable probiotics (red spots) was always significantly lower than that of alive ones (green spots) in the time interval here explored (5–30 min).

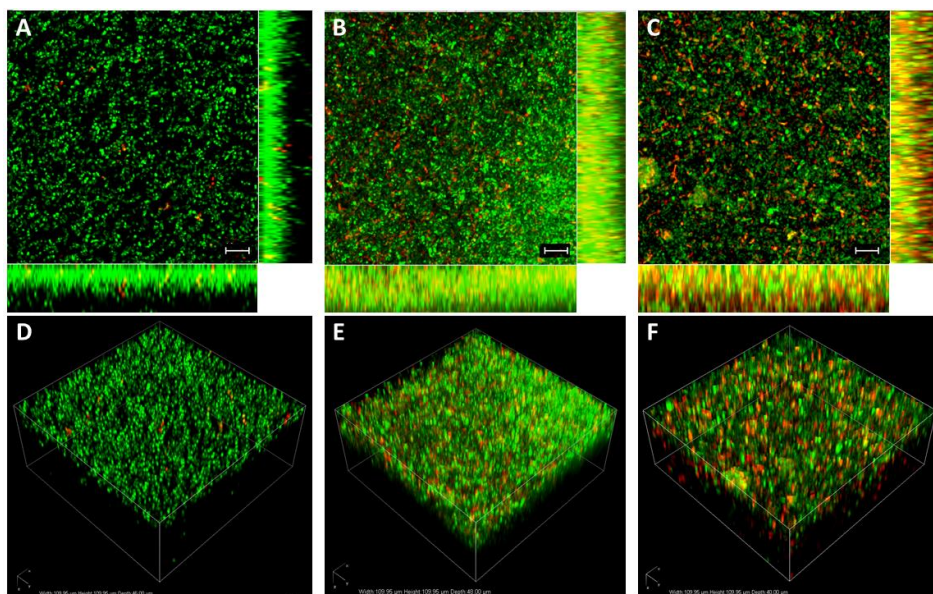


Figure 2. CLSM of BC-*Lf* at different incubation times in AgNPs solution. Samples were stained with SYTO9/PI dyes. The images are maximum intensity projections of 20 µm in-depth of **(A)** BC after *Lf* adsorption (BC-*Lf*), **(B)** BC-*Lf* after 15 min of incubation in AgNPs (AgNP-BC-*Lf*), and **(C)** BC-*Lf* after 30 min of incubation in AgNPs. Scale bars = 10 µm. **(D–F)** images are three-dimensional reconstructions of **(A–C)**, respectively.

The biomaterial containing the highest AgNPs concentration with null effect on the probiotic viability was obtained by incubating BC-*Lf* for 15 min in the AgNPs solution (Figure 2B, E). The incorporation level of *Lf* in the final biomaterial, AgNP-BC-*Lf*, was determined after sample digestion with cellulase (see Materials and methods), by counting CFUs in MRS-agar plates after 24 h of incubation (37 °C) in anaerobic conditions. A value of 2×10^9 CFUs/g ($\pm 8\%$) was obtained. Field-emission scanning electron microscopy (FESEM) images of AgNP-BC-*Lf* confirmed that, as expected, it consists of a two-sided material: one face showing a high density of *Lf* with its typical morphology (Figure 3A), while the opposite face contained AgNPs, entrapped in the BC fiber network (Figure 3B). It is interesting to note that FESEM images of AgNP-BC-*Lf* showed neither AgNPs on the probiotic-containing face nor probiotic on the AgNPs-containing one. This material was further used to study the antibacterial activity (*vide infra*). In contrast, the concomitant presence of probiotics and AgNPs was observed at the probiotic-containing side of the sample obtained at longer incubation times (>15 min) (Figure 3C). The antibacterial activity of the two AgNP-BC-*Lf* surfaces, containing either probiotics or AgNPs, was assessed against *PA*, an opportunistic pathogen responsible of a broad range of skin infections. The activities were compared to those of the materials containing only one of the antibacterials (AgNP-BC or BC-*Lf*). As expected, BC exhibited no activity against *PA*, while AgNP-BC-*Lf*, AgNP-BC, and BC-*Lf* materials produced clear inhibition zones against this pathogen (Figure 4). Importantly, the bifunctional AgNP-BC-*Lf* was more active against *PA* than BC-*Lf* or AgNP-BC, independently of the face exposed to the pathogen (AgNP-BC-*Lf* or AgNP-BC-*Lf*, Figure 4). These results confirm the existence of an additive effect between the two antimicrobial faces.

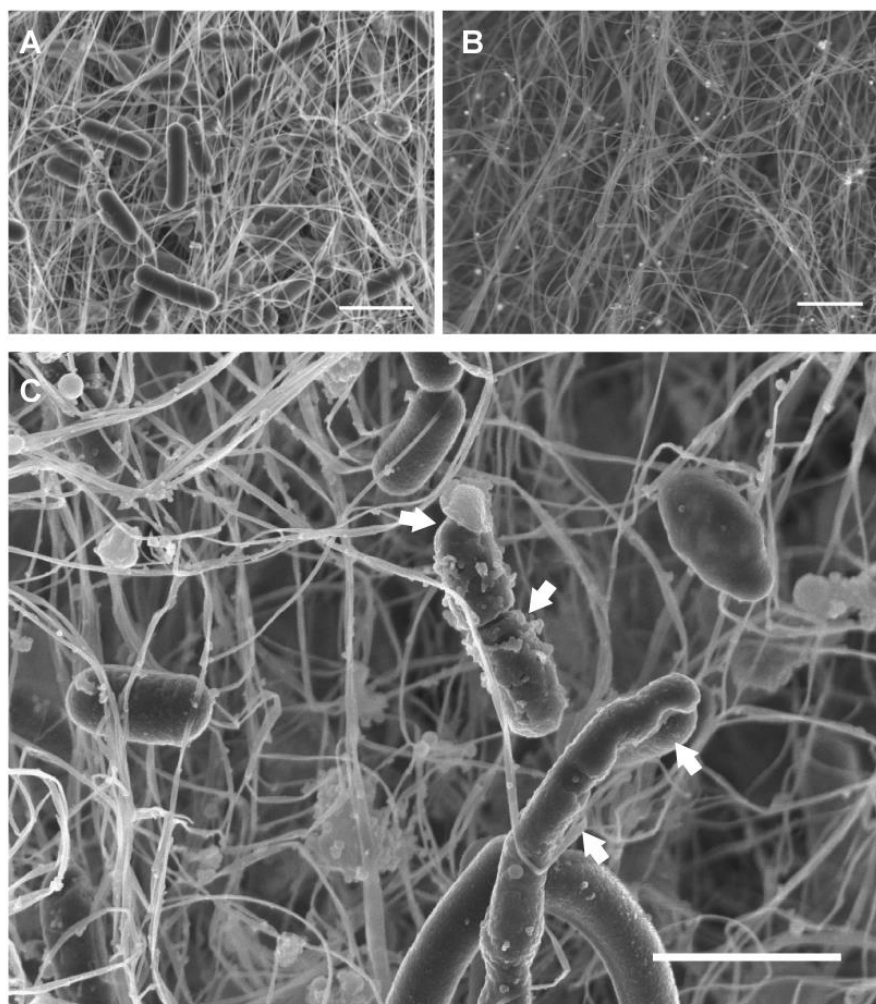


Figure 3. FESEM images of the two-sided biomaterials. **(A)** The side containing *Lf* exhibited the typical rod-like morphology of this bacterium. **(B)** BC side containing AgNPs. **(C)** *Lf*-functionalized BC surface, containing a higher amount of AgNPs (30 min of incubation in the AgNPs solution). Arrows show the cell wall damage. Scale bars: 2 μm .

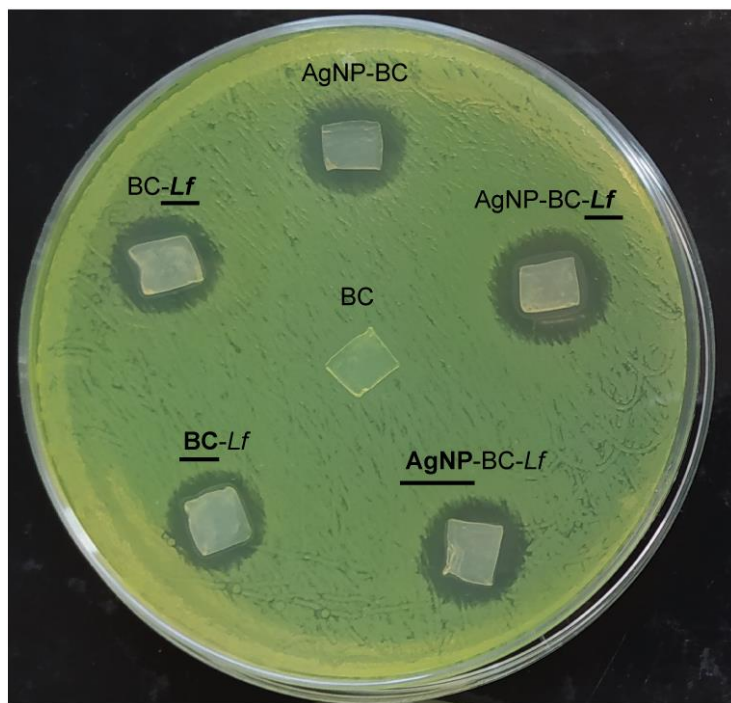


Figure 4. Inhibitory activity of the composite materials against *PA*. Inhibition zones of BC, AgNP-BC, BC-*Lf* and AgNP-BC-*Lf*. The corresponding BC side in contact with agar is marked in bold and underlined. The diameter of the Petri dish is 9 cm.

To understand this additive effect, it is interesting to note that the activity of the *Lf*-side of BC-*Lf* against *PA* (**BC-*Lf*** in Figure 4) was only slightly higher than that of the probiotic-free face (**BC-*Lf*** in Figure 4). This finding suggests that the activity of BC-*Lf* is due to excreted species that diffuse through the BC structure and reach the pathogen media.

On the other hand, it is interesting to note that the antibacterial activity of AgNPBC-*Lf*, no matter its face, is really a sum of the two antibacterial components (AgNPs and *Lf*) (Table 1). The possible silver cations diffusion inside the biomaterial during the agar diffusion test, from AgNPs to *Lf*, and the consequent probiotic death, resulted low. In fact, the probiotic viability before and after the antibacterial test assays was close, with CFUs decreasing lower than 10% (see *Materials and Methods*).

Table 1. Area of the inhibition zones around the cellulosic samples in the antimicrobial assays shown in Figure 4. Results are shown as means of three replicates \pm standard deviation (SD). Statistical analysis was carried out by the one-way ANOVA (Bonferroni's method). Letters indicate significant differences ($p < 0.05$) between samples. The BC side in direct contact with agar is indicated in bold and underline letters.

Muestra	Inhibition zones \pm SD (mm ²)
BC	0 \pm 0 a
AgNP-BC	89 \pm 2 b
BC- <u>Lf</u>	81 \pm 3 b
<u>BC</u> -Lf	80 \pm 2 b
AgNP-BC- <u>Lf</u>	137 \pm 9 c
<u>AgNP</u> -BC-Lf	110 \pm 10 c

3. Conclusions

A new concept of bifunctional BC, based on the combination of two antibacterial agents, i.e., probiotics (*Lf*) and AgNPs was here developed. The antibacterials were intentionally placed on opposite faces to avoid the killer effect of AgNPs on the probiotics. The antibacterial assays against *PA* pointed out that the activity of AgNP-BC-*Lf* is the result of an additive effect of both antibacterial components. This activity against *PA*, together with the extraordinary features of BC as a wound dressing, makes AgNP-BC-*Lf* an antibacterial with potential applications in skin infections without the use of antibiotics.

4. Materials and Methods

Reagents and Solutions. High-grade quality reagents were used as received from commercial suppliers. Aqueous solutions were prepared with ultrapure water (18.2 MW cm, Bacteria < 0.1 CFU/mL at 25 °C, Milli-Q, Millipore, Burlington, MA, USA).

Synthesis of Silver Nanoparticles. Silver nanoparticles (AgNPs) were prepared by the well-known Turkevich method, using citrate as a reducing and capping agent²⁷. Briefly, 10 mL of a 1 mM AgNO₃ (Sigma) solution in deionized water was heated until it started to boil. After that, 10 mL of an aqueous solution of 5 mM sodium citrate (Sigma) was dropwise to the silver nitrate solution. The heating was continued for 10 min, and then cooled to room temperature. The solution was filtered using a 0.22 µm Sartorius filter prior to use. An absorption spectrum was recorded with the Unicam UV 300 spectrophotometer to observe the plasmon absorbance of Ag colloids. Diameter of the particles was determined by electron microscopy. High-resolution Transmission electron microscopy (HR-TEM) images were recorded with a 300 kV FEI TITAN G2 60–300 microscope (Thermo Fisher Scientific, Waltham, MA, USA) of the Centre for Scientific Instrumentation, University of Granada (CIC-UGR, Granada, Spain). AgNPs were also imaged by Scanning transmission electron microscopy (STEM) using a high-angle annular dark field (HAADF) detector. AgNPs diameter distribution (histogram) was estimated by measuring the diameter of 100 nanoparticles with ImageJ software (version 1.48v; NIH, Bethesda, MD, USA).

Bacteria Culture. Lyophilized *Pseudomonas aeruginosa*, PA (ATCC 27853, CECT 108), and *Acetobacter xylinum*, Ax (ATCC 11142, CECT 473), were supplied by the Colección Española de Cultivos Tipo (CECT). The pathogenic strain was grown in nutrient broth (NB, Sigma-Aldrich, *Molecules* **2021**, 26, 2848 7 of 9 St. Louis, MO, USA) and Ax in Hestrin-Schramm (HS) agar²⁸ at 30 °C. All HS medium constituents were purchased from Sigma-Aldrich.

Lactobacillus fermentum, *Lf*, was kindly provided by Biosearch Life S.A. and grown in de Man, Rogosa and Sharpe medium (MRS, Oxoid, Hampshire, UK) at 37 °C.

Synthesis of Bacterial Cellulose. The synthesis of bacterial cellulose (BC) was carried out by culturing a single *Ax* colony, grown on agar culture medium, in 6 mL of HS medium. After 3 days of incubation at 30 °C, the BC pellicle was vortexed in order to remove active cells embedded in the membrane. One milliliter of the suspension was transferred to a 250 mL Erlenmeyer flask containing 100 mL of HS liquid medium, and incubated at 30 °C in static conditions for a week. After incubation, BC pellicles produced on the liquid–air interface of each culture were harvested, cut into pieces of similar size and weighted. The pieces had a thickness of 3 mm and weighted 0.15 ± 0.002 g. The pellicles were then purified by immersing in EtOH, boiled in water for 40 min, immersed in NaOH 0.1 M at 90 °C for 1 h (with four dissolution replacements), and neutralized in distilled water. Finally, the pellicles were sterilized for 20 min in an autoclave at 121 °C.

Incorporation of Probiotics into BC. BC pieces were placed over MRS medium previously inoculated with 10⁶ colony forming units (CFU)/mL of lyophilized *Lf*, avoiding the complete immersion of samples, for 3 h at 37 °C.

Incorporation of Silver Nanoparticles. The side free of probiotics was immersed in the filtered-AgNPs solution for times ranging from 5 to 30 min. Afterwards, the pellicles were repeatedly rinsed with sterile ultrapure water in order to remove the excess of citrate, silver ions and non-adsorbed AgNPs. The biomaterial containing the highest AgNPs concentration with null effect on the probiotic viability was obtained by incubating BC-*Lf* for 15 min. This biomaterial was referred to as AgNP-BC-*Lf*.

Quantification of Immobilized Probiotics on BC. The protocol used to quantify the number of probiotics adsorbed on the BC pellicles was recently described²⁶. Briefly, functionalized BC (0.15 g) was digested with cellulase

from *Trichoderma reesei* (No C2730-50ML, Sigma–Aldrich). Then, probiotics were suspended in 5 mL of saline solution and colony-forming units (CFU) were determined by counting in MRS-agar plates after 24 h of incubation (37 °C) in anaerobic conditions (using the BD GasPak™ ES Anaerobe Container System, Hamilton, NJ, USA). The serial dilution with a number of visible colonies around 20–300 was used to calculate CFU, and plating was performed in triplicate.

Field Emission Scanning Electron Microscopy (FESEM). Cellulosic samples were fixed in 1 mL of cacodylate buffer (0.1 M, pH 7.4) containing 2.5% of glutaraldehyde at 4 °C for 24 h. Subsequently, samples were washed with cacodylate buffer three times for 30 min at 4 °C. The samples were stained with osmium tetroxide (OsO₄) solution (1% v/v) for 2 h in the dark, being then repeatedly rinsed with Milli-Q water to remove the excess of OsO₄ solution. Samples were then dehydrated at room temperature with ethanol/water mixtures of 50%, 70%, 90% and 100% (v/v) for 20 min each, being the last concentration repeated three times and dried at the CO₂ critical point. Finally, dehydrated samples were mounted on aluminium stubs using a carbon tape, sputtered with a thin carbon film, and analyzed using a FESEM (Zeiss SUPRA40V, Oberkochen, Germany) of the Centre for Scientific Instrumentation (University of Granada, CIC-UGR, Granada, Spain).

Bacterial Viability Assay. Viability of probiotics adhered to BC was assessed by confocal laser scanning microscopy (CLSM). The samples were washed with sterile water and stained with LIVE/DEAD BacLight Bacterial Viability Kit (ThermoFisher, Waltham, MA, USA) following manufacturer's instructions. This assay combines membrane-impermeable DNA-binding stain, i.e., propidium iodide (PI), with membrane-permeable DNA-binding counterstain, SYTO9, to stain dead and live and dead bacteria, respectively. Cell viability along the BC matrix was evaluated with a confocal microscope (Nikon Eclipse Ti-E A1, Nikon, Tokyo, Japan) of the CIC-UGR equipped with 20x objective. For acquiring SYTO9 signals (green channel), a 488 nm laser

and 505–550 nm emission filter was used. For PI (red channel), a 561 nm laser and 575 nm long-pass emission filter were used. Images were analyzed with NIS Elements software (Nikon, Tokyo, Japan).

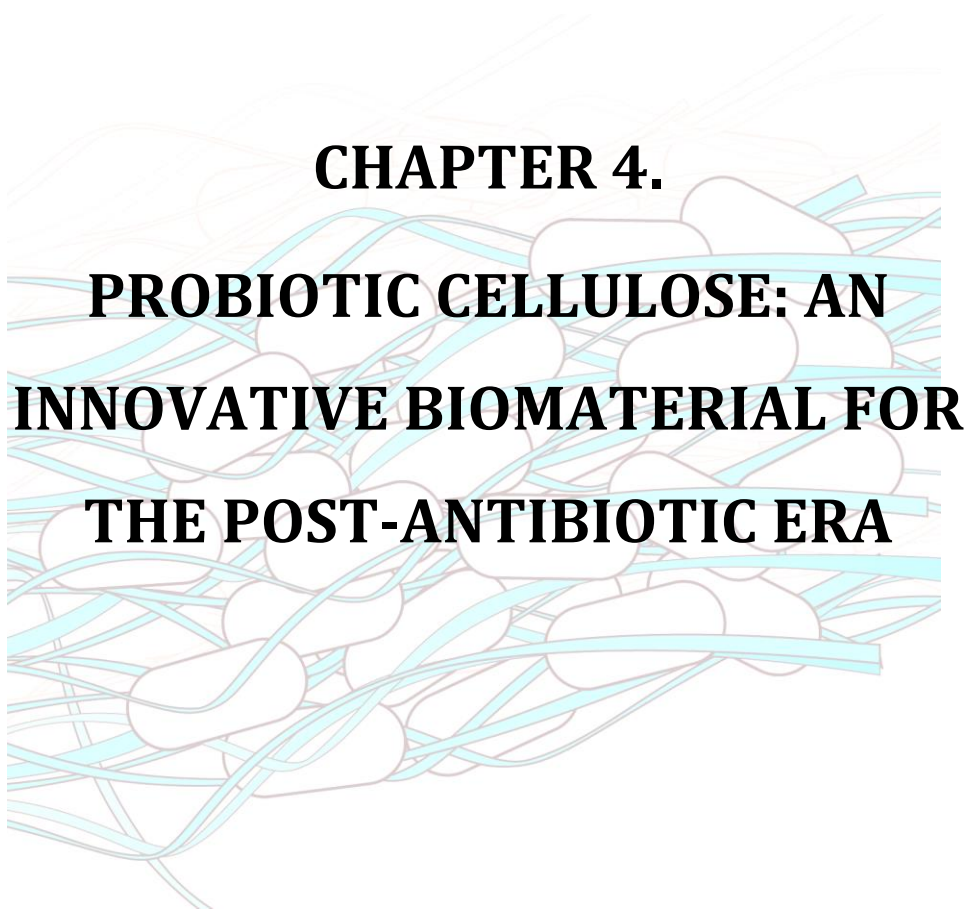
Antimicrobial Activity Studies: Agar-Diffusion Method. Antimicrobial activity of pure BC (as a negative control), BC with AgNPs (as a positive control), BC with *Lf* and BC with AgNPs and *Lf* against *PA* was assessed by the agar diffusion method²⁹. In brief, 0.1 mL of an overnight culture of *PA* was spread on nutrient agar Petri dish. Then, cellulosic samples were placed on the agar plate containing the pathogen and incubated 24 h at 37 °C before examination of inhibition zones. Probiotic CFUs before and after every antibacterial test were determined as described above (quantification of immobilized probiotics on BC). Differences lower than 10% were observed. Results were analyzed with the software GraphPad Prism 5, and data are expressed as mean ± standard deviation. For the statistical analysis, we applied the one-way ANOVA, Bonferroni's method.

5. References

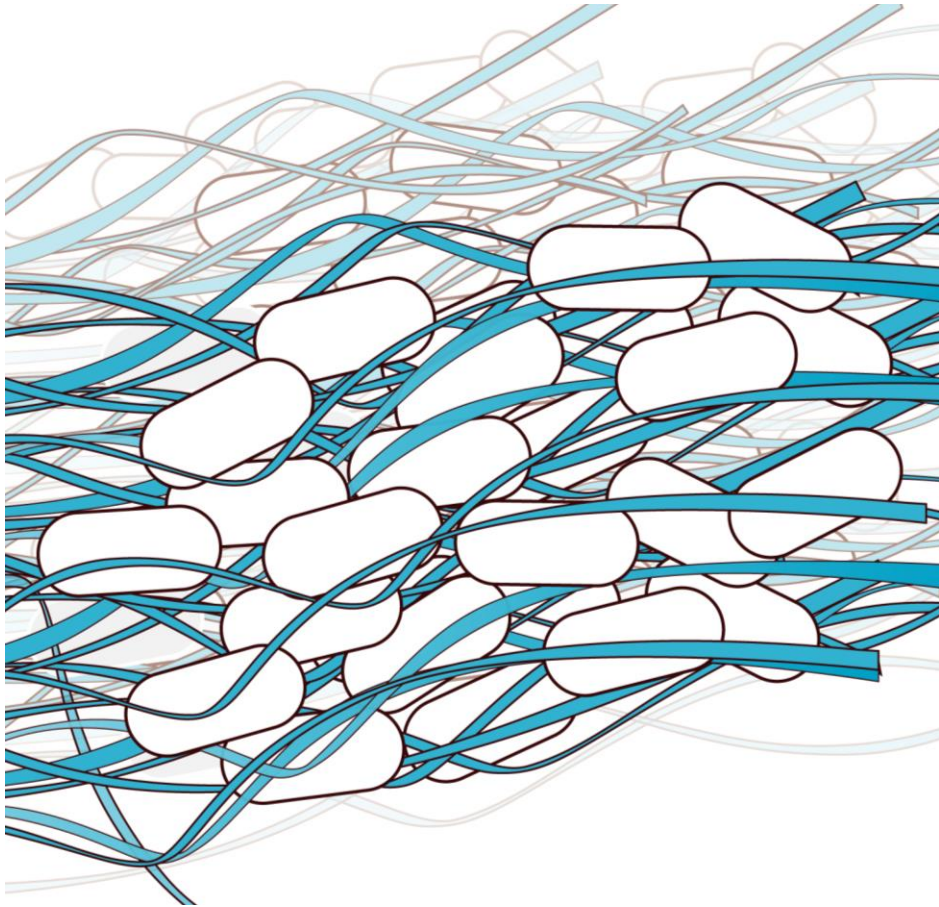
1. Willyard, C. The drug-resistant bacteria that pose the greatest health threats. *Nature* **543**, 15 (2017).
2. Luo, H. *et al.* Polymeric antibacterial materials: design, platforms and applications. *J. Mater. Chem. B* **9**, 2802–2815 (2021).
3. Borjihan, Q. & Dong, A. Design of nanoengineered antibacterial polymers for biomedical applications. *Biomater. Sci.* **8**, 6867–6882 (2020).
4. Guo, Z., Chen, Y., Wang, Y., Jiang, H. & Wang, X. Advances and challenges in metallic nanomaterial synthesis and antibacterial applications. *J. Mater. Chem. B* **8**, 4764–4777 (2020).
5. Pryshchepa, O., Pomastowski, P. & Buszewski, B. Silver nanoparticles: Synthesis, investigation techniques, and properties. *Adv. Colloid Interface Sci.* **284**, 87–100 (2020).
6. Zhu, Y. *et al.* One-step synthesis of an antibacterial and pro-healing wound dressing that can treat wound infections. *J. Mater. Chem. B* **5**, 8451–8458 (2017).
7. Gao, C. *et al.* Antibacterial activity and osseointegration of silver-coated poly(ether ether ketone) prepared using the polydopamine-assisted deposition technique. *J. Mater. Chem. B* **5**, 9326–9336 (2017).
8. Rizzello, L. & Pompa, P. P. Nanosilver-based antibacterial drugs and devices: Mechanisms, methodological drawbacks, and guidelines. *Chem. Soc. Rev.* **43**, 1501–1518 (2014).
9. Pal, S., Nisi, R., Stoppa, M. & Licciulli, A. Silver-Functionalized Bacterial Cellulose as Antibacterial Membrane for Wound-Healing Applications. *ACS Omega* **2**, 3632–3639 (2017).
10. Zhang, G., Liu, Y., Gao, X. & Chen, Y. Synthesis of silver nanoparticles and antibacterial property of silk fabrics treated by silver nanoparticles. *Nanoscale Res. Lett.* **9**, 1–8 (2014).
11. De Moura, M. R., Mattoso, L. H. C. & Zucolotto, V. Development of cellulose-based bactericidal nanocomposites containing silver nanoparticles and their use as active food packaging. *J. Food Eng.* **109**, 520–524 (2012).
12. Kokura, S. *et al.* Silver nanoparticles as a safe preservative for use in cosmetics. *Nanomedicine Nanotechnology, Biol. Med.* **6**, 570–574 (2010).
13. Chernousova, S. & Epple, M. Silver as antibacterial agent: Ion,

- nanoparticle, and metal. *Angew. Chemie - Int. Ed.* **52**, 1636–1653 (2013).
14. Panáček, A. *et al.* Bacterial resistance to silver nanoparticles and how to overcome it. *Nat. Nanotechnol.* **13**, 65–71 (2018).
 15. Vuotto, C., Longo, F. & Donelli, G. Probiotics to counteract biofilm-associated infections: promising and conflicting data. *Int. J. Oral Sci.* **6**, 189 (2014).
 16. Tsiouris, C. G. & Tsiouri, M. G. Human microflora, probiotics and wound healing. *Wound Med.* **19**, 33–38 (2017).
 17. González, A. *et al.* Entrapping Living Probiotics into Collagen Scaffolds: A New Class of Biomaterials for Antibiotic-Free Therapy of Bacterial Vaginosis. *Adv. Mater. Technol.* **5**, 2000137 (2020).
 18. Tian, X. *et al.* Bactericidal Effects of Silver Nanoparticles on *Lactobacilli* and the Underlying Mechanism. *ACS Appl. Mater. Interfaces* **10**, 8443–8450 (2018).
 19. Picheth, G. F. *et al.* Bacterial cellulose in biomedical applications: A review. *Int. J. Biol. Macromol.* **104**, 97–106 (2017).
 20. Czaja, W., Krystynowicz, A., Bielecki, S. & Brown Jr, R. M. Microbial cellulose—the natural power to heal wounds. *Biomaterials* **27**, 145–151 (2006).
 21. Homaeigohar, S. & Boccaccini, A. R. Antibacterial biohybrid nanofibers for wound dressings. *Acta Biomater.* **107**, 25–49 (2020).
 22. Bethke, K. *et al.* Functionalized Cellulose for Water Purification, Antimicrobial Applications, and Sensors. *Adv. Funct. Mater.* **28**, 1–14 (2018).
 23. Weishaupt, R. *et al.* Antibacterial, Cytocompatible, Sustainably Sourced: Cellulose Membranes with Bifunctional Peptides for Advanced Wound Dressings. *Adv. Healthc. Mater.* **9**, 1–13 (2020).
 24. Roig-Sanchez, S. *et al.* Nanocellulose films with multiple functional nanoparticles in confined spatial distribution. *Nanoscale Horizons* **4**, 634–641 (2019).
 25. Anton-Sales, I., Roig-Sanchez, S., Sánchez-Guisado, M. J., Laromaine, A. & Roig, A. Bacterial Nanocellulose and Titania Hybrids: Cytocompatible and Cryopreservable Cell Carriers. *ACS Biomater. Sci. Eng.* **6**, 4893–4902 (2020).
 26. Sabio, L. *et al.* Probiotic cellulose: Antibiotic-free biomaterials with enhanced antibacterial activity. *Acta Biomater.* (2021). doi:10.1016/j.actbio.2021.01.039

27. Turkevich, J., Stevenson, P. C. & Hillier, J. A study of the nucleation and growth processes in the synthesis of colloidal gold. *Discuss. Faraday Soc.* **11**, 55–75 (1951).
28. Schramm, M. & Hestrin, S. Factors affecting production of cellulose at the air/liquid interface of a culture of *Acetobacter xylinum*. *J. Gen. Microbiol.* **11**, 123–129 (1954).
29. Khalid, A., Khan, R., Ul-Islam, M., Khan, T. & Wahid, F. Bacterial cellulose-zinc oxide nanocomposites as a novel dressing system for burn wounds. *Carbohydr. Polym.* (2017). doi:10.1016/j.carbpol.2017.01.061



CHAPTER 4.
**PROBIOTIC CELLULOSE: AN
INNOVATIVE BIOMATERIAL FOR
THE POST-ANTIBIOTIC ERA**



1. Introduction. Skin infections

According to the World Health organization (WHO), the dramatic increase of antibiotic-resistant bacteria is one of the biggest threats to global health. Antibiotic resistance is responsible for around 700,000 deaths per year worldwide, with the potential to cause 10 million deaths by 2050¹. The WHO reported in 2014 that “a post-antibiotic era –in which common infections and minor injuries can kill– far from being an apocalyptic fantasy, is instead a very real possibility for the 21st century”. New antibiotic-free approaches are thus urgently needed for the treatment and prevention of bacterial infections.

A promising alternative to antibiotics is the use of probiotics. Probiotics are live microorganisms known to provide health benefits by restoring the gut microbiome or by excreting antipathogenic compounds, as bacteriocins or hydrogen peroxide². Likewise, they may be helpful to prevent diarrhoea when taking antibiotics and to ease some symptoms of irritable bowel syndrome. Nowadays, the term probiotic goes beyond commensal bacteria for the gut microbiota since probiotics can provide health benefits to other tissues and, in particular, Lactobacilli strains have already shown antimicrobial properties and the ability to accelerate the healing process³.

Nonetheless, non-encapsulated probiotics are vulnerable when nesting and proliferating in the hostile environment of the target tissue, thus jeopardising their viability and consequently their beneficial health effects⁴. Therefore, one of the keys to the health applications associated with probiotics is the choice of an appropriate matrix to host and protect them, since dead or unprotected probiotics have reduced or no activity⁵. Most studies into engineering protective matrices for probiotics were intended for food and nutraceuticals⁵⁻⁹, yet little has been done regarding potentially fatal skin infections, including those occurring at hard-to-heal wounds such as following major surgery, war wounds, burns, and so on.

Bacterial cellulose (BC) combines all the characteristics necessary to serve as a host matrix for active species of medical interest¹⁰. BC is a fascinating biopolymer synthesised by some aerobic bacteria^{10,11}. It has received special attention due to its unique properties in comparison with plant cellulose (PC). Both BC and PC consist of $\beta(1\rightarrow4)$ linked D-glucose units that self-assemble into fibres through a complex hierarchical process. However, BC, in contrast to PC, is chemically pure and free of components such as hemicellulose, lignin or pectin¹⁰. This means BC is nontoxic and biocompatible. Furthermore, BC has a higher crystallinity than PC. The thin cellulose fibres of BC, ranging from 40-80 nm in diameter (approximately 100 times smaller than those of PC), confer bacterial cellulose a higher surface area, exceptional mechanical properties, a high water-holding capacity and a high adsorption capacity. Thanks to these properties, BC has been widely studied for biomedical applications¹² and, in particular, for tissue engineering, reconstruction of damaged tissues, and as a wound dressing material. BC provides optimum moisture balance to dry wounds, absorbs wound exudates, provides an effective physical barrier against external infection and does not adhere to the wound surface, thereby avoiding tissue damage upon removal¹³. Wound dressing materials based on bacterial cellulose are already commercially available under several trademarks XCell®, Biofill®, Bioprocess®, Nanocell®, Bionext® and Membracel®^{11,12}. Moreover, *in vivo* wound healing studies have demonstrated that BC-based materials feature faster epithelialisation and regeneration than other commercially available products¹¹.

However, BC itself has no activity against bacterial infection, which is a recurrent issue affecting hard-to-heal chronic wounds. The synthesis of BC derivatives with antibacterial properties has long been, in fact, a challenge for biomaterial scientists. Most approaches dealt with BC functionalization by physical surface interactions or chemical bonding. Thus, antibacterial polymers, peptides or nanoparticles were incorporated to BC¹⁴⁻¹⁸. However,

both physical and chemical approaches have limitations. BC contains available hydroxyl groups on its surface that facilitate the possibility of coating, but due to the weak interaction between BC and the coating, it potentially suffers from shedding. The chemical modification becomes difficult due to the poor solubility of BC, which makes necessary the use of solvents that influences the green safety of products, and limits its large-scale production.

BC has been recently functionalized with *Bacillus subtilis* resulting in a composite biomaterial with antimicrobial properties and the capacity of promoting skin wound healing¹⁹. However, the functionalization process required first the isolation and purification of BC and then the inoculation and further growth of the *bacillus*, which only penetrates few layers of the bacterial cellulose.

In this work, we have developed a one-pot approach under mild conditions to obtain antibiotic-free antibacterial biomaterials, so-called probiotic cellulose, which consist of cellulose films where probiotics progressively grow until completely invading the entire scaffold. Antibacterial assays (agar-diffusion and time-kill tests) demonstrated that probiotic cellulose is able to kill *Staphylococcus aureus* (*SA*) and *Pseudomonas aeruginosa* (*PA*), the most active pathogens in severe skin infections and chronic wounds, even in pathogen-favourable media. Noticeably, probiotic cellulose was also found to be effective to inhibit the proliferation of methicillin-resistant *SA* (*MRSA*) and of multidrug-resistant *PA* isolated from clinical urine sample. To overcome this important limitation, we have developed a new class of BC – probiotic cellulose – that also exhibits antibacterial activity.

2. Results and discussion

2.1. A new protocol for probiotic cellulose synthesis

The synthetic approach used to obtain probiotic cellulose is presented in Figure 1. It is based on the fact that *Acetobacter xylinum* (*Ax*), the cellulose-producing bacterium, is strictly aerobic while probiotics *Lactobacillus fermentum* (*Lf*) and *Lactobacillus gasseri* (*Lg*) are facultative anaerobic bacteria. Two types of probiotic were explored, selected according to their activity in terms of the prevention and/or treatment of infections^{20,21}. Specifically, *Lf* is a immunostimulant that strengthens the microbiota and *Lg* has exhibited antimicrobial activity against *Staphylococcus aureus*²⁰, one of the most common bacteria involved in chronic skin ulcers²².

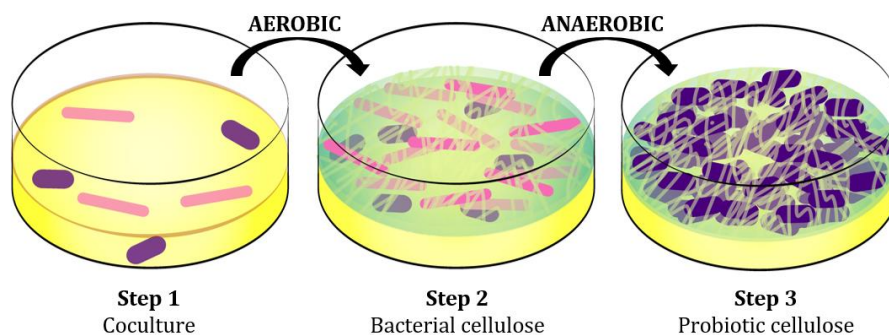


Figure 1. Experimental protocol to obtain probiotic cellulose: production of cellulose films under aerobic conditions followed by the gradual proliferation/invasion of the cellulose by probiotics under anaerobic conditions.

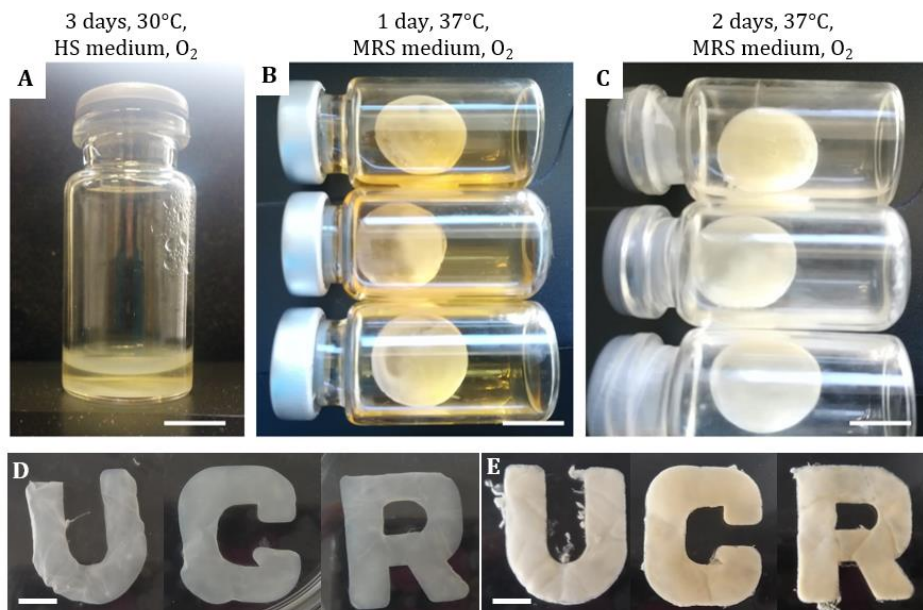


Figure 2. One-pot synthetic method of probiotic cellulose. **(A)** Bacterial cellulose obtained with the coculture of *Ax* and *Lf* in HS medium, under aerobic conditions; **(B)** cellulose after 24 h of incubation in MRS under anaerobic conditions; **(C)** cellulose after 48 h of incubation in MRS medium. The resulting biomaterial is the so-called probiotic cellulose. Note that cellulose films were not extracted during the process. The probiotic cellulose can be produced with arbitrary shapes: **(D)** BC before invasion of probiotics, and **(E)** probiotic cellulose. Scale bar = 1 cm.

2.2. Characterization of the probiotic cellulose: structure and viability

Gram staining shed light on the growth mechanism of probiotic cellulose. The coculture of Gram-negative *Ax* and Gram-positive *Lf/Lg* in the optimal growing conditions of the first (Hestrin-Schramm (HS) medium and anaerobic conditions) resulted in the formation of a thick cellulose gel (Figure 2A,D) containing both bacteria (*Ax/Lf* or *Ax/Lg*). The facultative anaerobic probiotics were situated at the bottom of the cellulose, as far away from the air-culture interface (Figure 3E). After adjusting the growing conditions to optimal for probiotics (by replacing HS medium with MRS medium and

removing oxygen), the lactobacilli proliferated and completely invaded the cellulose network (Figure 2C,E and Figure 3G).

BC produced aerobically in the presence of *Ax* and *Lf/Lg* was a two-sided material. FESEM micrographs of the air-exposed surface showed the typical fibrous morphology of *Ax* (Figure 4), whereas bacteria at the submerged face presented the typical bacilliform appearance of probiotics. In fact, FESEM micrographs of the cross-section of this cellulose (Figure 4C) revealed two clearly differentiated areas: one exposed to air, containing exclusively *Ax*, and the other exposed to the bulk aqueous phase, which only included probiotics. When culture conditions are modified to optimal for probiotics (MRS and anaerobic atmosphere), they extensively proliferated and invaded the entire cellulose matrix to such an extent that SEM micrographs of both faces were similar, highlighting the presence of a huge number of probiotics (Figure 4E,F). Under these latter conditions, no evidences of reminiscent *Ax* were detected on probiotic cellulose.

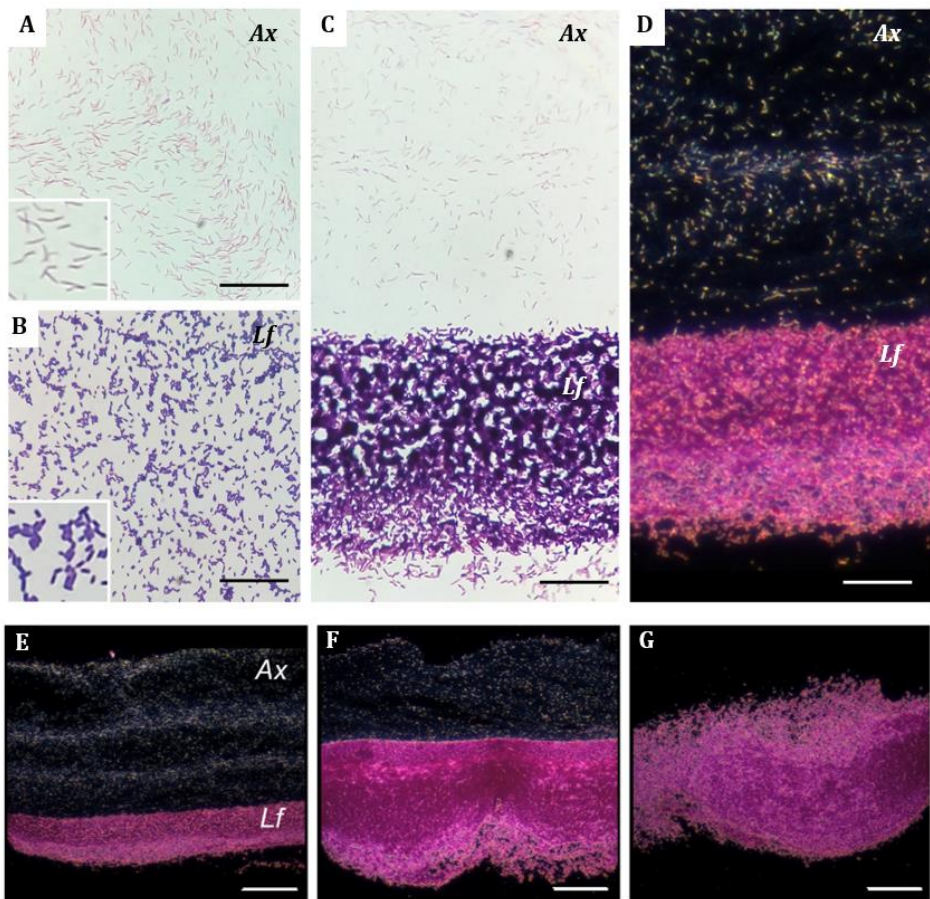


Figure 3. Gram staining micrographs of cellulosic samples. **(A)** Gram-negative *Acetobacter xylinum* (Ax) with fibrous morphology, and **(B)** Gram-positive *Lactobacillus fermentum* (Lf) with bacilliform appearance. **(C)** Cross-section of Lf-cellulose showing the two bacteria, which can be clearly distinguished. Note that Gram-negative Ax are stained with safranin (red), and the Gram-positive probiotics acquires the colour of crystal violet (purple). Samples were observed under a 100x immersion oil objective and bright field mode. **(D)** Transversal section of Lf-cellulose under dark-field mode. The greyish zones indicate a high density of cellulose fibers. Scale bar = 50 μm . **(E - G)** Dark-field optical micrographs of cross-sections of Gram-stained pellicles showing the gradual invasion of the probiotics as a function of increasing incubation time (from left to right). Scale bar = 100 μm .

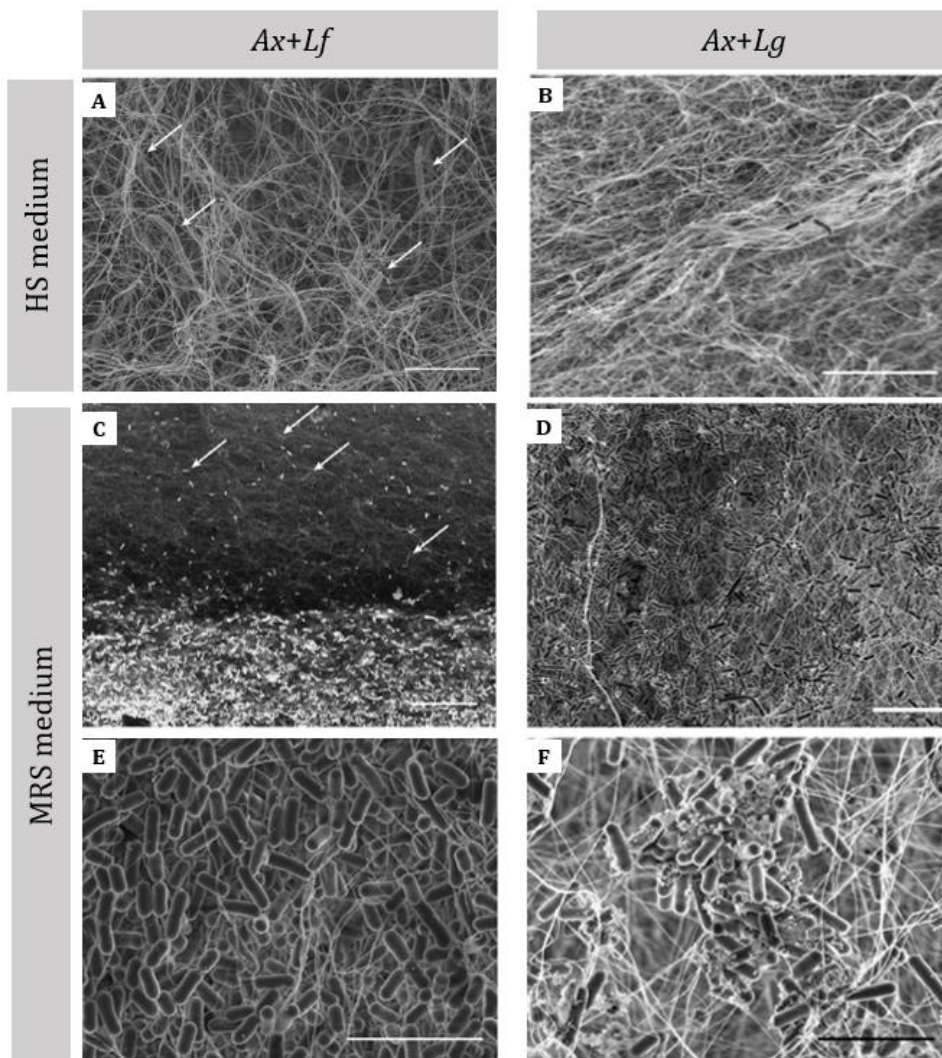


Figure 4. SEM micrographs of cellulose cocultured with *Ax* and *Lf* (*Ax+Lf* column) or *Ax* and *Lg* (*Ax+Lg* column). Pictures of the air-exposed surface of cellulose cocultured with *Ax+Lf* (**A**) or *Ax+Lg* (**B**). Note that most of the bacteria (highlighted with arrows for clarity) present the typical long rod-shaped morphology of *Ax*. (**C**) Micrograph of the cross-section of the two-sided material obtained under anaerobic conditions: one side contains *Ax* (arrows) and the other *Lf*. Micrographs of cellulose cocultured under anaerobic conditions with *Ax* and *Lf* (**E**) or *Ax* and *Lg* (**D, F**). In these cases, both surfaces of the materials provided similar results. Note that all the bacteria exhibit the typical rod-shape morphology of lactobacilli. Scale bar = 5 μm .

Therefore, probiotic cellulose contains only probiotics, which are distributed throughout the cellulose network. Despite the high density of probiotics (Figure 4E,F), i.e., $1.4 \cdot 10^{11}$ colony forming units per mg of cellulose (CFU mg^{-1}) for *Lf*, and $8.7 \cdot 10^{10}$ CFU mg^{-1} for *Lg*, the entrapment did not affect the size of the cellulose nanofibers, with diameters ranging between 20 and 90 nm (Figure 5). It is important to highlight that probiotic cellulose is produced under mild conditions in a one-pot synthesis, as described above. By contrast, the synthesis of bacterial cellulose and its derivatives requires the isolation of pure BC through a long and expensive procedure involving successive treatments with ethanol and alkali at high temperatures to eliminate any remnants of cellulose-producing bacteria^{18,23-25}. This point is of the utmost importance when considering the economic and environmental factors associated with the industrial production of probiotic cellulose.

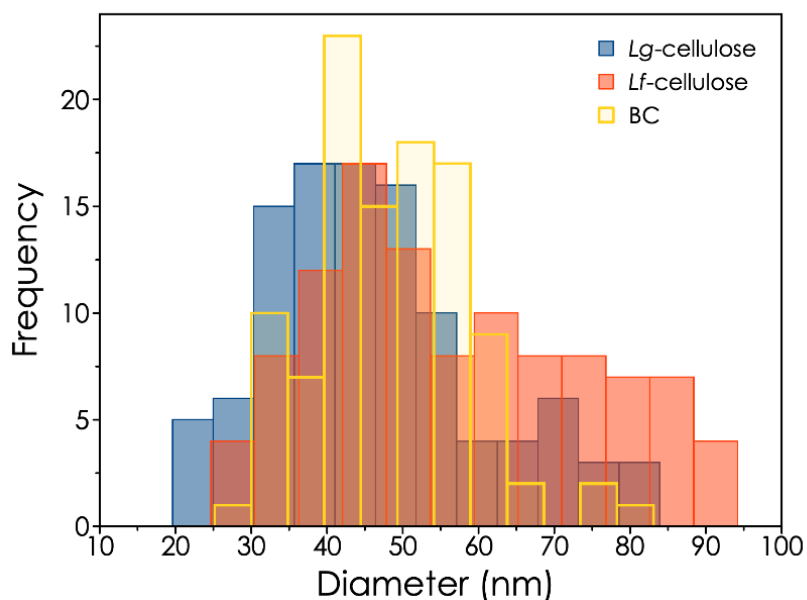


Figure 5. Size distribution of cellulosic materials. Histogram of fibril diameters of bacterial cellulose (BC, yellow empty bars) and of *Lf*-cellulose (red bars) and *Lg*-cellulose (blue bars). The diameters of 100 fibbers from different SEM image were measured for each condition.

Live/dead viability test, based on SYTO 9/propidium iodide (PI) fluorescent dyes, demonstrated that the probiotics entrapped in the cellulose remained viable (Figure 6). Confocal laser scanning microscopic (CLSM) images of BC contained a mixture of green spots (live) with a high density of red spots (dead) of fibrous *Ax* and shorter bacilliform *Lf* bacteria (Figure 6a-f). Contrastingly, the probiotic cellulose showed an extremely high density of live probiotics (green spots) and very few dead ones (red spots) (Figure 6g-j). Moreover, the 3D CLSM reconstruction confirmed that probiotic cellulose is a homogeneous material, since live probiotics migrated and colonised the entire cellulose matrix after 48 h (Figure 6k,l).

Importantly, the entrapped probiotics were also metabolically active. Within a few hours, the pH of the MRS media in contact with the probiotic cellulose (containing *Lf* or *Lg*) dropped from 7 to approximately 4, a value very close to the pK_a of lactic acid (Figure 7a). In addition, we observed that probiotic cellulose can gradually reduce electrochromic polyoxometalate [P₂Mo^{VI}₁₈O₆₂]⁶⁻ (POM, Figure 7b), which is complementary evidence of the probiotics' metabolic activity²⁶ once entrapped in the probiotic cellulose matrix.

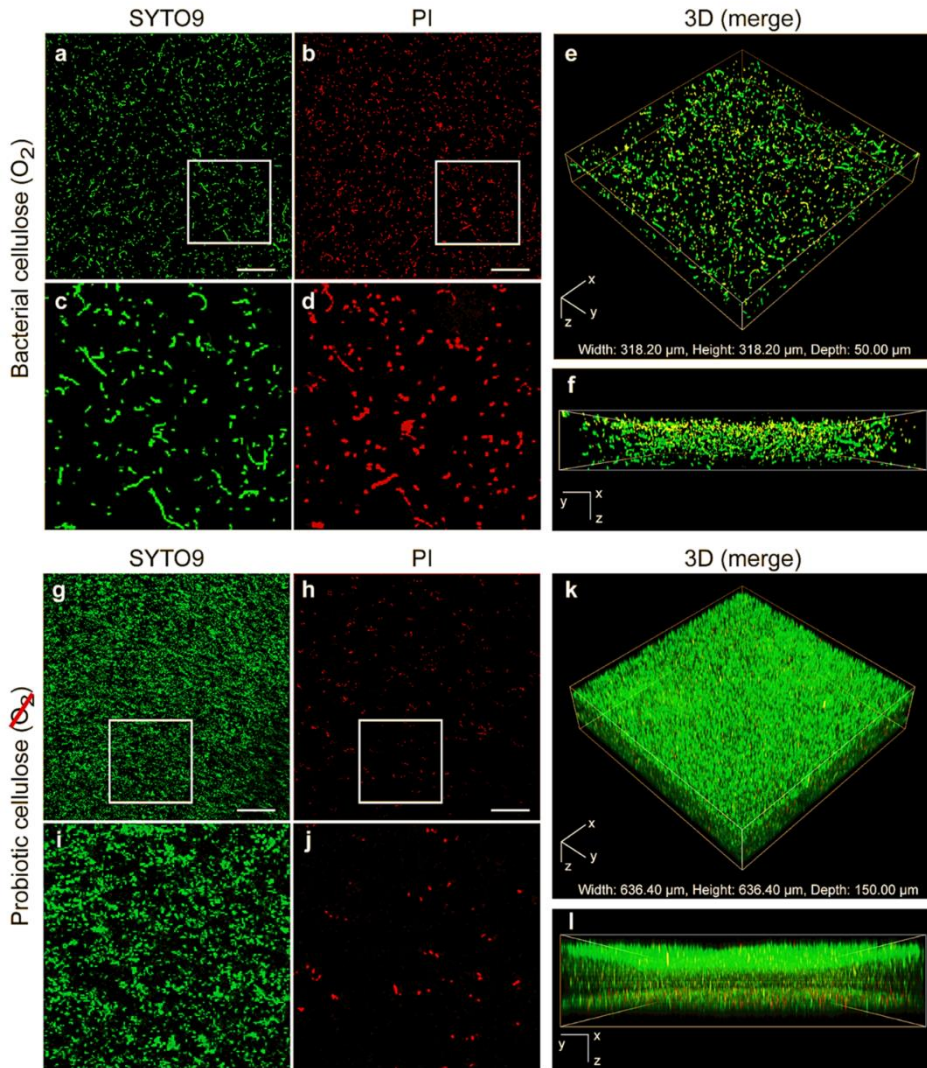


Figure 6. Live/dead viability assays. CLSM images of BC cocultured with *Ax* and *Lf* under aerobic (**a-f**), and then, anaerobic conditions (**g-l**). Green channel (SYTO 9, live bacteria), and red channel (propidium iodide, dead bacteria) are shown. Panels **c,d** and **i,j** correspond to expanded views of the boxes (3x) in images **a,b** and **g,h**, respectively. The 3D maps are representative of the merged images. Scale bars = 50 μm.

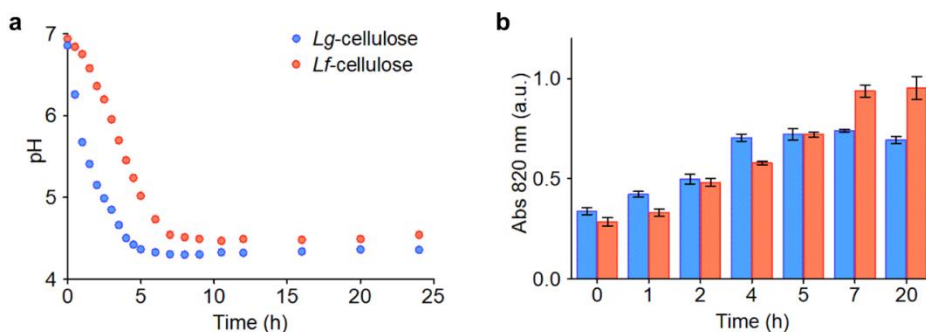


Figure 7. Metabolic activity of probiotic cellulose. **(a)** Time evolution of the pH of MRS media containing a film of probiotic cellulose. **(b)** Time dependence of the UV-vis absorbance at 820 nm of probiotic cellulose supernatant in contact with a solution containing POM. Data are expressed as mean with the corresponding standard deviation as error bars.

In order to test the viability of the probiotics immobilized in the cellulose, we determined the viable CFU (Figure 8) and record the time evolution of the pH of MRS containing the probiotic cellulose after their storage at 4 °C and 25 °C, for one week (Figure 9a,c) and one month (Figure 9b,d). We compared the results obtained with probiotic celluloses with those of probiotic pellets obtained after the digestion of cellulosic samples. The pellets, with an equivalent number of bacteria than celluloses, showed a similar CFU counting and acidification when stored at 4 °C (Figure 8 and 9a,c, respectively). However, significant differences were found after one month at 25 °C. Both *Lf*- and *Lg*-cellulose were able to low the pH of the MRS media faster than the equivalent pellet formed solely by *Lf* and *Lg*. (Figure 9b,d). Similarly, the survival obtained for these pairs were higher for the probiotics embedded in the cellulosic network (Figure 8). These results pointed out the protective effect of bacterial cellulose over the probiotics, keeping better conditions for their maintenance.

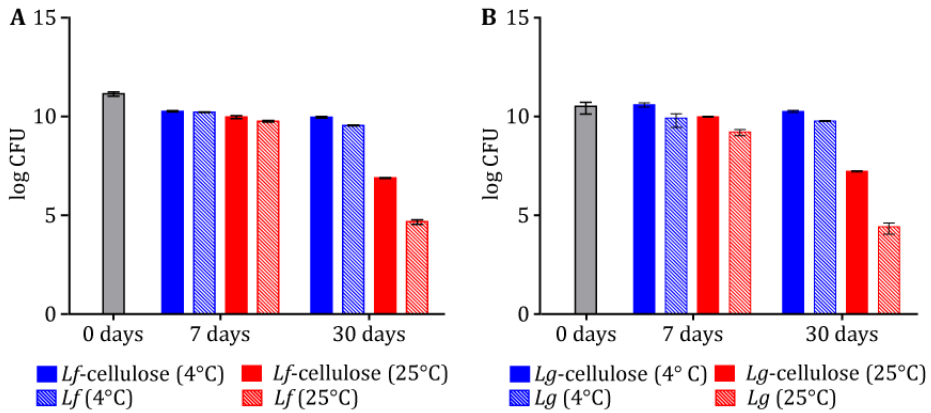


Figure 8. Colony forming units (CFU) count of probiotic celluloses *Lf*-cellulose (A) and *Lg*-cellulose (B) after storage at 4 °C and 25 °C.

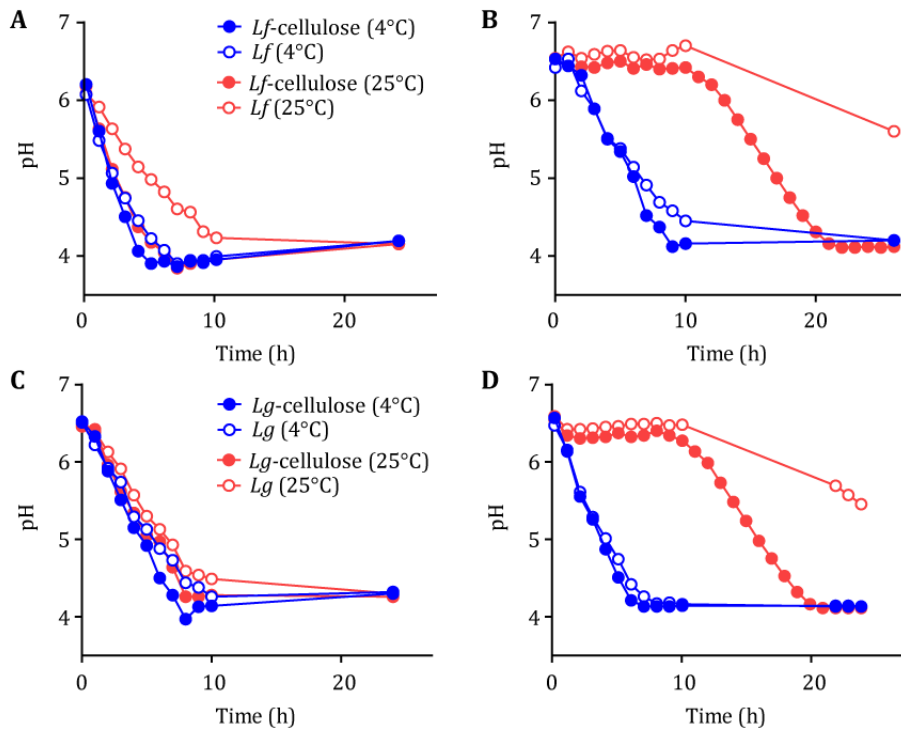


Figure 9. Time evolution of the pH of MRS media containing *Lf*/*Lf*-cellulose after one week (A) and one month (B), or *Lg*/*Lg*-cellulose after one week (C) and one month of storage (D).

2.3. Antibacterial activity: *S. aureus* and *P. aeruginosa*

The antibacterial activity of probiotic cellulose was assessed against *Staphylococcus aureus* (*SA*) and *Pseudomonas aeruginosa* (*PA*), two opportunistic pathogens responsible for a broad range of skin infections, some of which are potentially fatal (severe and chronic wounds)^{22,27}. Although many studies have tried to develop effective vaccines against these pathogens, none of them have so far gained approval from regulatory authorities.

It is important to emphasise that both *Lf* and *Lg* have shown antimicrobial activity against *SA* and *PA*, but only in media that favour the proliferation of probiotics^{20,28} (Figure 10A). However, we found that neither *Lf* nor *Lg* could inhibit the growth of *SA* or *PA* in optimal pathogenic media such as tryptic soy agar (TSA) (Figure 10B). This subtle nuance is of paramount importance, because in a real-life infection scenario the pathogen and probiotic meet in an environment that is optimal for the former but not the latter. With this in mind, we initially tested the antibacterial activity of probiotic cellulose using the disk diffusion set-up depicted in Figure 11A, where the pathogens were dispersed in TSA. Even in these unfavourable conditions, probiotic cellulose produced inhibition zones against both pathogens (Figure 11B). Noticeably, under these unfavourable conditions for probiotics, BC functionalized with *Lf* or *Lg* through an “adsorption-incubation” procedure (BC+*Lf* or BC+*Lg*) as that proposed by Digel *et al.*¹⁹ did not inhibit in the same extent the pathogenic proliferation in TSA media (Figure 11B).

These observations were confirmed by time-kill experiments. *SA* or *PA* were cultivated in tryptic soy broth (TSB), an unfavourable medium for probiotics^{27,29}. Both pathogens proliferated from initial loads of 10^6 - 10^7 to 10^9 CFU after 24 h (Figure 12A). Then, in a control experiment, we observed that the addition of bacterial cellulose did not affect the proliferation of either *SA*

or *PA* cultures (Figure 12A, *SA*+*BC* or *PA*+*BC* bars). Nonetheless, when probiotic cellulose (either *Lf*- or *Lg*-cellulose) was added instead of bacterial cellulose, we witnessed a dramatic decline in pathogen viability. In particular, *Lg*-cellulose eliminated *PA* and *SA* after 24 hours, while *Lf*-cellulose practically killed *PA* and notably decreased *SA* viability (Figure 12).

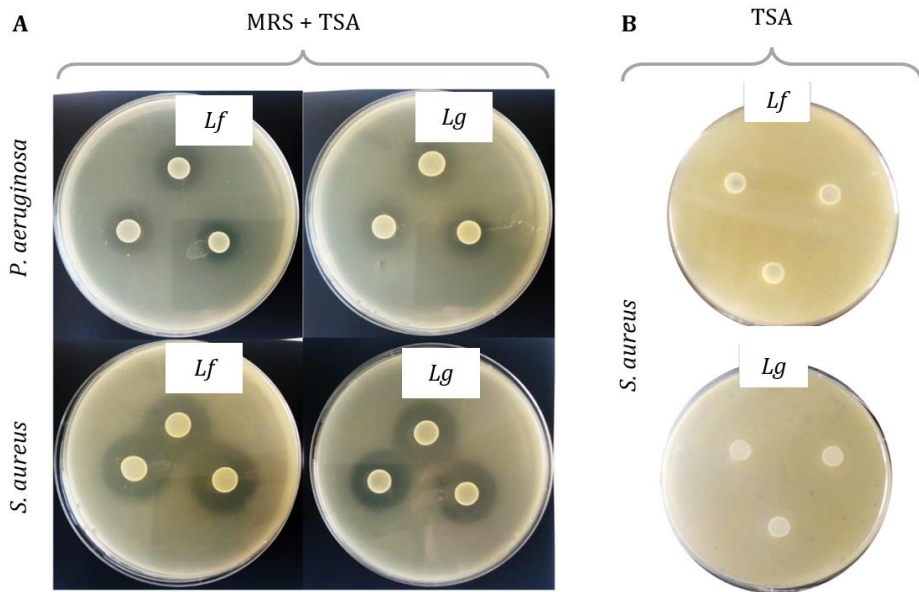


Figure 10. Media-dependent inhibition activity of non-encapsulated *Lf* and *Lg* probiotics. Inhibitory activity of the probiotics in MRS-agar+TSA medium against *SA* and *PA* (A), and in TSA against *SA* (B).

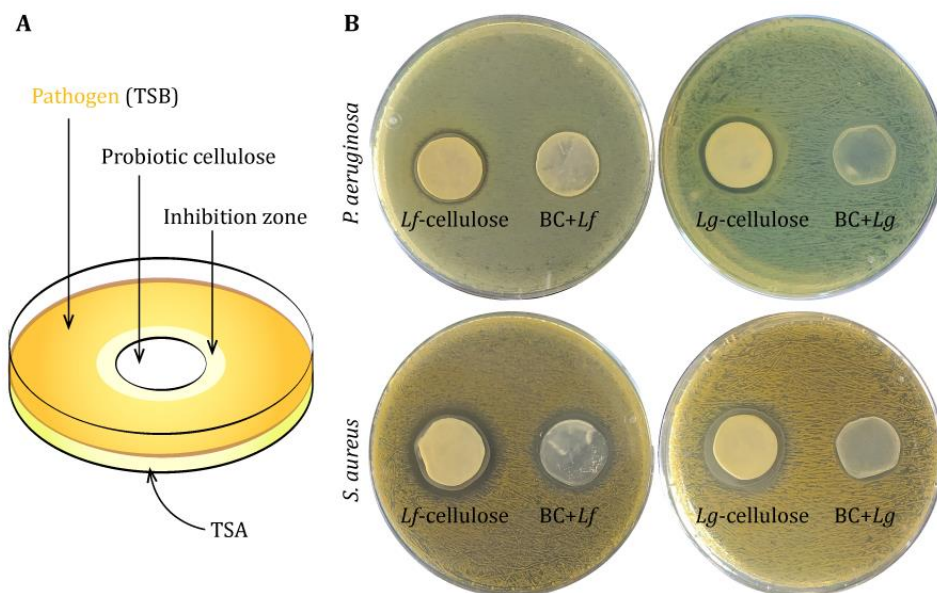


Figure 11. (A) Diagram of the experimental protocol used to assess the inhibitory activity **(B)** of probiotic cellulose (*Lf*- and *Lg*-cellulose) and BC with adsorbed probiotics (*BC+Lf* and *BC+Lg*) against *Staphylococcus aureus* and *Pseudomonas aeruginosa*. Even though each pathogen was cultivated in an optimal medium, we observed clear inhibition zones around the probiotic celluloses for both *PA* and *SA*.

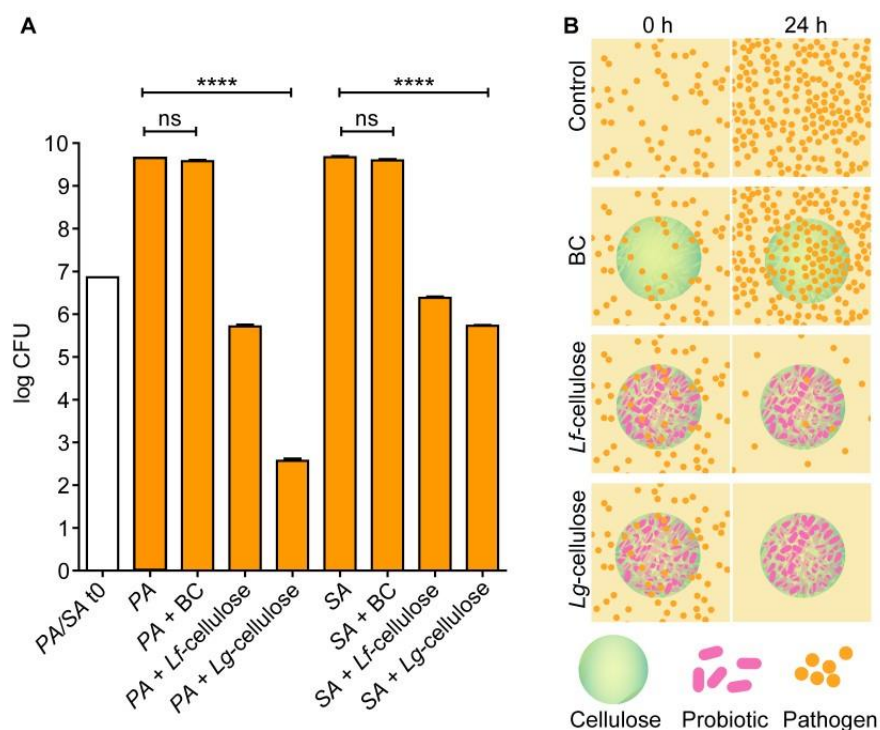


Figure 12. Time-kill assay experiments in tryptic soy broth (TSB). **(A)** *Pseudomonas aeruginosa* (PA) and *Staphylococcus aureus* (SA) survival after coincubation with BC or probiotic celluloses (*Lf*- and *Lg*-cellulose) in TSB. Asterisks and ns denote statistical significance ($p < 0.001$) and no significance, respectively. **(B)** Diagram depicting the bactericidal properties of *Lf*- and *Lg*-cellulose compared to the corresponding control assays.

These interesting findings motivated us to explore the activity of probiotic cellulose against *MRSA* by agar diffusion assays. As found in Figure 13 A,B, both *Lf*- and *Lg*-cellulose inhibited the growth of *MRSA*. Although some inhibitory effects were also found for BC+*Lf* and BC+*Lg* (biomaterials prepared by an adsorption-incubation procedure), the inhibition zones were smaller than those found for probiotic celluloses (Figure 13A,B). Indeed, *Lf*-cellulose also inhibited the growth of multidrug-resistant PA, as shown in Figure 13C.

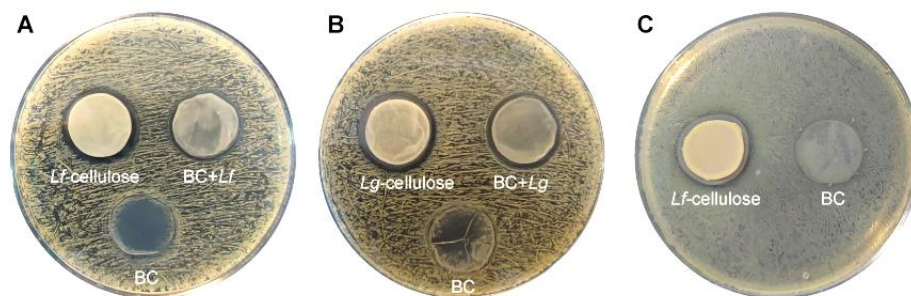


Figure 13. Inhibitory activity of probiotic cellulose (**A**, *Lf*-cellulose and **B**, *Lg*-cellulose) against *MRSA* by agar diffusion tests on TSA plates. BC+*Lf* (**A**), BC+*Lg* (**B**) and pure BC were also tested. Even though the media was optimal for the pathogens, clear inhibition zones appeared around the probiotic cellulose and in a less extent around the biomaterials prepared through an adsorption-incubation procedure (BC+*Lf* and BC+*Lg*). (**C**) Inhibitory activity of *Lf*-cellulose against multidrug-resistant *PA* by agar diffusion test on TSA plates. Pure BC was used as control (BC).

3. Conclusions

In summary, we have developed a new type of antibiotic-free antibacterial –probiotic cellulose– which consists of bacterial cellulose containing live and active probiotics. The two probiotic celluloses (*Lg*- and *Lf*-cellulose) showed extraordinary antibacterial activity against *Staphylococcus aureus* and *Pseudomonas aeruginosa*, the two most active pathogens in severe skin infections. Furthermore, probiotic celluloses, in contrast to probiotics, are antibacterial even in conditions that are favourable for pathogens or unfavourable for probiotics. Our smart strategy to produce probiotic cellulose can be extended to other facultative anaerobic probiotics and easily scaled for industrial production. In fact, the production of probiotic cellulose does not require the lengthy and quite expensive chemical treatments necessary to isolate bacterial cellulose. We presented here an antibiotic-free antibacterial agent with excellent practical application today, and tomorrow, in a hypothetical post-antibiotic era, where common infections and minor injuries could kill.

4. Materials and methods

Reagents and solutions. High-grade quality reagents were purchased from Sigma-Aldrich. Aqueous solutions were prepared with ultrapure water (18.2 M Ω -cm, Bacteria < 0.1 CFU/mL at 25 °C, Mili-Q, Millipore).

Bacterial strains and culture conditions. The lyophilized *Acetobacter xylinum* (ATCC 11142 / CECT 473, *Ax*) was supplied by the Colección Española de Cultivos Tipo (CECT) and grown at 30 °C in Hestrin and Schramm medium (HS)³⁰ with (w/v) 2% glucose, 0.5% yeast extract, 0.5% peptone, 0.115% citric acid, 0.68% Na₂HPO₄ · 12 H₂O (Sigma). *Ax* was first grown on solid agar (1.5%) and stored at 4 °C. *Lactobacillus fermentum* (*Lf*) and *Lactobacillus gasserii* (*Lg*) were kindly provided by Biosearch Life S.A. and grown in de Man, Rogosa and Sharpe medium (MRS, Oxoid) at 37 °C.

The pathogenic strains of *Staphylococcus aureus* (CECT 976, *SA*) and *Pseudomonas aeruginosa* (CECT 108, *PA*) were supplied by the CECT. The pathogenic strains were grown in tryptic soy broth (TSB No2, Sigma-Aldrich) at 30 °C and 37 °C, respectively. Methicillin-resistant *Staphylococcus aureus* (*MRSA*) and multidrug-resistant *Pseudomonas aeruginosa* (*PA*) bacteria were isolated from clinical urine sample at the Microbiology Laboratory of the “Virgen de las Nieves” University Hospital (Granada, Spain). The MicroScan system (Beckman Coulter, Brea, CA, USA) and mass spectrometry (Maldi-Tof®, Bruker Daltonik GmbH, Bremen, Germany) were used to identify the isolate. The MicroScan microdilution system was employed to characterize resistance to antibiotics. Minimum Inhibitory Concentration (MIC) assays were performed and the lowest concentration of the following antimicrobials (in mg·mL⁻¹) was interpreted according to the EUCAST 2020 recommendations. The *MRSA* strain was found to be resistant to penicillin (> 0.25), oxacillin (2), ciprofloxacin (> 2), levofloxacin (> 4), fosfomicin (64) and daptomycin (2); and susceptible to erythromycin (< 0.5), clindamycin (< 0.25), gentamicin (< 1), vancomycin (2), teicoplanin (< 1), mupirocin (< 4),

trimethoprim- sulfamethoxazole (< 1/19), linezolid (2), rifampicin (< 0.5) and tetracycline (< 1). *MRSA* bacteria were grown in TSB at 36 °C. The MDR *PA* isolate was found to be resistant to imipenem (> 16), levofloxacin (> 8) and amikacin (> 64).

Synthesis of bacterial cellulose (BC) and probiotic cellulose. The synthesis of probiotic celluloses (*Lf*- and *Lg*-cellulose) were carried out by co-culturing 0.1 mL of an *Ax* suspension (OD_{600nm} = 0.3) and 0.1 mL of a probiotic (*Lf* or *Lg*) suspension (OD_{600nm} = 0.4) in 1 mL of HS medium and aerobic conditions at 30 °C. The material obtained after 3 days of culture is referred to as bacterial cellulose (BC) in this work. Afterwards, HS medium was replaced by 5 mL of MRS and BC was incubated in an anaerobic atmosphere at 37 °C for 48 hours. The MRS medium was replaced after 24 hours. After 48 hours of culturing in MRS, probiotic-celluloses (*Lf*- or *Lg*-cellulose) were obtained.

With the aim of exploring the reproducibility of probiotic growth into the cellulose matrix, we performed three independent experiments with fresh batches of *Ax*, *Lf* or *Lg* and fresh solutions on different weeks obtaining 3 samples of *Lf*- and *Lg*-cellulose per batch. Subsequently, the probiotics into the matrix of each sample were quantified (see “Quantification of immobilized probiotics”). For the sake of comparison, bacterial cellulose was also purified and then functionalized with probiotics. The purification of BC was achieved as follows: immersion in ethanol, boiling in water for 40 min, immersion in NaOH 0.1M at 90 °C for 1 hour (with four dissolution replacements), and neutralization in distilled water. Cellulose was then functionalized with adsorbed probiotics by incubation in MRS broth inoculated with *Lf* (BC+*Lf*) or *Lg* (BC+*Lg*), at the same conditions as probiotic celluloses. *Lf* and *Lg* are included in the list of Qualified Presumption of Safety (QPS) of the European Food Safety Authority (EFSA) and Food and Drug Administration (FDA). QPS provides a safety status for microorganisms intentionally used in the food and feed chain. These microorganisms can be also used as living entities that may reach the consumer as such, or may be used as production organisms or as

dead biomass³¹. Likewise, FDA approved some wound dressing devices based on bacterial cellulose³².

Characterization of probiotic cellulose

Gram staining. This staining protocol allows differentiating between two major bacterial groups, Gram-positive (stained purple) and Gram-negative (stained red) cells. *Ax* is a Gram-negative bacterium, whereas *Lf* and *Lg* are Gram-positive bacteria. After 1, 2 and 7 days of incubation in MRS, *Lf*-cellulose was dehydrated in gradient ethanol and washed with xylene³³. Then, the samples were embedded in paraffin and transversally cut in 4 μm sections using a microtome. Slides were deparaffinized, cleared in xylene, and rehydrated before the staining. Then, a standard Gram staining protocol was performed. In brief, crystal violet was applied for 1 minute at room temperature, and slides were briefly rinsed under running water to remove the excess of staining. Iodine mordant was applied for 30 seconds and washed with water. To remove violet crystal from Gram-negative bacteria, slides were covered with EtOH for 15 seconds and quickly rinsed under running water until the water run clear. Finally, Gram-negative bacteria were stained with safranin for 1 minute and rinsed with water. The slides were observed using an iScope (Euromex) microscope, in bright field mode and under a 100x immersion oil objective to differentiate between Gram-positive and Gram-negative. The same slides were also observed using a Nikon Eclipse E200 microscope, in dark field mode and under a 10x objective to obtain macroscopic images of the whole *Lf*-cellulose section. Images were acquired with an AxioCam ERc 5s (ZEISS) camera.

Field Emission Scanning Electron Microscopy (FESEM). Probiotic celluloses were fixed in 1 mL of cacodylate buffer (0.1 M, pH 7.4) containing 2.5% of glutaraldehyde at 4 °C for 24 h. Subsequently, samples were washed with cacodylate buffer three times for 30 min at 4 °C. The samples were stained with osmium tetroxide (OsO_4) solution (1% v/v) for 2 hours in the dark, being

then repeatedly rinsed with Milli-Q water to remove the excess of OsO₄ solution. Samples were then dehydrated at room temperature with ethanol/water mixtures of 50%, 70%, 90% and 100% (v/v) for 20 min each, being the last concentration repeated three times and dried at the CO₂ critical point. Finally, dehydrated samples were mounted on aluminum stubs using a carbon tape, sputtered with a thin carbon film, and analyzed using a FESEM (Zeiss SUPRA40V) of the Centre for Scientific Instrumentation (University of Granada, CIC-UGR).

The fiber width distribution of each condition was obtained by measuring 100 fibers of different SEM micrographs with ImageJ software (version 1.48v; NIH, Bethesda, MD).

Quantification of immobilized probiotics. Probiotic cellulose (2 cm-diameter, 1.5 mm-thick) was digested with cellulase from *Trichoderma reesei* (No C2730-50ML, Sigma–Aldrich). For this purpose, each sample was immersed in 2 mL of enzyme solution (50 µL cellulase/mL potassium phosphate buffer, 50 mM, pH 6) and incubated at 37 °C for 1 h, with orbital shaking (180 rpm)³⁴. Then, the samples were centrifuged to collect the probiotics and washed three times with saline solution. Probiotics were suspended in 5 mL of saline solution and colony forming units (CFU) were determined by counting in MRS-agar plates after 24 h of incubation at 37 °C in anaerobic conditions (using the BD GasPak™ ES Anaerobe Container System). The serial dilution with number of visible colonies around 20-300 was used to calculate CFU, and plating was performed in triplicate. Nine independent samples of probiotic cellulose (*Lf*- of *Lg*-cellulose) were digested and analyzed. Data are expressed as mean of experimental triplicates (n = 9) ± standard deviations.

The mass of BC was weighted to denote the concentration of probiotics as CFU per milligram of cellulose. To this aim, samples were immersed in ethanol after the co-culture in HS medium (aerobiosis), boiled in deionized water for 30 min, treated with 0.1 M NaOH at 90 °C for 1h, and washed with deionized

water until neutral pH was achieved²⁴. With this treatment BC was purified and bacteria were removed. Finally, purified celluloses were dried at 100 °C and weighted using a BOECO BAS31plus microbalance. Three replicates were measured.

In vitro Live-dead viability assays by confocal laser scanning microscopy. Bacteria viability of BC and probiotic celluloses was qualitatively assessed by confocal laser scanning microscopy (CLSM). The samples were washed with sterile saline solution and stained with LIVE/DEAD BacLight Bacterial Viability Kit (ThermoFisher) following manufacturer's instructions. This assay combines membrane-impermeable DNA-binding stain, i.e., propidium iodide (PI), with membrane-permeable DNA-binding counterstain, SYTO 9, to stain dead and live bacteria, respectively. Cell viability along the BC matrix was evaluated with a confocal microscope (Nikon Eclipse Ti-E A1) equipped with 20x oil immersion objective. For acquiring SYTO 9 signals (green channel), 488 nm laser and 505–550 nm emission filter were used. For PI (red channel), 561 nm laser and 575 nm long-pass emission filter were used. Images were analyzed with NIS Elements software.

Bacterial activity. pH monitoring and POM reduction capacity. The metabolic activity of *Lf* and *Lg* on probiotic cellulose was evaluated by pH monitoring (HACH SensION™ pHmeter) and measuring its reductive capacity against electrochromic polyoxometalates (POM, $[P_2Mo^{VI}_{18}O_{62}]^{6-}$), following a previously reported protocol.³⁵ Briefly, *Lf*-cellulose and *Lg*-cellulose samples were incubated in 100 mL of diluted MRS broth (1:10) in anaerobic conditions, at 37 °C and 180 rpm. At scheduled times (0, 1, 2, 4, 5, 7 and 20 h), 1mL-aliquot was collected, centrifuged (3000 g, 5 min) and filtered with a 0.2 µm filter to remove any residual bacteria. Then, 190 µL of the sample was mixed with 10 µL of POM solution (10 mM) on a 96-well and irradiated with UV light (365 nm) for 10 min. The absorbance at 820 nm was measured in a

Tecan's NanoQuant plate reader (CIC-UGR). Data are expressed as mean of triplicates \pm standard deviations.

Probiotic survival. The survival rate of *Lf*- and *Lg*-cellulose samples were tested after their storage at 4 °C and 25 °C, for one week and one month, and compared with that of equivalent free CFU. To this aim, we quantified the probiotics and monitored the pH, as described in section 4.3 and 4.5.

Inhibitory and antimicrobial activity of probiotic cellulose against Staphylococcus aureus (SA) and Pseudomonas aeruginosa (PA)

The antimicrobial activity of non-encapsulated probiotics against *SA* and *PA*, two common pathogens involved in wound infection, was initially evaluated by an agar spot test in MRS³⁶. In brief, overnight cultures of probiotics (10^9 CFU mL⁻¹) were inoculated as a 5 μ L spot on MRS agar plates (3 spots/plate). After 24 h of incubation at 37 °C under anaerobic conditions, the plates were overlaid with 6 mL of TSA (0.7 % w/v agar) at 45 °C, previously inoculated with 0.1 mL of an overnight culture of *SA* or *PA*. The plates were incubated 24 h at 30 °C and 37 °C, respectively, before examination of the corresponding inhibition zones. Subsequently, the antimicrobial activity of probiotic cellulose was evaluated by agar diffusion assays³⁷ but in pathogen-favorable tryptic soy media²⁹. The agar diffusion assay was carried out as follows: 0.1 mL of an overnight culture of *SA*, *PA* or *MRSA* was spread on Petri dishes containing TSA. Then, *Lf*- or *Lg*- cellulose were placed on agar plates containing the selected bacterial strains and incubated 24 hours at pathogen optimal temperature (37 °C for *PA*, 30 °C for *SA* and 36 °C for *MRSA*) before examination of inhibition zones. Aliquots of the inhibition zones were selectively grown in MRS or TSB media. In the experiment with *SA*, we only found proliferation in MRS, pointing out the presence of some probiotic cellulose detachment (see Figure 11B). Control experiments with non-encapsulated probiotics, bacterial cellulose (BC) and cellulose with adsorbed probiotics (BC+*Lf*, BC+*Lg*) were also carried out following the same protocol

and using equivalent CFU of *Lf* and *Lg*. After 24 hours of incubation, the inhibition zones of non-encapsulated probiotics and celluloses were imaged and compared. The inhibitory activity of probiotic cellulose was evaluated by time-kill assays³⁸. *Lg*- and *Lf*-cellulose were introduced into TSB medium containing 7×10^6 CFU of pathogen and incubated with orbital shaking for 24 h at 30 °C for *SA* and at 37 °C for *PA*^{29,39}. The pathogen survival was assayed by the serial dilution method, plating on TSA in triplicate and counting after 24 hours of incubation. Control experiments with bacterial cellulose (BC) were also carried out following the same protocol.

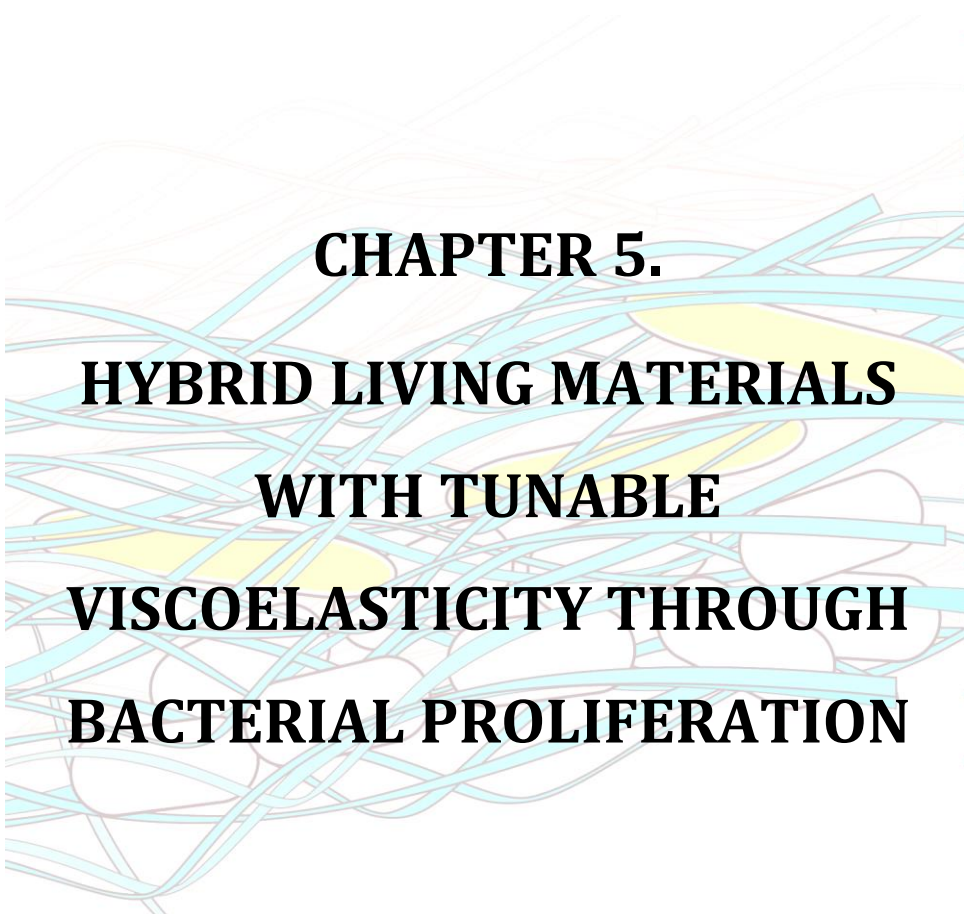
Statistics. Results were analyzed with the software GraphPad Prism and data are expressed as mean \pm standard deviation. For the statistical analysis, we applied the one-way ANOVA, Bonferroni's method.

5. References

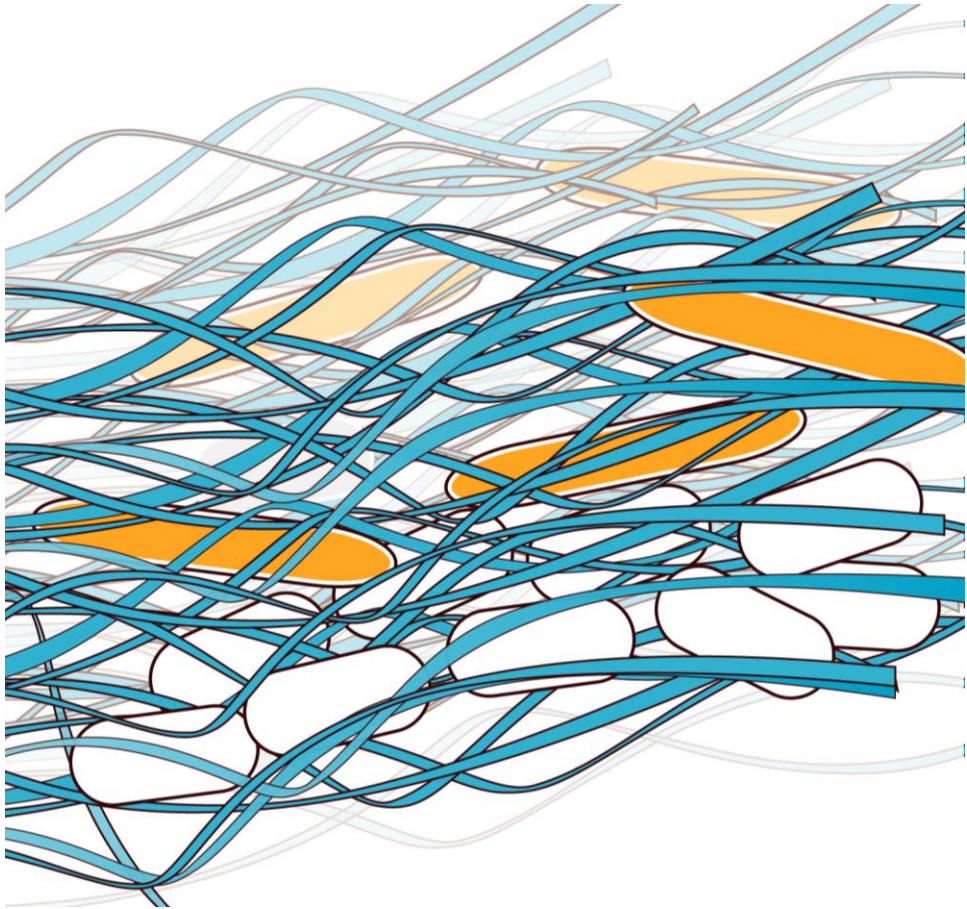
1. Willyard, C. The drug-resistant bacteria that pose the greatest health threats. *Nature* **543**, 15 (2017).
2. Vuotto, C., Longo, F. & Donelli, G. Probiotics to counteract biofilm-associated infections: promising and conflicting data. *Int. J. Oral Sci.* **6**, 189 (2014).
3. Tsiouris, C. G. & Tsiouri, M. G. Human microflora, probiotics and wound healing. *Wound Med.* **19**, 33–38 (2017).
4. Saarela, M., Mogensen, G., Fonden, R., Mättö, J. & Mattila-Sandholm, T. Probiotic bacteria: safety, functional and technological properties. *J. Biotechnol.* **84**, 197–215 (2000).
5. Burgain, J., Gaiani, C., Linder, M. & Scher, J. Encapsulation of probiotic living cells: From laboratory scale to industrial applications. *J. Food Eng.* **104**, 467–483 (2011).
6. Vilela, C., Moreirinha, C., Almeida, A., Silvestre, A. J. D. & Freire, C. S. R. Zwitterionic Nanocellulose-Based Membranes for Organic Dye Removal. (2019).
7. Huq, T. *et al.* Alginate based nanocomposite for microencapsulation of probiotic: Effect of cellulose nanocrystal (CNC) and lecithin. *Carbohydr. Polym.* (2017). doi:10.1016/j.carbpol.2017.03.032
8. Singh, P. *et al.* Cellulose-based edible films for probiotic entrapment. *Food Hydrocoll.* (2019). doi:10.1016/j.foodhyd.2018.08.057
9. Singh, P. *et al.* On the viability, cytotoxicity and stability of probiotic bacteria entrapped in cellulose-based particles. *Food Hydrocoll.* (2018). doi:10.1016/j.foodhyd.2018.04.027
10. Moon, R. J., Martini, A., Nairn, J., Simonsen, J. & Youngblood, J. *Cellulose nanomaterials review: Structure, properties and nanocomposites.* *Chemical Society Reviews* **40**, (2011).
11. Ullah, H., Wahid, F., Santos, H. A. & Khan, T. Advances in biomedical and pharmaceutical applications of functional bacterial cellulose-based nanocomposites. *Carbohydr. Polym.* **150**, 330–352 (2016).
12. Picheth, G. F. *et al.* Bacterial cellulose in biomedical applications: A review. *Int. J. Biol. Macromol.* **104**, 97–106 (2017).
13. Czaja, W., Krystynowicz, A., Bielecki, S. & Brown Jr, R. M. Microbial cellulose—the natural power to heal wounds. *Biomaterials* **27**, 145–151 (2006).
14. Bethke, K. *et al.* Functionalized Cellulose for Water Purification, Antimicrobial Applications, and Sensors. *Adv. Funct. Mater.* **28**, 1–14

- (2018).
15. Weishaupt, R. *et al.* Antibacterial, Cytocompatible, Sustainably Sourced: Cellulose Membranes with Bifunctional Peptides for Advanced Wound Dressings. *Adv. Healthc. Mater.* **9**, 1–13 (2020).
 16. Roig-Sanchez, S. *et al.* Nanocellulose films with multiple functional nanoparticles in confined spatial distribution. *Nanoscale Horizons* **4**, 634–641 (2019).
 17. Anton-Sales, I., Roig-Sanchez, S., Sánchez-Guisado, M. J., Laromaine, A. & Roig, A. Bacterial Nanocellulose and Titania Hybrids: Cytocompatible and Cryopreservable Cell Carriers. *ACS Biomater. Sci. Eng.* **6**, 4893–4902 (2020).
 18. Maneerung, T., Tokura, S. & Rujiravanit, R. Impregnation of silver nanoparticles into bacterial cellulose for antimicrobial wound dressing. *Carbohydr. Polym.* **72**, 43–51 (2008).
 19. Savitskaya, I. S., Shokatayeva, D. H., Kistaubayeva, A. S., Ignatova, L. V. & Digel, I. E. Antimicrobial and wound healing properties of a bacterial cellulose based material containing *B. subtilis* cells. *Heliyon* **5**, e02592 (2019).
 20. Olivares, M., Díaz-Ropero, M. P., Martín, R., Rodríguez, J. M. & Xaus, J. Antimicrobial potential of four *Lactobacillus* strains isolated from breast milk. *J. Appl. Microbiol.* **101**, 72–79 (2006).
 21. Martín, R. *et al.* Human milk is a source of lactic acid bacteria for the infant gut. *J. Pediatr.* **143**, 754–758 (2003).
 22. Gjødsbøl, K. *et al.* Multiple bacterial species reside in chronic wounds: a longitudinal study. *Int. Wound J.* **3**, 225–231 (2006).
 23. Olsson, R. T. *et al.* Making flexible magnetic aerogels and stiff magnetic nanopaper using cellulose nanofibrils as templates. *Nat. Nanotechnol.* **5**, 584–588 (2010).
 24. Chi, K. & Catchmark, J. M. The influences of added polysaccharides on the properties of bacterial crystalline nanocellulose. *Nanoscale* **9**, 15144–15158 (2017).
 25. Gao, M. *et al.* A natural in situ fabrication method of functional bacterial cellulose using a microorganism. *Nat. Commun.* **10**, 1–10 (2019).
 26. González, A., Gálvez, N., Clemente-León, M. & Dominguez-Vera, J. M. Electrochromic polyoxometalate material as a sensor of bacterial activity. *Chem. Commun.* **51**, 10119–10122 (2015).
 27. Kwiecinski, J., Kahlmeter, G. & Jin, T. Biofilm formation by staphylococcus aureus isolates from skin and soft tissue infections. *Curr. Microbiol.* **70**, 698–703 (2015).

28. Li, Z. *et al.* Biofilm-inspired encapsulation of probiotics for the treatment of complex infections. *Adv. Mater.* **30**, 1–7 (2018).
29. Wang, Y., Leng, V., Patel, V. & Scott Phillips, K. Injections through skin colonized with *Staphylococcus aureus* biofilm introduce contamination despite standard antimicrobial preparation procedures. *Sci. Rep.* **7**, 1–9 (2017).
30. Schramm, M. & Hestrin, S. Factors affecting production of cellulose at the air/liquid interface of a culture of *Acetobacter xylinum*. *J. Gen. Microbiol.* **11**, 123–129 (1954).
31. Herman, L. *et al.* The qualified presumption of safety assessment and its role in EFSA risk evaluations: 15 years past. *FEMS Microbiol. Lett.* **366**, 1–7 (2019).
32. Gorgieva, S. Bacterial Cellulose as a Versatile Platform for Research and Development of Biomedical Materials. *Processes* **8**, 1–26 (2020).
33. Becerra, S. C., Roy, D. C., Sanchez, C. J., Christy, R. J. & Burmeister, D. M. An optimized staining technique for the detection of Gram positive and Gram negative bacteria within tissue. *BMC Res. Notes* **9**, 1–10 (2016).
34. Hu, Y. & Catchmark, J. M. Integration of cellulases into bacterial cellulose: Toward bioabsorbable cellulose composites. *J. Biomed. Mater. Res. Part B Appl. Biomater.* **97**, 114–123 (2011).
35. González, A., Gálvez, N., Clemente-León, M. & Dominguez-Vera, J. M. Electrochromic polyoxometalate material as a sensor of bacterial activity. *Chem. Commun.* **51**, 10119–10122 (2015).
36. Tejero-Sariñena, S., Barlow, J., Costabile, A., Gibson, G. R. & Rowland, I. In vitro evaluation of the antimicrobial activity of a range of probiotics against pathogens: Evidence for the effects of organic acids. *Anaerobe* **18**, 530–538 (2012).
37. Khalid, A., Khan, R., Ul-Islam, M., Khan, T. & Wahid, F. Bacterial cellulose-zinc oxide nanocomposites as a novel dressing system for burn wounds. *Carbohydr. Polym.* (2017). doi:10.1016/j.carbpol.2017.01.061
38. Balouiri, M., Sadiki, M. & Ibsouda, S. K. Methods for in vitro evaluating antimicrobial activity: A review. *J. Pharm. Anal.* **6**, 71–79 (2016).
39. Wang, Y., Tan, X., Xi, C. & Phillips, K. S. Removal of *Staphylococcus aureus* from skin using a combination antibiotic approach. *npj Biofilms Microbiomes* (2018). doi:10.1038/s41522-018-0060-7



CHAPTER 5.
HYBRID LIVING MATERIALS
WITH TUNABLE
VISCOELASTICITY THROUGH
BACTERIAL PROLIFERATION



1. Introduction

Hybrid Living Materials (HLMs) are an emergent class of materials formed by combining living biological entities with soft materials, such that the resulting biomaterial takes on the functional properties of both building blocks. In HLMs, the properties of the abiotic component can modify the functionality of the living entity, and conversely, the cellular component can switch the properties of the material counterpart¹⁻⁴. Switching materials have indeed the ability to turn their properties in response to external stimuli, enabling or disabling the on-off state. This class of materials have a great presence in our daily life since they are present in many and varied applications. Examples of switching materials include dielectrics that switch to conductors, colorless to colored materials, paramagnets to ferromagnets, etc. The external input triggering the switch can be the pressure, as in piezoelectric materials, that after sensing a higher pressure, switch from dielectric to conductors⁵; the light, as it occurs in photochromic materials, that change color after light irradiation⁶; magnetic field⁷, heat⁸, etc.

In the field of biomedicine, the best-known example of switching material is probably that constituted by a family of resins, which cure or harden after UV irradiation^{9,10}. This procedure is useful for enamel or dentin repair, which can be irradiated by the UV light, but it is not useful for repairing chipped or cracked internal bones, as the UV radiation is absorbed by tissues and cannot reach the bone. In general, the possibility to tune the properties of a material in an internal tissue in the body becomes difficult since external stimuli have limitations to reach the material. However, it is still possible to use internal stimuli, such as pH, to tune adequately the properties of a material¹¹. In fact, the pH change from the bloodstream to the lysosome is used to open closed structures of some drug-containing biomolecules, thus triggering the drug delivery. However, this option is restricted to specific applications mostly related to drug delivery.

Viscoelasticity, i.e., the tendency of a material to act both like a solid and fluid, is a very interesting material property for a broad range of applications. Viscoelastic materials show an intermediate behavior between a linear viscous (Newtonian) liquid and an elastic (Hookean) solid¹². Viscoelasticity plays a key role in many processes ranging from the extrusion of polymer melts into molds to the bread-making performance of a dough. Viscoelasticity is also crucial in natural biological materials such as cartilage and skin, and synthetic ones such as shaving foams and paints. Bone, for instance, is a good example of viscoelastic material that exhibits both creep (deformation) and stress relaxation¹³.

Here, we present a new HLM, so-called probiotic cellulose (PC)¹⁴, with programmable viscoelasticity. This biohybrid consists of a non-living matrix of bacterial cellulose (BC) in which, living and active probiotic bacteria are perfectly integrated. We demonstrated that probiotic proliferation strongly modifies the viscoelasticity of the cellulose matrix, i.e., obtaining celluloses with lower-than-matrix fluidity at low probiotic density, but with viscoelastic moduli close to those of elastic solids at higher probiotic density. PC is the first example of a HLM with tunable viscoelasticity by life (probiotic proliferation).

2. Results and discussion

2.1. Production of HLMs

BC is produced by certain types of bacteria, being the *Gluconacetobacter xylinus* (*Gx*) the most effective¹⁵. In contrast to that produced by plants, BC forms long fibers with nanometric diameters (10-80 nm), which confers it with a very high specific surface area, water-holding, and absorption capability¹⁶. As produced, the fibrillar network of BC contains the cellulose-producing bacteria *Gx* (BC-*Gx*, Scheme 1B). However, the treatment of BC-*Gx* with ethanol and alkali at high temperature eliminates *Gx*, giving rise to pure bacterial cellulose¹⁷ (BC, Scheme 1B).

Conversely, we have recently shown that the co-cultivation of aerobic *Gx* and facultative anaerobic probiotic (such as *Lactobacillus fermentum*, *Lf*) under aerobic conditions results in the formation of a cellulose film containing both *Gx* and *Lf*¹⁴. Switching to anaerobic environment and the media to MRS (optimal conditions for *Lf* but harsh for *Gx*), *Lf* gradually proliferates and invades the whole cellulose matrix, at the expense of *Gx* (Figure 1B). This approach allows the probiotic density within the BC network to be tuned with the incubation time. Samples obtained at 0, 5, 24 and 48 hours of incubation in anaerobic MRS media (referred to as PC-*Lf*₀, PC-*Lf*₅, PC-*Lf*₂₄ and PC-*Lf*₄₈) contained a gradually increased density of *Lf*, respectively (Figure 1A).

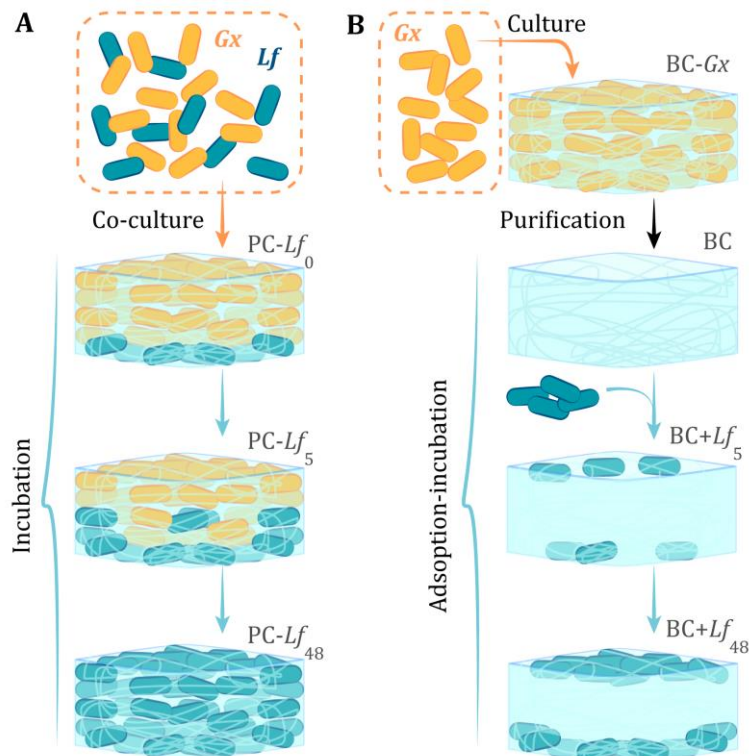


Figure 1. Graphical representation of the experimental protocols used to build PC, through the co-incubation of *Gx* and *Lf* (A), and BC-*Gx*, BC (after purification of BC-*Gx*) and then functionalized with probiotics (BC+*Lf*) through the adsorption incubation method (B).

Field Emission Scanning Electron Microscopy (FESEM) micrographs of BC, BC-*Gx* and PC samples with increasing *Lf* probiotic density are shown in Figure 2. The diameter of the cellulose fibers (60 nm in average, Figure 3A) was similar in all the samples and the corresponding X-ray diffraction (XRD) patterns (Figure 3B), with the characteristic diffraction peaks of cellulose nanocrystals assembled forming long fibers, neither showed noticeable structural differences (despite the increase of diffuse scattering coming from the increasing bacteria density)¹⁸. These results confirmed that the presence of probiotics in the culture media did not affect the microstructure of the cellulose fibers (Figure 3A). As expected, FESEM micrograph of BC-*Gx* showed the presence of elongated *Gx* with its typical fibrous morphology (Figure 2B), whereas no bacteria were visible in BC (Figure 2A), obtained after purification of BC-*Gx*. FESEM images of PCs revealed the extensive proliferation of *Lf* upon incubation time, until invading the entire cellulose matrix (PC-*Lf*₄₈, Figure 2D). Average lengths of 3.0 and 1.5 μm were obtained for *Gx* and *Lf* from FESEM micrographs of BC-*Gx* and PC-*Lf*₄₈, respectively (Figure 2E). The length of *Gx* is reduced at the early stages of cultivation in anaerobic MRS media (PC-*Lf*₅, Figure 2C).

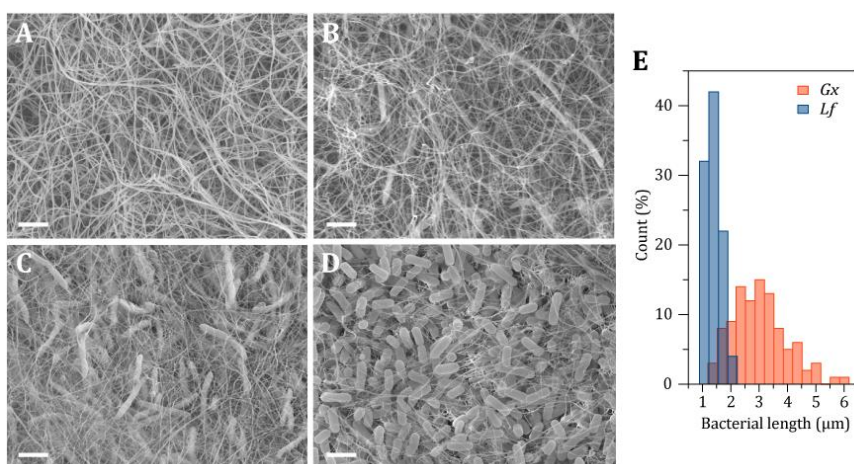


Figure 2. FESEM images of (A) BC, (B) BC-*Gx*, (C) PC-*Lf*₅ and (D) PC-*Lf*₄₈. Scale bars = 2 μm . (E) Histogram of *Gx* and *Lf* lengths as obtained from FESEM micrographs of BC-*Gx* and PC-*Lf*₄₈, respectively (n = 100).

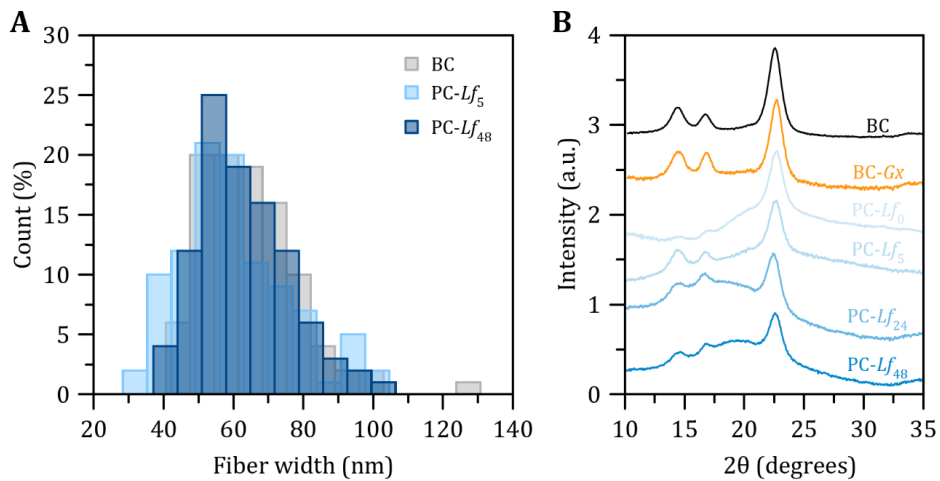


Figure 3. (A) Histogram of the fiber widths of BC, PC- Lf_5 and PC- Lf_{48} . As obtained from FESEM micrographs ($n = 100$). **(B)** XRD patterns of BC, BC-Gx and PC with different probiotic densities.

Similar conclusions were obtained by confocal laser scanning microscopy (CLSM) (Figure 4) after labelling the samples with the pair SYTO9/propidium iodide fluorescent dyes. The CLSM image of PC- Lf_0 consisted of a mixture of live (green-labelled) *Gx* and *Lf* bacteria, whereas that of PC- Lf_5 showed a mixture of live and dead bacteria (red-labelled), the latter corresponding to *Gx*. As expected, CLSM images of PC- Lf_{48} exhibited high density of living *Lf* invading the entire cellulose matrix. We used CLSM images collected at different depth to measure the area fraction of bacteria (*Gx* and *Lf*) into the cellulose matrix. The minimal fraction was found for PC- Lf_5 (Figure 4F), most likely due to the shrinkage of *Gx* occurring during probiotic proliferation, as commented before. Subsequently, the massive proliferation of probiotics (PC- Lf_{48} , Figure 4C) caused an increase of the area ratio (Figure 4C).

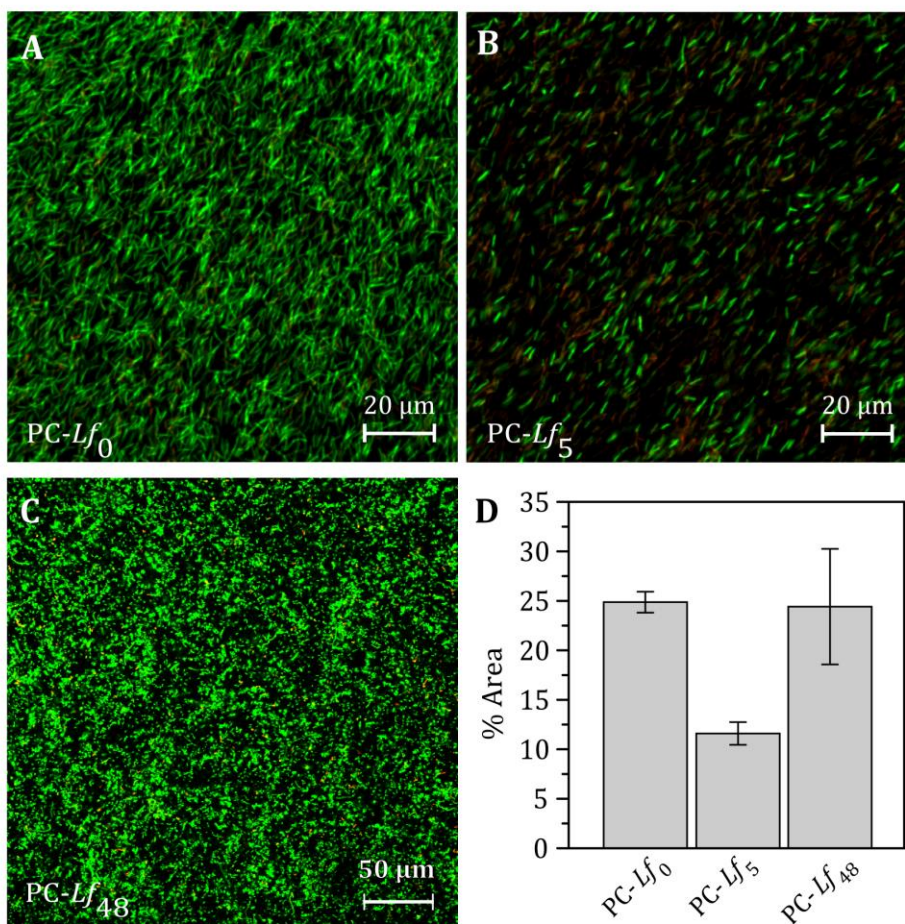


Figure 4. CLSM images of **(A)** PC-Lf₀, **(B)** PC-Lf₅, and **(C)** PC-Lf₄₈. Green channel (SYTO 9) and red channel (propidium iodide) represents live and dead bacteria, respectively. **(D)** Histogram showing the percentage of green/red areas.

In parallel, we have prepared a set of celluloses with *Lf* probiotics by the adsorption-incubation method¹⁹ (BC+*Lf*, Figure 1B). In this case, probiotics were not integrated in the matrix but only located at the surface (Figure 5), since the dense cellulose fibril network does not allow the penetration.

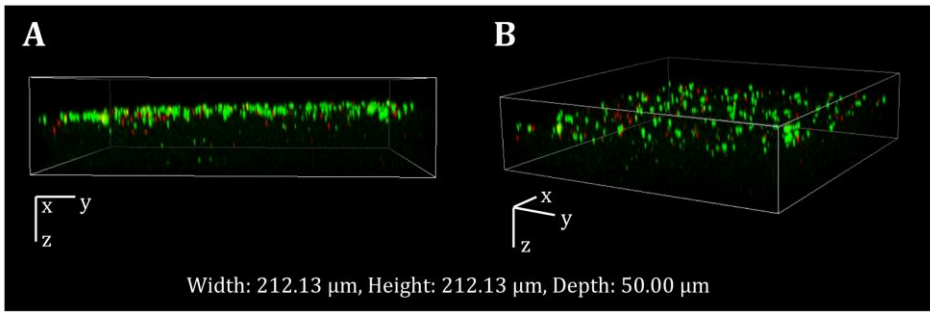


Figure 5. CLSM images of BC functionalized with Lf (BC + Lf) demonstrating that the probiotic does not penetrate through the cellulose network by this preparation method (adsorption-incubation). **(A)** side-view and **(B)** perspective view of a CLSM three-dimensional reconstruction. Green channel (SYTO 9) and red channel (propidium iodide) represents live and dead bacteria, respectively.

2.2. Compression tests

The mechanical response of the PC biomaterials was initially assessed by compression tests. All the rheological experiments were performed under the supervision of Juan de Vicente Álvarez Manzaneda, from the Department of Applied Physics (UGR). Cellulosic samples were progressively squeezed at constant velocity until reaching a normal force (F_N) of 0.3 N (954.93 Pa). The experimental setup and raw data of F_N as a function of the gap separation (h) are represented in Figure 6. BC and PC samples exhibited a two-step response. At large initial gaps, water was gradually expelled from the samples so the normal force increases slowly when closing the gap. At the end of the compression process (small gaps) the plate was inelastically deforming the cellulose matrix so that the normal force increases quicker when decreasing the gap separation. The compression moduli E , i.e., the slope of the stress (σ) vs strain (ε) curves, were calculated in the range $0 < \varepsilon < 0.3$ (Figure 6D). The compression modulus accounts for the resistance of the material to be compressed. As observed, the compression modulus in the low strain region was very

similar (no significant differences) for all the samples (Figure 6E). This result was expected because, as discussed before, the cellulosic matrix was not affected by the presence of the different bacteria over culture time. However, the situation at higher strains is rather different. Samples with high density of probiotics (PC- Lf_{48}) were inelastically deformed at lower strain than BC (Figure 6D). On the contrary, higher strains were needed to deform inelastically the samples with low density of probiotics (PC- Lf_0 , PC- Lf_5 , PC- Lf_{24}), being needed strains close to 1 to deform inelastically the sample PC- Lf_5 (Figure 6D).

We also monitored the gap separation between the plates of the rheometer (Figure 7); h_0 corresponds to the initial gap separation when the plates initially get in contact with the sample (i.e., F_N starts to increase). On the other hand, h_1 corresponds to the final gap separation at the end of the compression when the $F_N = 0.3$ N criteria is fulfilled. As expected, h_0 was very similar for all the samples tested, having practically the same thickness (ca. 1.5 mm) (Figure 7A). However, h_1 was strongly sample-dependent (Figure 7B). PC- Lf_{48} showed a significantly larger h_1 than that observed in BC. These differences are a consequence of the high density of Lf inside the cellulose backbone. On the contrary, samples with low probiotic density (PC- Lf_0 and PC- Lf_5) showed an unusual high compressibility. In fact, the final gap h_1 of these samples was around 10-times thinner than that of the BC matrix (Figure 7). All these observations confirm that bacterial density within the matrix play a key role in the mechanical response of the PCs biomaterials.

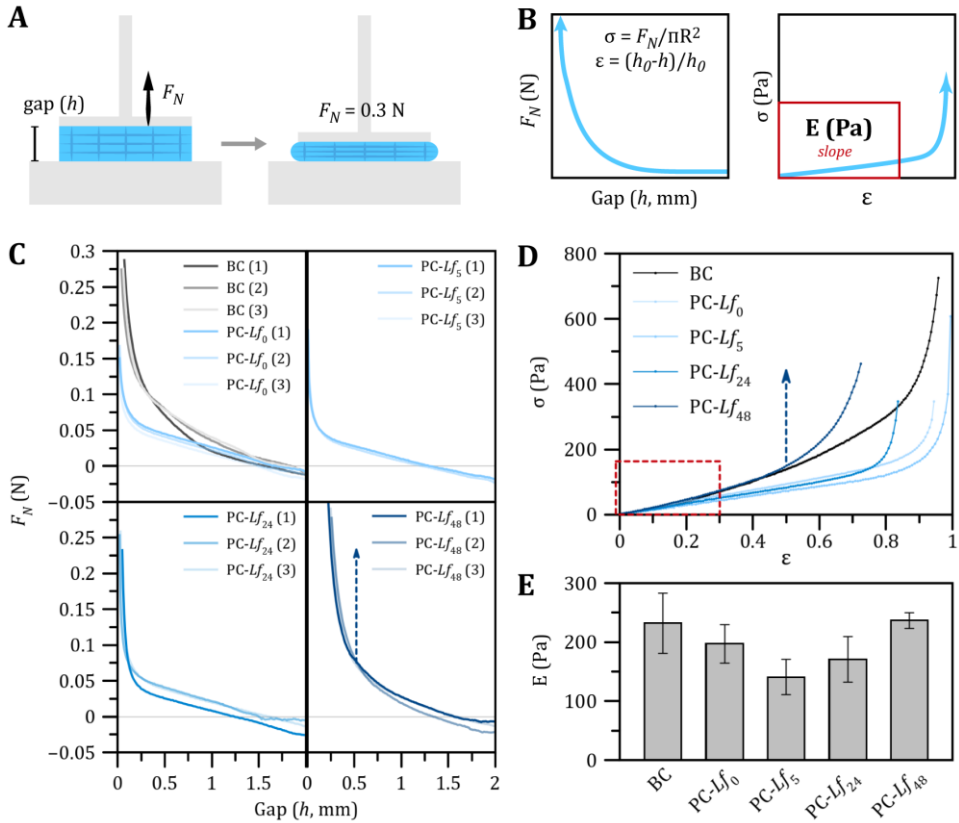


Figure 6. (A) Scheme of the experimental setup used during the compression tests. **(B)** Graphical representation of the extracted information. **(C)** Plots of the normal force (F_N) as a function of the gap separation distance (h) measured during compression tests of BC and PC. Each measurement was performed in triplicate (1-3) to confirm the good reproducibility between experiments with different samples prepared under the same experimental conditions. Compression curves are typical of samples with a two-step response. The blue arrow represents the force at which the plate starts to deform inelastically the cellulosic sample. **(D)** Plots of the compressive stress ($\sigma = F_N / \pi r^2$, being r the radius of the plate, 1 cm) vs strain ($\epsilon = (h_0 - h) / h_0$, being h_0 the gap separation when the plate contacts the sample, $F_N > 0$). Data errors are lower than 11 Pa (in the first-step response). The slope of the interval $\epsilon \in [0, 0.3]$ is estimated as the compression modulus E , represented in panel **(E)** as vertical bars. Non-significant differences were found for E values ($p < 0.05$) after perform one-way ANOVA, Bonferroni's post-test.

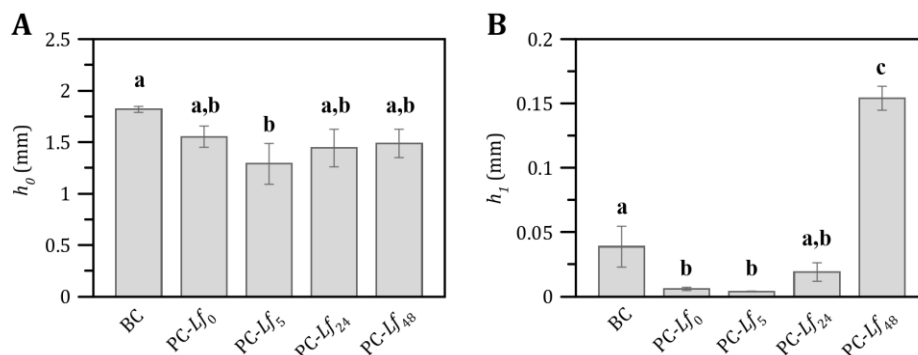


Figure 7. Gap separation between the plates of the rheometer (h) when the upper plate is set in motion and contacts the sample (**A**, $h = h_0$), and after a normal force of 0.3 N is achieved (**B**, $h = h_1$). Different letters indicate significant differences ($p < 0.05$) between samples after one-way ANOVA, Bonferroni's method analysis.

2.3. Strain amplitude sweep tests

Once the samples were confined between the plates ($F_N = 0.3$ N), dynamic oscillatory shear tests were carried out by increasing the strain amplitude from 10^{-4} % to 200 % at a constant frequency of 1 Hz to explore their viscoelastic characteristics under shear. The experimental setup and the resulting averaged curves are shown in Figure 8C. For sufficiently small strains both viscoelastic moduli remain flat (this is the so-called linear viscoelastic region, LVR). Here, the storage modulus (G') is greater than the loss modulus (G''), indicating an elastic behavior. Plateau values of these linear regions are shown in Figure 9A. When the strain amplitude increases, G' and G'' decrease indicating the onset of non-linearity (linearity limit or yield point, Figure 8B). For strains above the flow point (i.e., $G' = G''$), the sample dissipates more energy than it can store.

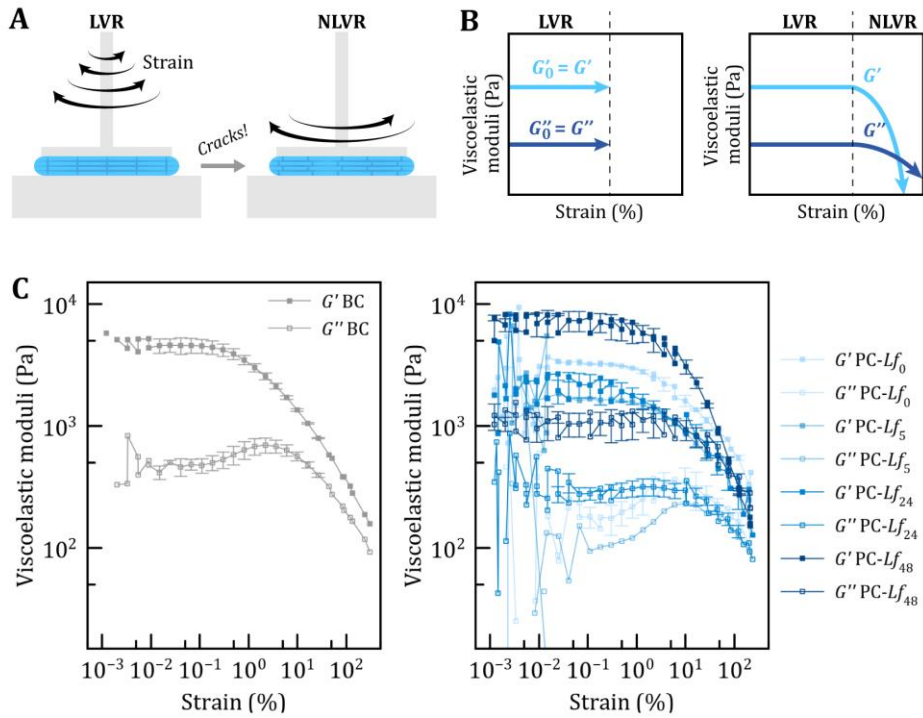


Figure 8. (A) Scheme of the experimental setup used during the strain-amplitude sweep tests. (B) Graphical representation of the extracted information. (C) Averaged data of strain amplitude sweep tests of BC (left), and PC- Lf_0 , PC- Lf_5 , PC- Lf_{24} , and PC- Lf_{48} (right). Data show means \pm SD of triplicates.

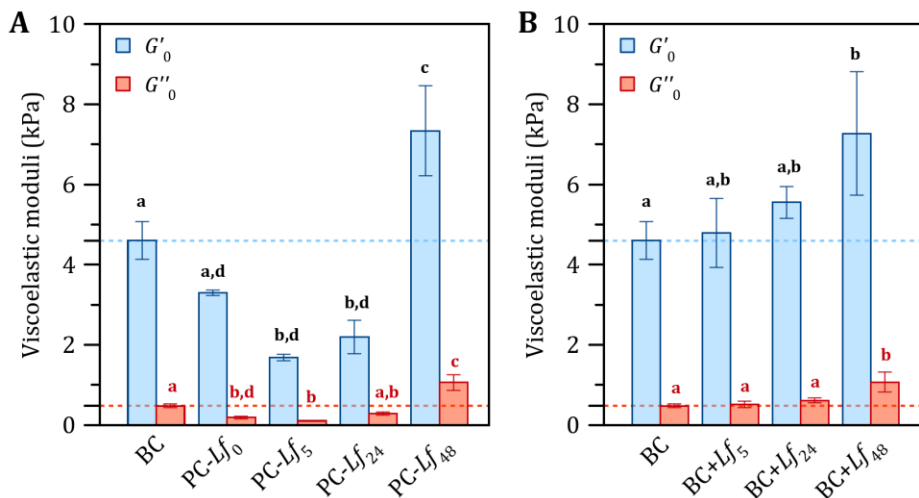


Figure 9. Viscoelastic moduli (G'_0, G''_0) in the linear viscoelastic region (LVR) as obtained from strain amplitude sweep tests for **(A)** BC and PC, and for **(B)** BC+Lf (obtained by the adsorption-incubation method), with increasing contents of bacteria. Statistical analysis was carried out by the one-way ANOVA (Bonferroni's method). Different letters indicate significant differences ($p < 0.05$) between samples (black and red letters for G'_0 and G''_0), respectively).

Substantial differences are found for G'_0 and G''_0 being both moduli highly dependent on bacterial density. The incorporation of probiotics produces a huge impact in the viscoelastic moduli. Interestingly, PC-Lf₀ and PC-Lf₅ exhibited lower viscoelastic moduli than that of the BC matrix. From these samples, the moduli start to increase with the exponential growth of probiotics (PC-Lf₂₄ and PC-Lf₄₈). Qualitatively, the evolution of moduli in these samples matches that of the volume fraction that bacteria occupy in the cellulose matrix (Figure 4D). The viscoelasticity of these materials seems to be the result of a compromise between two factors: a small bacterial fraction favors sliding between cellulose fibers, while a large fraction hinders such sliding. In this sense, it has to be noted that a similar correlation exists between dislocation density and the hardness of a metallic material. At low dislocation density, plastic deformation occurs when

dislocations move. However, high dislocation density hinders dislocation motion and renders the material stronger than previously. In the context of PC samples, the entrapped bacteria in the cellulose network can be considered as sliding cylinders. A reduced bacterial density favors the slipping between fibers. However, this sliding effect is lost above a certain number of cylinders, which becomes an impediment for the fibers to slide.

This interesting density-dependent sliding effect is only observed when the bacteria is perfectly integrated into the matrix and a real hybrid material is at work. Indeed, the behavior is completely different when the living cellulose biomaterials are produced by the adsorption-incubation procedure (Figure 1B). When probiotics are exclusively located at the surface, the sliding effect was not observed. Thus, in contrast to PC-*Lf* samples, the viscoelastic moduli of BC+*Lf* samples increased with the incubation time (bacterial proliferation), and were all larger than that of the BC matrix (Figure 9). A similar trend was observed when the bacteria proliferated free in aqueous media (Figure 10). In this case, the viscosity (η) of the bacterial suspension increases with bacteria concentration as typically occurs in colloidal dispersions.

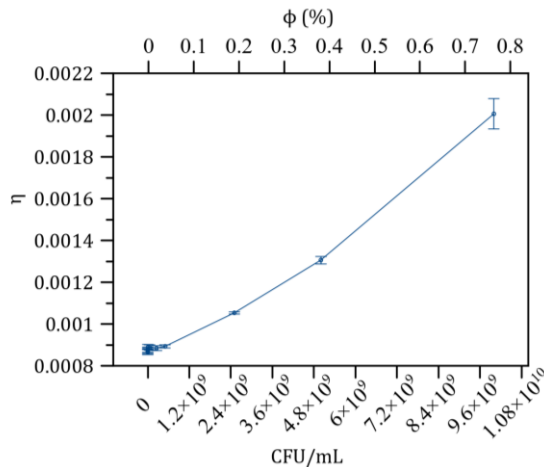


Figure 10. Shear viscosity (η) of a *Lf* suspension with increasing probiotic densities. Data are expressed as mean of triplicates \pm SD.

Figure 11 illustrates the impact of the change of viscoelasticity in these living celluloses. PC-*Lf*₅, the sample having the lowest viscoelastic moduli, is a transparent gel-like fluid pellicle, whereas PC-*Lf*₄₈, that of the highest moduli, looks like an opaque solid, due to the high density of probiotics inside.

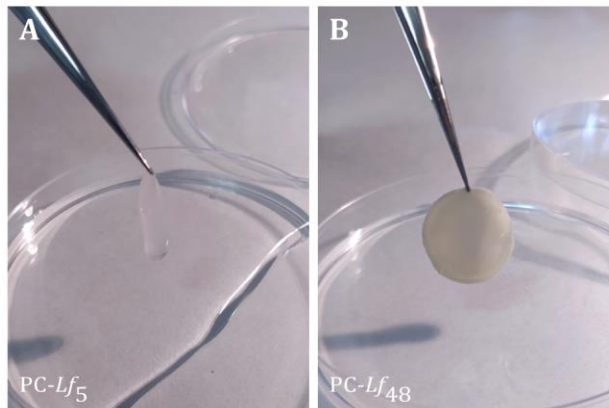


Figure 11. Photographs of **(A)** PC-*Lf*₅ and **(B)** PC-*Lf*₄₈. The diameter of the samples was 2 cm.

3. Conclusions

The co-cultivation of (aerobic) cellulose-producing bacteria and (facultative anaerobic) probiotics produce HLMs in which the metabolically active probiotics are fully integrated into the fibrillar cellulose network. Dedicated rheological measurements confirmed that the viscoelasticity of the resulting biohybrids can be tuned with probiotic proliferation (bacterial density). Indeed, biomaterials with lower-than-matrix fluidity were obtained at low probiotic density, which turn to elastic solids at high probiotic density. This new concept is a very promising alternative to obtain bio-inks for *in vivo* bioprinting using, for the first time, life (proliferation) as external stimuli to switch the material fluidity.

4. Materials and methods

Reagents and solutions. High-grade quality reagents were used as received from commercial suppliers unless otherwise stated. Aqueous solutions were prepared with ultrapure water (18.2 M Ω .cm, Bacteria < 0.1 CFU/mL at 25°C, Milli-Q, Millipore).

Bacteria culture. The lyophilized *Gluconacetobacter xylinum* (ATCC 11142, CECT 473), *Gx*, was supplied by the Colección Española de Cultivos Tipo (CECT) and grown in Hestrin-Schramm (HS) agar²⁰ at 30 °C. HS medium formula is (w/v) 2% glucose, 0.5% yeast extract, 0.5% peptone, 0.115% citric acid, 0.68% Na₂HPO₄ · 12 H₂O (Sigma). *Lactobacillus fermentum*, *Lf*, was kindly provided by Biosearch Life S.A. and grown in de Man, Rogosa and Sharpe medium (MRS, Oxoid) at 37°C.

Bacterial cellulose synthesis and incorporation of probiotics by co-culture. The synthesis of bacterial cellulose was carried out by culturing 0.1 mL of an *Ax* suspension (OD_{600 nm} = 0.3) in 1 mL of HS broth and aerobic conditions at 30°C for 3 days. After incubation, a thick gel-like membrane was produced in the liquid-air interface, composed of *Gx* bacteria and cellulose (BC-*Gx*). To obtain purified bacterial celluloses (BC), these pellicles were treated following the traditional procedure. Briefly, the membranes were immersed in ethanol 96° for 15 min, followed by immersion in boiling water for 40 min, and four washings of NaOH 0.1M at 90°C of 20 min each. Finally, the pure cellulosic pellicles were washed with distilled water until neutral pH was achieved.

On the other hand, bacterial celluloses with probiotics were synthesized as previously reported¹⁴. Briefly, 0.1 mL of an *Gx* suspension (OD_{600 nm} = 0.3) was mixed with 0.1 mL of a *Lf* suspension (OD_{600 nm} = 0.3) in 1 mL of HS medium and co-cultured in aerobic conditions at 30°C, for 3 days. We referred to this material as PC-*Lf*₀. Afterwards, HS medium was replaced with MRS and PC-*Lf*₀ was incubated in anaerobic conditions at 37 °C for 5, 24

and 48 h, resulting in the obtention of PC- Lf_5 , PC- Lf_{24} and PC- Lf_{48} , respectively. The MRS broth was replaced after 24 h. BC samples cultured in MRS after Lf adsorption for identical times (BC+ Lf_5 , BC+ Lf_{24} and BC+ Lf_{48}) were used for comparison. Every synthesis was performed by using 2 cm-diameter vials in order to obtain circular BC samples with appropriate dimensions to carry out the rheological experiments.

Rheological experiments. A torsional rheometer (MCR302 Anton Paar) was used to interrogate the mechanical properties of cellulose matrices both in compression and shearing mode. Experiments for BC, BC- Gx , PC- Lf and BC+ Lf samples were carried out at 25 °C in a parallel plate configuration (20 mm diameter). We used plates with rough surfaces to prevent sample slippage. Rheological experiments are conducted in two intervals using triplicates.

Interval #1.- Compression test. The sample is placed on the bottom plate and the upper one is displaced downward (i.e., closing the gap) at a constant velocity ($v = 10 \mu\text{m/s}$). During the plate motion, the normal force acting on it, due to the sample, is monitored. This interval ends when the normal force reaches $F_N = 0.3 \text{ N}$.

Interval #2.- Shearing test. During this interval, the sample is confined between the two plates at a constant normal force of $F_N = 0.3 \text{ N}$ and subjected to an oscillatory strain of increasing strain amplitude at a constant frequency ($f = 1 \text{ Hz}$).

Using this particular protocol, it is possible to investigate both the compressive and shearing properties of the same sample. From the first interval it is possible to obtain the compressive modulus. From the second interval it is possible to elucidate the storage and loss moduli in the viscoelastic linear region as well as the onset of non-linearity under shear.

Viscosity of Lf suspensions: We also analysed Lf suspensions at different concentrations in sterile saline solution 0.9% (w/v). A volume of 0.7 mL of

different bacterial concentrations were used, ranging from 10^{10} colony forming units (CFU) per mL to $5 \cdot 10^4$ CFU/mL. The experiments were performed in a cone-plate geometry (50 mm diameter and 1° angle) in three intervals by triplicate. The first interval consists in a preshear to remove the mechanical history of the sample (shear rate of 500 s^{-1}). In the second interval the sample is allowed to rest for a short time. In the third interval the sample is sheared at an increasing shear rate from 0.01 to 1 s^{-1} .

Bacterial viability test. Bacterial viability and distribution of PC- Lf_0 , PC- Lf_5 , and PC- Lf_{48} , was qualitatively assessed by confocal laser scanning microscopy (CLSM). The samples were washed with sterile saline solution and stained with LIVE/DEAD BacLight Bacterial Viability Kit (ThermoFisher) following manufacturer's instructions. This assay combines membrane-impermeable DNA-binding stain, i.e., propidium iodide (PI), with membrane-permeable DNA-binding counterstain, SYTO9, to stain dead and live and dead bacteria, respectively. Cell viability along the BC matrix was evaluated with a confocal microscope (Nikon Eclipse Ti-E A1, Centre for Scientific Instrumentation, University of Granada, CIC-UGR) equipped with 20x objective. For acquiring SYTO 9 signals (green channel), 488 nm laser and 505–550 nm emission filter was used. For PI (red channel), 561 nm laser and 575 nm long-pass emission filter were used. Images were analysed with NIS Elements software.

Field-emission scanning electron microscopy (FESEM). BC and PC- Lf samples were fixed in 1 mL of cacodylate buffer (0.1 M, pH 7.4) containing 2.5% of glutaraldehyde at 4°C for 24 h. Subsequently, samples were washed with cacodylate buffer three times for 30 min at 4°C . The samples were stained with osmium tetroxide (OsO_4) solution (1% v/v) for 2 h in the dark, being then repeatedly rinsed with Milli-Q water to remove the excess of OsO_4 solution. Samples were then dehydrated at room temperature with ethanol/water mixtures of 50%, 70%, 90% and 100% (v/v) for 20 min each,

being the last concentration repeated three times and dried at the CO₂ critical point. Finally, dehydrated samples were mounted on aluminium stubs using a carbon tape, sputtered with a thin carbon film, and analysed using a FESEM (Zeiss SUPRA40V) of the CIC-UGR.

Bacterial dimensions and volume fraction estimation. The length of G_x and L_f ($n = 100$) were measured from FESEM micrographs of BC- G_x and PC- L_{f48} , respectively, using ImageJ 1.52a software (<http://imagej.nih.gov/ij>). For L_f volume estimation, we also measured the width of the probiotic from FESEM images and we correlated bacteria with a cylinder, thus resulting the volume calculation as the product of $\pi \cdot (\text{width}/2)^2 \cdot \text{length}$. The volume fraction (Φ) calculation was estimated considering the CFU concentration.

Cellulose fiber width distribution. Fiber widths ($n=100$) of BC, PC- L_{f5} and PC- L_{f48} were measured from FESEM images using ImageJ software.

X-ray diffraction patterns (XRD). XRD patterns were collected from the surface of lyophilized cellulose films using a Bruker D8 Discover diffractometer (CIC-UGR) equipped with a 2D-detector (Pilatus3R 100K-A, Dectris), at 25 °C, with Cu K α ($\lambda = 1.5406 \text{ \AA}$) radiation generated at 50 kV and 1 mA. The XRD diffraction patterns were recorded at a rate of 40 s/step from 10° to 40° with a step size of 0.02°. Each spectrum was baseline-corrected and normalized to the maximum intensity at around 2θ value of 22.5°.

The freeze-drying of the samples was carried out by freezing in liquid nitrogen for 10 min before drying under vacuum at -60 °C for 2 days using a Telstar Cryodos-50.

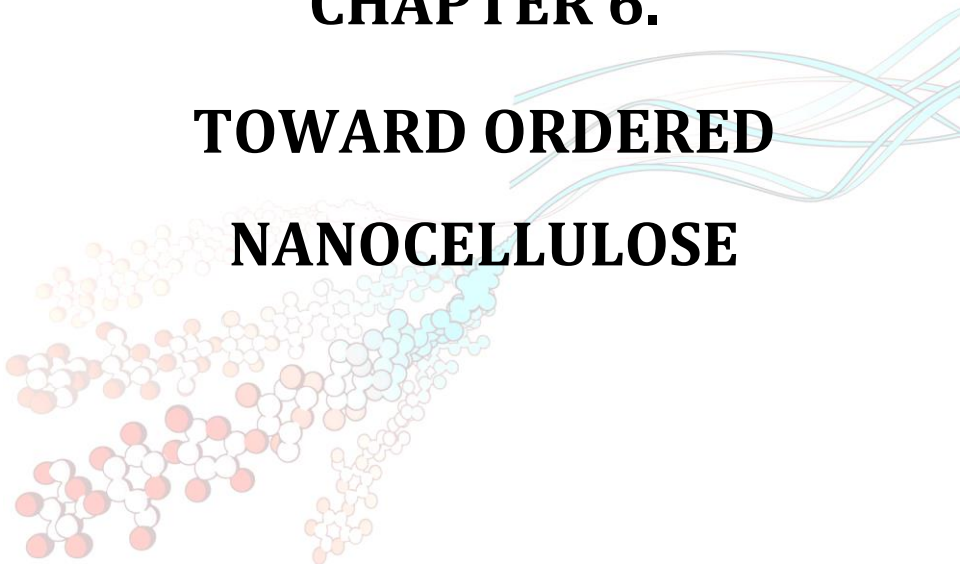
Statistics and graphs. Results were analysed with the software OriginPro 8 and Excel, and data are expressed as mean of three replicates \pm standard deviations. The software MagicPlot Pro 2.9.3 was used for plotting the data and statistical analysis were performed with GraphPad Prism v5.0.

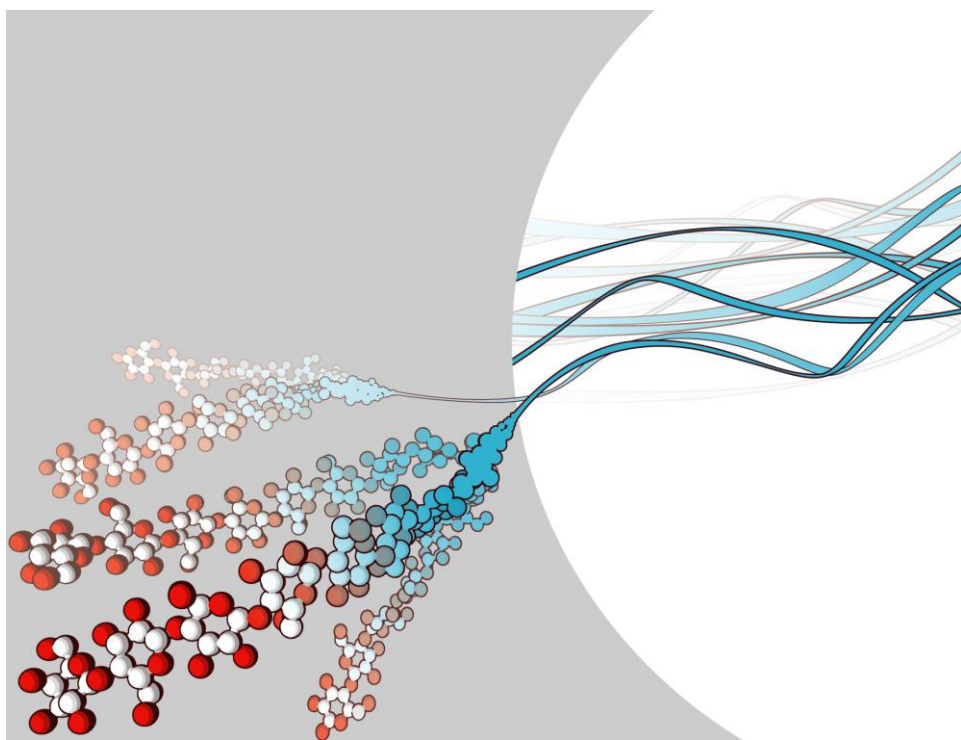
5. References

1. Rodrigo-Navarro, A., Sankaran, S., Dalby, M. J., del Campo, A. & Salmeron-Sanchez, M. Engineered living biomaterials. *Nat. Rev. Mater.* **6**, 1175–1190 (2021).
2. Nguyen, P. Q., Courchesne, N.-M. D., Duraj-Thatte, A., Praveschotinunt, P. & Joshi, N. S. Engineered Living Materials: Prospects and Challenges for Using Biological Systems to Direct the Assembly of Smart Materials. *Adv. Mater.* **30**, 1704847 (2018).
3. Tang, T.-C. *et al.* Materials design by synthetic biology. *Nat. Rev. Mater.* **6**, 332–350 (2021).
4. Smith, R. S. H. *et al.* Hybrid Living Materials: Digital Design and Fabrication of 3D Multimaterial Structures with Programmable Biohybrid Surfaces. *Adv. Funct. Mater.* **30**, (2020).
5. Wei, H. *et al.* An overview of lead-free piezoelectric materials and devices. *J. Mater. Chem. C* **6**, 12446–12467 (2018).
6. Irie, M. Photochromism: Memories and Switches s Introduction Diarylethenes for Memories and Switches. *Chem. Rev.* **100**, 1685–1716 (2000).
7. Municoy, S., Ibañez, I. L., Durán, H. & Bellino, M. G. A catalase-magnetic switch for cell proliferation. *RSC Adv.* **4**, 15077–15080 (2014).
8. Chen, X. G. *et al.* Above room-temperature dielectric and nonlinear optical switching materials based on [(CH₃)₃Sn]₂[MBr₄] (M = Cd, Mn and Zn). *Dalt. Trans.* **48**, 11292–11297 (2019).
9. Liu, F., Liu, A., Tao, W. & Yang, Y. Preparation of UV curable organic/inorganic hybrid coatings-a review. *Prog. Org. Coatings* **145**, 105685 (2020).
10. Revilla-León, M., Meyers, M. J., Zandinejad, A. & Özcan, M. A review on chemical composition, mechanical properties, and manufacturing work flow of additively manufactured current polymers for interim dental restorations. *J. Esthet. Restor. Dent.* **31**, 51–57 (2019).
11. Wang, R. *et al.* pH-Controlled drug delivery with hybrid aerogel of chitosan, carboxymethyl cellulose and graphene oxide as the carrier. *Int. J. Biol. Macromol.* **103**, 248–253 (2017).
12. Phan-Thien, N. *Understanding Viscoelasticity*. (Springer Berlin Heidelberg, 2013). doi:10.1007/978-3-642-32958-6
13. Lakes, R. S., Katz, J. L. & Sternstein, S. S. Viscoelastic properties of wet cortical bone-I. Torsional and biaxial studies. *J. Biomech.* **12**, (1979).

14. Sabio, L. *et al.* Probiotic cellulose: Antibiotic-free biomaterials with enhanced antibacterial activity. *Acta Biomater.* (2021). doi:10.1016/j.actbio.2021.01.039
15. Gorgieva, S. & Trček, J. Bacterial cellulose: Production, modification and perspectives in biomedical applications. *Nanomaterials* **9**, 1–20 (2019).
16. Moon, R. J., Martini, A., Nairn, J., Simonsen, J. & Youngblood, J. *Cellulose nanomaterials review: Structure, properties and nanocomposites. Chemical Society Reviews* **40**, (2011).
17. Gao, M. *et al.* A natural in situ fabrication method of functional bacterial cellulose using a microorganism. *Nat. Commun.* **10**, 1–10 (2019).
18. French, A. D. Idealized powder diffraction patterns for cellulose polymorphs. *Cellulose* **21**, 885–896 (2014).
19. Savitskaya, I. S., Shokatayeva, D. H., Kistaubayeva, A. S., Ignatova, L. V. & Digel, I. E. Antimicrobial and wound healing properties of a bacterial cellulose based material containing *B. subtilis* cells. *Heliyon* **5**, e02592 (2019).
20. Schramm, M. & Hestrin, S. Factors affecting production of cellulose at the air/liquid interface of a culture of *Acetobacter xylinum*. *J. Gen. Microbiol.* **11**, 123–129 (1954).

CHAPTER 6.
TOWARD ORDERED
NANOCELLULOSE





1. Introduction

As stated along this manuscript, bacterial cellulose (BC) has extraordinary potential for biomedical applications due to its exceptional properties: biocompatibility, chemical purity, high water-absorption capacity, and high adsorption capabilities. In addition, the combination of a hierarchical microstructure, hydrogen bonds and structural anisotropy result in a wide range of strength, stiffness and toughness values. Obtaining unidirectional (UD) fibre orientation would be highly desirable since this arrangement would fully exploit the high strength and stiffness of the cellulose biopolymer. In fact, the highest strength and stiffness values (910 MPa and 40 GPa, respectively) have been found for unidirectional composites based on regenerated cellulose (Bocell). Other structural features as high crystallinity, high degree of polymerisation and high orientation of cellulose macromolecules also contribute positively to improve the mechanical properties of cellulose¹.

The formation of unidirectional fibres in BC would definitively expand even further the, already broad, applicability of this material allowing²: i) The modulation of their anisotropic properties; ii) the balance of the stiffness versus the strength of structural materials. It has been shown that the stiffness of Kevlar can be achieved along the fibre direction; iii) to maximize the efficiency of fibre-reinforced materials. It would allow the mechanical properties improvement of polymeric materials; iv) its use as scaffolds to allow cells to be aligned *in vitro* with the aim of imitating the morphology they present *in vivo* since cultures tend to adopt the shape of the substrate (template effect). This cell orientation is critical in the case of extracellular matrix remodeling (e.g., in tendons and bones³).

In this context, it is well known that the BC microstructure is mainly affected by culture conditions, purification and drying methods. The cultivation in static or dynamic (agitated conditions) results in significantly

different BC structures. Static conditions yield denser networks of higher crystallinity⁴ whereas dynamic ones are faster, due to the better contact with the provided oxygen. In fact, culture conditions affect the $I\alpha/I\beta$ BC polymorphs ratio, decreasing under dynamic conditions⁵.

In order to obtain a highly pure cellulose, cells, residual molecules and metabolic products must be eliminated. Usually, the treatment consists of the immersion of the cellulose pellicles in NaOH (0.1–1 M) solutions at around 90 °C for 1 h, or at room temperature for 24–48 h⁶. The strong alkali treatment of cellulose I can disrupt the crystalline regions, forming new crystalline lattice that led to the formation of the cellulose II polymorph. This results in a non-desirable weakening of mechanical properties. In fact, some works have analysed the effect of NaOH concentration and immersion time on the final structure of BC⁷. The conversion of cellulose I to cellulose II occurs at NaOH concentrations above 6% w/v (1.5 M). However, other researchers concluded that the polymorphic transition to cellulose II begun at NaOH concentrations at the order of 5-10 %w/v (1.25 – 2.5 M)⁸. In this regard, it is assumed that the most widely used purification treatment, which employ NaOH concentrations of 0.1 – 1M, did not affect the initial crystallinity of the BC, but the effect of alkali treatments to obtain pure BC is still a subject of debate.

Depending on the application, the BC can be used as a hydrogel in a wet state⁹, or as a dry matrix, such as an aerogel¹⁰ or a film¹¹. There are a considerable number of different drying methods that have been employed in the literature. The most popular ones are drying at different temperatures (from room temperature until 100 °C), under pressure, freeze-drying, supercritical point, or combinations when possible. In general, dried samples are employed to analyse its crystallinity by performing X-ray diffraction (XRD), Fourier-transform infrared (FTIR) and Raman spectroscopies. Although it is generally assumed that the crystallinity of dried films can be correlated with the crystallinity of the wet samples (with or without bacteria), there are several works that employed different drying methods in order to

modulate the microstructure and mechanical properties depending on the application^{12,13}. Thus, assuming that crystallinity of dried BC correlates with that of the cellulose synthesized *in situ* by the bacteria is an inaccuracy. For example, Illa *et al.* studied the effect of oven and freeze drying on several physio-chemical properties of BC produced by two strains¹². Their results concluded that oven-dried and freeze-dried samples have drastically different optical and mechanical properties: oven-dried BC showed higher transparency, Young's modulus and tensile strength, and lower strain and crystal size compared to freeze-dried BC. This is attributed to the higher crystallinity, higher order, less porosity, less fiber diameter, and a denser fibrous network of the oven-dried sample than that of the lyophilized ones. Thus, considering the application, the drying method is decisive for achieving the desired microstructure, and therefore, the mechanical properties.

According to the literature, method of synthesis (dynamic or static), purification and drying procedures induces modifications of BC microstructure, but it does not introduce a significant improvement of the mechanical properties. In fact, there are several methods intended to increment the cellulose fibers' alignment and crystallinity to enhance their mechanical properties. These methods usually involve the previous production of cellulose nanomaterials (CNMs)². CNMs obtained through mechanical fibrillation combined with chemical or biological treatments yield cellulose nanocrystals (CNCs) or cellulose nanofibers (CNFs). The main difference between them is their dimensions: while CNCs are rigid, 100-200 nm long and 5-20 nm wide, CNFs are fibrillar structures with length of >1 μm and a width of 5-200 nm.

On the other hand, other *in situ* and *ex situ* approaches are being investigated to obtain ordered BC. The former includes methods that change culture conditions to induce the formation of aligned cellulose fibers, as unidirectional shear-induced culturing¹⁴, wrinkling³, the application of

electric fields (which produce an oxygen gradient in the culture)³, using rising bubble stream¹⁵, etc. The latter comprise post-synthesis approaches such as directional freeze-drying¹⁶, stretching^{17,18}, twisting¹⁹, crosslinking, used alone or in combination.

Despite the large number of investigations devoted to aligning BC, the resulting materials did not show macroscopic structural order. Achieving unidirectional orientation of the long and interweaving fibrils of cellulose is very complex. Moreover, the approaches used for ordering BC were based on the manipulation of post-synthesized BC, being necessary its previous isolation. Thus, the development of a methodology to directly produce BC with unidirectional fiber orientation at large-scale remains a challenge in the cellulose world.

In this chapter, we evaluated the impact that modifications in culture conditions, purification treatment, and drying methods have in the microstructure of BC. This was done with the aim to establish a methodology framework to analyze the structure and fibril arrangement of BC. Then, preliminary results aimed at developing new approaches to render ordered BC fibrils, based on the use of magnetic nanoparticles and engineered 'magnetic' bacteria, are shown.

2. Results and discussion

In a first step, the impact of the culture condition (static or dynamic) and drying conditions (RT, FD and scCO₂ drying) on the crystallinity and preferential fibre orientation were analysed by a combination of techniques providing complementary information at different length scales (from nano- to macro-scales, Figure 1). The samples were characterized by X-ray diffraction (XRD), Fourier-transform infrared (FTIR) spectroscopy, and field-emission scanning electron microscopy (FESEM). In addition, the properties of pure cellulose (after alkali treatment) were compared to that of the native

BC (in the presence of all the biofilm components, including the cellulose producing-bacteria).

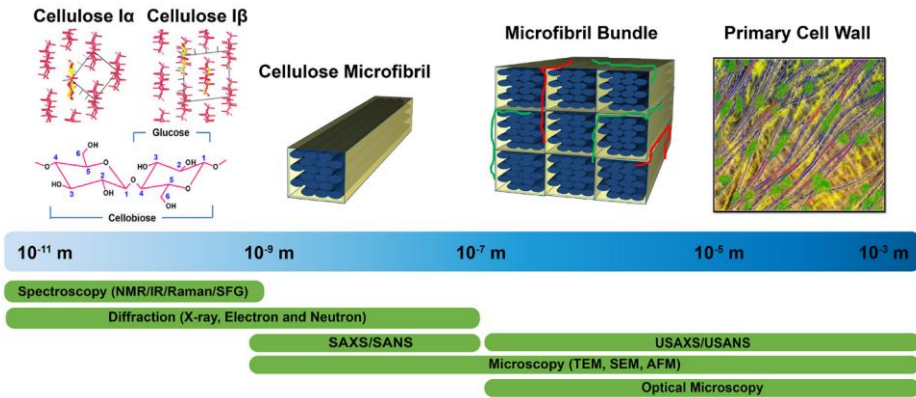


Figure 1. Characterization tools to study the cellulose arrangement at different length scales. Image extracted from Rongpipi *et al.* (2019)²⁰.

We employed *A. xylinum* as the cellulose-producing bacterium and glucose as the main carbon source. Hestrin-Schramm (HS) medium was employed for culturing in all cases. The membranes prepared either under static or agitated conditions presented a yellowish colour due to the presence of nutrients and fermentation by-products inside the network. When static fermentations were performed, thick and homogeneous vial-shaped BC pellicles were synthesized at the solution-air interface (Figure 2A,B), in contrast to agitated cultures, which rendered BC with spherical-like shapes. The size of these BC pellets strongly depended on the orbital agitation speed, so that higher speeds resulted in smaller BC particles (Figure 2C,D).

After the purification treatment of native pellicles (by static or dynamic conditions), including immersion of the pellicle in ethanol, followed by boiling in distilled water, treatment with alkali at 90 °C and finally rinsed with water until neutral pH, transparent membranes of pure BC were obtained (Figure 3A). Optical images of the BC were taken at each step of the purification (Figure 3B-C).

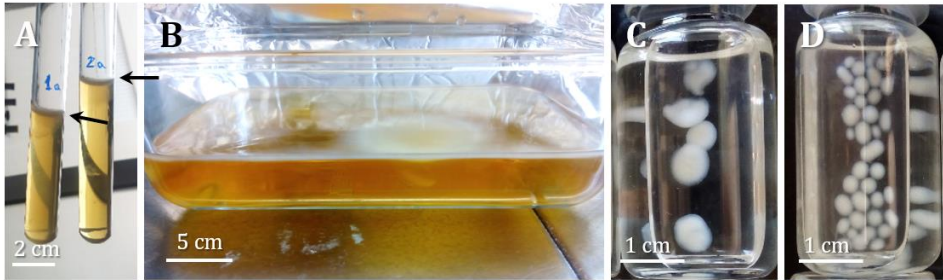


Figure 2. Native BC in HS medium after 5 days **(A)** and 10 days **(B)** of incubation in static conditions. Note that the cellulosic pellicle is formed at the surface of the culture medium (black arrows). Native BC pellets obtained after 2 days of incubation in HS at 180 rpm **(C)** and 200 rpm **(D)**, and transferred to distilled water.

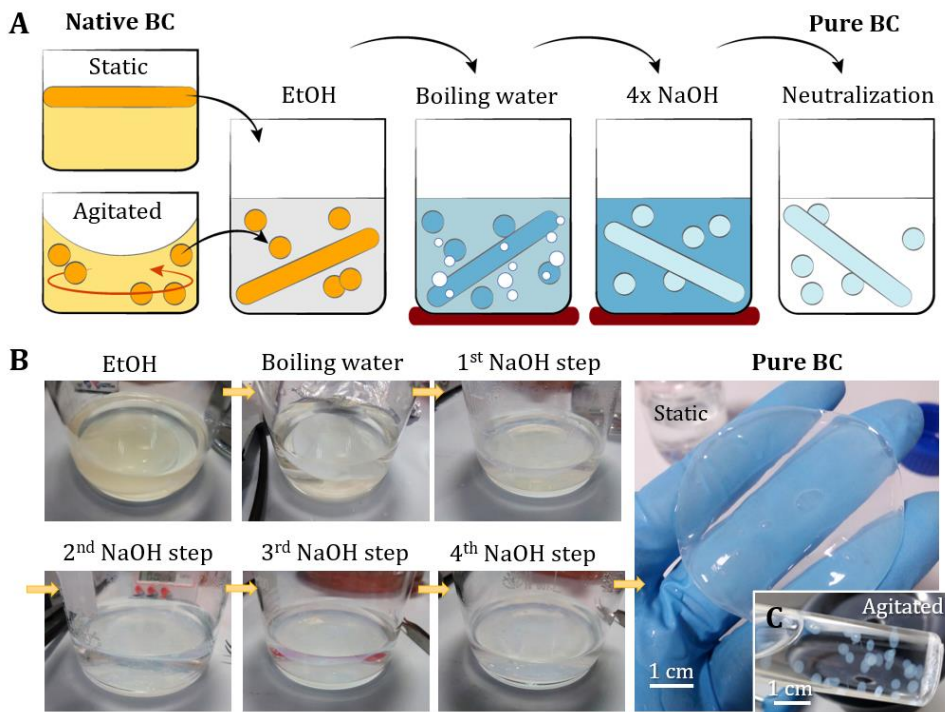


Figure 3. (A) Schematic representation of the treatment for eliminating bacteria and obtention of pure-cellulose pellicles. **(B)** Optical images of the purification treatment performance in a static BC, step by step. Native BC was immersed in ethanol, followed by boiling water, and four alkali treatments at 0.1 M NaOH and 90°C for 20 minutes. Finally, the pellicle was rinsed with distilled water until neutral pH was achieved. **(C)** Pure BC pellets obtained after the purification treatment of native agitated BCs.

2.1. Influence of synthesis conditions (static or dynamic) on BC crystallinity

The microstructure of native and pure BC samples, obtained after static and dynamic fermentations, was initially analysed by field-emission scanning electron microscopy (FESEM, Figure 4). Samples were dried in a first attempt with $scCO_2$, since this drying method is fast, efficient, and one of the most employed techniques²¹. No differences were found between fiber morphology and thickness of both BCs, which were also similar to those of the corresponding pure BC. The FESEM micrographs of static native BC (Figure 4A) illustrate a homogeneous biofilm whose embedded bacteria size around 1.5 microns in length, in contrast with the longer bacteria from agitated BC, which doubled that size (Figure 4B), accordingly with better oxygenation and nutrient distribution of that produced in dynamic conditions. On the other hand, static BC showed a more compact fibrillar structure than that obtained in dynamic conditions (Figure 4 A-D), due to a proper stacking of the cellulosic sheets during the static fermentation⁴.

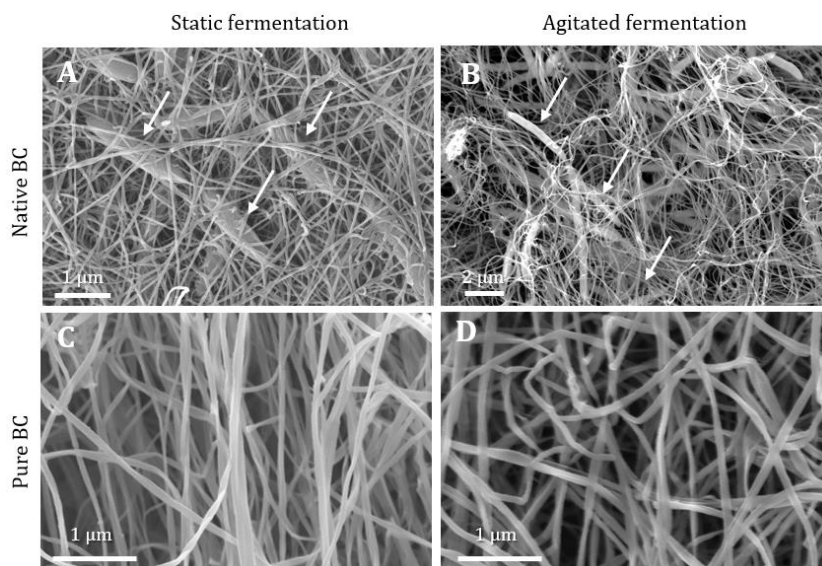


Figure 4. Static and agitated BC membrane before (A, B) and after the purification treatment (C, D). Native and pure BC samples were dried with $scCO_2$. White arrows show *A. xylinum* bacteria.

2.2. Influence of drying methods in BC crystallinity

The possible existence of preferred orientation of RT dried BCs was further analysed by XRD. This technique is sensitive to variations of the crystalline structure (mainly crystal size/morphology and defects) and to the existence of oriented arrangement of crystals. To evaluate the formation of textured samples, we collected XRD patterns by rotating the sample (0° and 90°) using a 2D detector (DECTRIS PILATUS3R 100K-A), as shown schematically in Figure 5A. Figure 5B shows the two-dimensional XRD frames of cellulosic samples dried at RT. Three Bragg reflections (rings) corresponding to the 100, 010 and 011 of $I\alpha$ crystalline phase can be observed²². The rings are not complete in some of the samples (dynamic pure BC), being the pattern collected at 0 and 90° different. This may be indicative of textured samples (preferred orientation). This is more clearly observed in the 1D pattern obtained after the integration of the 2D images (Figure 5C,D).

Preliminary analysis using the Rietveld method of the 1D XRD patterns from static pure BC dried at RT (Figure 5C,D) was carried out to confirm the existence of such preferred orientation. This analysis was performed with MAUD (Materials Analysis Using Diffraction) software, which allows the calculation of the crystal size and crystallinity degree (defined as the crystalline fraction of the sample). As previously stated, bacterial cellulose is composed mainly of cellulose $I\alpha$ (ca. 90%), with little percentage of $I\beta$ (ca. 10%). Although the Rietveld refinement suggested that both phases are textured, $I\beta$ crystals appeared to be more oriented along the $(110)_{I\beta}$ plane since the intensity of the $I\beta$ diffraction peaks depended on the sample position. On the other hand, when cellulose from cotton linters were analysed with the Rietveld method, only cellulose $I\beta$ and amorphous contribution were observed (*data not shown*). Since the typical peaks of $I\alpha$ and $I\beta$ (750 cm^{-1} and 710 cm^{-1} , respectively) can be observed in the FTIR spectra in all the BC samples assayed (Figure 6), we can consider that $I\beta$ is present after the BC

biosynthesis and that purification treatment or drying methods had little influence on their abundance, but may have an effect in its texture.

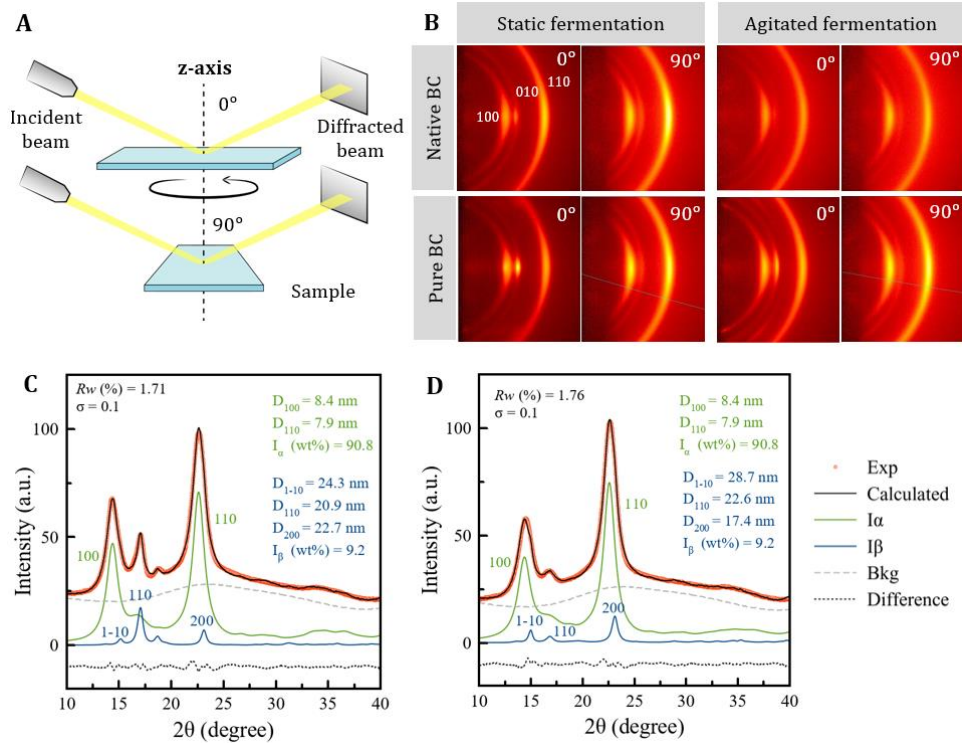


Figure 5. (A) Diagram depicting the strategy to assess the qualitative orientation of cellulose fibers by 2D XRD. **(B)** 2D frames collected by XRD at 0° and 90° of native or pure BC films after culturing in static or dynamic conditions, and dried at RT. The more intense regions correlate with the cellulose α diffraction peaks (100), (010) and (011), at $2\theta = 14.5^\circ$, 16.6° and 22.6° , respectively. **(C-D)** In red, integrated intensity profiles of the 2D XRD frames of static pure BC dried at RT (panel B) between $2\theta = 10^\circ$ - 40° . Rietveld analysis of the XRD pattern collected at 0° **(C)** and 90° **(D)**, calculated with MAUD (Materials Analysis Using Diffraction) program.

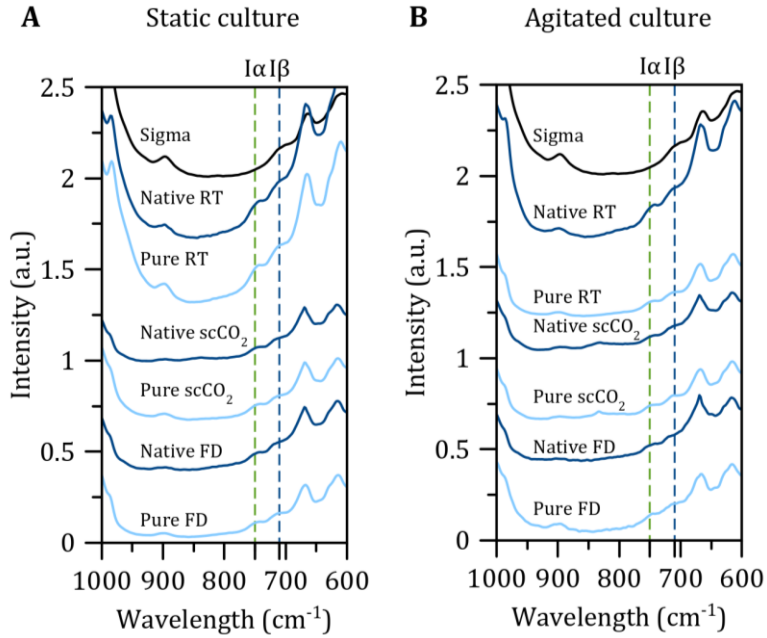


Figure 6. FTIR spectra of native and pure BC produced in **(A)** static and **(B)** agitated fermentations, after FD, RT and scCO₂ dryings. FTIR peaks of cellulose I α (750 cm⁻¹) and cellulose I β (710 cm⁻¹) are marked with dashed lines. Cellulose I β powder from cotton linters (Sigma-Aldrich) is also included in the analysis as control.

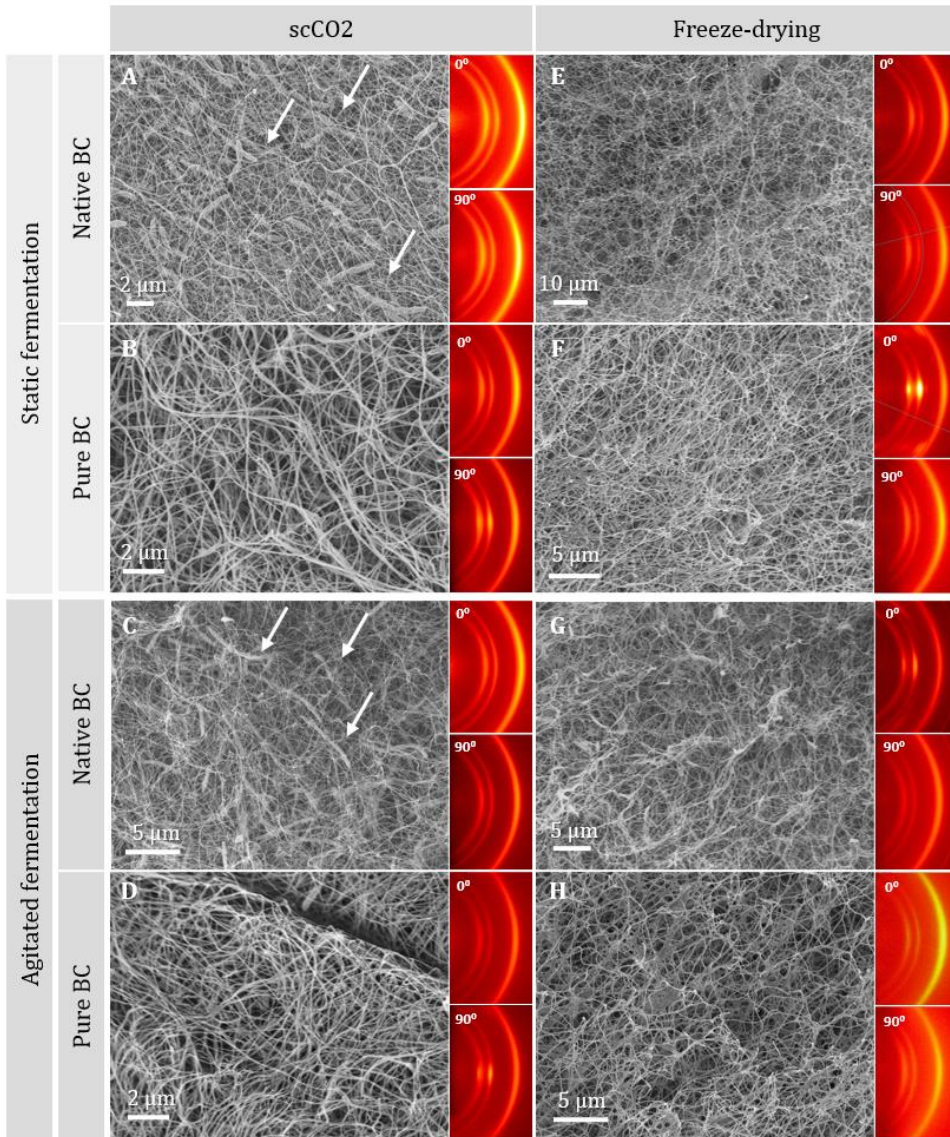


Figure 7. FESEM images of different BC samples in native state or treated, and after scCO₂ drying and freeze-drying. The insets in each image correspond to the BC XRD patterns collected at 0° and 90°. White arrows show *A. xylinum* bacteria.

Therefore, we can conclude that crystal order does not change significantly with synthesis, purification and drying procedures. Static pure BCs displayed this tendency irrespective of the drying method performed,

although the XRD patterns of scCO_2 dried samples showed a lower alignment (Figure 7B) in comparison to freeze-dried samples (Figure 8F). However, further experiments are needed to confirm this tendency. Dried static BCs at RT led to more compact fibrillar structures with quite small pores, resulting in thin and flexible transparent cellulosic films (Figure 8). Hence, in view of these results, we used RT drying for further experiments, considering also that it is the drying method that requires the least handling of the samples.



Figure 8. (A) Static pure BC after drying at RT. This drying technique leads to films with higher density than aerogels, almost transparent appearance, and a more compact microstructure, as shown in FESEM micrograph (B).

In view of these results, we explored new approaches to produce ordered BC based on the use of magnetic nanoparticles or engineering magnetic bacteria, and the application of external magnetic fields to induce preferential orientation of the magnetic entities, which in turn, would induce preferential orientation of BC fibers. Two approaches were explored: *i) ex-situ* functionalization of pure BC with superparamagnetic nanoparticles and subsequent application of external magnetic fields, and *ii) an innovative in situ* approach consisting in producing, first, engineering magnetic *Acetobacter xylinum* (*Ax*) bacteria, which were cultivated in the presence of external magnetic fields to directly produce ordered structural-magnetic native BC, which was purified to lead ordered pure BC.

The first approach, a post-synthetic approach, consisted of the impregnation of pure BC hydrogel with maghemite nanoparticles (average

size 10 nm). These magnetic nanoparticles penetrated the cellulosic structure and changed the BC aspect from clear to brown, as shown in Figure 9A-B. The FESEM image in Figure 9C shows nanoparticles homogeneously attached to the BC fibers. The magnetic functionalization seems quite stable as after washing with sterile water for 48h, no colour change was appreciable in the cellulose material.

When a hard magnet was placed near maghemite-functionalized BC, the sample moved through the liquid medium onto the magnet. Unfortunately, this process did not modify BC structure. In fact, after applying the same magnet for a week, the XRD analysis of the resulting cellulose sample did not show a higher preferential orientation compared to the samples described above (Figure 9D,E). Works are in progress on this approach but using larger superparamagnetic and ferromagnetic nanoparticles.

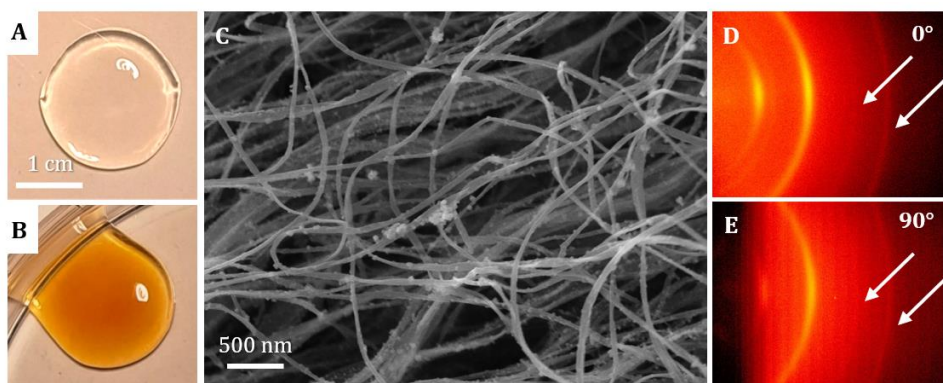


Figure 9. Optical images of a pure BC (A) and maghemite-impregnated pure BC (B). C) FESEM image of maghemite-impregnated pure BC. 2D XRD frames of magnetic-BC at 0° (D) and 90° (E). White arrows mark typical diffraction peaks of maghemite that can be observed at $2\theta = 30.3^\circ$ and 35.7° .

As a further step in terms of complexity, we developed a new strategy to produce ordered BC as an Engineering Living Material (ELM). We first functionalized the cellulose-producing *A. xylinum* bacteria with maghemite

nanoparticles (average size 10 nm) following a procedure developed by our group to obtain magnetic probiotics²³. The *A. xylinum* suspension acquired a brownish colour after the adhesion of the maghemite to cell surface. Moreover, when the suspension was observed under the optical microscope, the bacteria appeared coloured while the background was colourless, which means that nanoparticles adhered preferentially to bacterial surface (Figure 10B). After incubation of the magnetic *A. xylinum* in HS medium at optimal conditions and under a permanent magnetic field (Figure 10C), a thin cellulose membrane was obtained. Although the yield of BC synthesis was lower than that from pure *A. xylinum* in HS medium, these results point out that magnetic-*A. xylinum* maintained enough activity to produce cellulose. This result is not unexpected as magnetic probiotics reported by our group also kept their activity after magnetic functionalization.

Therefore, the magnetic *A. xylinum* synthesized cellulose at the same time as they moved through the culture medium following the external magnetic field. An optical microscopy image of the cellulose pellicle obtained is shown in Figure 10D, which suggests that the BC also acquired the typical brownish colour of the maghemite. Noticeable, the preferred orientation of fibber can be figured out from this image (the direction marked by the arrow).

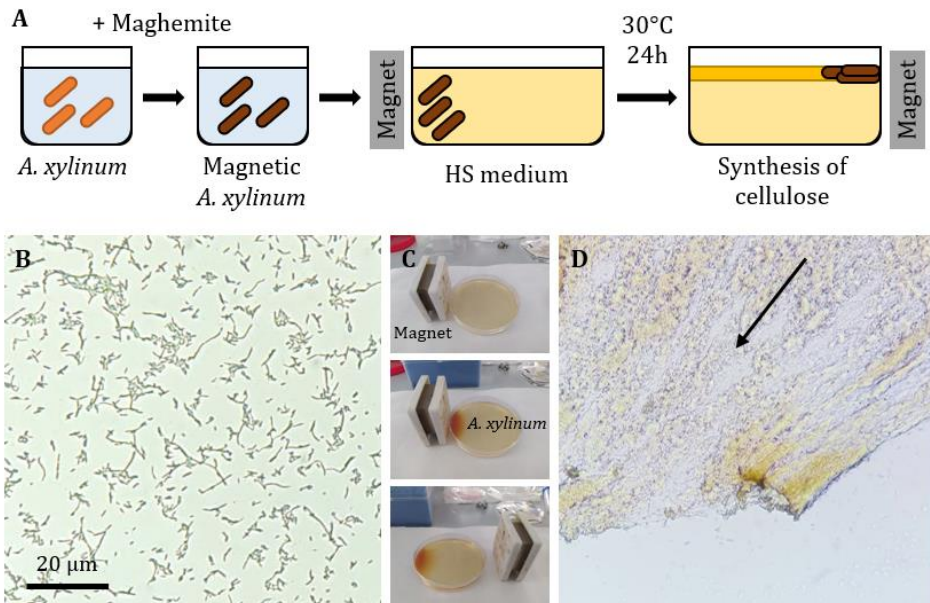


Figure 10. (A) Scheme depicting the protocol to obtain oriented cellulose by incubating under magnetic fields *A. xylinum* with maghemite nanoparticles. (B) Optical microscopy image under 40x objective of the magnetic *A. xylinum* suspension. (C) From top to down: location of the magnet and culture media before, after the inoculation of the magnetic bacterial pellet, and relocation of the magnet to perform the incubation. (D) BC pellicle obtained after fermentation observed by optical microscopy (20x). Black arrow indicates the direction of the orientation.

With the aim to obtain pure ordered BC, the cellulose was purified by removing bacterial cells, biofilm components and maghemite nanoparticles. We performed a modified purification treatment, consisting of the immersion of the sample in L-ascorbic acid as first step to remove magnetic nanoparticles by the reduction of iron oxide to soluble Fe(II). Afterwards, the resulting BC was washed with distilled water and submerged in NaOH 0.1 M for 48 h. Then, it was rinsed with water until neutral pH was achieved and dried at room temperature on a Kapton film. This cleaning treatment adaptation was performed in order to avoid excessive manipulation of the membrane.

Morphological study by AFM and X-ray diffraction at small- and wide-angles (SAXS and WAXS, respectively) were performed at the Institut des Sciences de la Terre (ISTerre) and at the BM02 - D2AM Beamline of the European Synchrotron Radiation Facility (ESRF, Grenoble, France), under the supervision of Alexander Van Driessche and Alicia Moya Cuenca. AFM images showed some preferential orientation of the cellulose-producing cells (Figure 11A). Indeed, some region with no bacteria permitted the visualization of cellulose fibres, also showing some preferred orientation (Figure 11B). On the contrary, AFM images of control samples of pure BC showed a randomly arrangement of BC fibers (Figure 11D,E). We used SAXS to confirm the formation of such fibril preferential orientation. The 2D SAXS patterns of the control sample showed a uniform intensity indicating a random arrangement of fibrils (Figure 11F). In contrast, SAXS pattern of magnetically oriented BC sample showed much more intense reflections in the equatorial direction, confirming the preferential alignment of fibers (Figure 11C).

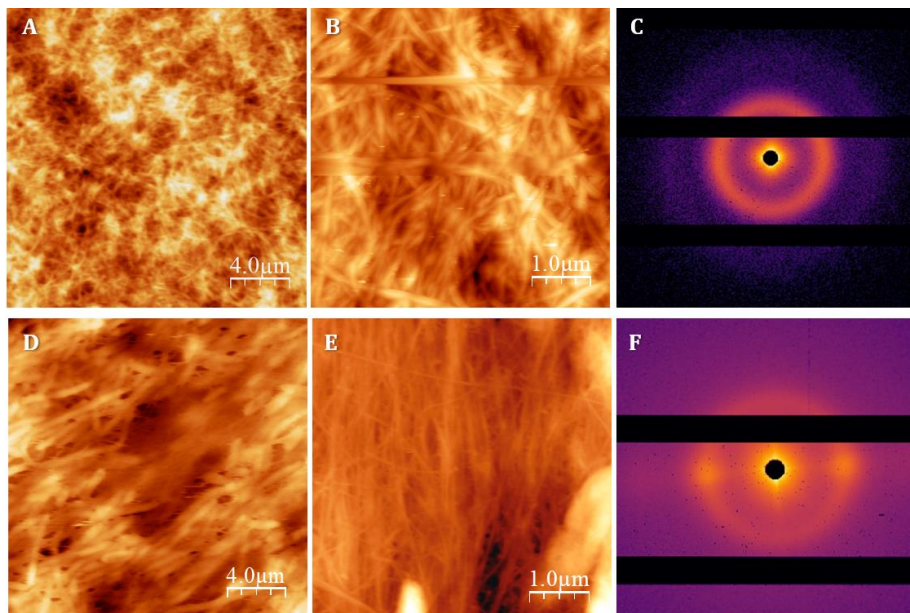


Figure 11. AFM images of BC pure as control (**A, B**) and of the BC biofilm synthesized after culturing the magnetic *A. xylinum* in optimal conditions (**D-E**). 2D SAXS patterns of the control pure BC (**C**) and the magnetically oriented BC (**F**).

3. Conclusions

The development of direct methods of synthesis of BC with unidirectional fibre orientation could mark a turning point in the cellulose world. In addition to the conceptual challenge of ordering a material that Nature produces in a non-ordered form, the improvement of strength and toughness of ordered BC would expand the potential of this material even further.

In this chapter dedicated to 'work in progress' and future perspectives, new approaches have been explored for contributing to succeed to this challenge. These approaches are based on the use of magnetic nanoparticles and magnetic cellulose-producing bacteria that in the presence of external magnetic fields can orientate the cellulose fibers. Preliminary results pointed out that the post-synthesis approach of decorating pure BC with 10-sized maghemite nanoparticles was unsuccessful. Although maghemite nanoparticles were attached to pure BC fibers, they did not result ordered in the presence of an external magnetic field. Work is in progress to reproduce this approach but using larger maghemite nanoparticles and iron and nickel ferromagnetic nanoparticles.

However, the pre-synthesis approach, consisting of the production of magnetic ELM cellulose allowed us to produce pure BC having some preferential fiber orientation. Works are in progress to optimize experimental conditions and fully characterized the obtained materials.

4. Materials and methods

Synthesis of Bacterial cellulose

The lyophilized *Acetobacter xylinum* (ATCC 11142 / CECT 473, Ax) was supplied by the Colección Española de Cultivos Tipo (CECT) and grown in Hestrin and Schramm medium (HS)²⁴ with (w/v) 2% glucose, 0.5% yeast extract, 0.5% peptone, 0.115% citric acid, 0.68% Na₂HPO₄ · 12 H₂O (Sigma). Ax was first grown on solid agar (1.5%) and stored at 4 °C.

The synthesis of bacterial celluloses was carried out by culturing a single colony of Ax in liquid HS medium, at 30 °C and in aerobic conditions. Two different culture conditions were assayed. On one hand, for static conditions, Ax was cultured in 10 mL of HS medium for 3 days before scaling the culture to 100 mL. After 5 days of incubation, the cellulose pellicles were collected. On the other hand, Ax was cultivated in 3 mL of HS medium under orbital agitation (200 rpm) for 3 days. Bacterial cellulose samples were washed in sterile saline solution (0.9% NaCl) to eliminate the residual components of culture media and stored at 4 °C until its further use. Half of the pellicles were treated for obtaining pure cellulose, and all samples were finally rinsed with distilled water in order to eliminate NaCl immediately before drying procedures for further characterization.

Obtention of pure cellulose

Pure cellulose was obtained from static and agitated cultures following a protocol well established²⁵⁻²⁷. Briefly, bacterial cellulose pellicles were submerged in ethanol (96°) for at least 15 min, boiled in water for 40 min, treated three times with NaOH 0.1 M at 90 °C for 20 min, and finally, washed in distilled water until neutral pH was achieved. The static-cultured celluloses were cut into squares of approximately 1 cm² after neutralization.

Obtention of maghemite-impregnated pure BCs

Pure BC with 2 cm in diameter were immersed in a maghemite solution (concentration?) for 5 min and washed during 72h with water changes every 24h (until no colour changes were appreciable). To induce the orientation of the fibers, an external magnetic field was applied for a week using a nickel-plated NdFeB magnet (N42 magnetisation, strength of approx. 588 N, ID: Q-40-40-20-N, <https://www.supermagnete.es>). Afterwards, room temperature drying and XRD assays were performed in order to assess preferential orientation.

Synthesis of cellulose by artificial magnetic *A. xylinum*

A BC pellicle was digested with cellulase from *Trichoderma reesei* (No C2730-50ML, Sigma-Aldrich). The membrane was immersed in 2 mL of enzyme solution (50 μ L cellulase/mL potassium phosphate buffer, 50 mM, pH 6) and incubated at 37 °C for 2h, with orbital shaking (180 rpm). Then, the sample was centrifuged to collect the cellulose-producing bacteria and washed three times with sterile water. The bacterial suspension was adjusted to an optical density of $OD_{600} = 0.3$ (5 mL). Subsequently, we performed the protocol described by Martín *et al.* (2014)²³. Finally, the pellet was resuspended in 1 mL of sterile water at pH 2 and inoculated in 14 mL of Hestrin-Schramm culture medium²⁴. The fermentation was performed in static conditions at 30°C for 24h under magnetic field induced with a nickel-plated NdFeB magnet (ID: Q-40-40-20-N). The purification treatment was adapted to avoid excessive manipulation of the pellicle. In brief, the maghemite nanoparticles were eliminated by immersion in 20 mL of L-ascorbic acid 1M at 37 °C for 24h, followed by washing with distilled water and treatment with NaOH 0.1M at 37°C for 48 h. Finally, the pellicle was neutralized.

Drying methods and characterization of the pure BC networks

In order to analyse how the presence of A_x in the cellulosic structure affects the fibers arrangement, three drying methods were applied separately to samples containing or not-containing the producing bacteria -drying at room temperature, freeze-drying and supercritical CO_2 drying-. Afterwards, the films were characterized by X-Ray Diffraction (XRD), small-angle X-ray scattering (SAXS), Fourier-Transform Infrared spectroscopy (FTIR), and Field Emission Scanning Electron Microscopy (FESEM).

The drying methods were performed as follow:

Room temperature drying (RT-D) was carried out by placing the pellicles between filter papers and under slight pressure, for at least 4 days.

For freeze-drying (F-D), samples were submerged in distilled water, freeze in liquid nitrogen for 10 min, and dry under vacuum at $-60\text{ }^\circ\text{C}$ for 2 days using a Telstar Cryodos-50 freeze-dryer.

For the third drying method, *supercritical CO_2 drying (C-D)*, we employed duplicates of samples after processing for FESEM analysis (before covering with the carbon film).

For structural characterization:

X-Ray Diffraction (XRD) patterns were collected from the surface of cellulose films using a Bruker D8 Discover diffractometer (Centre of Scientific Instrumentation, University of Granada) equipped with a 2D-detector (Pilatus3R 100K-A, Dectris), at $25\text{ }^\circ\text{C}$, with $Cu\ K\alpha$ ($\lambda = 1.5406\text{ \AA}$) radiation generated at 50 kV and 1 mA. The XRD diffraction patterns were recorded at a rate of 2° min^{-1} from 10° to 40° with a step size of 0.02° . In order to check the presence of preferred orientation, two patterns were collected (0° and 90°) by rotating the sample. Each spectrum was baseline-corrected and normalized to the maximum intensity at around 2θ value of 22.5° .

Fourier-Transform Infrared (FTIR) spectra were collected on a Bruker Tensor 27 spectrometer under attenuated total reflection configuration with resolution of 3 cm^{-1} by accumulation of 100 scans covering the $4000\text{-}400\text{ cm}^{-1}$ spectral range. The spectra were collected at room temperature in the absorption mode.

Raman spectroscopy. Cellulose films were placed on a microscope glass. Raman spectra were collected on a Micro-Raman Spectrometer JASCO NRS-5100 (Centre of Scientific Instrumentation, University of Granada) with laser 785 nm , 500 mW (Torsana StarBright). The spectra were recorded over the range $1700\text{-}340\text{ cm}^{-1}$ with resolution of 1 cm^{-1} , averaged over 10 scans and 20 s exposure. Each spectrum was baseline-corrected and normalized to the maximum absorbance at 1096 cm^{-1} .

Field Emission Scanning Electron Microscopy (FESEM). Bacterial celluloses were fixed in 1 mL of cacodylate buffer (0.1 M, pH 7.4) containing 2.5% of glutaraldehyde at $4\text{ }^{\circ}\text{C}$. After 24 hours, the samples were washed 3 times (30 min at $4\text{ }^{\circ}\text{C}$) with cacodylate buffer. The samples were stained with osmium tetroxide solution (1% v/v) for 2 hours in the dark and then repeatedly rinsed with Mili-Q water to remove the excess of osmium. Samples were then dehydrated at room temperature with ethanol/water mixtures of 50%, 70%, 90% and 100% (v/v) for 20 each, being the last concentration repeated three times and dried at the CO_2 critical point. Finally, dehydrated samples were mounted on metal stubs with conductive adhesive, covered with a thin carbon film and analysed using a FESEM (Zeiss SUPRA40V, Centre of Scientific Instrumentation, University of Granada).

Optical microscopy

A drop of magnetic *A. xylinum* suspension and the BC pellicle obtained after its incubation were fixed in poly-L-Lys glass slides (Superfrost®Plus, ThermoScientific) and observed under bright field using a 40x objective using an optical microscope (iScope, Euromex)

Atomic force microscopy (AFM)

AFM imaging was performed with an MFP-3D™ Origin+ device (Asylum Research, Oxford Instruments). All the samples were dried on glass slides at room temperature and screened in air and contact mode using silicon nitride tips (Bruker SNL-10), with a spring constant of 327.76 pN/m. Image processing and representation were carried out with WSxM 5.0 Develop 10.2 software²⁸.

Small-angle X-ray scattering

The samples were dried at room temperature on Kapton films prior to SAXS and WAXS data collection. The experiments were performed at the French CRG beamline BM02-D2AM (at room temperature with a wavelength of 1.1808 Å) of the European Synchrotron Radiation Facility (ESRF). A beam size of 500 x 500 μm² and a Pixel photon counting detector were used for data collection.

5. References

1. Jakob, M. *et al.* The strength and stiffness of oriented wood and cellulose-fibre materials: A review. *Prog. Mater. Sci.* **125**, 100916 (2022).
2. Li, K. *et al.* Alignment of Cellulose Nanofibers: Harnessing Nanoscale Properties to Macroscale Benefits. *ACS Nano* **15**, 3646–3673 (2021).
3. Prathapan, R. *et al.* In Situ Alignment of Bacterial Cellulose Using Wrinkling. *ACS Appl. Bio Mater.* **3**, 7898–7907 (2020).
4. Singhsa, P., Narain, R. & Manuspiya, H. Physical structure variations of bacterial cellulose produced by different *Komagataeibacter xylinus* strains and carbon sources in static and agitated conditions. *Cellulose* **25**, 1571–1581 (2018).
5. Watanabe, K., Tabuchi, M., Morinaga, Y. & Yoshinaga, F. Structural features and properties of bacterial cellulose produced in agitated culture. *Cellulose* **5**, 187–200 (1998).
6. Mikkelsen, D., Flanagan, B. M., Dykes, G. A. & Gidley, M. J. Influence of different carbon sources on bacterial cellulose production by *Gluconacetobacter xylinus* strain ATCC 53524. *J. Appl. Microbiol.* **107**, 576–583 (2009).
7. Gea, S. *et al.* Investigation into the structural, morphological, mechanical and thermal behaviour of bacterial cellulose after a two-step purification process. *Bioresour. Technol.* **102**, 9105–9110 (2011).
8. Oudiani, A. El, Chaabouni, Y., Msahli, S. & Sakli, F. Crystal transition from cellulose I to cellulose II in NaOH treated *Agave americana* L. fibre. *Carbohydr. Polym.* **86**, 1221–1229 (2011).
9. Sulaeva, I., Henniges, U., Rosenau, T. & Potthast, A. Bacterial cellulose as a material for wound treatment: Properties and modifications. A review. *Biotechnol. Adv.* **33**, 1547–1571 (2015).
10. Sai, H. *et al.* Surface modification of bacterial cellulose aerogels' web-like skeleton for oil/water separation. *ACS Appl. Mater. Interfaces* **7**, 7373–7381 (2015).
11. Gomes, N. O., Carrilho, E., Machado, S. A. S. & Sgobbi, L. F. Bacterial cellulose-based electrochemical sensing platform: A smart material for miniaturized biosensors. *Electrochim. Acta* **349**, 136341 (2020).
12. Illa, M. P., Sharma, C. S. & Khandelwal, M. Tuning the physiochemical properties of bacterial cellulose: effect of drying conditions. *J. Mater. Sci.* **54**, 12024–12035 (2019).
13. Liebner, F. *et al.* Aerogels from unaltered bacterial cellulose:

- Application of scCO₂ drying for the preparation of shaped, ultra-lightweight cellulosic aerogels. *Macromol. Biosci.* **10**, 349–352 (2010).
14. Chae, I. *et al.* Shear-induced unidirectional deposition of bacterial cellulose microfibrils using rising bubble stream cultivation. *Carbohydr. Polym.* **255**, 117328 (2021).
 15. Chae, I. *et al.* Shear-induced unidirectional deposition of bacterial cellulose microfibrils using rising bubble stream cultivation. *Carbohydr. Polym.* **255**, 117328 (2021).
 16. Chen, Y. *et al.* Anisotropic nanocellulose aerogels with ordered structures fabricated by directional freeze-drying for fast liquid transport. *Cellulose* **26**, 6653–6667 (2019).
 17. Wang, S. *et al.* Transparent, Anisotropic Biofilm with Aligned Bacterial Cellulose Nanofibers. *Adv. Funct. Mater.* **28**, 1–10 (2018).
 18. Ye, D. *et al.* Ultrahigh Tough, Super Clear, and Highly Anisotropic Nanofiber-Structured Regenerated Cellulose Films. *ACS Nano* **13**, 4843–4853 (2019).
 19. Wang, S. *et al.* Super-Strong, Super-Stiff Macrofibers with Aligned, Long Bacterial Cellulose Nanofibers. *Adv. Mater.* **29**, 1–8 (2017).
 20. Rongpipi, S., Ye, D., Gomez, E. D. & Gomez, E. W. Progress and opportunities in the characterization of cellulose – an important regulator of cell wall growth and mechanics. *Front. Plant Sci.* **9**, 1–28 (2019).
 21. Taokaew, S., Phisalaphong, M. & Newby, B. Z. Bacterial Cellulose. in 255–283 (2017). doi:10.4018/978-1-5225-1971-3.ch012
 22. French, A. D. Idealized powder diffraction patterns for cellulose polymorphs. *Cellulose* **21**, 885–896 (2014).
 23. Zeng, M., Laromaine, A. & Roig, A. Bacterial cellulose films: influence of bacterial strain and drying route on film properties. *Cellulose* **21**, 4455–4469 (2014).
 24. Schramm, M. & Hestrin, S. Factors affecting production of cellulose at the air/liquid interface of a culture of *Acetobacter xylinum*. *J. Gen. Microbiol.* **11**, 123–129 (1954).
 25. Kuo, C. H., Chen, J. H., Liou, B. K. & Lee, C. K. Utilization of acetate buffer to improve bacterial cellulose production by *Gluconacetobacter xylinus*. *Food Hydrocoll.* **53**, 98–103 (2016).
 26. Mohammadkazemi, F., Azin, M. & Ashori, A. Production of bacterial cellulose using different carbon sources and culture media. *Carbohydr. Polym.* **117**, 518–523 (2015).

27. Tronser, T., Laromaine, A., Roig, A. & Levkin, P. A. Bacterial Cellulose Promotes Long-Term Stemness of mESC. *ACS Appl. Mater. Interfaces* **10**, 16260–16269 (2018).
28. Horcas, I. *et al.* WSXM: A software for scanning probe microscopy and a tool for nanotechnology. *Rev. Sci. Instrum.* **78**, (2007).



CONCLUSIONS

The general conclusion of this PhD is that it is possible to generate new (multipurpose) biomaterials by adequately/suitably integrating live and active probiotic bacteria into biocompatible matrices of biopolymers of biological importance, i.e., collagen or bacterial cellulose. The experimental results combining the synthesis, complete structural characterization and evaluation of cell viability and activity of the biomaterials support the proposed hypotheses. Each biomaterial of this work has been developed for a specific challenge, for a specific biomedical application. The specific conclusions are as follows:

A biomaterial based on collagen and probiotics for the treatment of bacterial vaginosis (BV). The most common strategy today for the treatment of this bacterial infection is the use of probiotics for restoring the balance of the vaginal. The main limitation of current treatments lies in the lack of adherence of probiotics to the vagina and their difficulty in colonizing it, which generates short-term efficacy and frequent relapses.

The biomaterials developed in this PhD (col-*Lf* and col-*La*) can provide a possible solution to this problem. The two probiotics used, *L. fermentum* (*Lf*) and *L. acidophilus* (*La*), were integrated in a matrix of collagen fibers (col), using the EPS probiotics as glue to adhere to col. Once *Lf* and *La* are entrapped in the collagen fiber network, they remain alive, proliferate, and show enhanced metabolic activity. These col-*Lf* and col-*La* biomaterials are capable of acclimatizing and proliferating in a hostile BV environment, whereas the respective non-entrapped probiotics, *Lf* and *La*, do not show this performance. Through proliferation under BV conditions, these entrapped probiotics are able to restore the pH of the BV medium (pH 5) to a healthy pH of around 4. In addition to the stability that the collagen matrix confers to the entrapped probiotics, col-*Lf* and col-*La* exhibit excellent adhesion to mucin, significantly higher than those of *Lf* and *La*. The combination of these properties makes these biomaterials ideal candidates for the treatment of BV, as they overcome the two critical limitations of the

current probiotic-based therapies: high adhesion to the vaginal mucosa and protection of the probiotics in the hostile BV environment.

We are currently developing vaginal tampons of this class of biomaterials containing probiotic cocktails for their commercialization in the prevention and therapy of BV.

Two-sided bifunctional cellulose. A bifunctional BC based on the combination of two antibacterial agents, i.e., probiotics (*Lf*) and silver nanoparticles (AgNPs) was developed in this PhD. The antibacterials were intentionally placed on opposite BC faces to avoid the toxic effect of AgNPs on the probiotics. The antibacterial assays against *Pseudomonas aeruginosa* pointed out that the activity of the two-sided AgNP-BC-*Lf* is the result of an additive effect of both antibacterial components. efficacy of these two-sided biomaterials against multi-resistant pathogens is also being evaluated.

An antibacterial cellulose. Due to its extraordinary properties, BC is in the market as a wound dressing material. However, BC itself has no activity against bacterial infection, which is a recurrent issue affecting hard-to-heal chronic wounds. The synthesis of BC derivatives with antibacterial properties has long been, in fact, a challenge for biomaterial scientists. BC functionalization has limitations due to its poor solubility, which makes necessary the use of organic solvents and high temperatures.

In this PhD, a new approach has been applied to succeed in the challenge of developing antibacterial celluloses. A new class of cellulose, which we have named probiotic cellulose, has been produced by integrating probiotics (*L. fermentum Lf* or *L. gasseri Lg*) into the bacterial cellulose matrix. The two probiotic celluloses (*Lf*- and *Lg*-cellulose) showed enhanced antibacterial activity against *Staphylococcus aureus* and *Pseudomonas aeruginosa*, the two most active pathogens in severe skin infections. Interestingly, they also were active against methicillin-resistant *S. aureus* and *P. aeruginosa* isolated from urine samples of patients of the Hospital

Virgen de las Nieves (Granada). Therefore, probiotic cellulose is a new class of antibiotic-free antibacterial with practical application today, and tomorrow, in a hypothetical post-antibiotic era, where antibiotics would no be longer effective.

The strategy to produce probiotic cellulose can be extended to other facultative anaerobic probiotics or even combining different probiotics with the aim of obtaining multifunctional biomaterials towards complex microbial infections. Moreover, the production of probiotic cellulose involves a single-step process under mild conditions and does not require the lengthy and expensive chemical treatments necessary to isolate bacterial cellulose, and thus can be easily scaled for industrial production.

We are currently testing the activity of a library of probiotic celluloses against other antibiotic-resistant pathogens and even multi-resistant bacteria.

Life tunes viscoelasticity of probiotic cellulose. Hybrid Living Materials (HLMs) are an emergent class of materials with extraordinary potential for different biomedical applications. Probiotic cellulose is a genuine example of HLM. In probiotic cellulose, the viscoelasticity is tuned by probiotic proliferation. Indeed, the proliferation of probiotics within cellulose acts as a key modulator of the viscoelasticity, providing from celluloses with lower-than-matrix fluidity (at low probiotic density) to celluloses with viscoelastic moduli closer to those of elastic solids (at higher probiotic density). Probiotic cellulose is the first example of a material where viscoelasticity is tuned by no external input (like UV light, heat, etc) but by life (bacteria proliferation). We are currently exploring the possibility of using probiotic cellulose as a bio-ink for 3D bioprinting.

Towards ordered bacterial cellulose. Bacterial cellulose (BC) is considered one of the biomaterials of the future. Biocompatibility, chemical purity, high water-holding, and high adsorption capabilities make BC an

extraordinary material for different biomedical applications. The methodology used for producing, isolating, purifying, and drying BC defines its crystallinity but in no case can result in ordered BC.

In this PhD, a strategy to render some order to cellulose fibers has been explored. It consists of the use of magnetite-containing cellulose-producing bacteria, which are able to produce cellulose films under external magnetic fields. SEM and AFM images showed some aligned fibres, which was then corroborated by SAXS and WAXS data collected with synchrotron radiation.

The development of ordered cellulose could mark a turning point in the cellulose world, since the structural order of cellulose fibers may expand, even more, the potential of this material. A detailed rheological study of a library of ordered celluloses is in progress to understand the impact of the structural order in the rheological/mechanical properties of the films.



La conclusión general de este doctorado es que es posible generar nuevos biomateriales (polivalentes) mediante la integración adecuada/conveniente de bacterias probióticas vivas y activas en matrices biocompatibles de biopolímeros de importancia biológica, es decir, colágeno o celulosa bacteriana. Los resultados experimentales que combinan la síntesis, la caracterización estructural completa y la evaluación de la viabilidad y actividad celular de los biomateriales apoyan las hipótesis propuestas. Cada biomaterial de este trabajo se ha desarrollado para un reto específico, para una aplicación biomédica concreta. Las conclusiones específicas son las siguientes:

Un biomaterial basado en colágeno y probióticos para el tratamiento de la vaginosis bacteriana (VB). La estrategia más común hoy en día para el tratamiento de esta infección bacteriana es el uso de probióticos para restaurar el equilibrio de la vagina. La principal limitación de los tratamientos actuales radica en la falta de adherencia de los probióticos a la vagina y su dificultad para colonizarla, lo que genera una eficacia a corto plazo y frecuentes recaídas.

Los biomateriales desarrollados en este doctorado (col-*Lf* y col-*La*) pueden aportar una posible solución a este problema. Los dos probióticos utilizados, *L. fermentum* (*Lf*) y *L. acidophilus* (*La*), se integraron en una matriz de fibras de colágeno (col), utilizando los probióticos EPS como pegamento para adherirse a col. Una vez que *Lf* y *La* quedan atrapados en la red de fibras de colágeno, permanecen vivos, proliferan y muestran una mayor actividad metabólica. Estos biomateriales col-*Lf* y col-*La* son capaces de aclimatarse y proliferar en un entorno hostil de BV, mientras que los respectivos probióticos no atrapados, *Lf* y *La*, no muestran este rendimiento. Mediante la proliferación en condiciones de BV, estos probióticos atrapados son capaces de restaurar el pH del medio de BV (pH 5) a un pH saludable de alrededor de 4. Además de la estabilidad que la matriz de colágeno confiere a los probióticos atrapados, col-*Lf* y col-*La* muestran una excelente adhesión

a la mucina, significativamente mayor que la de *Lf* y *La*. La combinación de estas propiedades hace que estos biomateriales sean candidatos ideales para el tratamiento de la VB, ya que superan las dos limitaciones críticas de las actuales terapias basadas en probióticos: la alta adhesión a la mucosa vaginal y la protección de los probióticos en el entorno hostil de la VB.

Actualmente estamos desarrollando tampones vaginales de esta clase de biomateriales que contienen cócteles probióticos para su comercialización en la prevención y terapia de la VB.

Celulosa bifuncional de dos caras. En este doctorado se desarrolló un BC bifuncional basado en la combinación de dos agentes antibacterianos, es decir, probióticos (*Lf*) y nanopartículas de plata (AgNPs). Los antibacterianos se colocaron intencionadamente en caras opuestas del BC para evitar el efecto tóxico de las AgNP sobre los probióticos. Los ensayos antibacterianos contra *Pseudomonas aeruginosa* señalaron que la actividad de las AgNP-BC-*Lf* de dos caras es el resultado de un efecto aditivo de ambos componentes antibacterianos. También se está evaluando la eficacia de estos biomateriales de dos caras contra patógenos multirresistentes.

Una celulosa antibacteriana. Debido a sus extraordinarias propiedades, la BC está en el mercado como material de apósito para heridas. Sin embargo, la BC por sí misma no tiene actividad contra la infección bacteriana, que es un problema recurrente que afecta a las heridas crónicas de difícil curación. La síntesis de derivados del BC con propiedades antibacterianas ha sido durante mucho tiempo, de hecho, un reto para los científicos de biomateriales. La funcionalización de BC tiene limitaciones debido a su escasa solubilidad, que hace necesario el uso de disolventes orgánicos y altas temperaturas.

En este doctorado, se ha aplicado un nuevo enfoque para tener éxito en el reto de desarrollar celulosas antibacterianas. Se ha producido una nueva clase de celulosa, que hemos denominado celulosa probiótica,

mediante la integración de probióticos (*L. fermentum Lf* o *L. gasseri Lg*) en la matriz de celulosa bacteriana. Las dos celulosas probióticas (*Lf*- y *Lg*-celulosa) mostraron una mayor actividad antibacteriana contra *Staphylococcus aureus* y *Pseudomonas aeruginosa*, los dos patógenos más activos en las infecciones cutáneas graves. Curiosamente, también fueron activos contra *S. aureus* y *P. aeruginosa* resistentes a la metilicina aislados de muestras de orina de pacientes del Hospital Virgen de las Nieves (Granada). Por lo tanto, la celulosa probiótica es una nueva clase de antibacteriano sin antibióticos con aplicación práctica hoy, y mañana, en una hipotética era post-antibiótica, donde los antibióticos ya no serían efectivos.

La estrategia de producción de celulosa probiótica puede extenderse a otros probióticos anaerobios facultativos o incluso a la combinación de diferentes probióticos con el objetivo de obtener biomateriales multifuncionales frente a infecciones microbianas complejas. Además, la producción de celulosa probiótica implica un proceso de un solo paso en condiciones suaves y no requiere los largos y costosos tratamientos químicos necesarios para aislar la celulosa bacteriana, por lo que puede escalarse fácilmente para la producción industrial.

Actualmente estamos probando la actividad de una biblioteca de celulosas probióticas contra otros patógenos resistentes a los antibióticos e incluso contra bacterias multirresistentes.

La viscoelasticidad de la celulosa probiótica en función de la vida.

Los materiales vivos híbridos (HLM) son una clase emergente de materiales con un potencial extraordinario para diferentes aplicaciones biomédicas. La celulosa probiótica es un auténtico ejemplo de HLM. En la celulosa probiótica, la viscoelasticidad se ajusta mediante la proliferación de probióticos. De hecho, la proliferación de probióticos dentro de la celulosa actúa como un modulador clave de la viscoelasticidad, proporcionando desde celulosas con una fluidez inferior a la de la matriz (a baja densidad

probiótica) hasta celulosas con módulos viscoelásticos más cercanos a los de los sólidos elásticos (a mayor densidad probiótica). La celulosa probiótica es el primer ejemplo de un material en el que la viscoelasticidad no se ajusta por una entrada externa (como la luz ultravioleta, el calor, etc.) sino por la vida (la proliferación de bacterias). Actualmente estamos explorando la posibilidad de utilizar la celulosa probiótica como biotinta para la bioimpresión en 3D.

Hacia la celulosa bacteriana ordenada. La celulosa bacteriana (BC) se considera uno de los biomateriales del futuro. Su biocompatibilidad, pureza química, alta capacidad de retención de agua y alta capacidad de adsorción hacen de la BC un material extraordinario para diferentes aplicaciones biomédicas. La metodología utilizada para producir, aislar, purificar y secar el BC define su cristalinidad, pero en ningún caso puede dar lugar a un BC ordenado.

En este doctorado se ha explorado una estrategia para dar cierto orden a las fibras de celulosa. Consiste en el uso de bacterias productoras de celulosa con magnetita, que son capaces de producir películas de celulosa bajo campos magnéticos externos. Las imágenes de SEM y AFM mostraron algunas fibras alineadas, lo que fue corroborado por los datos de SAXS y WAXS recogidos con radiación de sincrotrón.

El desarrollo de la celulosa ordenada podría marcar un punto de inflexión en el mundo de la celulosa, ya que el orden estructural de las fibras de celulosa puede ampliar, aún más, el potencial de este material. Se está realizando un estudio reológico detallado de una biblioteca de celulosas ordenadas para comprender el impacto del orden estructural en las propiedades reológicas/mecánicas de las películas.